Optimization-based Synthesis of Hybrid Separation Processes

Von der Fakultät für Maschinenwesen der
Rheinisch-Westfälischen Technischen Hochschule Aachen
zur Erlangung des akademischen Grades eines
Doktors der Ingenieurwissenschaften genehmigte Dissertation

vorgelegt von

Korbinian Krämer

Berichter: Universitätsprofessor Dr.-Ing. Wolfgang Marquardt
Universitätsprofessor Dr.-Ing. Andrzej Górak

Tag der mündlichen Prüfung: 31. Januar 2012

Fortschritt-Berichte VDI

Reihe 3

Verfahrenstechnik

Dipl.-Ing. Korbinian Krämer,
Köln

Nr. 934

Optimization-based Synthesis of Hybrid Separation Processes

Berichte aus der
Aachener Verfahrenstechnik - Prozesstechnik

RWTH Aachen University

Krämer, Korbinian
Optimization-based Synthesis of Hybrid Separation Processes
Fortschr.-Ber. VDI Reihe 3 Nr. 934. Düsseldorf: VDI Verlag 2012.
243 Seiten, 59 Bilder, 78 Tabellen.
ISBN 978-3-18-393403-4, ISSN 0178-9503,
€ 73,00 / VDI-Mitgliederpreis € 65,70.

Keywords: Process design – Conceptual design – Process optimization – Shortcut method – Rigorous optimization – MINLP – Distillation – Heteroazeotropic distillation – Extraction – Crystallization

Hybrid separation processes offer a great potential for the design of energy-efficient, sustainable separation processes through a combination of different separation techniques. However, the design of these highly integrated processes is challenging due to the multitude of structural and operative degrees of freedom. A lack of modeling experience and reliable synthesis methods has so far hindered the application of these promising designs in industry. It is the scope of this thesis to provide methodologies which facilitate an efficient and reliable conceptual design of hybrid separation processes. For this purpose, a synthesis framework for the optimization-based design of hybrid processes is proposed. Powerful shortcut and rigorous evaluation methods for distillation, heteroazeotropic distillation, extraction, crystallization and reactive distillation are developed. These methods are fully algorithmic and computationally efficient in order to allow an optimization-based design of large-scale hybrid processes. The proposed synthesis framework is validated by industrial case studies.

Bibliographische Information der Deutschen Bibliothek
Die Deutsche Bibliothek verzeichnet diese Publikation in der Deutschen Nationalbibliographie; detaillierte bibliographische Daten sind im Internet unter http://dnb.ddb.de abrufbar.

Bibliographic information published by the Deutsche Bibliothek
(German National Library)
The Deutsche Bibliothek lists this publication in the Deutsche Nationalbibliographie (German National Bibliography); detailed bibliographic data is available via Internet at http://dnb.ddb.de.

D 82 (Diss. RWTH Aachen University, 2012)

ISSN 0178-9503
ISBN 978-3-18-393403-4

Vorwort

Die vorliegende Arbeit entstand während meiner Zeit als wissenschaftlicher Mitarbeiter an der Aachener Verfahrenstechnik-Prozesstechnik der RWTH Aachen University.

Ich möchte meinem Doktorvater, Herrn Professor Dr.-Ing. Wolfgang Marquardt, für die Betreuung und Förderung während dieser Zeit herzlich danken. Seine fachliche Kompetenz und seine Offenheit gegenüber neuen Forschungsansätzen haben die Basis für diese Dissertation gelegt. Für sein Vertrauen in meine Arbeit und die Möglichkeit zum eigenständigen und kreativen Arbeiten bin ich ihm sehr dankbar.

Weiterhin danke ich Herrn Prof. Dr.-Ing. Andrzej Górak von der Technischen Universität Dortmund für die Übernahme des Koreferates. Die Kooperation mit Prof. Górak im Bereich der Hybridverfahren aus Destillation und Pervaporation habe ich als sehr angenehm empfunden. Herrn Prof. Dr.-Ing. Andre Bardow möchte ich für die Übernahme des Prüfungsvorsitzes danken.

Die offene, familiäre und herzliche Atmosphäre am Lehrstuhl hat das produktive Arbeiten ungemein unterstützt und über manche Hürde hinweggeholfen. Dafür danke ich allen Mitarbeitern.

Die enge Kooperation innerhalb der Synthesegruppe hat einen großen Anteil am Gelingen dieser Arbeit. Sven Kossack, der mir vier Jahre lang gegenüber saß, möchte ich besonders für sein Engagement und seine Geduld bei meiner Einarbeitung danken. Wir haben viel gemeinsam geforscht, diskutiert, publiziert und gelacht. Er hat nicht nur einen großen Teil zum Erfolg der Dissertation beigetragen sondern auch zum Spass an der Arbeit. Andreas Harwardt möchte ich für seine zahlreichen Ideen, seine Hilfsbereitschaft und die angenehme Zusammenarbeit bei vielen Themen dieser Arbeit danken. Mirko Skiborowski, der mich bei der robusten Berechnung von Phasengleichgewichten unterstützt hat, sei ebenfalls herzlich gedankt.

Weiterhin möchte ich Akram Avami, mit der ich im Bereich der Näherungsverfahren für Reaktivdestillation zusammengearbeitet habe, und meinen Diplomarbeitern, Studienarbeitern und studentischen Hilfskräften für ihren Beitrag zu dieser Arbeit danken.

Mein größter Dank gilt meinen Eltern, die schon früh das Interesse an Wissenschaft in mir geweckt haben, und meiner Frau Friederike für ihre Unterstützung und Liebe.

Köln, im Juli 2012 *Korbinian Krämer*

Contents

Notation

A	area	[m^2]
B	bottoms stream	[mol/s]
b	binary variable	[-]
C	number of components, coefficient, cost	[-],[-],[€]
c	continuous variable	[-]
c_p	heat capacity	[J/kmol·K]
D	distillate stream, diameter, distribution coefficient	[mol/s],[m],[g/g]
E	extract stream, reaction extent	[mol/s]
F	feed stream	[mol/s]
F_G	F-factor	[$Pa^0.5$]
f_c	capital charge factor	[1/a]
H	height	[m]
H_0	height of liquid distributors	[m]
h	enthalpy	[J/mol]
ΔH_{vap}	enthalpy of vaporization	[J/kmol]
ΔH_m	enthalpy of fusion	[J/mol]
K	equilibrium constant, number of feed streams	[-]
K	crystallization effort	[-]
k	heat transfer coefficient,	[W/m^2·K]
K_{eq}	chemical equilibrium constant	[-]
L	liquid stream, length	[mol/s],[m]
M	molar weight, proportionality constant	[g/mol],[-]
m	binary decisions, collinearity factor	[-]
MF	module factor	[-]
MPF	material and pressure factor	[-]
$\dot{m}$	mass flow	[t/h]
N	number of trays	[-]
n	normal vector	[-]

N_{col}	number of column trays	[-]
N_{reac}	number of reactions	[-]
q	feed state	[-]
Q	energy	[W]
p	pressure	[bar]
P	number of pinches	[-]
R	gas constant	[J/mol·K]
R	reflux/reboil ratio, raffinate stream, residue melt stream	[-],[mol/s]
r	chemical equilibrium, heat of vaporization	[-],[J/mol]
r_f	freezing ratio	[-]
S	side stream, solvent stream, solid stream	[mol/s]
T	temperature	[K]
t	time	[s]
t_a	annual operation time	[h/a]
T_c	critical temperature	[°C]
T_m	melting temperature	[°C]
TAC	total annualized cost	[€/a]
V	vapor stream, volume	[mol/s],[m^3]
w	velocity	[m/h]
x	liquid composition	[-]
$\tilde{x}$	feed point for ZVC/MAC	[-]
y	vapor composition, binary variable	[-]
z	total composition, solid composition	[-]
z_0	reference state	[-]
α	angle	[°]
γ	activity coefficient	[-]
ϵ	load factor	[-]
λ	continuation parameter	[-]
μ	relaxation parameter	[-]
ν	stoichiometric coefficient	[-]
ν	molar volume	[m^3/mol]
ϱ	density	[kg/m^3]
τ	binary interaction parameter	[-]
φ	phase distribution	[-]

Superscripts

0	on vapor line
ig	ideal gas
L	liquid
V	vapor
∞	infinite dilution
I,II	liquid phases

Subscripts

B	bottom, reboiler, stripping section
C	cooling
c	column
cap	capital
col	column
con	condenser
cool	chilled water (5°C)
cryst	crystallization
cw	cooling water
D	distillate, condenser, rectifying section
dec	decanter
E	extract
e	eutectic trough
f	feed tray
F	feed
FP	feed pinch point
H	heating
hex	heat exchanger
i	component, counter
ic	crystallizing component
int	column internals
j	counter, component, reaction
k	feed stream, last heterogeneous tray
l	liquid

max	maximum, last
min	minimum
n	tray number
op	operating
p	pinch
R	raffinate, residue melt
r	reflux
reb	reboiler
S	side stream, solvent
s	column shell, solids
SP	relevant saddle pinch points
steam	steam
T	trays
t	tanks
tot	total

Sets

E	set of eutectic troughs
I	set of components
I_e	set of two isomers at binary eutectic points
P	set of pinch points

Kurzfassung

Hybride Trennverfahren bieten durch die Verschaltung unterschiedlicher Grundoperationen Vorteile gegenüber herkömmlichen Trennverfahren hinsichtlich der Energieeffizienz und der Überwindung von Trenngrenzen. Somit ermöglicht der Einsatz von Hybridprozessen eine entscheidende Reduzierung des energetischen und apparativen Aufwands für die Auftrennung azeotroper und engsiedender Mehrkomponentengemische.

Trotz der inhärenten Vorteile der Hybridverfahren werden diese bisher nur sehr begrenzt in der Industrie eingesetzt. Ein entscheidender Grund hierfür liegt in der fehlenden Modellierungserfahrung. Zudem wird die Komplexität des Prozessentwurfs durch die aus der Verschaltung der Grundoperationen resultierenden Vielzahl an strukturellen und operativen Freiheitsgrade deutlich erhöht. Daraus ergibt sich eine Mannigfaltigkeit an denkbaren Prozessvarianten, die im Prozessentwurf hinsichtlich Machbarkeit und wirtschaftlichem Potenzial untersucht werden müssen.

Zielsetzung dieser Arbeit ist daher die Entwicklung leistungsfähiger Modellierungswerkzeuge für den Entwurf hybrider Trennverfahren, die den Zeitaufwand und die Komplexität der Prozesssynthese reduzieren und damit entscheidend zur Akzeptanz hybrider Prozesse beitragen können. Der Prozessentwurf soll dabei systematisch und mit Hilfe von rein algorithmischen Methoden erfolgen, die eine Anwendung von Optimierungsalgorithmen erlauben. Nur auf diese Weise kann ein effizienter Entwurf optimaler Hybridprozesse für nicht-ideale Gemische mit beliebiger Komponentenzahl erzielt werden.

Die Entwicklung der Entwurfsmethoden in dieser Arbeit basiert auf der Systematik eines in Vorgängerarbeiten entwickelten Syntheserahmenwerks, das aber bisher nur für rein destillative Trennprozesse angewandt werden konnte. Dieses Rahmenwerk begegnet der Komplexität des Prozessentwurfs durch eine mehrstufige Vorgehensweise mit schrittweise erhöhtem Detaillierungsgrad der Modellformulierungen. Dabei wird die Dimensionalität der Enwurfsprobleme durch die sukzessive Elim-

inierung von Lösungsvarianten reduziert. Im ersten Schritt, der Variantengenerierung, werden Prozessvarianten für das zu trennende Gemisch generiert. Diese Fließbildvarianten werden im zweiten Schritt mit robusten und effizienten Näherungsverfahren hinsichtlich Machbarkeit und Energiebedarf evaluiert. Im dritten Schritt wird dann eine Auswahl erfolgversprechender Varianten mit rigorosen Modellen hinsichtlich der Gesamtkosten optimiert, um schließlich die beste Trennsequenz am optimalen Betriebspunkt zu erhalten.

In der vorliegenden Arbeit wird dieses Syntheserahmenwerk erweitert, so dass die Entwurfsmethodik auch für Hybridprozesse angewandt werden kann, in denen Destillation mit Dekantierung, Extraktion, Kristallisation oder Reaktion kombiniert wird. Zu diesem Zweck wurden leistungsfähige Näherungsverfahren für die Evaluierung von Heteroazeotropdestillation, Extraktion, Kristallisation und Reaktivdestillation entwickelt. Weil diese Näherungsverfahren rein algorithmisch sind, kann die Evaluierung von Prozessfließbildern in eine Optimierungsaufgabe überführt werden, die einen effektiven Vergleich alternativer Varianten am optimalen Betriebspunkt erlaubt. Dank der numerischen Effizienz der Nährungsverfahren beträgt die Rechenzeit für die Minimierung des Energiebedarfs von Trennprozessen mit mehreren Apparaten und Rückführungen nur wenige Sekunden.

Eine zentrale Aufgabe der vorliegenden Arbeit war zudem die Formulierung von gemischt-ganzzahligen Optimierungsproblemen basierend auf rigorosen Stufenmodellen für alle betrachteten Trennoperationen. Anhand dieser Modelle können im dritten Schritt des Rahmenwerks Informationen über die optimalen Apparatekonfigurationen und die minimalen Betriebs- und Investitionskosten gewonnen werden. Die Lösungseigenschaften dieser komplexen Optimierungsprobleme konnten durch die Initialisierung mit den Ergebnissen der näherungsweisen Evaluierung und die kontinuierliche Reformulierung des gemischt-ganzzahligen Problems entscheidend verbessert werden.

Der Entwurf hybrider Trennprozesse anhand des entwickelten Syntheserahmenwerks wird an zahlreichen, zum Teil großtechnischen Fallbeispielen demonstriert. Dabei werden Gemische mit mehr als drei Komponenten und Probleme aus der industriellen Praxis betrachtet. Es wird gezeigt, das der optimierungsbasierte Entwurf im vorgestellten Rahmenwerk zu energieeffizienteren und kostengünstigeren Prozessen im Vergleich zu konventionellen Lösungen führen kann.

Chapter 1

Introduction

The widely predicted shortage of natural carbon resources will not only affect the availability of fuels for transportation but also the availability of raw materials for the production of basic chemicals. Alternative fossil fuels like natural gas and coal as well as renewable resources, i.e. biomass, are being evaluated as carbon source for the existing chemical value-adding chains. The expected propagation of bio-based processes will induce a shift from known production routes to novel routes based on water-rich feedstock, from gas-phase to liquid-phase reactions, from hot to cold downstream processes, from low- to high-viscous media, and from conventional to novel solvents (Marquardt, Harwardt, Hechinger, Kraemer, Viell and Voll, 2010). Ultimately, the design of new sustainable processes based on these new carbon sources will be necessary, even for basic chemicals with mature production routes. As a consequence, an increased interest in methods and tools for robust and efficient process synthesis is expected as well.

Distillation, which is still the major separation technique in chemical engineering, will remain essential in many separation processes for the purification of reaction products. Unlike other techniques like membrane separation or chromatography, batch and continuous distillation are very mature technologies and provide high separation volumes and purities. Additional advantages of distillation are the low capital investment, the operational flexibility, and the low operational risk. However, distillation columns are very energy-intensive unit operations, which consume about 95% of the total separation energy used in the refining and chemical processing industries, or about 20% of the U.S. manufacturing energy use (Eldridge, Seibert, Robinson and Rogers, 2005).

Many distillation processes can be made more energy-efficient by the application

of heat integration. Possibilities include heat exchange between process reboilers and condensers (cf. Section 3.4.2), vapor recompression, and internally heat-integrated columns (cf. Section 3.5.3). Yet, when distillation boundaries or low relative volatilities complicate distillation, it is desirable to substitute distillation with unit operations operating at low temperature levels like extraction, crystallization, adsorption, or membrane separation, if possible. These "cold separation techniques" are particularly advantageous for the separation of products from highly diluted reactor effluents such as fermentation broths. Still, distillation remains essential in many applications due to the limitation of these alternatives by separation boundaries, the lack of suitable solvents and equipment, or the requirement of high purities and volumes. Hence, the most effective way to save energy is often to augment distillation with alternative separation technologies in a hybrid separation process. In general, hybrid separation processes are characterized by the combination of two or more different unit operations, which contribute to the same separation task by different physical separation principles. Thus, separation boundaries or inefficiencies of a single separation mechanism can be overcome. If applied correctly, hybrid processes offer significant cost savings and allow the cost-efficient (bio)chemical synthesis of new products.

Examples for the successful implementation of hybrid processes can be found in the work of Franke (2006). He reviews processes, where distillation is combined with decantation, absorption, adsorption, extraction, crystallization, and membrane separation, as well as hybrid processes which do not rely on distillation. In their report on research opportunities for energy reduction, Eldridge et al. (2005) identify the highest potential for hybrid processes which combine distillation with adsorption, extraction, or membrane separation. Fewer opportunities with significant energy-savings potential were identified for absorption and crystallization.

Despite of the inherent advantages of hybrid separation processes, they are not systematically exploited in industrial applications (Eldridge et al., 2005). A major reason is rooted in the complexity of the synthesis of these highly integrated processes. The combination of unit operations leads to a multitude of structural and operative degrees of freedom, i.e. a multitude of alternative process variants and possibly entrainer candidates, which have to be evaluated in order to identify feasible and cost-effective variants. Considering that the operating points of structurally different process variants have to be optimized for a meaningful comparison, it is clear that the design procedure can be very complex and time consuming.

In addition, there is a lack of modeling experience for many unit operations apart from distillation, which results in an uncertainty towards the design of these unit operations. Hence, there is a need for powerful modeling and design methodologies

to reflect the non-ideal and coupled phenomena of hybrid processes. Likewise, in their report to the U.S. department of energy, Eldridge et al. (2005) state that the development of design methodologies for hybrid processes are priority R&D needs to overcome their economic barriers and gain market acceptance.

1.1 Structure of this thesis

In the light of the above mentioned barriers, it is the scope of this thesis to provide methodologies which facilitate an efficient and reliable conceptual design of hybrid separation processes. First, methods for the conceptual design of hybrid separation processes are reviewed in Section 2. These are grouped into heuristics, thermodynamic analysis, shortcut evaluation methods, rigorous optimization, and structural flowsheet optimization.

Subsequently, Section 2.6 presents the process synthesis framework proposed by Marquardt, Kossack and Kraemer (2008), which combines shortcut evaluation and rigorous optimization steps for a systematic design of separation processes. This process synthesis framework has so far been applied predominantly to distillation processes (Kossack, Kraemer, Gani and Marquardt, 2008; Kraemer, Kossack and Marquardt, 2009; Kossack, 2010). In this thesis, the extension of the framework to the optimization-based design of hybrid separation processes will be developed.

Yet before the extension to hybrid processes is addressed, Chapter 3 illustrates the consistent application of the framework to the design of large-scale distillation processes. Since distillation is still the backbone of many hybrid processes, powerful shortcut evaluation and rigorous optimization methods for distillation are essential for the subsequent extension to hybrid processes. Progress concerning the rigorous optimization of distillation processes is made mainly through the continuous reformulation and stepwise initialization of discrete-continuous optimization problems.

Chapters 4 to 6 then introduce the extension of the synthesis framework to the design of hybrid separation processes, where distillation is coupled with decantation, extraction, and crystallization, respectively. Here, fully algorithmic shortcut and rigorous models are developed for the evaluation of the hybrid systems. In order to demonstrate the effectiveness of the design methods, large-scale industrial case studies involving multicomponent mixtures are presented in each chapter.

Subsequently, Chapter 7 gives a brief outlook on the extension of the developed methods to reactive distillation systems. Chapter 8 concludes this thesis and identifies topics for further research.

Chapter 2

Conceptual design of hybrid separation processes

The cost of a chemical process is mainly determined by the first development step, the conceptual process design. This step is therefore of extraordinary importance and should be executed carefully. According to Kossack (2010), conceptual design needs to address three central issues:

- support the invention of conceptual design alternatives,
- assess the feasibility of these conceptual design alternatives, and
- evaluate the alternatives to determine the best of the feasible design alternatives.

General reviews of different tools and design methodologies to answer these questions are given in the works by Barnicki and Siirola (2004), Li and Kraslawski (2004), and Westerberg (2004) and in the theses of Brüggemann (2005) and Kossack (2010). For the design of distillation processes, particularly the latter two works give comprehensive synopses of synthesis methods. The following subsections review the literature on design methodologies proposed for the synthesis of hybrid processes.

2.1 Flowsheet generation by heuristics

In industrial practice, a flowsheet is often pragmatically fixed first using heuristics from literature, solutions of similar problems, experience and intuition. The most prominent representative of heuristic methods is the hierarchical design strategy proposed by Douglas (1985, 1988, 1995), which helps to systematize the design procedure. Expert systems like Jacaranda (Fraga, Steffens, Bogle and Hind, 2000), Prosyn (Kra-

vanja and Grossmann, 1993), or TEAGPERT (Schembecker and Simmrock, 1997) aim at automating this design step.

The synthesis of hybrid separation processes comprising different separation techniques is significantly more complex than the synthesis of pure distillation processes. Here, the use of heuristics can contribute significantly towards the identification of promising flowsheet alternatives. In their well-cited works, Barnicki and Fair (1990, 1992) have developed a knowledge-based, structured expert system for the selection and sequencing of unit operations for multicomponent separation. Their task-oriented approach reduces the magnitude of the overall separation synthesis problem by decomposing the complex design problem into subtasks, for which design guidelines are given. Wahnschafft, Le Rudulier and Westerberg (1993) suggested a problem decomposition approach, which also relies on the identification of subtasks and attainable product regions. In addition, the strategic use of recycles is studied in their work. In the work by Siirola (1996), the hierarchical approach to process synthesis is further elaborated and combined with a means-end analysis, which is an operator-based state transformation paradigm used in automated goal-orientated problem solving. Later, Pajula, Seuranen, Koiranen and Hurme (2001) presented a process synthesis methodology which uses case-based reasoning to benefit from the systematic storing and reuse of accumulated knowledge. In their work, the phases of reasoning for a separation system include the search for creative new solutions by using analogies, the use of negative cases to exclude some solutions, and the adaptation of cases corresponding to the separation problem. Harmsen (2004) has gathered the best practices of conceptual process design applied in the chemical process industry in the last 15 years. He particularly reviews heuristic-based methods for the selection of unit operations and recycle structures and the integration of units to multi-functional equipment. Concerning solids processes, a hierarchical procedure for the conceptual design has been presented by Rajagopal, Ng and Douglas (1992). These authors introduce rules for the selection of unit operations and equipment configurations. Guidelines for the determination of design variables and economic trade-offs are also given.

2.2 Flowsheet generation by thermodynamic analysis

The use of heuristics alone may lead to suboptimal flowsheets and cannot substitute the information gained by thermodynamic insight of the mixture topology. In Section 3.4.1, an example will be presented, where the application of heuristics suggested by Thong and Jobson (2001) does not lead to the best flowsheet structure. Typically, the generation of flowsheets is therefore accompanied by some kind of thermodynamic

analysis to gain information about the feasibility of the unit operations and the flowsheet structure. In case of distillation processes, such an analysis usually involves the graphical inspection of residue curves and distillation boundaries. For extraction, the shape of the miscibility gap and the location of tie-lines are studied, while the location of eutectic troughs is inspected for crystallization.

Jaksland, Gani and Lien (1995) and Gani and Constantinou (1996) suggested a method for the synthesis of hybrid separation processes by means of a systematic analysis of the relationships between physicochemical properties and the conditions at which the separation techniques become feasible. The selection of unit operations for certain separation tasks is then based on the thermodynamic insight gained by this analysis. Subsequently, Steffens, Fraga and Bogle (1999) proposed a methodology for flowsheet generation of hybrid processes by means of a discretization of the design space. The methodology, which was implemented in Jacaranda (Fraga et al., 2000), minimizes both the environmental impact and the process costs by multicriteria optimization. The feasibility of the unit operations is assessed by feasibility indices taken from Jaksland et al. (1995). Later, Bek-Pedersen, Gani and Levaux (2000) analyzed the separation driving forces of possible unit operations for the synthesis of energy-efficient hybrid separation schemes. Based on the information of phase composition data only, the method enables the visual determination of optimal separation sequences. The work of Pressly and Ng (1999) on the other hand focuses on the consideration of separation boundaries in process synthesis. In conjunction with the available separation task selection methods, a step-by-step procedure is proposed in order to generate complete flowsheet alternatives, which allow bypassing both thermodynamic and equipment boundaries to achieve a given separations objective.

The generation of flowsheets by heuristics and thermodynamic analysis must be combined with a quantitative evaluation such that the feasibility and the economic fitness of the flowsheet alternatives can be assessed. In industrial practice, this is usually accomplished by repetitive simulation studies, where each flowsheet variant is evaluated individually. These simulation studies are very time consuming and tedious, therefore only a small number of possible flowsheets can be studied. Moreover, a meaningful ranking of flowsheets can only be accomplished when the variants are compared at the respective optimal operating points. Commercial sequential-modular process simulators, however, cannot perform these optimization tasks fully algorithmically, such that tedious manual optimization of operating points is required. Hence, the design of the most cost-effective flowsheet within commercial process simulators cannot be guaranteed.

2.3 Shortcut methods

Compared to simulation studies, shortcut methods provide a more efficient way to assess the feasibility and cost of flowsheet variants. These methods allow an approximate but computationally efficient evaluation of the process economics without the need for a detailed specification of the units. Paired with representations for separation boundaries like the pinch distillation boundary, the inspection of feasibility and the optimization of operating points are also possible. Reviews of the literature on shortcut methods for the evaluation of the unit operations distillation, extraction, crystallization, and reactive distillation will be included in Chapters 3 - 7, respectively. Novel powerful shortcut methods for these unit operations will also be proposed in these chapters. In the following, literature on the shortcut evaluation of hybrid processes is referenced. It needs to be noted that the vast majority of the published works on the synthesis of hybrid processes, however, concentrate on flowsheet generation by means of heuristics, case-based reasoning or superstructure optimization (Section 2.5).

A few authors (e.g. Pham, Ryan and Doherty (1989); Ryan and Doherty (1989); Wasylkiewicz, Kobylka and Castillo (2003)) have published shortcut methods for the design and evaluation of distillation coupled with decantation (heteroazeotropic distillation). These works, which are reviewed in detail in Chapter 4, typically resort to models for two-phase distillation and consider three phases only in the decanter. Bausa (2001) and Urdaneta, Bausa, Brüggemann and Marquardt (2002) have proposed shortcut methods for the evaluation of heteroazeotropic distillation, which rely on an accurate identification of vapor-liquid-liquid equilibrium on column trays.

Concerning the combination of distillation with membrane separation, first studies for the shortcut-based design were presented by Moganti, Noble and Koval (1994), Stephan, Noble and Koval (1995), and Pettersen and Lien (1995). These authors analyzed the optimal membrane operating points for a minimization of the number of distillation trays. In order to reduce complexity, only binary separations have been considered and the membrane units and distillation columns were optimized separately. Pressly and Ng (1998) developed a screening method to determine the break-even costs of distillation-membrane separation processes but also consider only binary mixtures. Bausa and Marquardt (2000b) studied the evaluation of hybrid distillation-membrane separation processes by means of algorithmic shortcut methods. Here, the minimum energy demands of the distillation tasks are determined by the rectification body method (cf. Section 3.1.2.3). The economic potential of membrane cascades is described by the minimum membrane area, which is calculated under the assumption of an infinite number of membrane modules and constant maximum

temperature. Recently, Caballero, Grossmann, Keyvani and Lenz (2009) developed a shortcut model for the evaluation of the energy savings potential of distillation columns combined with vapor membrane systems. They use Underwood's method (Underwood, 1948) as distillation shortcut and either a simple black-box model or an ideal perfect cross-flow model for the membrane system. Ayotte-Sauve, Sorin and Rheault (2010) present a similar approach, where shortcut models based on the notion of power of separation are used. Only binary separations are considered.

The energy-efficient design of hybrid extraction-distillation separation processes has been studied by Lucia, Amale and Taylor (2006). They model the distillation tasks using their concept of shortest separation lines (cf. Section 3.1.3). A simple extraction shortcut is applied, since only ternary mixtures are to be separated in the considered examples. Wallert (2008) extended the shortcut-based evaluation of hybrid extraction-distillation processes to quaternary mixtures (cf. Section 5.1.2). The extraction shortcut proposed in her work requires an analysis of feasibility by graphical inspection of the separation topology. In Section 5.1.3, a fully algorithmic shortcut model for extraction will be proposed, which allows an optimization-based evaluation of extraction-distillation hybrid processes.

Franke (2006), Wallert (2008), and Franke, Nowotny, Ndocko, Gorak and Strube (2008) studied the shortcut-based evaluation of hybrid crystallization-distillation processes for the separation of close-boiling isomers. Due to the computational efficiency of their methodology, a manifold of flowsheet variants was ranked based on energy-efficiency. In Chapter 6, their works will be discussed in more detail and a refinement of the design methodology will be proposed. Franke (2006) has also studied the design of hybrid processes comprising crystallization and dissociation extraction units with the help of shortcut models.

2.4 Rigorous optimization

Shortcut methods rely on various simplifying assumptions and cannot provide information about tray numbers or the optimal dimensions of the unit operations. This information, however, can be gained by a rigorous optimization of units or processes.

These rigorous optimization problems are usually of discrete-continuous nature due to the cascade-like structure of many unit operations like distillation, extraction, crystallization, and membrane separation. The solution of these problems is therefore challenging, even when the flowsheet structure of the process is fixed. The convergence properties can be improved by a favorable initialization with shortcut methods.

In Chapter 2.6, a process synthesis framework exploiting this property by means of successive shortcut and rigorous evaluation steps will be described in detail. The following paragraphs give an overview on the literature covering rigorous optimization of hybrid processes.

Szitkai, Lelkes, Rev and Fonyo (2002), Barakat and Sørensen (2008) and Skiborowski, Mhamdi, Kraemer and Marquardt (2012) studied the rigorous optimization of hybrid processes where distillation is coupled with pervaporation or permeation to separate binary mixtures or desalinate water. While Szitkai et al. and Skiborowski et al. optimize the membrane cascades by means of mixed-integer nonlinear programming (MINLP) techniques, Barakat and Sørensen apply genetic optimization algorithms. Buchaly, Kreis and Górak (2007) also use genetic algorithms for the rigorous optimization of the operating point of a reactive distillation column coupled with vapor permeation modules.

Farkas, Rev and Lelkes (2005) proposed binarily minimal MINLP representations for rigorous process optimization problems by reducing the binary multiplicity and redundancy of the optimization superstructures. Their approach allows the efficient structural optimization of a hybrid distillation-pervaporation process for ethanol dehydration.

Franke (2006) addressed the rigorous optimization of hybrid processes combining crystallization with distillation and dissociation extraction units for the efficient separation of close-boiling isomers (see also Chapter 6). A modified generalized Benders decomposition algorithm was developed to enhance the solution properties of the complex MINLP problems for the optimization of feed locations and stage numbers.

Caballero, Odjo and Grossmann (2007) presented the rigorous MINLP optimization of flowsheets using modular process simulators and discontinuous cost and sizing equations. The implicit equations of the process simulator are connected to the explicit constraints for the MINLP optimization via an input-output black box structure. The approach benefits from the availability of thermodynamic data and a wide range of process models through the use of commercial process simulators. On the other hand, the use of these modular simulators significantly increases the computational time required for the solution of the optimization problems. While the examples given in the work by Caballero et al. (2007) are confined to distillation processes, Caballero et al. (2009) extend the method to the rigorous optimization of hybrid processes where distillation is coupled with vapor permeation to separate binary ethylene-ethane mixtures.

2.5 Structural flowsheet optimization

The optimal flowsheet for a separation task can theoretically be obtained and evaluated by the optimization of a general and large superstructure comprising all flowsheet alternatives (Duran and Grossmann, 1986). Thus, the variant generation is reduced to the selection of a suitable flowsheet superstructure. The separation units are modeled by shortcut or rigorous models connected by possible flowsheet streams. The resulting large-scale nonlinear optimization problems are discrete-continuous by nature and are usually solved with mixed-integer nonlinear programming (MINLP) techniques. Large and complex superstructures have to be defined and solved if all possible flowsheet alternatives are to be considered. Given this complexity, it becomes clear that these optimization problems are computationally expensive and that the quality of the final solution strongly depends on the specified initial values.

Several examples of structural flowsheet optimization can be found in literature, most notably the works of Grossmann and his co-workers. Kocis and Grossmann (1989) and Kravanja and Grossmann (1990) proposed MINLP formulations for process synthesis, where the optimization models are given in equation form and modeling/decomposition strategies are applied to reduce the size of the subproblems. Subsequently, Diwekar, Grossmann and Rubin (1992) and Kravanja and Grossmann (1996) suggested implementations of MINLP topology optimization in process simulators. Here, the units are described by implicit models.

For hybrid processes, an early example of structural flowsheet optimization was presented by Glanz and Stichlmair (1995). In their work, superstructures for extraction-distillation processes are generated and simplified by the application of heuristics. Since rigorous process models are used, only small superstructures can be solved.

Similarly, Hostrup, Harper and Gani (1999) suggest a method which integrates mathematical modeling with heuristic approaches in order to tackle the increased complexity of superstructure optimization for hybrid separation flowsheets. The main feature of the proposed method is that it applies a mathematical solution approach but simplifies the resulting mathematical problem through thermodynamic insights. The authors illustrate their approach by the synthesis of extraction-distillation processes for the removal of environmental harmful chemicals from process or wastewater streams.

Diaz, Gros and Brignole (2000) study the structural optimization of hybrid processes comprising high-pressure extraction and dehydration columns. Their modeling approach relies on the use of a sequential process simulator and a black box strategy

for the solution of the unit models. Key separation properties are predicted by a group contribution method with association equations of state. The considered examples give rise to only few structural decisions, but the resulting superstructures are solved robustly.

Liu, Fan, Seib, Friedler and Bertok (2004) identify optimal hybrid separation flowsheets for bio-based downstream processes by structural flowsheet optimization based on graph-theoretical methods. First, a process-graph (P-graph, cf. Friedler, Tarján, Huang and Fan (1992)) representation of the flowsheet superstructure is generated. The superstructure with minimum complexity is then identified by the application of maximal structure generation (MSG) algorithms and optimal or near optimal flowsheets are ranked by means of branch-and-bound methods. It is important to note that Liu et al. (2004) evaluate the cost and feasibility of the single separation tasks a-priori by heuristics or commercial process simulators. While this approach allows a very efficient optimization of the flowsheet superstructure, separation boundaries and recycles cannot be considered in the optimization.

2.6 A framework for systematic process synthesis

In Sections 2.1-2.5 different approaches to the conceptual design of hybrid processes have been reviewed. These have been grouped into heuristics, thermodynamic analysis, shortcut methods, rigorous optimization, and structural flowsheet optimization. While it has been shown that the reviewed works offer promising progress for the model-based design of hybrid processes, various limitations of the different approaches have also been pointed out.

In order to provide methodologies for the robust and efficient design of large-scale separation processes, Marquardt et al. (2008) have proposed a systematic synthesis framework which combines shortcut and rigorous optimization steps (cf. Fig. 2.1). Thus, the shortcomings of each individual design tool as outlined in Sections 2.3 and 2.4 can be minimized while the strengths can be ideally exploited. A similar approach has been used by Caballero et al. (2009) for the design of hybrid distillation-vapor membrane separation systems.

The steps of the design framework are performed at different levels of model refinement. The level of model refinement of each step is adapted to the specific design task in order to meet the model requirements and facilitate an efficient design procedure. This combination of synthesis methods with increasing level of detail allows the efficient evaluation of separation processes for multicomponent mixtures on the

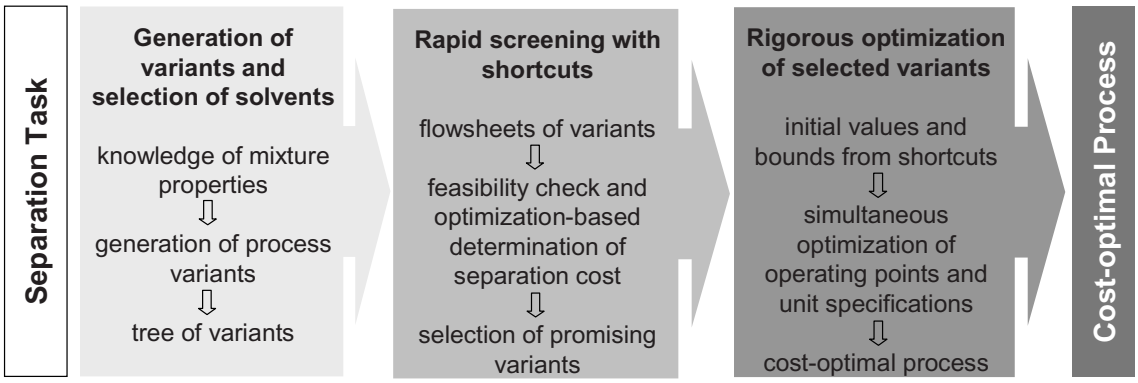

Figure 2.1: Process synthesis framework for the systematic optimization-based design of separation processes.

basis of rigorous thermodynamics. Thus, the optimal distillation flowsheet, the optimal process operating point and the optimal unit specifications (number of trays and diameters, location of feeds, heat exchanger duties) can be determined reliably. In the following, the individual steps are described in the order of the framework. As noted by Kossack (2010), however, the framework does not prescribe a linear workflow. Iterations, especially between the generation of alternatives and the shortcut evaluations, are expected, since the shortcut methods usually allow the design engineer to get a better understanding of the thermodynamic behavior of the process.

In the first step of the proposed framework, possible flowsheet alternatives for the desired separation task are generated and, if needed, suitable entrainers are identified. The generation of flowsheets can be automated for zeotropic multicomponent distillation with simple columns as presented by Harwardt, Kossack and Marquardt (2008). However, for azeotropic or close-boiling mixtures, flowsheet alternatives are created manually, typically in experts brainstorming sessions. The hierarchical concepts based on heuristics and thermodynamical insight outlined in Sections 2.1 and 2.2 are applied and a study of the mixture topology is performed. Distillation feasibility can be analyzed by the calculation of the pinch distillation boundaries (Brüggemann and Marquardt, 2011a). In addition, superstructure optimization (cf. Section 2.5) with shortcut models can be applied to reduce the number of flowsheet variants. However, to date its applicability for large-scale processes and non-ideal mixtures still remains limited.

Considering the large number of separation mechanisms and the even larger number of possible entrainer candidates for the separation of azeotropic mixtures, it is clear that not all envisioned alternatives generated in the first step can be covered with

simulation studies. The framework therefore relies on shortcut tools to determine a few economically attractive flowsheet designs.

In the second step of the framework, the flowsheet variants and possible entrainer candidates are therefore screened with respect to feasibility and minimum energy demand by means of shortcut methods. The application of these methods allows for a robust and efficient evaluation of a high number of alternatives. In literature, the evaluation of distillation flowsheets by shortcut methods is usually accomplished by Underwood's method (Underwood, 1948) or the boundary value method (Levy, Van Dongen and Doherty, 1985), which are confined to different limitations like binary mixtures, ideal thermodynamics or graphical feasibility checks. In the works by Kossack et al. (2008), Kraemer, Harwardt and Marquardt (2009a), and Kraemer, Kossack and Marquardt (2009), the screening of flowsheet variants is performed with the rectification body method (RBM, cf. Bausa, von Watzdorf and Marquardt (1998)), a reliable and efficient shortcut method for the evaluation of azeotropic multicomponent distillation based on rigorous thermodynamics (cf. Section 3.1.2.3). The RBM is algorithmically accessible and therefore allows an optimization of process operating points. The feasibility can be guaranteed by an algebraic feasibility test based on the calculation of pinch distillation boundaries. As a consequence, azeotropic multicomponent mixtures and processes with multiple columns and recycles can be evaluated. The only specifications needed to inspect feasibility and optimize the minimum energy demand in this step are column pressures and product purities.

In the third step, a selection of the most promising flowsheet variants is then rigorously optimized with an economic objective function containing capital and operating costs. It should be noted that a large number of flowsheet alternatives can typically be discarded after the shortcut step, such that only few alternatives remain for rigorous optimization in this last step. The aim is to determine the process and unit specifications which yield the lowest total annualized costs. This involves the simultaneous optimization of recycle and intermediate streams, energy duties, column diameters, heat exchanger areas, as well as column tray numbers and feed tray locations. Since the latter two variables are discrete, a mixed-integer nonlinear optimization problem (MINLP) has to be solved. Considering the large scale and complexity of multi-unit processes and the nonlinearity of the underlying non-ideal thermodynamics, it is obvious that these MINLP problems are particularly hard to solve.

The design within the synthesis framework, however, offers excellent opportunities for an efficient initialization and a tight bounding of the rigorous optimization variables by the results of the preceding shortcut evaluation. Thus, the solution properties of the MINLP problems can be improved significantly (Kossack, Kraemer and Mar-

quardt (2006); Kraemer, Kossack and Marquardt (2009), see also Section 3.3.3). The handover of the shortcut results can be automated, such that no manual intervention is necessary once the shortcut calculations are completed. In addition, the MINLP problems in the work of Kossack et al. and Kraemer et al. are reformulated as purely continuous NLP problems to further speed up the solution procedure (cf. Section 3.3.2). Integer solutions for the continuous reformulation are achieved by the introduction of special nonlinear constraints which force the continuous decision variables to integer values.

To summarize, the process synthesis framework as a procedure of incremental refinement and successive initialization allows for a rapid synthesis of the cost optimal process while taking into account multiple flowsheet alternatives. Although the economic optimization is confined to local optimization, the favorable initialization and bounding of variables within the stepwise procedure results in very good locally optimal solutions. In future work, the framework can be extended by a fourth evaluation step offering further model refinement, e.g. by rate-based models, as suggested by Noeres, Kenig and Gorak (2003). It remains highly problem specific, however, whether the equilibrium-based evaluation suffices (e.g. for simple distillation) or a refinement offers additional valuable information (e.g. for rate-controlled unit operations such as reactive distillation).

The process synthesis framework has so far been predominantly applied to distillation processes (Kossack et al., 2008; Kraemer, Kossack and Marquardt, 2009; Kossack, 2010). In the following chapters, the extension of the framework to the systematic design of hybrid processes will be developed. This involves both the advancement of the design methodology of the framework and the development of novel shortcut and rigorous models for the considered unit operations.

It needs to be emphasized that it is the proposition of this thesis to offer methodologies which meet two critical requirements. First, novel methods need to be suitable for optimization-based process design such that the ranking of process variants can be based on optimal process parameters in each evaluation step. This approach reduces the design effort and warrants a meaningful comparison of process alternatives at their respective optimal operating points. A manual optimization by repetitive simulation studies is clearly too tedious when a manifold of process alternatives needs to be compared. While today's commercial process simulators like Aspen Plus offer limited optimization possibilities, it is the purpose of this thesis to provide methodologies for a consistent optimization-based process synthesis.

Second, the design methods will be tested and verified by means of large-scale,

industrial case studies. Hence, the shortcut and rigorous evaluation steps need to handle the challenges of multicomponent mixtures, multiple units, recycles, and rigorous thermodynamics.

Both requirements imply the need for fully algorithmic evaluation methods for all unit operations considered in this thesis. In addition, these methods need to be sufficiently robust and efficient to allow their application to large-scale problems. Furthermore, all models must be implemented using an optimization platform such as GAMS (Brooke, Kendrick, Meeraus and Raman, 2005), which offers powerful optimization solvers.

This thesis is partly based on work which results from close collaborations with colleagues at the Aachener Verfahrenstechnik as documented by a number of joint publications. The initialization of the rigorous optimization of distillation columns was developed together with Sven Kossack. While the PhD thesis of Sven Kossack focuses on the rigorous optimization of single distillation columns and the conceptual design of extractive and reactive distillation processes, this thesis focuses on the optimization-based design of multicolumn and hybrid separation processes. The automatic generation of (heat-integrated) distillation processes was integrated into the synthesis framework in close collaboration with Andreas Harwardt. A more detailed perspective on this approach to flowsheet generation is given in the original works by Andreas Harwardt which are referenced in this thesis. Furthermore, the design of heteroazeotropic distillation and liquid-liquid extraction was facilitated by a powerful phase split test, which was implemented by Mirko Skiborowski. The extension of the shortcut methods to reactive distillation was developed in close collaboration with Akram Avami.

Chapter 3

Optimization-based synthesis of distillation processes

Distillation columns are the backbone of many hybrid separation processes. This chapter therefore presents the optimization-based synthesis of distillation processes for homogeneous azeotropic mixtures by means of the framework described in Chapter 2.6. The main section of the chapter covers the development of novel methodologies for the robust and efficient rigorous optimization of distillation processes. These methods will be carried over to heteroazeotropic distillation, extraction columns, crystallization cascades, and reactive distillation in subsequent chapters. Hence, this chapter lays the groundwork for the extension of the process synthesis framework to the conceptual design of processes, where distillation columns are coupled with additional unit operations.

The work presented in this chapter is based on earlier publications by Kraemer, Kossack and Marquardt (2009) and Kraemer, Harwardt and Marquardt (2009a). In Section 3.1, recent shortcut methods for the evaluation of non-ideal distillation are briefly reviewed. Section 3.2 illustrates the calculation of the pinch distillation boundaries for an algorithmic check of split feasibility within the shortcut evaluation step. Next, the literature on rigorous optimization of distillation processes is reviewed in Section 3.3. Unfortunately, the solution of these large-scale discrete-continuous optimization problems usually suffers from a lack of robustness, long computational times and a low reliability towards good local optima. In Section 3.3.1, a novel approach to the rigorous optimization of complex distillation processes is proposed, which allows the solution of these large-scale optimization problems with outstanding robustness, reliability and efficiency through progress on two levels: First, the integration in the

process synthesis framework allows a reduction of the complexity of the optimization superstructure and provides an excellent initialization by shortcut evaluation with the rectification body method. Second, the reformulation as a purely continuous optimization problem enables a solution with reliable and efficient NLP solvers. A careful initialization phase and a stepwise solution procedure with gradually tightened bounds to enforce integer solutions facilitate a robust and efficient solution.

The conceptual process design by the methodology of the synthesis framework is illustrated by a case study of large scale in Section 3.4, which considers the flowsheet synthesis as well as the rigorous optimization of a curved boundary process for the complete separation of an azeotropic quaternary mixture. It will be shown that the most energy-efficient flowsheet is identified by means of an optimization-based shortcut evaluation of flowsheet alternatives. The subsequent discrete-continuous rigorous optimization is initialized by the results of the shortcut evaluation and reformulated as a continuous problem. We will observe that the reformulated tray optimization problem can be solved significantly faster than the corresponding MINLP problem.

Further case studies involving the optimization of complex column setups, internally heat-integrated columns and extractive distillation processes will be briefly reviewed in Sections 3.4.4 and 3.5.

3.1 Shortcut methods for non-ideal distillation

Various authors have presented shortcut methods for the quantitative evaluation of distillation processes. A start was made with graphical design methods such as the Ponchon-Savarit method or the McCabe-Thiele method for binary mixtures. Underwood (1948) proposed a well known numerical method to calculate the minimum energy demand (MED) of multicomponent distillation for ideal mixtures under the assumption of constant relative volatility and constant molar overflow throughout the column. Shortcut methods for non-ideal and azeotropic mixtures have been developed subsequently. Bausa et al. (1998) and Bausa (2001) provide a comprehensive review of shortcut methods for the prediction of the MED for multicomponent, azeotropic, homogeneous distillation. The most prominent concepts including some new developments are briefly reviewed in this section. These methods are demonstrated by the separation of a homogeneous non-ideal mixture of acetone, methanol, and ethanol. For this separation, a ternary feed is split into a bottoms product of pure ethanol and a distillate on the binary acetone-methanol edge. The activity coefficients of the liquid phase are calculated by the Wilson model.

3.1.1 Boundary value method

Levy et al. (1985) proposed the boundary value method (BVM) for an assessment of feasibility and MED in non-ideal distillation. Column tray-to-tray profiles are calculated for each column section from the respective column ends. For a given distillate composition $\mathbf{x}_D$, distillate flow rate D and condenser duty Q_D, tray-to-tray profiles for the rectifying section are computed starting at the distillate by balancing components and energy and considering chemical equilibrium on each tray (cf. Fig. 3.1):

$$0 = V_{n+1} - L_n - D, \qquad n = 1, ..., n_F, \tag{3.1}$$

$$0 = V_{n+1} y_{n+1,i} - L_n x_{n,i} - D x_{D,i}, \qquad n = 1, ..., n_F,\ i = 1, ..., C, \tag{3.2}$$

$$0 = V_{n+1} h^V_{n+1} - L_n h^L_n - D h_D + Q_D, \qquad n = 1, ..., n_F, \tag{3.3}$$

$$1 = \sum_{i=1}^{C} x_{n,i}, \qquad 1 = \sum_{i=1}^{C} y_{n,i}, \qquad n = 1, ..., n_F, \tag{3.4}$$

$$y_{n,i} = K_{n,i}(\mathbf{x}_n, T_n, p_n) x_{n,i}, \qquad n = 1, ..., N,\ i = 1, ..., C, \tag{3.5}$$

$$h^V_n = h^V(\mathbf{y}_n, T_n, p_n), \qquad n = 1, ..., N, \tag{3.6}$$

$$h^L_n = h^L(\mathbf{x}_n, T_n, p_n), \qquad n = 1, ..., N. \tag{3.7}$$

For the stripping section, Eqs. (3.1)-(3.3) are replaced by

$$0 = L_{n-1} - V_n - B, \qquad n = n_F, ..., N, \tag{3.8}$$

$$0 = L_{n-1} x_{n-1,i} - V_n y_{n,i} - B x_{B,i}, \qquad n = n_F, ..., N,\ i = 1, ..., C, \tag{3.9}$$

$$0 = L_{n-1} h^L_{n-1} - V_n h^V_n - B h_B + Q_B, \qquad n = n_F, ..., N. \tag{3.10}$$

Note that the tray-to-tray calculations are carried out recursively starting from both column ends. Separation feasibility is determined by an inspection of intersection of the column profiles. The lowest energy duty which allows an intersection of column profiles defines the MED.

For sharp splits, traces of impurities have to be specified for the pure column end product, since the profiles would not leave the subspace of the product components otherwise. The manifold of stripping section profiles for different trace components in the bottoms product of the example separation are shown in Fig. 3.1. The determination of feasibility and the search for the MED therefore require a simultaneous optimization of the energy duty and the amounts of all trace components. This procedure can be tedious, especially for mixtures with more than three components. Since the intersection of profiles needs to be checked manually, the application of the BVM is effectively limited to ternary mixtures.

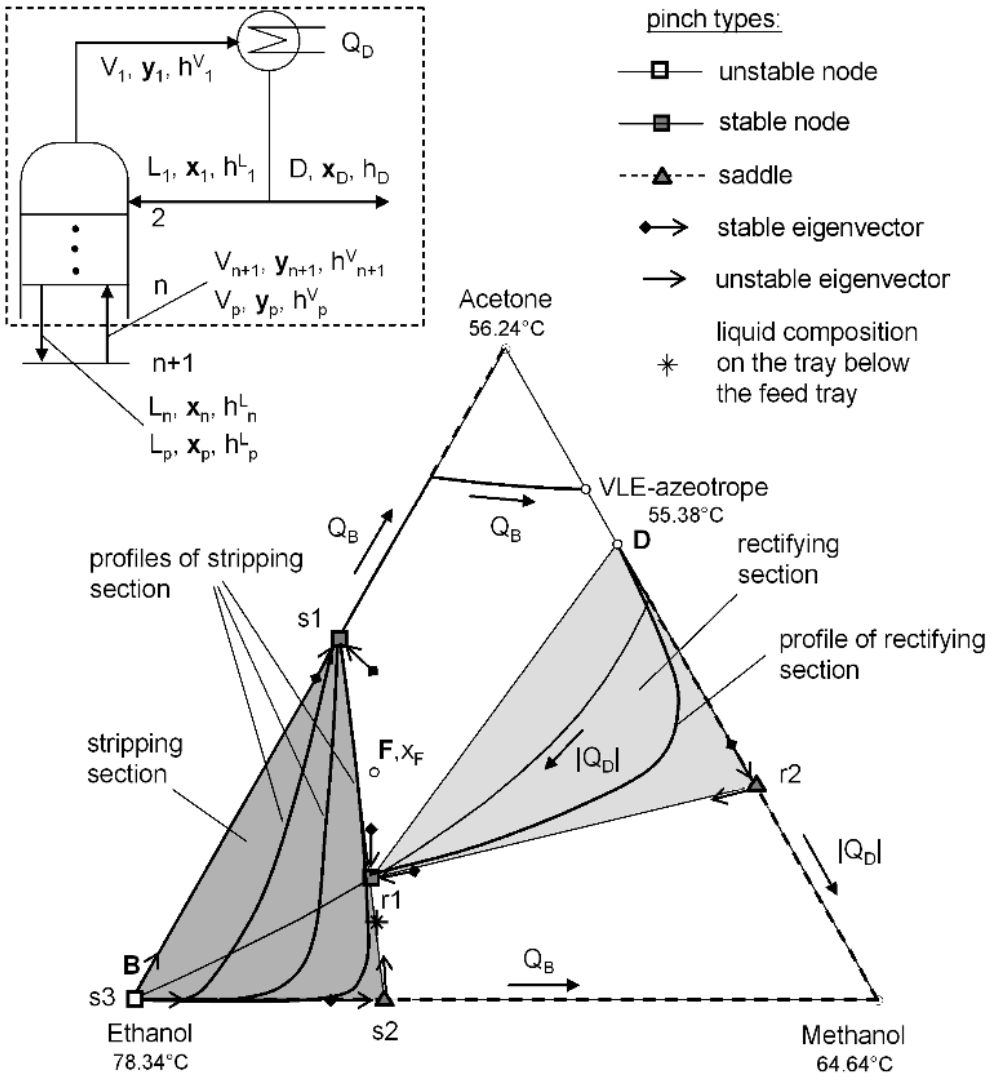

Figure 3.1: Balance envelope for the rectifying section (upper left) and composition simplex with section profiles, pinch points, rectification bodies, and liquid composition on the tray below the feed tray for the example separation of the mixture of acetone, methanol, and ethanol.

Recently, Zhang and Linninger (2004) have proposed the evaluation of distillation by a temperature collocation algorithm based on the BVM to reduce the problem size and computational effort for the calculation of column profiles. This approach reduces the problem size and the computational effort by replacing the conventional tray-to-tray calculation with a bubble point temperature distance function and orthogonal collocation on finite elements. They achieve an efficient and robust assessment of

feasibility and minimum reflux for the separation of multi-component ideal mixtures. Subsequently, they have extended their approach to homogeneous azeotropic distillation and optimal column sequencing (Zhang and Linninger, 2006).

3.1.2 Pinch-based methods

In order to overcome the dependency of the BVM results on the specification of trace components in the products, pinch-based shortcut methods have been proposed by various authors. Pinch points describe the compositions on a distillation profile where the driving force of the separation vanishes. Pinch point curves can be calculated for a given product for each column section as the branches of the fixed-points of the tray-to-tray equations if the reboiler (or condenser) duty is varied. More specifically, the pinch equation system, derived for a balance envelope around the rectifying section (cf. Fig. 3.1),

$$0 = V_p - L_p - D, \qquad p \in P_D, \tag{3.11}$$
$$0 = V_p y_{p,i} - L_p x_{p,i} - D x_{D,i}, \qquad p \in P_D,\ i = 1, ..., C, \tag{3.12}$$
$$0 = V_p h_p^V - L_p h_p^L - D h_D + Q_D, \qquad p \in P_D, \tag{3.13}$$
$$1 = \sum_{i=1}^{C} x_{p,i}, \qquad 1 = \sum_{i=1}^{C} y_{p,i}, \qquad p = 1, ..., P, \tag{3.14}$$
$$y_{p,i} = K_{p,i}(\mathbf{x}_p, T_p, p_p) x_{p,i}, \qquad p = 1, ..., P,\ i = 1, ..., C, \tag{3.15}$$
$$h_p^V = h^V(\mathbf{y}_p, T_p, p_p), \qquad p = 1, ..., P, \tag{3.16}$$
$$h_p^L = h^L(\mathbf{x}_p, T_p, p_p), \qquad p = 1, ..., P, \tag{3.17}$$

is solved for the pinch points of the rectifying section for a given energy duty Q_D. Similarly, the pinch points of the stripping section can be calculated for a balance envelope around the stripping section by replacing eqs. (3.11)-(3.13) by

$$0 = L_p - V_p - B, \qquad p \in P_B, \tag{3.18}$$
$$0 = L_p x_{p,i} - V_p y_{p,i} - B x_{B,i}, \qquad p \in P_B,\ i = 1, ..., C, \tag{3.19}$$
$$0 = L_p h_p^L - V_p h_p^V - B h_B + Q_B, \qquad p \in P_B. \tag{3.20}$$

Pinch points are insensitive towards the choice of trace components. They can be classified as stable nodes, unstable nodes, or as saddles depending on the number of stable eigenvectors. In this thesis, we consider the nomenclature for pinch points as introduced by Julka and Doherty (1990): the pinch points are denoted by r or s for the rectifying and stripping section and by the number of unstable eigenvectors plus

one. The pinch points for the example separation are shown in Fig. 3.1. Here, the stable pinch point *r1* is the feed pinch. All column profiles run through this point, regardless of the specification of trace components in the products. *r2* and *s2* are the saddle pinches. The section profiles pass by these points when sufficiently pure products are specified. Tapp, Holland, Hildebrandt and Glasser (2004) also consider pinch points which lie outside of the composition space. By deriving so-called column profile maps they have proposed a graphical tool to assess the feasibility of complex column designs (Hildebrandt, Beneke, Abbas, Holland, Vrey and Glasser, 2010).

It needs to be noted that not all splits exhibit a feed pinch and saddle pinches. The appearance of pinch points, and ultimately the applicability of pinch-based shortcut methods, depends on the type of split. In literature, the notation of the different types of splits is not consistent. Hence, we briefly define a notation of the splits for this thesis and illustrate the implications of the splits on the occurrence of pinch points:

- *Direct/indirect splits* usually refer to separations, where a pure product, i.e. the lightest or heaviest boiling component, is removed at the top or bottom. In this thesis, this category also includes separations, where the lightest or heaviest boiling azeotrope of the respective distillation region is removed at the top or at the bottom. We will use this broader definition of direct and indirect splits here, since these separations exhibit the same pinch point behavior: A feed pinch, i.e. a pinch at the feed tray, usually occurs in the section where the impure product is drawn off. Note that the impure product does not necessarily have to be located at an edge of the composition space or at a distillation boundary.
- In *intermediate splits*, both column end products are not pure but are located at the edges of the composition space or at a distillation boundary. For mixtures with more than three components, these splits often have no feed pinch.
- *Sloppy or nonsharp splits* correspond to separations, where all components of the mixture are present in both column end products and the products are not located at a distillation boundary. For mixtures with more than three components, these splits typically have no feed pinch. Usually, there are no saddle pinches either. For ternary mixtures, however, sloppy (and intermediate) splits usually exhibit a feed pinch due to the reduced dimensionality.

In the following four subsections, pinch-based shortcut methods for non-ideal distillation are reviewed.

3.1.2.1 Zero-volume and minimum angle criterion

For the approximation of minimum reflux conditions, the zero-volume criterion (ZVC) introduced by Julka and Doherty (1990) and the minimum angle criterion (MAC) suggested by Köhler, Aguirre and Blass (1991) require the feed concentration and a subset of relevant pinch points to be on a straight line or to form a minimum angle, respectively.

The ZVC identifies the approximate minimum reflux for the example separation when the feed $\mathbf{x}_F$, the stable node pinch of the rectifying section *r1*, and the saddle pinch of the stripping section *s2* lie on a straight line (see Fig. 3.1). When the feed is not a saturated liquid, the point $\tilde{\mathbf{x}} = (1-q)(\mathbf{x}_{r1} - \mathbf{y}_{r1}) + \mathbf{x}_F$ is used instead of $\mathbf{x}_F$. The ZVC for multicomponent systems uses the information of the feed, the feed pinch, and C-2 pinch solutions in the non-pinched section. The ZVC can only be applied to splits with a feed pinch, i.e. to direct or indirect splits, since it requires collinearity (or coplanarity) of the selected points and the feed pinch. Moreover, Julka and Doherty assumed constant molar overflow for the calculation of the pinch points, which is often not valid in highly non-ideal systems.

The MAC estimates the minimum reflux in case of the separation in Fig. 3.1 by minimizing the angle between the line connecting $\mathbf{x}_F$ (or $\tilde{\mathbf{x}}$) with the stable node pinch of the rectifying section *r1* and the line connecting $\mathbf{x}_F$ (or $\tilde{\mathbf{x}}$) with the saddle pinch of the stripping section *s2*. For the indirect split of the ternary example, the MAC and ZVC are equivalent. Contrary to the ZVC, however, the MAC considers always only one pinch point in each section for multi-component separations. It can therefore be inaccurate for mixtures with more than three components, where the profiles often pass by multiple pinches in one section. Since the lines through $\tilde{\mathbf{x}}$ and the pinches do not need to be collinear in the MAC, it can, in principle, be applied to separations without a feed pinch. However, the MAC lacks a physical explanation in such cases. It is therefore not astonishing that the MAC is reported to be rather inaccurate for separations without a feed pinch (Bausa et al., 1998). An example underlining this observation is given in Appendix B.

A physical explanation of the ZVC for separations with a feed pinch is given in Appendix D in the work of Bausa et al. (1998). While the ZVC and the MAC are computationally efficient due to the lack of tray-to-tray calculations, both criteria suffer from the drawback that the selection of the relevant pinch points can be rather complicated and time-consuming, particularly for mixtures with more than three components.

3.1.2.2 Eigenvalue criterion

The eigenvalue criterion (EC) introduced by Pöllmann, Glanz and Blass (1994) can be considered a pinch-based BVM. Instead of calculating profiles starting from both column ends, the tray-to-tray computation is started from points close to the saddle pinches in the direction of the unstable eigenvectors. The minimum reflux condition is achieved at the smallest reflux ratio which makes an intersection of the profiles possible. Again, the selection of the relevant subset of active pinch points is not trivial. For multicomponent mixtures with more than one unstable eigenvector per pinch point, multi-dimensional manifolds of column profiles have to be checked for intersection, which can be a costly procedure, the more so as the automation of the check for intersection remains difficult.

3.1.2.3 Rectification body method

Bausa et al. (1998) introduced the rectification body method (RBM) as an algorithmically accessible procedure to estimate the MED in multicomponent azeotropic distillation. Here, all pinch point solutions of the candidate separation are computed reliably from a robust implementation of the pinch equation system (Bausa, 2001). Then, possible paths along pinch points with an increasing number of stable eigenvectors are generated and checked for thermodynamic consistency by excluding paths where the entropy production does not increase strictly monotonously. Convex rectification bodies which approximately describe the manifold of all profiles are then constructed for each section by linearly connecting the pinch points contained in the paths (cf. Fig. 3.1). The minimum energy duty is calculated by iteratively identifying the lowest reboiler duty that results in an intersection of a set of bodies. Since all pinch points are used, no a-priori selection of relevant pinch solutions is required. The check for intersection of the convex rectification bodies can be performed very efficiently. Therefore, the method can be automated and applied to mixtures with any number of components. Harwardt et al. (2008) have calculated the MED by means of the RBM for separations with more than 10 components in about 10 CPU seconds on a standard PC. In fact, these authors show that the computational efficiency of the RBM facilitates a rapid optimization of large column sequence superstructures for the separation of zeotropic multicomponent mixtures of up to 8 components. The RBM has been extended to handle complex columns (Von Watzdorf, Bausa and Marquardt, 1999; Brüggemann, 2005) and extractive columns Brüggemann and Marquardt (2004). It should also be noted that the RBM is applicable to direct, indirect, as well as intermediate splits, which often have no pinch at the feed tray when the mixture contains

more than three components. In this case, the rectification bodies for the rectifying section and the stripping section intersect at the edges (see Bausa et al. (1998) or Appendix B). In case of a tangent pinch, three pinch points can be determined on one pinch point curve. Hence, only the first pinch on each pinch point curve is used. When the energy is increased such that the tangent pinch disappears, the rectification bodies overlap at MED. Sloppy splits, however, often exhibit no saddle pinches such that the RBM with linear rectification bodies returns an inaccurate estimation of MED for these splits.

Furthermore, the RBM, only returns a good estimate of MED in those cases where the profiles between the pinch points are not strongly curved. Still, most homogeneous mixtures exhibit only a weak nonlinear behavior such that the linearization of the rectification bodies is a good assumption. Heterogeneous mixtures, however, often exhibit strongly curved column profiles in and around the miscibility gap, which complicate the application of the RBM (Bausa (2001), see also Section 4.3.2).

3.1.2.4 Petlyuk's methodology

Petlyuk (2004) proposed a comprehensive methodology for the optimal design of multicomponent azeotropic distillation. In his works, design procedures are developed for infinite reflux, minimum reflux and reversible distillation conditions and for all kinds of splits. Petlyuk uses the information of the separation pinch points but derives their location by calculating tray-to-tray profiles with constant molar overflow instead of directly solving the pinch equation system.

In a first approximate design step, the methodology for the calculation of the minimum reflux of a direct or indirect split requires a subset of pinches in the non-pinched section and the tray above or below the feed tray, respectively, to be on a straight line. The liquid composition on the tray above or below the feed tray is determined by a simplified mass balance around the feed tray assuming constant molar overflow. In the example in Fig. 3.1, the tray below the feed tray is brought to intersection with the line connecting the pinch points *s1* and *s2* of the non-pinched stripping section. More tedious iterative procedures are required for intermediate and non-sharp splits without a feed pinch.

Petlyuk's methodology can be applied to a wide variety of separations. However, the approximate design step suffers from low accuracy for highly non-ideal mixtures due to the assumption of constant molar overflow and the linearization of the profiles between the pinch points. In addition, the selection of the relevant pinch points is not trivial for mixtures with more than three components. Petlyuk suggests to refine the

prediction of minimum reflux in a more rigorous second design step, where attainable regions are derived with the help of iterative tray-to-tray profile calculations. As a drawback, this design step is computationally expensive.

3.1.3 Shortest stripping line method

Lucia, Amale and Taylor (2008) proposed the shortest stripping line method (SSLM) to find minimum energy designs in multicomponent azeotropic distillation. The authors show that the shortest stripping line which produces a feasible separation, i.e. where the product purities are reached by the section profiles, marks the MED. When the feed pinch occurs in the stripping section, the SSLM suggests the calculation of a large number of stripping section trays, e.g. 300, starting from the bottoms product such that the feed pinch is reached. Then, the rectifying profile is calculated upwards from the feed pinch. When the feed pinch occurs in the rectifying section, a search for the stripping profile passing through the feed is started. The rectifying profile is then calculated upwards from the intersection of the stripping profile with the pinch line of the feed pinch in the rectifying section. This procedure involves the solution of a MINLP problem to find the required intersections. In both cases, the MED is found by a minimization of a distance function along the discrete stripping trajectory while the product purities must be reached.

While the SSLM is based on the constant molar overflow assumption, it has been successfully applied to homogeneous zeotropic and azeotropic mixtures of up to six components and to multi-unit processes (Lucia et al., 2008). The concept has also been extended to non-pinched minimum energy designs, which can be identified by the solution of a subsequent MINLP problem (Amale and Lucia, 2008). While the feasibility check can easily be automated for direct and indirect splits, automation is more challenging for intermediate or sloppy splits. For these splits, the unstable nodes are not located at the section end. As a consequence, the profile does not terminate at the end product for a large number of trays, but passes by or continues past the end product. Hence, the entire section profile needs to be checked for intersection with the end product, which is much more difficult algorithmically.

Due to the large number of tray-to-tray calculations, the SSLM demands a higher computational effort particularly for the evaluation of large processes, where the occurrence of recycles requires an optimization of the process operating point.

3.2 Process evaluation with shortcut methods

A meaningful assessment of separation cost and comparison of alternatives can only be accomplished at the respective optimal operating points of the considered flowsheets. For a numerical optimization of the process operating point, a fully algorithmic and computationally efficient shortcut method is required. For most homogeneous mixtures, the RBM (cf. Section 3.1.2.3) offers both sufficient accuracy and computational efficiency such that the method is suited for use in process optimization. The RBM, however, can be inaccurate for heteroazeotropic, highly non-ideal, or reactive distillation. For these applications, a novel shortcut method based on the RBM will be introduced in Sections 4.5 and 7.2.

When the RBM or a related pinch-based shortcut method is used for the numerical optimization of process recycles, an algorithmic formulation of a feasibility criterion is necessary in addition. This feasibility test has to be algebraically accessible and needs to provide information on the distance of a selected point to a distillation boundary. Both of these criteria are met by the so called pinch distillation boundary (PDB), which marks the distillation boundary at minimum reflux (Davydian, Malone and Doherty, 1997; Brüggemann and Marquardt, 2011a). It is therefore very well suited to be used in conjunction with the RBM, since here the columns are also assumed to operate at minimum reflux. In contrast, the simple distillation boundary reflects the distillation boundary at infinite reflux.

The mathematical formulation of the PDB is based on the (pitchfork) bifurcation phenomena of the pinch lines, which can be detected using a test function and continued by a homotopy continuation method. An algebraic criterion then checks the distance of the column products from the distillation boundary. Further mathematical details are given in the work of Brüggemann and Marquardt (2011a). It needs to be noted that the feasibility check is general and can be applied to arbitrary azeotropic mixtures. It can be used without limitations regarding the number of components or certain types of splits since it does not require graphical inspection.

Supplemented by the RBM for the calculation of the MED and an objective function to minimize the total process energy demand, the PDB can then be used for the numerical optimization of process operating points. Several case studies can be found in the works of Brüggemann (2005), Brüggemann and Marquardt (2011b) and Kossack, Refinius, Brüggemann and Marquardt (2007). However, it will be shown in Section 3.4.1 that the repeated call of the PDB homotopy continuation in every iteration step of such an optimization procedure can significantly slow down the solution times, even to an extent that the process optimization with shortcut methods

requires longer solution times than a rigorous process optimization. A speedup of the PDB-based feasibility check by a-priori calculation and approximation of the PDB is a topic of current research (see also Section 8.1.2). It has therefore not been available for application in the case studies of this thesis. Hence, a simplified approach, which requires no calculation of PDBs, is proposed in Section 4.5.2 and used for the process optimization within the shortcut evaluation steps in Chapters 4 and 5.

3.3 Rigorous optimization

The evaluation of a distillation process with the RBM in combination with the PDB as portrayed in Section 3.2 serves as a good approximation to inspect feasibility and compare different process flowsheets by means of minimum energy demand. However, no conclusions can be made regarding the optimal tray numbers, the optimal location of feeds and side streams, product purities, and capital costs. This information can be gained by a rigorous optimization of the process with an economic objective function, where the columns are represented by tray-to-tray models. The resulting optimization problem is of discrete-continuous nature due to the discrete decisions concerning the tray numbers and stream locations, and the continuous values of energy duties, flow rates, and compositions. While the rigorous optimization of a single distillation column is already non-trivial due to the discrete-continuous nature and the nonlinearity and non-convexity of the underlying thermodynamics, the optimization of distillation processes with recycles poses an even more difficult challenge. Large and complex superstructures have to be defined and solved if all possible splits and column configurations are to be considered (Bauer and Stichlmair, 1998). Given the large scale and the complexity, it becomes clear that these optimization problems are computationally expensive and that the quality of the final solution strongly depends on the specified initial values (Dünnebier and Pantelides, 1999).

As a consequence of these difficulties, the examples of rigorous optimization of distillation processes in the literature are confined to different assumptions, simplifications or limitations. Viswanathan and Grossmann (1990) were the first to publish a general MINLP formulation for tray optimization of single columns. They apply this formulation to an ideal binary mixture and later to azeotropic mixtures (Viswanathan and Grossmann, 1993). Dünnebier and Pantelides (1999) have extended this method to include multi-column systems and an economic objective function but also only consider ideal separations. Bauer and Stichlmair (1998) have developed a rigorous optimization procedure for azeotropic separations which first generates separation

splits based on preferred separations and complements this sequence generation with a MINLP tray optimization. However, they only look at ternary mixtures and report long computational times. In a series of papers, Barttfeld and Aguirre (2002, 2003) develop a method for the optimal synthesis of ternary zeotropic distillation processes based on the concept of reversible separation. They solve the MINLP problem efficiently due to a preprocessing phase but cannot handle sharp splits, which are not allowed in reversible separation schemes.

The tray optimization formulations in the works mentioned above all suffer from the numerical difficulties inherent to large-scale MINLP optimization: lack of robustness, long computational times and sensitivity to local optima. As a consequence, efforts have been made to apply alternative optimization approaches to the column optimization problem. Yeomans and Grossmann (2000) formulate general disjunctive programming (GDP) representations for the economic optimization of distillation columns for reversible separations and Barttfeld, Aguirre and Grossmann (2003) compare its solution properties to MINLP formulations. They claim that the GDP representation increases the robustness in the solution as non-existent trays are not included in the subproblems. Still, the GDP has to be reformulated and solved as a MINLP since the development of logical solvers which are capable of handling logical constraints has not yet progressed sufficiently. The numerical results of their case studies for non-sharp separation of ternary mixtures in a single column suggests that the GDP formulation requires less solution time but is more sensitive towards local optima than MINLP formulations. Farkas, Czuczai, Rev and Lelkes (2008) reformulate GDP representations of complex distillation systems as MINLP problems and apply a modified outer approximation algorithm which provides good initial values for the NLP subproblems. They optimize a complex distillation process for an azeotropic quaternary example but still report solution times larger than 1 h. In general, the GDP representations modeling the column size by existing or non-existing (i.e. by-passed) trays cannot benefit from the tight relaxations of the MINLP formulations, where the column size is modeled by a variable reflux/reboil location, variable condenser/reboiler location or variable product stream location.

Various authors, including Barkmann, Sand and Engell (2008), solve rigorous column optimization problems by genetic algorithms. While this approach benefits from good robustness, the computational times prove to be significantly longer than for gradient-based optimization.

Linninger and his co-workers extend their temperature collocation algorithm (cf. Section 3.1.1) to the rigorous design of complex column networks in a series of papers (Kim, Ruiz and Linninger, 2010; Kim and Linninger, 2010; Ruiz, Kim, Moes and Lin-

ninger, 2011). In their case studies, the authors include multicomponent and non-ideal mixtures but do not study processes with recycles. In addition, economic objective functions are not considered.

Recently, continuous reformulations of MINLP problems which can be solved with robust NLP solvers have gained increased attention due to the remaining drawbacks of discrete optimization. Lang and Biegler (2002) proposed a column optimization formulation, where the discrete decisions, i.e. number of trays and feed tray location, are modeled by continuous variables. The authors place the continuous decision variables on bell-shaped curves with the help of a differentiable distribution function in order to locate optimal regions for the feed and the reflux/reboil streams. The optimization is then carried out in a series of continuous NLP problems where the variance of the bell-shaped distribution function is gradually reduced. While this approach is very promising, some of the following simplifications apply for each of their published case studies: linear objective functions, non-sharp splits, fixed feeds, single columns or ideal mixtures. In addition, they only obtain a narrow distribution of the decision variables instead of an integer solution. Neves, Silva and Oliveira (2005) presented an alternative strategy for the continuous optimization of tray optimization problems, where they replace the differentiable distribution functions by numerically easier to handle nonlinear constraints that force the continuous decision variables to integer values. Like Lang and Biegler (2002), they solve the continuous problem in a sequence while reducing relaxation parameters. The robustness is increased due to the continuous approach, a pre-processing phase based on shortcuts and the addition of slack variables. However, the published case studies are confined to the tray optimization of either single columns or distillation processes with a fixed number of trays.

Kraemer, Kossack and Marquardt (2009) have studied the rigorous optimization of large-scale and complex distillation processes for the separation of homogeneous azeotropic mixtures. In their work, substantial progress has been made towards the robust and efficient solution of these optimization problems through measures on two levels:

- **Initialization by shortcut evaluation.** The integration of the rigorous optimization into the process synthesis framework (cf. Chapter 2.6) allows a reduction of the process superstructure a priori. Thus, elementary design decisions like the selection of splits, the flowsheet structure, the column pressures or the choice of entrainer are already made before the rigorous optimization is set up. In addition, the shortcut evaluation provides excellent initial values and bounds for the rigorous optimization (see Section 3.3.3).

- **Continuous reformulation.** The resulting MINLP problems are reformulated as purely continuous problems, which are solved as a series of a few easier to solve NLP problems with successively tightened bounds as presented in Sections 3.3.2 and 3.3.4. These rigorous tray optimization problems are solved with outstanding efficiency and robustness by formulating a particular tight continuous representation. Because of the tight optimization formulation, the local optima are located in a narrow range in the continuous space and, thus, special nonlinear constraints to force integer decisions can be handled robustly. We will see that continuously reformulated tray optimization problems can be solved significantly faster than the corresponding MINLP problems. The reduction of the computational time is of great benefit when varying specifications for product purities, pressures, feed compositions or cost parameters necessitate numerous design evaluations.

3.3.1 MINLP column model

In general, a tray-to-tray optimization problem can be formulated as a GDP, where the column size is modeled by existing or non-existing (i.e. by-passed) trays, or as a MINLP, where the column size is modeled by variable column ends. Contrary to the GDP column representations, MINLP column formulations exhibit very tight relaxations and are therefore better suited for continuous reformulation. Different column superstructures for the MINLP tray optimization can be found in the literature (Bauer and Stichlmair, 1998; Barttfeld et al., 2003). MINLP formulations for three different superstructure variants as illustrated in Fig. 3.2 were reformulated as continuous problems by Kraemer, Kossack and Marquardt (2009) and compared for robustness, reliability and efficiency.

Superstructure variant (a) determines the number of column trays by a variable reflux scheme as proposed by Viswanathan and Grossmann (1993). The top tray models the condenser and as the reflux is moved to lower trays, the trays between the reflux location and the top tray dry up, i.e. the liquid overflow disappears for these trays. Note that the introduction of smoothing functions, which Lang and Biegler (2002) formulate to handle the loss of phases on dried-up plates becomes redundant since pressure drops and heat losses are neglected in this thesis. Superstructure variant (b) has the condenser heat exchange as variable to control the tray number. Heat is exchanged on the top tray in any case when the distillate product leaves the column as boiling liquid. Comparable to variant (a), the trays above the last existing tray dry up. Again, no smoothing function for dried up trays is required when the column

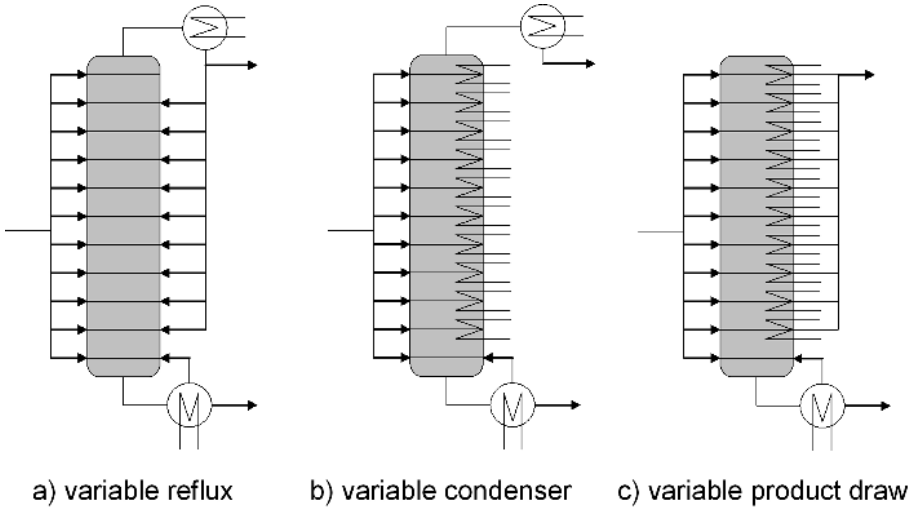

Figure 3.2: Alternative superstructures for the tray optimization of distillation columns. The top ends of the columns are variable in this case.

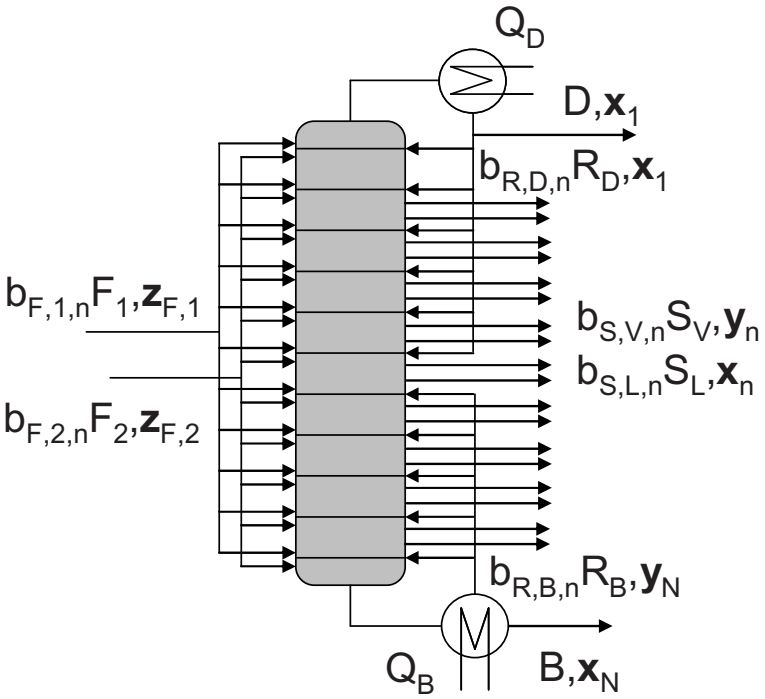

Figure 3.3: Tray optimization superstructure used in this thesis. Both column ends are variable. Multiple feeds and vaporous as well as liquid side draws are considered.

pressure drop and heat losses are neglected. Superstructure variant (c) models the size of the column by a variable distillate product stream and condenser heat location. The trays above the product draw are still calculated but are of no relevance.

Superstructure variant (a) offered the best results as far as solution times and quality of the local optima are concerned. Hence, only superstructure variant (a) is applied in the case studies in this thesis. While all column configurations can be modeled by variable feed and either variable reflux or variable reboil positions, it needs to be noted that the feed and both the reflux and the reboil positions are variable in the superstructure applied in this thesis. This superstructure, which is depicted in Fig. 3.3, proved to yield even better local optimal solutions. Multiple feeds and side draws are also considered in the superstructure in Fig. 3.3.

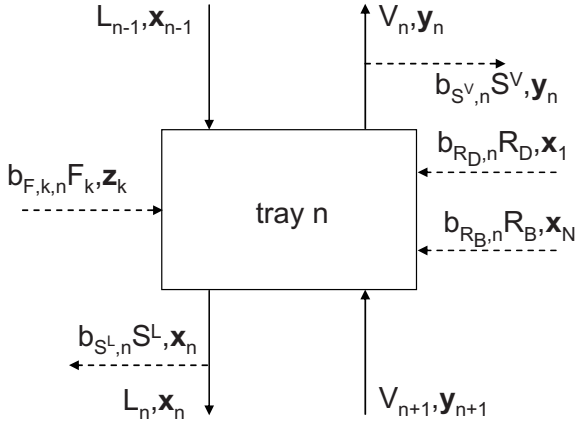

Figure 3.4: Equilibrium tray with streams for the superstructure depicted in Fig. 3.3.

The rigorous column optimization model for a single column and the superstructure depicted in Fig. 3.3 is listed as follows:

$$\min \quad \text{TAC} = \dot{C}_{op} \cdot t_a + f_c \cdot C_{cap}, \tag{3.21}$$

s.t.

$$\begin{aligned} 0 = &\sum_{k=1}^{K} b_{F,k,n} F_k z_{k,i} + L_{n-1} x_{n-1,i} + V_{n+1} y_{n+1,i} - L_n x_{n,i} - V_n y_{n,i} - b_{S^L,n} S^L x_{n,i} \\ &- b_{S^V,n} S^V y_{n,i} + b_{R_D,n} R_D x_{1,i} + b_{R_B,n} R_B y_{N,i}, \qquad n = 2, ..., N-1,\ i = 1, ..., C, \end{aligned} \tag{3.22}$$

$$\begin{aligned} 0 = &\sum_{k=1}^{K} b_{F,k,n} F_k h_{F,k} + L_{n-1} h^L_{n-1} + V_{n+1} h^V_{n+1} - L_n h^L_n - V_n h^V_n - b_{S^L,n} S^L h^L_n \\ &- b_{S^V,n} S^V h^V_n + b_{R_D,n} R_D h^L_1 + b_{R_B,n} R_B h^V_N, \qquad n = 2, ..., N-1, \end{aligned} \tag{3.23}$$

$$0 = \sum_{k=1}^{K} b_{F,k,n} F_k z_{k,i} + V_{n+1} y_{n+1,i} - D x_{n,i} - R_D x_{n,i}, \qquad n = 1,\ i = 1, ..., C, \tag{3.24}$$

$$0 = \sum_{k=1}^{K} b_{F,k,n} F_k h_{F,k} + V_{n+1} h^V_{n+1} - D h^L_n - R_D h^L_n + Q_D, \quad n = 1, \tag{3.25}$$

$$0 = \sum_{k=1}^{K} b_{F,k,n} F_k z_{k,i} + L_{n-1} x_{n-1,i} - B x_{n,i} - R_B y_{n,i}, \qquad n = N,\ i = 1, ..., C, \tag{3.26}$$

$$0 = \sum_{k=1}^{K} b_{F,k,n} F_k h_{F,k} + L_{n-1} h^L_{n-1} - B h^L_n - R_B h^V_n + Q_B, \quad n = N, \tag{3.27}$$

$$0 = L_1, \tag{3.28}$$

$$0 = V_N, \tag{3.29}$$

$$\sum_{i=1}^{C} x_{n,i} = 1, \qquad \sum_{i=1}^{C} y_{n,i} = 1, \qquad n = 1, ..., N, \tag{3.30}$$

$$y_{n,i} = K_{n,i}(\mathbf{x}_n, \mathbf{y}_n, T_n, p_n) x_{n,i}, \qquad n = N,\ i = 1, ..., C, \tag{3.31}$$

$$h^V_n = h^V(\mathbf{y}_n, T_n, p_n), \qquad n = 1, ..., N, \tag{3.32}$$

$$h^L_n = h^L(\mathbf{x}_n, T_n, p_n), \qquad n = 1, ..., N. \tag{3.33}$$

$$\sum_{n=1}^{N} b_{F,k,n} = 1, \quad \sum_{n=1}^{N} b_{S^L,n} = 1, \quad \sum_{n=1}^{N} b_{S^V,n} = 1,$$

$$\sum_{n=1}^{N} b_{R_D,n} = 1, \quad \sum_{n=1}^{N} b_{R_B,n} = 1, \qquad k = 1, ..., K, \tag{3.34}$$

$$\sum_{n}^{N} b_{R_D,n} + b_{F,k,n} \leq 1, \quad \sum_{1}^{n} b_{R_B,n} + b_{F,k,n} \leq 1, \qquad n = 1, ..., N,\ k = 1, ..., K, \tag{3.35}$$

$$x_{n,i} \geq x_{D,\text{purity}}, \qquad n = 1, \qquad i = \text{light component}, \tag{3.36}$$

$$x_{n,i} \leq x_{B,\text{purity}}, \qquad n = N, \qquad i = \text{light component}, \tag{3.37}$$

$$N_{col} = N - \sum_{n=1}^{N}\sum_{n=1}^{N} b_{R_D,n} - \sum_{n=1}^{N}\sum_{n=1}^{N} b_{R_B,n}, \tag{3.38}$$

$$C_{op} = f(Q_B, Q_D), \tag{3.39}$$

$$C_{cap} = f(N_{col}, D_{col}, A_{reb}, A_{con}). \tag{3.40}$$

The column model is based on the MESH equations, which specify tray-to-tray mass and energy balances and assume VLE conditions on every column tray. The streams to and from a tray are visualized in Fig. 3.4. The symbol b (with particular

indices) denotes binary variables to indicate whether the stream is present or not. Component mass balances and energy balances are given in eqs. (3.22) and (3.23) for each tray except the topmost and the lowest trays, which represent the condenser and the reboiler, respectively. For these, component mass and energy balances are given in eqs. (3.24)-(3.29). Eq. (3.30) refers to the closure relations for the liquid and vapor compositions on each tray. The vapor-liquid equilibrium and the vapor and liquid enthalpies are described by eqs. (3.31)-(3.33). For the K-values, the liquid activity coefficients γ are calculated by means of a common g^E model (e.g. Wilson, UNIQUAC, NRTL, UNIFAC). The pure component vapor pressure is determined by the extended Antoine equation whereas vapor phase fugacities coefficients are set to 1 for the mixtures in this thesis. DIPPR equations are employed for the calculation of the enthalpies. It needs to be noted that column pressure drop is neglected in this thesis. The addition of slack variables to the balances and the equilibrium condition for better convergence properties as in the work by Neves et al. (2005) can be neglected due to the sound initialization of the optimization problem (see Section 3.3.3). Closure relations apply for the binary variables modeling the column feed locations, $b_{F,k,n}$, side draw locations, $b_{S^L,n}, b_{S^V,n}$, and the reflux and reboil locations $b_{R_D,n}$, $b_{R_B,n}$ (eq. (3.34)). Eq. (3.35) guarantees that the column feeds are located between the trays where the reflux and reboil is introduced. Purity constraints are added for the distillate and bottom products in eqs. (3.36) and (3.37) to ensure product quality. A sharp split for the light component is specified here. Sharp splits for the heavy component or intermediate splits can be specified analogously.

The objective function reflects the total annualized column cost composed of operating cost (cost for cooling and heating, eq. (3.39)) and capital cost (investment for column shell, trays and heat exchangers, eq. (3.40)). The capital cost, which depends on the tray number, the column diameter and the areas of the heat exchangers, is calculated from nonlinear cost models given by Douglas (1988) and updated by the M&S index. The capital charge factor f_c accounts for the depreciation time including interest. The number of trays are calculated by eq. (3.38). The remaining sizing and costing functions for the equipment considered in this thesis are given in Appendix C.

In order to optimize a whole distillation process of several columns, the single column models are connected by flowsheet streams with variable flow rates and compositions. Furthermore, the purity constraints on column end products which constitute flowsheet intermediate and recycle streams are removed. The objective function is then specified as the minimization of the cumulated annualized operating and capital costs of all columns in the process.

3.3.2 Continuous reformulation of MINLP problems

Optimization problems in engineering are often of discrete-continuous nature and usually nonlinear or even nonconvex. In the field of chemical engineering for example, typical examples include the synthesis of reactor or heat exchanger networks, and unit or flowsheet structure optimization. The discrete variables in these examples usually stem from the structural decisions whereas typical continuous variables are compositions or energies, etc.. In addition, thermodynamics, reaction kinetics and economic objective functions add strong nonlinearities. Due to the combined computational challenges from both the discrete nature and the nonlinearity, these problems are particularly hard to solve. Specifically, the solution performance often suffers from the lack of robust solution algorithms, the necessity of a proper initialization with good starting points and long computational times. In the light of these challenges it is comprehensible that only few applications of large-scale discrete-continuous nonlinear optimization have been realized in industry.

Discrete-continuous nonlinear optimization problems are usually formulated as MINLP problems. Lastusilta, Bussieck and Westerlund (2009) give a comparison of the performances of different MINLP solvers, including recent developments such as CoinBonmin (Bonami, Biegler, Conn, Cornuéjols, Grossmann, Laird, Lee, Lodi, Margot, Sawaya and Wächter (2008)). In recent years, global MINLP solvers for nonconvex problems have been developed and successfully applied to problems of small to medium scale (BARON, Tawarmalani and Sahinidis (2005)). The high computational effort however still prohibits the use of these solvers for large-scale problems. Local optimization algorithms for MINLP problems are usually based on decomposition methods or tree-search algorithms. Decomposition methods, e.g. outer approximation (Viswanathan and Grossmann, 1990), rely on an iteration between overestimating nonlinear programming (NLP) subproblems and underestimating mixed-integer linear programming (MILP) subproblems. Tree search algorithms like branch & bound (Gupta and Ravindran, 1985) perform a search in the space of the NLP subproblems with intelligent node selection and elimination. While these local MINLP solvers have been applied to large-scale problems, the solution robustness, reliability, and efficiency still remain challenging.

In recent years, discrete-continuous nonlinear optimization problems have also been reformulated as purely continuous optimization problems. The resulting nonconvex NLP problems can then locally be solved with NLP solvers. Continuous reformulation was first successfully applied to optimization problems in the form of mathematical programs with equilibrium constraints (MPEC) (Fletcher and Leyffer, 2004). Here,

the equilibrium conditions in the MPEC problems are replaced by nonconvex continuous formulations enforcing the discrete decisions. More recently, general MINLP problems have also been reformulated as purely continuous problems by replacing the discrete variable set with continuous variables (Stein, Oldenburg and Marquardt, 2004; Kraemer, Kossack and Marquardt, 2007). Comparable to MPECs, the discrete decisions are then reached by adding special nonconvex constraints.

Certain discrete-continuous problems can be formulated as MPEC problems where discrete decisions are represented by equilibrium conditions. The equilibrium condition implies that either a constraint is enforced or a decision variable is at its bounds. MPEC problems are often reformulated as NLP problems and solved by NLP solvers. One way to reformulate the equilibrium constraint (EC) is to introduce a penalty function in the objective which penalizes non-discrete solutions. The EC can also be modeled by complementarity constraints in the form of binary multiplications. Various authors suggest to use NCP-functions for the formulation of the EC (Fletcher and Leyffer, 2004). However, all these reformulation strategies share one drawback: They violate the linear independence constraint qualification (LICQ) and the Mangasarian-Fromovitz constraint qualification (MFCQ) (Scheel and Scholtes, 2000). It was therefore proposed to relax the reformulations by adding a relaxation parameter μ to the EC. The problem is then solved in a series of successive NLPs as the relaxation parameter μ is reduced to zero. Stein et al. (2004) transferred the continuous reformulation approach to MINLP problems, which were derived from general disjunctive programs via big-M constraints. The Fischer-Burmeister (FB) NCP-function (Jiang and Ralph, 2000) was employed to enforce the discrete decisions. Later, Kraemer et al. (2007) proposed an extension of the continuous reformulation approach to include general formulations of MINLP problems with binary variables, which are given by

$$\begin{aligned} \min_{\mathbf{x},\mathbf{b}} \quad & f(\mathbf{x},\mathbf{b}), \\ \text{s.t.} \quad & g(\mathbf{x},\mathbf{b}) \leq 0, \\ & h(\mathbf{x},\mathbf{b}) = 0, \\ & \mathbf{x} \in \Re^n,\ \mathbf{b} \in \{0,1\}^m. \end{aligned} \tag{3.41}$$

For the continuous reformulation, the binary variables $b \in \{0,1\}$ were replaced by continuous variables $c \in [0,1]$. FB NCP-functions were used to force these continuous variables to take on binary values:

$$1 \leq \sqrt{{c_i}^2 + (1-c_i)^2} + \mu, \qquad i \in [1,m]. \tag{3.42}$$

Note that the FB NCP-function was relaxed by the relaxation parameter μ which was

reduced to zero in a series of successive NLPs. A discrete solution is returned by the last NLP where $\mu = 0$.

The continuous reformulation of MPECs and solution as NLPs has been applied to large MPEC problem libraries with good results (Fletcher and Leyffer, 2004; Baumrucker, Renfro and Biegler, 2008). Until the work of Kraemer and Marquardt (2010), however, continuous reformulation strategies have not been applied to MINLP problem libraries. Hence, Kraemer and Marquardt studied the performance of continuous reformulation of MINLP problems empirically by means of a large MINLP test problem library.

In their work, 98 representative test problems of the MINLP library MINLPLib were reformulated with the help of FB NCP-functions and solved in a series of NLP steps while a relaxation parameter is reduced. The solution properties are compared to the MINLP solution with branch & bound and outer approximation solvers. Since a large portion of the reformulated problems yield local optima of poor quality or cannot even be solved to a discrete solution, a reinitialization and a post-processing procedure were proposed. Extended with these procedures, the reformulation achieved a comparable performance to the MINLP solvers SBB and DICOPT for the 98 test problems. Details of this study and a comprehensive analysis of the results is given in Appendix A.

3.3.2.1 Continuous reformulation of MINLP column model

The MINLP tray optimization formulation proposed in Section 3.3.1 exhibits very tight relaxations. When the MINLP problem is relaxed, the feeds, reflux, reboil, and side streams are usually introduced on a few adjacent trays in the optimal relaxed solution. It is important to note that similar relaxation characteristics apply to the cascade optimization problems for extraction columns and crystallization cascades in Sections 5.2.1, 6.1 and 6.2. Because of this property, the MINLP tray optimization problems in this thesis are perfectly suited for continuous reformulation, where the tight relaxations can be ideally exploited. In order to gain a purely continuous formulation, the binary variables modeling the reflux and reboil location, i.e. the number of column trays in the MINLP model in Section 3.3.1, $b_{R_D,n}$ and $b_{R_B,n}$, and the feed and side stream locations, $b_{F,k,n}, b_{SL,n}, b_{SV,n}$, are replaced by the respective continuous decision variables $c_{R_D,n}$, $c_{R_B,n}$, $c_{F,k,n}$, $c_{S^L,n}$ and $c_{S^V,n}$.

Discrete decisions are then reached by the addition of nonlinear constraints in the

form of the Fischer-Burmeister function:

$$1 \leq \sqrt{{c_{m,n}}^2 + \left(1 - c_{m,n}\right)^2} + \mu, \qquad m \in \{F_k, R_D, R_B, S^L, S^V\}, \;\; n = 1, ..., N, \quad (3.43)$$

similar to eq. (3.42), which force the continuous decision variables $c_{m,n}$ to integer values when $\mu = 0$. Given that $\sum_n c_{m,n} = 1$ and $c_{m,n} \geq 0$, optimal discrete trays are determined for the feeds, reflux, reboil, and side stream locations. The relaxation parameter μ is added to the right hand side of eq. (3.43) in order to improve the numerical properties of the Fischer-Burmeister function. Typically, μ is reduced from $\mu = 0.5$ to $\mu = 0.2$ and $\mu = 0$ in a series of a few solution steps until an integer solution is reached when $\mu = 0$ (see Section 3.3.4).

As far as the feed distribution is concerned, Viswanathan and Grossmann (1993) already observed that a single column feed is optimally distributed when it is introduced on a single column tray. Kossack et al. (2006) has interpreted this property as a maximization of effective trays in each column section: the largest sections are obtained when the impure feed is introduced on a single tray and thus placed farthest away from both column ends. Kraemer, Kossack and Marquardt (2009) have observed, however, that multiple feed columns do not typically have discrete feed trays in the optimal solution of the relaxed problem. The costs for a two feed column, for example, are usually minimal when one feed is introduced on a single tray while the other feed is distributed among several trays. Here, Fischer-Burmeister constraints (eq. (3.43)) are added to enforce discrete decisions.

3.3.3 Initialization

The complex large-scale nonlinear tray optimization problem of Section 3.3.1 requires a sound initialization to allow for a robust, reliable and efficient solution. Different initialization concepts are known from the literature, which typically suffer from the drawback that a priori knowledge about the distillation process is required to specify initial values and bounds. Various authors (e.g. Barttfeld et al. (2003); Neves et al. (2005); Kossack et al. (2006)) have reported, however, that a favorable initialization of the column optimization improves both the robustness and the probability to identify good local optima. In order to identify appropriate initial values, different proposals for pre-processing phases have been published. Fletcher and Morton (2000) generate initial values by studying the limiting column condition at infinite reflux. Energy efficient columns, however, operate close to minimum rather than infinite reflux conditions. Barttfeld and Aguirre (2002, 2003); Barttfeld et al. (2003) use the theory of reversible distillation of Köhler et al. (1991) to identify the energy-efficient "preferred

separation" and to use it for initialization. As a drawback, this concept usually leads to non-sharp splits for azeotropic mixtures.

In this thesis (see also Kossack et al. (2006)), the integration of the rigorous optimization in the synthesis framework introduced in Chapter 2.6 offers excellent prospects for initialization as initial values and bounds can be directly retrieved from the preceding shortcut evaluation with the RBM. The initialization procedure not only provides a feasible starting point for the rigorous optimization but indeed an excellent one due to the proximity of the minimum reflux condition to the real column operating condition.

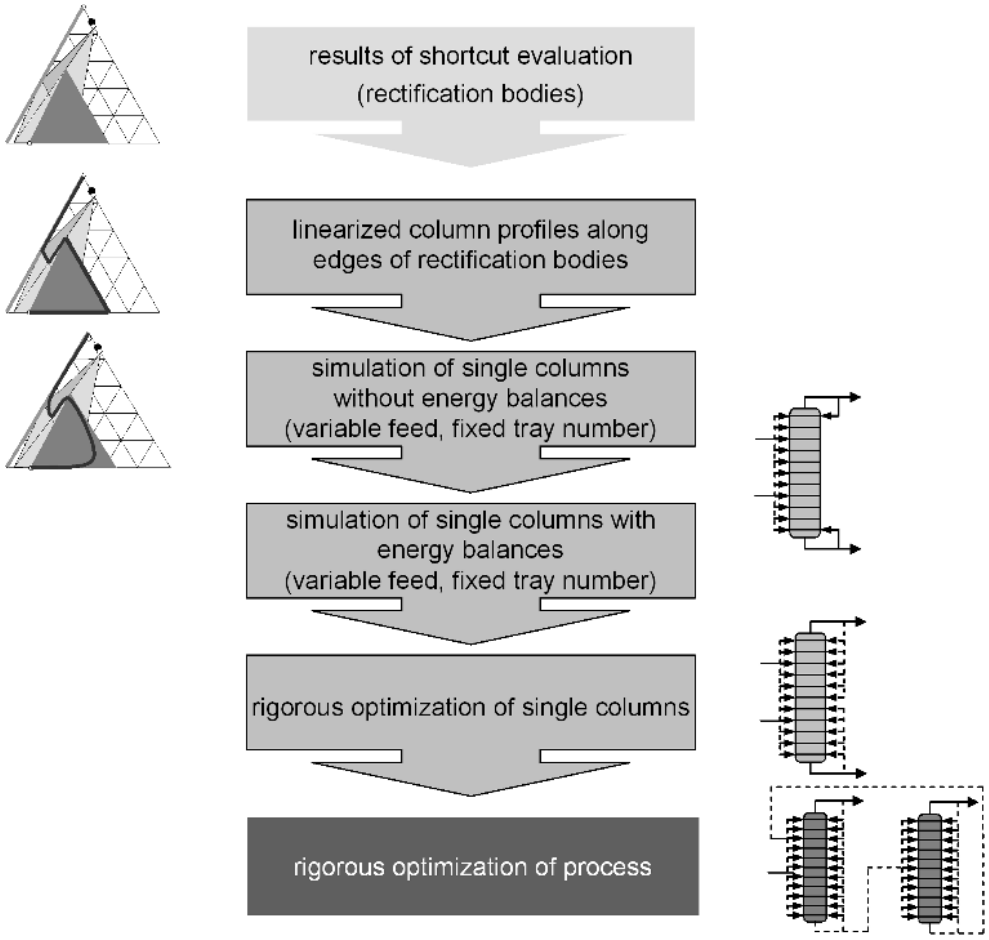

Figure 3.5: Steps of the initialization procedure. For illustration purposes, the rectification bodies and flowsheets at the respective initialization step of an extractive distillation process are included.

The initialization procedure for the rigorous optimization of distillation processes

is carried out in several steps as illustrated in Fig. 3.5. Kraemer, Kossack and Marquardt (2009) state that a stepwise initialization of the optimization problem with gradually refined models helps both robustness as well as efficiency, although more simulations and optimization runs have to be carried out. For the initialization, the process is therefore at first disaggregated into single columns which are initialized separately with the column feed and product streams being fixed at the optimal values from the preceding shortcut evaluation. Initial linear column composition and temperature profiles are derived for every column from the linear piece-wise combination of the pinch points calculated by the RBM in the shortcut step, providing very good approximations of the actual column profiles. These linear profiles then serve as initialization for a rigorous column simulation for which the tray number is fixed at a user-specified maximum value and energy balances are neglected in order to facilitate easy convergence of this initializing column model. Note that the feed tray location is set free to prevent an infeasible specification by the user. In the next step, energy balances are introduced and the relaxed feed tray location variable is optimized by a minimization of the reboiler duty to provide excellent initial values for the rigorous tray optimization. Subsequently, full rigorous column optimizations are performed for the separate columns where the total annualized costs are minimized by an optimization of the number of column trays and feed tray locations. Note that the highly nonlinear Fischer-Burmeister constraints which enforce integer tray decisions are not activated in this step for better convergence.

The initialization procedure is now completed. It needs to be noted that the rigorous optimization of the hybrid processes in the following chapters will be based on the same initialization steps as proposed in this section. Only slight changes will be implemented depending on the additional unit operations in these processes. In the following rigorous process optimization (see next section), the column models are connected by the flowsheet streams and the previously fixed flowsheet operating point is released. Due to the initialization, this last step will converge quickly to local optimal solutions of good quality.

3.3.4 Solution procedure

Now that the rigorous optimization is initialized by the procedure described in the previous section, we are able to solve the continuously reformulated process optimization problem robustly and efficiently. However, the reformulated column model with tightened Fischer-Burmeister constraints ($\mu = 0$) tends to yield local optimal solutions of bad quality due to the abundance of nonlinearities in the model. Therefore,

the problem formulation is relaxed first by setting the Fischer-Burmeister relaxation parameter μ in eq. (3.43) to 0.5 in order to diminish the effect of the nonlinearity inherent to the Fischer-Burmeister function. Thus, the decision variables (feed, reflux, reboil, and side stream locations, respectively) are optimally distributed among several column trays and the problem converges reliably to favorable solution regions. The formulations are then tightened by successively reducing the Fischer-Burmeister relaxation parameter μ to 0.2 and 0 such that discrete values for the decision variables are obtained. The successive steps of the solution procedure are comprehensively shown in Fig. 3.6.

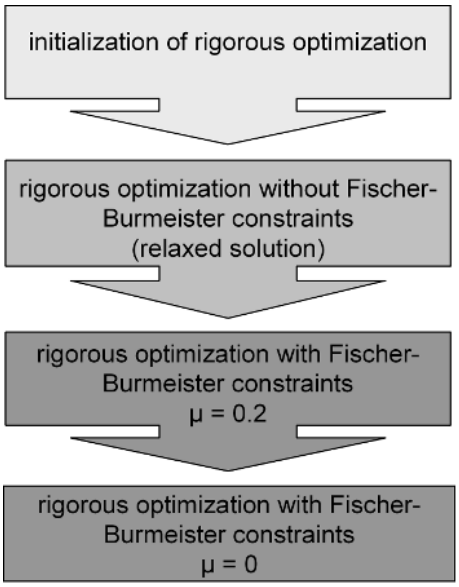

Figure 3.6: Steps of the solution procedure.

3.4 Case study: separation of an azeotropic quaternary mixture

The optimization-based process design by means of the synthesis framework is illustrated by a large-scale case study considering the separation of a quaternary azeotropic mixture in a multi-column curved-boundary process with recycle. The case study covers the whole design procedure of the process synthesis framework (cf. Chapter 2.6) with generation of alternative flowsheets, shortcut-evaluation with the RBM and

rigorous optimization of the most promising flowsheet variant. In addition, heat integration between the process condensers and reboilers by means of column pressure variation is considered in the shortcut and rigorous evaluation steps. It is shown that significant cost reductions in both capital and operating costs can be achieved by selecting the best flowsheet and rigorously optimizing the operating point and the column specifications. The solution properties of the continuously reformulated optimization problems, i.e. solution quality and computational time, are compared to the solution properties of the respective MINLP solution. Finally, Kraemer, Kossack and Marquardt (2009) have studied the possibility of further cost savings for the considered separation by means of a complex column setup, such as a dividing wall column. The dividing wall column setup is rigorously optimized such that the optimal tray numbers for all column sections are obtained. The costs for this integrated process are compared to the costs for the simple column process.

In the case study, an equimolar mixture of acetone, chloroform, benzene, and toluene is to be separated into its pure components in a multi-column process. The flow rate of the saturated liquid feed is set to 10 mol/s and all products are specified at 99% purity. The coefficients for the calculation of vapor pressures, ideal gas heat capacities, and heats of vaporization are given in Tables D.1, D.9, and D.18. The Wilson g^E-model is chosen for the calculation of the liquid activity coefficients of the homogeneous mixture. Parameters for the Wilson model are given in Tables D.1 and D.36. As shown in Fig. 3.7, the mixture exhibits a maximum boiling binary azeotrope on the acetone/chloroform edge and an associated distillation boundary between the azeotrope and the benzene/toluene edge. Fig. 3.7 illustrates the difference between the simple distillation boundary (boundary at infinite reflux) and the pinch distillation boundary (boundary at minimum reflux). Note that the pinch distillation boundary coincides with the chloroform/benzene/toluene plane at higher concentrations of benzene or toluene in the feed.

3.4.1 Manual flowsheet generation and shortcut evaluation

Thong and Jobson (2001) have generated feasible flowsheets for this separation task based on heuristic rules and a search among possible recycle options. They propose the flowsheet shown in Fig. 3.8, where a recycle stream of 2.5 mol/s (recycle/feed=0.25) and azeotropic composition is returned to the first column. A minimum process reboiler duty of 1.576 MW was quickly determined by Kraemer, Kossack and Marquardt (2009) by means of a flowsheet evaluation with the RBM at the operating point suggested by Thong and Jobson. As described in Section 3.2, the RBM allows

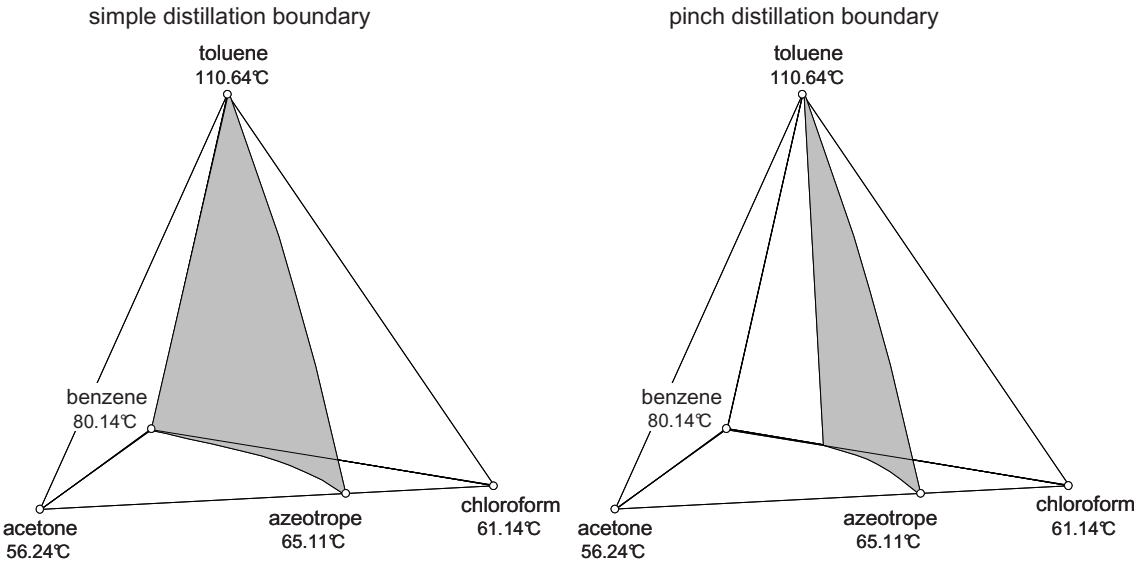

Figure 3.7: Distillation boundaries of acetone, chloroform, benzene, toluene at 1.013 bar: Simple distillation boundary (infinite reflux) and pinch distillation boundary (minimum reflux).

a numerical optimization of the process operating point, which leads to a reduction of the minimum process reboiler duty by 12.6% to 1.399 MW. Interestingly, the recycle flow rate increases to 7.38 mol/s at the optimum (see Table 3.4.1). The energy savings, however, result from a shift of the bottom product of the acetone column towards the benzene/toluene edge by an addition of benzene and toluene to the recycle. Since the pinch distillation boundary runs into the chloroform/benzene/toluene plane (Fig. 3.7), this shift allows a complete separation of acetone in the first column and, consequently, an acetone free mixture in the downstream columns.

The special curvature of the distillation boundary therefore enables a complete separation of the quaternary mixture in three columns. A recycle is still required for the given feed mixture, since the mass balance line of the acetone column, which stretches out to the boundary, needs to be shifted towards the benzene/toluene edge. Significant cost savings can be assumed for any three-column process when compared to processes which comprise four columns. In the light of these findings, the evaluation of further flowsheet variants is confined to flowsheets with three simple columns. A selection of these variants is shown in Fig. 3.9 together with the original flowsheet. The respective minimum process reboiler duties after evaluation with the RBM and optimization of the operating points are given in Table 3.4.1. A pinch distillation boundary constraint had to be considered only for the first column as the following

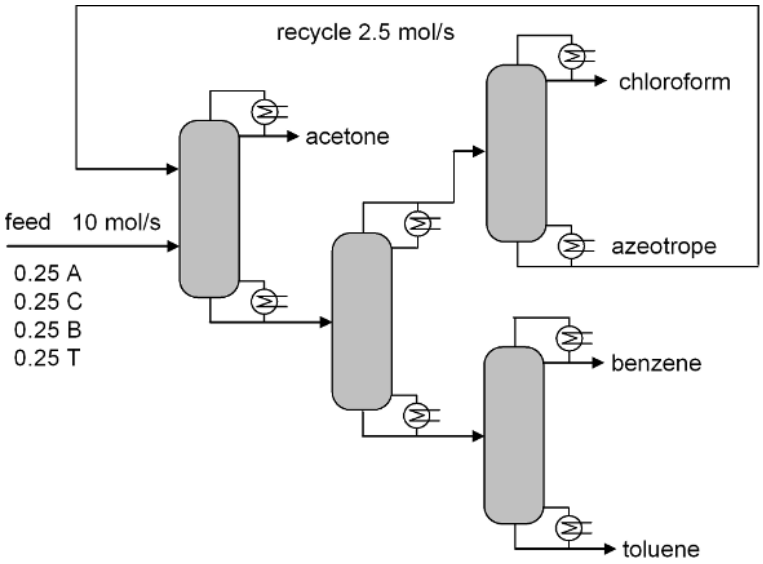

Figure 3.8: Flowsheet proposed by Thong and Jobson (2001) with a recycle of azeotropic composition.

columns are free of acetone and therefore not restricted by distillation boundaries. Note that flowsheet variant F2 exhibits the lowest minimum process reboiler demand (about 43% less than in the original work of Thong and Jobson (2001)).

Table 3.1: Recycles and minimal process reboiler duties for the flowsheet variants of Fig. 3.9. Compositions are given as molar fractions of acetone, chloroform, benzene and toluene, respectively.

flowsheet variant	recycle flow rate and composition		$Q_{B_{min}}$
F1	7.38 mol/s,	[0, 0.08, 0.65, 0.27]	1.399 MW
F2	5.44 mol/s,	[0, 0, 0, 1]	1.103 MW
F3	4.81 mol/s,	[0, 0, 0.5, 0.5]	1.201 MW
F4	5.59 mol/s,	[0, 0, 0, 1]	1.209 MW

The product streams of all flowsheet variants are withdrawn as saturated liquid. However, the distillate streams which are fed into another column are not condensed but transferred as saturated vapor as a measure of heat integration. This actually penalizes flowsheet variants F3 and F4 for the absence of intermediate distillate streams. Both a benzene and a toluene recycle with variable flow rates were considered for vari-

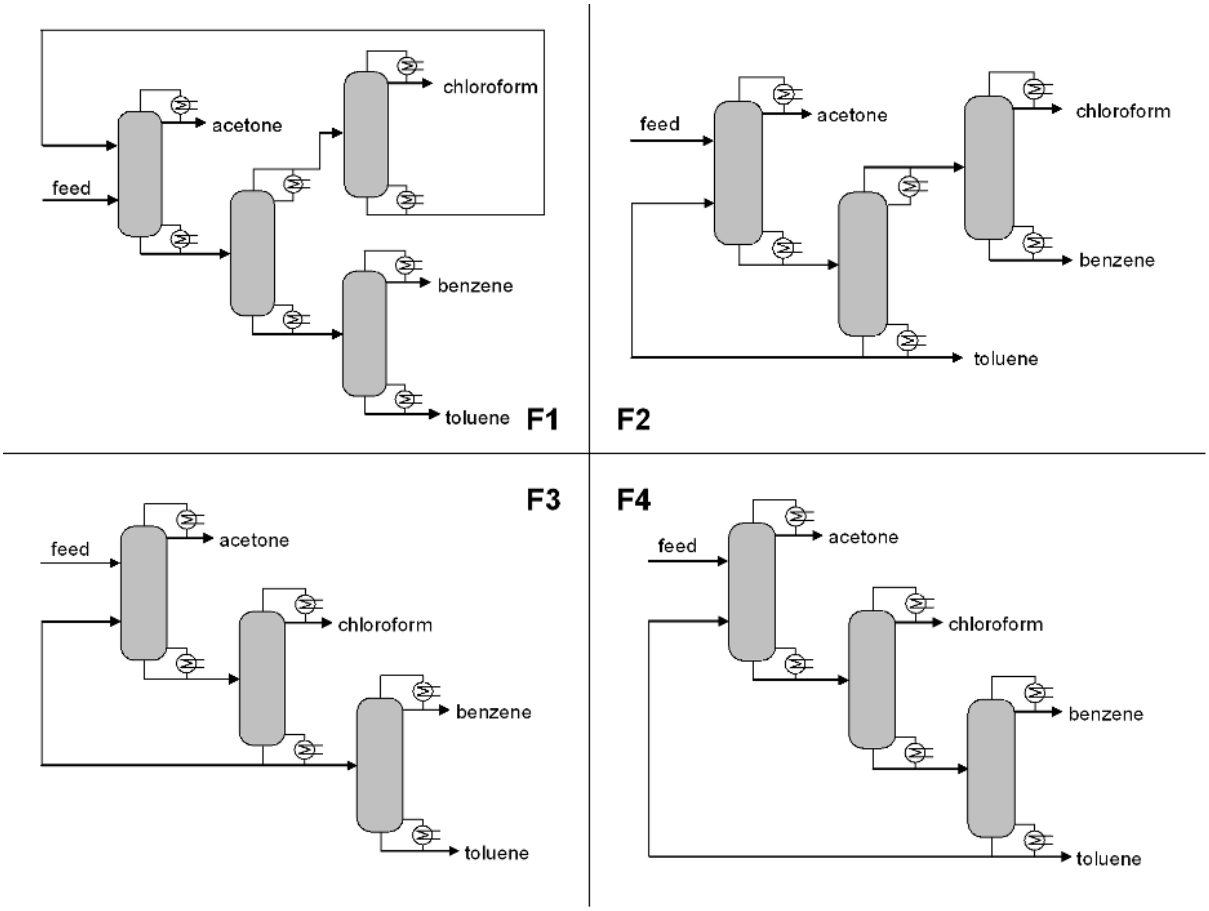

Figure 3.9: Flowsheet variants for the shortcut evaluation. 1: Four-column flowsheet of Thong and Jobson (2001). 2: Three-column flowsheet with toluene recycle. 3: Direct sequence with benzene/toluene recycle. 4: Direct sequence with toluene recycle.

ant 4. The benzene recycle, however, vanishes in the optimization.

As a drawback, the optimization runs turned out to be computationally costly. The optimization times lasted about 1000 seconds for each flowsheet variant. The computational times within the shortcut evaluation are thus significantly longer than the computational times of the rigorous optimization, which will be covered in Section 3.4.3. Compared to the rigorous optimization, however, the shortcut evaluation requires considerably less time for the problem setup and converges reliably without special initialization. It needs to be noted that by far the largest portion of the computational time for the shortcut evaluation is spent on the calculation of the PDB

in every iteration step. It is expected that this computational time can be significantly reduced by an a-priori calculation and polynomial interpolation of the PDB as suggested in Section 3.2.

3.4.2 Automatic generation and evaluation of heat-integrated flowsheets

The flowsheet alternatives in Fig. 3.9 were generated manually with insight in the mixture topology. To date, there are no fully automated and comprehensive procedures for the generation of flowsheets for multicomponent azeotropic distillation published in literature. An overview on flowsheet generation procedures, mostly based on graph theoretic methods, is given in the work of Kossack (2010). Note that the flowsheet synthesis procedure of Thong and Jobson (2001) suggests flowsheet variant F1 (cf. Fig. 3.9) as optimal for the separation considered in this chapter. Yet, it has been shown in the previous section that this flowsheet exhibits a significantly higher energy demand (see Table 3.4.1) and presumably also higher capital costs than the alternative flowsheets in Fig. 3.9.

For the separation of zeotropic mixtures, however, various authors have proposed reliable procedures for the automatic synthesis of distillation sequences (Rathore, Van Wormer and Powers, 1974; Andrecovich and Westerberg, 1985; Caballero and Grossmann, 2001; Agrawal, 2003). These are typically based on superstructure formulations such as the state-task network (Sargent and Gaminibandara, 1976), which is solved by optimization or enumeration. Usually, the distillation tasks are modeled by simple methods for ideal distillation such as Underwood's method. In contrast, Harwardt et al. (2008) and Harwardt, Kraemer and Marquardt (2009) use rigorous thermodynamics and the RBM as a powerful shortcut method for the evaluation of non-ideal distillation. In addition, Harwardt et al. consider heat integration between the process condensers and reboilers by variation of the column pressures within the sequence generation and evaluation.

It has been detected in Section 3.4.1 that the distillation boundary of the example mixture runs into the benzene/toluene/chloroform plane. Due to this property, acetone can be separated completely in the first distillation column of flowsheet variants F2, F3, and F4 in Fig. 3.9, when a recycle of toluene, benzene or a combination thereof is added. The minimum recycle flow rates, which allow a complete separation of acetone in the first column were determined in Section 3.4.1 by means of an optimization of the process operating points with the RBM under consideration of pinch distillation boundaries. The minimum recycle flow rates are 5.44 mol/s for a toluene

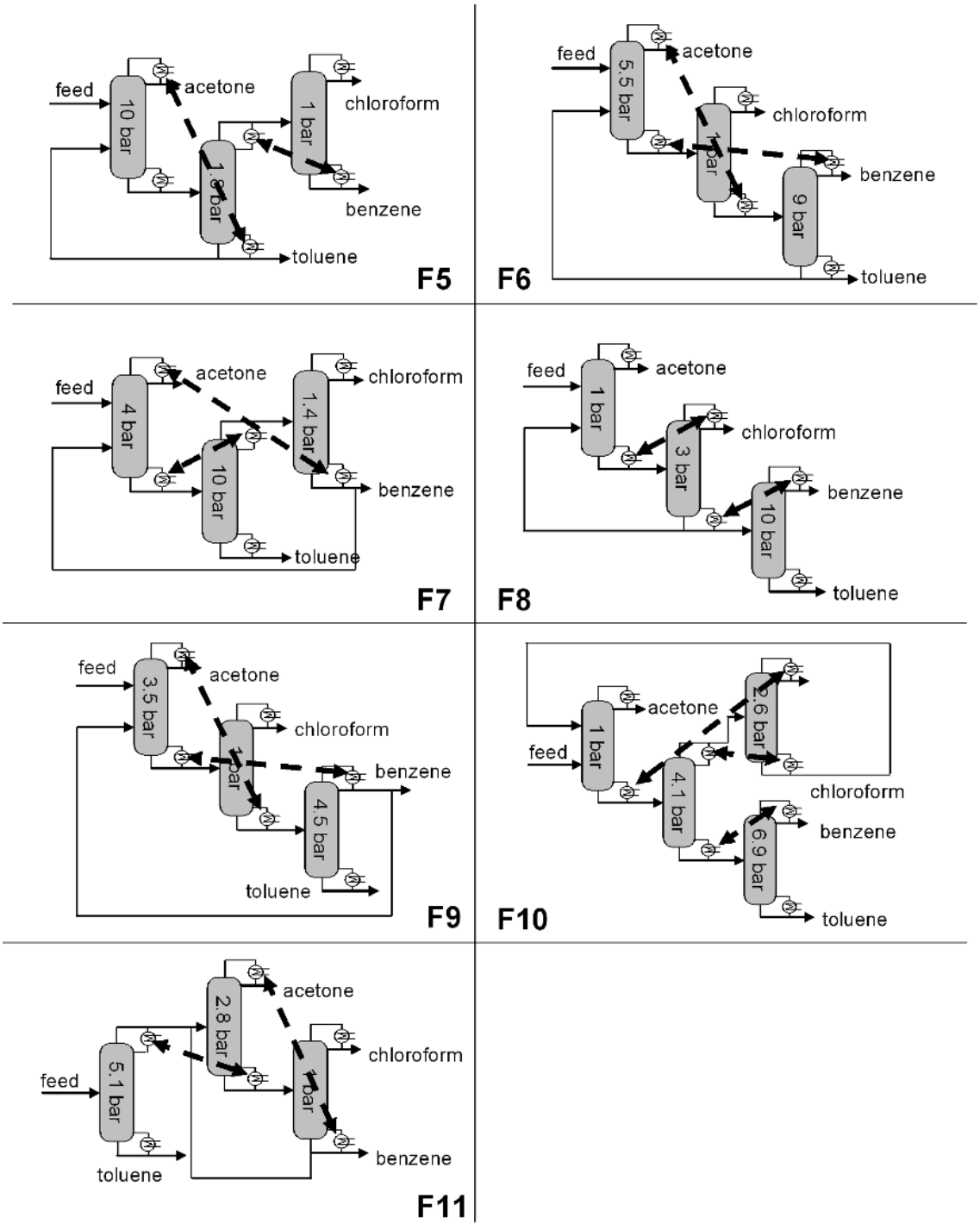

Figure 3.10: Generated flowsheet variants with pressure levels and heat exchanger connections.

recycle (variant F2), 4.54 mol/s for a benzene recycle, and 4.81 mol/s for an equimolar recycle of toluene and benzene (variant F3). When the recycle is fixed to one of these values, an automatic generation and evaluation of column sequences can be performed comparable to zeotropic separations. Harwardt et al. (2009) have therefore evaluated a superstructure of flowsheet alternatives given by a state-task network representation of unique separation tasks with mixed-integer linear programming (MILP) techniques based on the objective of minimum energy requirement. The column pressures are variable within discretized steps in the superstructure optimization such that the heat sinks (reboilers) and the heat sources (condensers) can be combined for a further reduction of the energy demand by heat integration. Temperature bounds are imposed such that inconveniently high and low temperatures in the heat exchangers are prevented. A detailed description is given in the work of Harwardt et al. (2009).

Table 3.2: Minimal process reboiler duties for the automatically generated flowsheet variants of Fig. 3.10.

flowsheet variant	$Q_{B_{min}}$
F5	475 kW
F6	501 kW
F7	561 kW
F8	574 kW
F9	609 kW
F10	615 kW
F11	730 kW

The generated flowsheets with pressure levels and heat exchanger connections are shown in Fig. 3.10. The process reboiler duties of these heat-integrated processes are given in Table 3.4.2. They are significantly lower than the reboiler duties of the processes without heat integration evaluated in Section 3.4.1 (Fig. 3.9 and Table 3.4.1). The flowsheet generation and evaluation could be performed in just 215 seconds using the CPLEX MILP solver within the optimization platform GAMS on a 1.8 GHz standard PC. Note that this computational time is significantly faster compared to the evaluation in Section 3.4.1. This is due to the fixing of the recycles to the optimal values determined in Section 3.4.1 such that the expensive calculation of pinch distillation boundaries becomes redundant.

3.4.3 Rigorous optimization

The heat-integrated flowsheet F5 (Fig. 3.10) was identified to be most energy-efficient for the separation task in Section 3.4.2. This flowsheet is now further evaluated with rigorous optimization to determine the cost-optimal column configurations. It is interesting to note that the same flowsheet structure was found to be optimal in the evaluation without heat integration in Section 3.4.1.

The rigorous optimization problem is formulated and solved on the optimization platform GAMS 22.7 (Brooke et al., 2005). The SQP-based solver SNOPT 7.2-4 (Gill, Murray, Saunders, Drud and Kalvelagen, 2008) is employed for the solution of the continuously reformulated problems on a 3 GHz standard PC. External functions are used in GAMS to calculate the thermodynamic properties (liquid activity coefficients and enthalpies) and the required derivatives. While this approach increases the required solution time because of the communication overhead between the solver and the external function, the robustness of the optimization problem is increased.

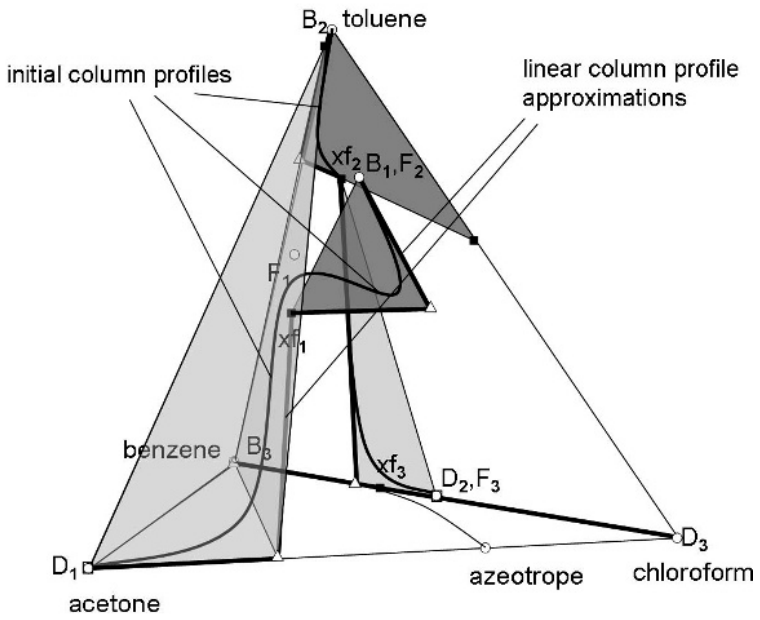

Figure 3.11: Rectification bodies, linear column profile approximations and initial column profiles of the initialization for the rigorous optimization of flowsheet F5.

The fresh feed is fed to flowsheet F5 (Fig. 3.10) as a boiling liquid at 1 bar. After

being pumped to 10 bar it is preheated in an additional heat exchanger by the hot acetone product stream. The distillate stream of the toluene column, which is fed into the chloroform/benzene column, is not condensed but transferred as saturated vapor, thus effectively reducing the required area of the heat exchanger linking these two columns. A depreciation time of 5 years is considered. While low pressure steam at 3 bar (12 €/t) suffices as additional hot utility for the chloroform/benzene column, high pressure steam at 20 bar (15 €/t) is required for the acetone and the toluene columns. The structural and operational degrees of freedom in the rigorous optimization are the number of column trays, feed tray locations, recycle and intermediate flows and compositions, and column energy duties.

At first, the initialization procedure for the rigorous optimization based on the results of the shortcut evaluation as presented in Section 3.3.3 is applied step by step. The linear column profile approximations along the relevant edges of the rectification bodies are shown in Fig. 3.11 together with the profiles of the initializing column simulation (penultimate step of the initialization procedure), where the tray numbers are fixed to 100, 40 and 60 for the acetone, toluene and chloroform/benzene columns, respectively.

Due to this thorough initialization phase, excellent initial values and bounds are provided for the following rigorous optimization. Here, all three columns are modeled with a variable feed position and top end, but a fixed bottom end. The maximum tray numbers were set to the same values as in the initialization phase, yielding optimization problems of about 4500 variables, including 620 decision variables. Fischer-Burmeister functions, eq. (3.43), were introduced for the reflux and reboil locations and for the recycle feed of the first column. The continuous decision variables for the feed locations of the remaining columns took on integer values in the optimal solution without being forced by a Fischer-Burmeister function as discussed in Section 3.3.2.1. The solution of the optimization problem was carried out by the solution procedure proposed in Section 3.3.4 and shown in Fig. 3.6.

The optimization results for all three columns of flowsheet F5 are displayed in Table 3.3 together with the optimization results for the structurally identical flowsheet F2 without heat integration, where all columns are operated at 1 bar and supplied with low pressure steam (cf. Kraemer, Kossack and Marquardt (2009) and Kraemer, Harwardt and Marquardt (2009a)). The heat-integrated process yields a total annualized cost (TAC) of about 76 k€/a less than the process without heat integration, which corresponds to a cost reduction of about 19 %. Reboiler duty savings of 52 % are observed. Note that the operating cost of the acetone column is higher for the heat-integrated process due to the expensive 20 bar hot utility. However, this cost increase

Table 3.3: Costs, column configurations and operating point for all columns of the heat-integrated flowsheet F5. The exchanged heat duties are underlined. Results for the same flowsheet without heat integration (F2) are shown for comparison.

	F5 (heat integration)			F2 (no heat integration)		
TAC [k€/a]	326.5			402.9		
column	acetone	toluene	chl./benz.	acetone	toluene	chl./benz.
TAC [k€/a]	203.1	62.1	61.3	152.7	136.4	113.9
capital cost [k€/a]	86.7	53.8	55.5	75.1	60.1	71.1
operating cost [k€/a]	116.3	8.3	5.8	77.6	76.3	42.7
condenser duty [kW]	0+290	69+281	440	447	289	386
reboiler duty [kW]	509	34+290	0+281	440	460	235
number of trays	94	33	41	58	32	50
feed tray	17	16	20	21	16	15
recycle feed tray	8			7		
diameter [cm]	48.4	65.5	73.4	67.6	69.7	80.8
recycle [mol/s]	4.52			7.23		

is more than compensated by the energy savings for the remaining columns. The acetone column of the heat-integrated process has a significantly higher tray number in the optimal solution when compared to the conventional process. This is due to the pressure increase for this column, which results in a smaller relative volatility, a smaller diameter, and, thus, a shift of the cost optimum towards a higher tray number. On the other hand, the cost optimum for the chloroform/benzene column of the heat-integrated process is found at a lower tray number since no hot utility is required for this column. Furthermore, the heat-integrated process has a significantly lower recycle flow rate to avoid heat losses in the high pressure acetone column, where the expensive hot utility is used. Interestingly, the feed tray of the high-boiling toluene recycle is located well above the tray of the fresh feed of equimolar composition in the optimal solution of both processes. Apparently, the toluene recycle has an extractive effect on the distillation of acetone in the first column.

For a comparison of the solution properties of the continuous reformulation and the

Table 3.4: CPU times and objective values (TAC) for the rigorous optimization of flowsheet F5. The left column shows optimization properties of the continuous reformulation solved with the NLP solver SNOPT. The optimization properties for the MINLP solution with the branch & bound solver SBB are given for comparison in the right column.

	NLP continuous reformulation	MINLP branch & bound
CPU time initialization	72 s	
CPU time optimization	258 s	2616 s
TAC	326.5 k€/a	326.5 k€/a

traditional MINLP solution, Table 3.4 lists the respective solution times and objective values for the heat-integrated process. The initialization phase, which is identical in all cases, took 72 CPU seconds. The computational time of the reformulated optimization problem is significantly lower than the computational time of the corresponding MINLP problem, which also benefited from the favorable initialization. The values of the minimized TAC are comparable. For the process without heat integration, similar optimization properties are reported by Kraemer, Kossack and Marquardt (2009).

Note that the whole process, i.e. all three columns, were optimized simultaneously. Thus, no specifications needed to be made for the intermediate streams, since their purity is optimized. Alternatively, the first two columns can be optimized separately from the chloroform/benzene column, which is not part of the recycle loop. In this case, the optimization problem can be solved faster but, on the other hand, solutions of lower quality are identified since the purity of the intermediate stream needs to be fixed.

3.4.4 Rigorous optimization of a dividing wall column system

Complex column systems such as dividing wall columns (DWC) have the potential to lower energy costs as well as capital costs when compared to sequences of simple columns (Kaibel, Miller, Stroezl, von Watzdorf and Jansen, 2004). At the same time, both the design and the assessment of the savings potential are particularly difficult because of little practical experience as well as an increased number of degrees of freedom.

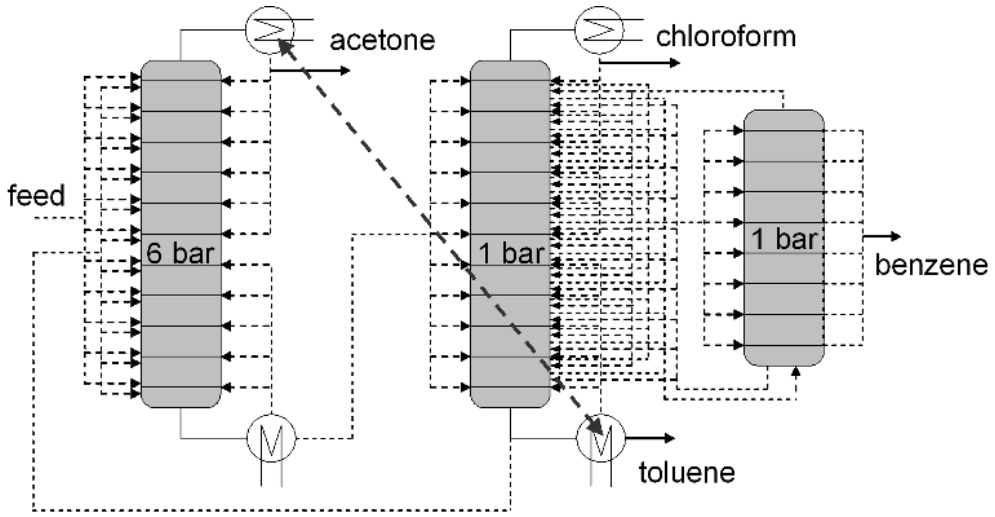

Figure 3.12: Tray optimization superstructure of the DWC process.

Von Watzdorf et al. (1999) have extended the RBM such that complex columns can be included in the shortcut evaluation. Yet the rigorous optimization of complex column systems is all the more useful, since shortcut calculations give no information about the location of side streams and the capital cost difference to simple column processes. The insight gained by a rigorous optimization, where the capital costs are included in the comparison of the economics, is essential here. At the same time, the integration of complex columns also leads to additional challenges for the mixed-integer optimization. Flowsheet F5 (cf. Fig. 3.10) is modified to incorporate a DWC. The resulting flowsheet and its structural degrees of freedom for the rigorous optimization are shown in Fig. 3.12. In addition to the energy savings of the DWC itself, heat integration is considered between the condenser of the acetone column and the reboiler of the DWC. Since the DWC operates at 1 bar, the pressure of the acetone column can be lowered to 6 bar such that 10 bar steam (13 €/t) is sufficient as hot utility for this column. As suggested by Dünnebier and Pantelides (1999), a

Table 3.5: Costs, column configurations and operating point for both columns of flowsheet F5 with heat integration and DWC. The exchanged heat duties are underlined.

	F5 with DWC	
TAC [k€/a]	294.7	
column	acetone	DWC
TAC [k€/a]	189.3	105.4
capital cost [k€/a]	97.0	98.5
operating cost [k€/a]	92.3	6.9
condenser duty [kW]	0+<u>365</u>	519
reboiler duty [kW]	496	0+<u>365</u>
number of trays	87	77
dividing wall between trays		18-69
feed tray	17	32
recycle feed tray	8	
side stream tray		55
diameter [cm]	51.6	79.6
recycle [mol/s]		

surcharge factor of 15% is added to the capital cost of the DWC to account for the increased installation cost of the complex column setup. Maximum tray numbers of 100, 100, and 60 are specified for the acetone column and the main and side sections of the DWC, respectively. Despite the increased complexity of the DWC process (about 1220 decision variables), the optimization could be solved in 554 seconds due to the favorable reformulation as a continuous problem. The MINLP solution with the branch & bound solver SBB returned the same total annualized cost but required 7552 CPU seconds.

Table 3.5 lists the optimization results for the DWC flowsheet. The energy requirement of the fully heat-integrated DWC process (496 kW) is only slightly lower than the energy requirement of the heat-integrated simple column process (543 kW). The capital cost of the DWC process is slightly lower as well, where the main cost saving can be allocated to the lower pressure of the acetone column. This results in a re-

duction of the TAC by 9.7% compared to the system of simple columns. Considering rising energy prices, the DWC setup might become even more interesting in the future.

3.5 Further case studies

Apart from the case study in Section 3.4, various distillation processes have been designed at Aachener Verfahrenstechnik by means of the process synthesis framework. A selection of interesting examples is given in the following subsections.

3.5.1 Pressure swing distillation of an azeotropic quinternary mixture

Kraemer, Kossack and Marquardt (2009) have demonstrated the potential of optimization-based conceptual design with shortcut and rigorous optimization steps by means of yet another large-scale and complex process synthesis problem. This example considers the separation of the homogeneous quinternary mixture of acetone, chloroform, methanol, ethanol, and benzene, for which the Wilson model calculates six binary, two ternary, and one quaternary azeotrope. Wasylkiewicz (2006) has generated a three-column pressure-swing distillation process with the help of the synthesis software ASPEN Distil for this mixture and the following separation task:

- feed of 25 mol% acetone, 40 mol% chloroform, 25 mol% methanol, 5 mol% ethanol and 5 mol% benzene,
- complete separation of pure benzene and pure ethanol,
- ethanol and benzene free residual as a recycle to the reactor.

A complete separation of ethanol and benzene in two simple columns at normal pressure is not possible because of the azeotropic behavior of the mixture with multiple separation regions. Hence, Wasylkiewicz proposed a pressure swing process as shown in Fig. 3.13: After the removal of the benzene in a first column all ethanol is separated in the second column with the help of excess methanol that is recycled from the third column. This column operates at low pressure (10 mbar) to shift the distillation boundary which prohibits a methanol recycle at normal pressure.

Kraemer, Kossack and Marquardt (2009) optimized the recycle flow and composition of this flowsheet by a minimization of the process energy duties in a shortcut evaluation with the RBM. A pinch distillation boundary constraint had to be considered for one column end product. When compared to the operating point suggested

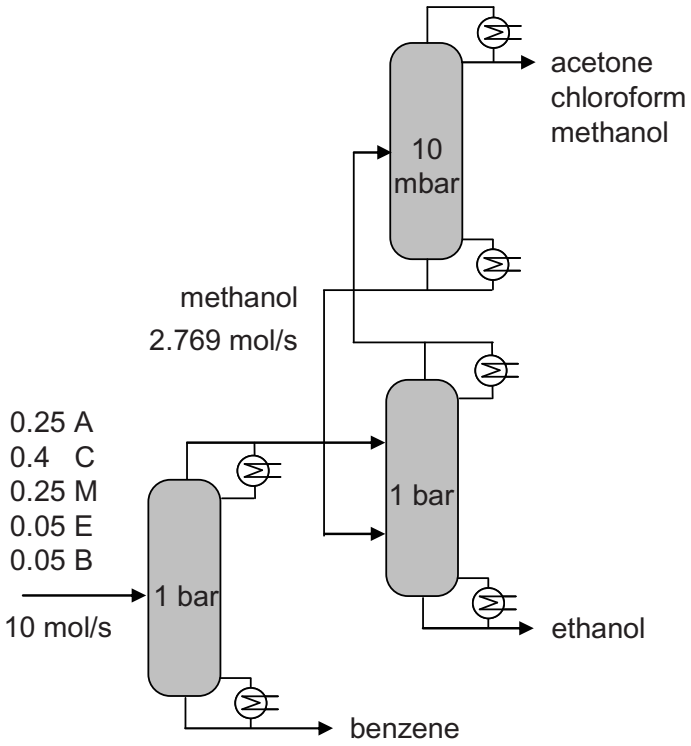

Figure 3.13: Three column flowsheet for the pressure swing process as proposed by Wasylkiewicz (2006).

by Wasylkiewicz (2006), a significantly lower recycle flow rate is obtained such that the process energy duty was reduced by 25%. With the insight gained by the shortcut evaluation, it was also determined that the separation task could be performed slightly more energy-efficient in a two-column flowsheet, where the separation of ethanol from the residual acetone, chloroform, and methanol is accomplished in a single low pressure column operated at 10 mbar.

Subsequently, both flowsheets were rigorously optimized with paramount robustness and efficiency. The computational time for the continuously reformulated rigorous optimization problem of the three-column process was 498 seconds on a 2.66 GHz standard PC including the initialization phase. By comparison, the MINLP solution of this optimization problem lasted 1992 seconds and yielded higher costs. The two-column process exhibited slightly higher costs compared to the three-column process due to larger column diameters.

3.5.2 Evaluation of entrainer alternatives for extractive distillation

Kossack et al. (2008) have generated various entrainer alternatives via computer-aided molecular design (Karunanithi, Achenie and Gani, 2005) for the separation of an azeotropic mixture of acetone and methanol in an extractive distillation process. It is shown that a screening based on entrainer selectivity alone is not sufficient and could possibly lead to an unfavorable entrainer choice. A selection of the most promising entrainers was therefore compared based on the minimum energy demand by a shortcut evaluation of the process with the RBM. These results are then used for the initialization of a rigorous process optimization to determine the total annualized costs of the separation depending on the entrainer choice. Chlorobenzene, although a harmful substance, was determined to be the entrainer yielding the lowest process costs. Later, Kraemer, Kossack and Marquardt (2009) studied the extractive distillation of acetone and methanol with the entrainer chlorobenzene in a complex column system with a side column and entrainer recycle. The complex column configuration was rigorously optimized, but yielded higher costs compared to the simple column process proposed by Kossack et al. (2008) due to significantly larger column diameters.

3.5.3 Evaluation of internally heat-integrated distillation columns

Internally heat-integrated distillation columns (HIDiC) allow for heat integration within a single distillation column. A compressor is applied to operate the rectifying section at an elevated pressure such that heat can be transferred to the stripping section. Although significant energy savings can be achieved using this setup, a considerable increase in investment cost penalizes the application. Furthermore, the additional degrees of freedom, i.e. the choice of the trays for internal heat exchange, complicates the optimal design. Harwardt and Marquardt (2012), Harwardt, Kraemer and Marquardt (2010) and Müller, Hoppe and Wagner (2010) have studied the cost-savings potential of HIDiC designs for the separation of ideal mixtures by means of a rigorous optimization with an objective function comprising energy and capital costs for the column and the compressor. Thanks to the continuous reformulation of the MINLP problem, the optimization could be performed robustly and efficiently.

The results of these studies indicate that HIDiC is only favorable for close boiling mixtures, for which the required pressure increase in the rectifying section is relatively small. The optimal solutions identified indicate that a small number of intermediate heat exchangers at the column ends is cost optimal. The optimal design is therefore conceptually very similar to a conventional column with a heat pump.

3.6 Summary

It was shown in Chapter 3 that the rigorous optimization of complex large-scale distillation processes for multicomponent homogeneous azeotropic mixtures can be accomplished robustly and efficiently when integrated into a process synthesis framework and reformulated as a continuous problem. The shortcut evaluation step preceding the rigorous optimization in the process synthesis framework serves two purposes: on the one hand, flowsheet alternatives for the separation task were screened with the RBM and ranked based on feasibility and minimum energy demand. Thus, the flowsheet superstructure could be efficiently reduced. On the other hand, excellent initial values and bounds for the rigorous optimization were generated due to the minimum reflux condition of the RBM and the optimization of the process operating point. The benefit of a rigorous optimization apart from obtaining useful information about optimal column configurations was demonstrated in Sections 3.4.4 and 3.5. In these studies with complex columns, the selection of the most economic process alternative could not be based on the comparison of the minimum energy duties alone but required the consideration of combined operating and capital costs.

The complex and large-scale tray optimization problems could be solved with unprecedented efficiency, robustness and reliability with the help of a suitable initialization procedure and a continuous reformulation of the MINLP problems. The solution of the reformulated problems was carried out in a procedure of a few successive NLPs with gradually tightened bounds in order to obtain local optima of good quality. The solution times and local optima (total annualized costs) of the reformulated problems were compared with the respective optimization properties for the MINLP solution. By applying the continuous reformulation, the computational time for the rigorous optimization problem of the case study could be cut by at least 90% when compared to the respective MINLP solution, which also benefits from the favorable initialization procedure. Note that the reduction of the computational time is of great benefit when varying specifications for product purities, pressures, feed compositions or cost parameters necessitates numerous design evaluations. In addition, better local optima were identified by the continuously reformulated problems than by the respective MINLP problems.

In the following chapters, the methods of the process synthesis framework are transferred to the synthesis of hybrid separation processes, which pose a major challenge for both conceptual and detailed design, since the coupling of distillation with other unit operations such as decanters, extraction columns, and crystallization cascades significantly increases the number of degrees of freedom.

Chapter 4

Distillation coupled with decantation

Many industrially relevant mixtures exhibit immiscibilities in the liquid phase. Moreover, the use of heterogeneous entrainers allows for the separation of azeotropic multicomponent mixtures in hybrid processes of distillation and decantation. Here, decantation permits a crossing of distillation boundaries. These hybrid processes are therefore usually termed heteroazeotropic distillation. Since both unit operations are well-understood and easy to operate, heteroazeotropic distillation occurs frequently in industrial practice. Cairns and Furzer (1990a), Stichlmair and Herguijuela (1992) and Franke (2006) list various published examples of heteroazeotropic processes. Hence, this type of hybrid process has to be covered by a comprehensive toolbox for conceptual design.

Yet, the design of heteroazeotropic distillation is considerably more complex and less understood than the design of simple distillation. Heterogeneous mixtures pose challenges for the application of shortcut as well as rigorous design methods for several reasons. First of all, the methods for homogeneous systems cannot be applied without an adaptation to handle the decomposition of the liquid phase in the decanter and also on the trays within the column. A robust and efficient phase stability test for the detection of the liquid phase behavior is essential for heteroazeotropic design (Cairns and Furzer, 1990a). Nevertheless, the modeling of phase splits on the column trays leads to additional degrees of freedom for the column profiles. Furthermore, heterogeneous systems always exhibit strong nonlinearities which complicate the application of design methods.

Hence, there are very few publications on design methods for heterogeneous distillation systems. Due to the lack of reliable and efficient phase stability tests, most of them consider immiscibilities only in the decanter but not on the column trays (Pham

et al., 1989; Ryan and Doherty, 1989; Wasylkiewicz, 1999). This practice, however, leads to the disregard of promising designs or miscalculations of the energy demand in many instances (Kovach and Seider, 1987; Cairns and Furzer, 1990b; Urdaneta et al., 2002). A thorough analysis of the properties of heteroazeotropic distillation has been provided by Urdaneta (2005).

The published works on the design of heteroazeotropic distillation are typically based on the inspection of column profiles by means of the BVM (Pham et al., 1989; Ryan and Doherty, 1989; Wasylkiewicz et al., 2003). It has been noted by Pham et al. (1989) that the profiles in heteroazeotropic distillation are very sensitive towards the specification of product impurities, which makes this design procedure even more cumbersome compared to the homogeneous case. Due to the graphical inspection of feasibility inherent to the BVM, the examples of heteroazeotropic distillation design in literature are restricted to separations of ternary mixtures. This restriction also applies to the continuous distillation region method, which was proposed by Urdaneta et al. (2002) for the evaluation of heteroazeotropic distillation. Additional drawbacks of these methods will be shown in Section 4.3.

Ryan and Doherty (1989) proposed a design procedure for the sequencing of ternary heteroazeotropic distillations. They generate alternative flowsheets manually and evaluate these for minimum reflux with the BVM. The operating points of the flowsheets are optimized by a combination of heuristics and simulation studies. The design procedure is therefore rather tedious and cannot guarantee good results. It will be shown in Section 4.7.2 that the heuristics proposed by Ryan and Doherty (1989) are not valid for a similar heteroazeotropic distillation example.

Due to the lack of reliable and efficient design methods, it is the scope of this chapter to extend the process synthesis framework presented in Chapter 2.6 to multicomponent heteroazeotropic distillation. The work presented in this chapter is based on earlier publications by Kraemer, Harwardt and Marquardt (2009b) and Kraemer, Harwardt, Skiborowski, Mitra and Marquardt (2011). A robust and efficient phase stability test for the detection of liquid phase behavior is presented in Section 4.1. Section 4.2 discusses the implications of liquid-liquid phase split within the column on the calculation of tray-to-tray profiles. In Section 4.3, we analyze the applicability of the shortcut methods reviewed in Section 3.1 to heterogeneous mixtures by means of a ternary heteroazeotropic example. The different restrictions of these methods, are pointed out in order to motivate the development of methods for highly non-ideal, heteroazeotropic distillation. Two novel methods are proposed in Sections 4.4 and 4.5. They combine elements of existing methods to overcome their limitations in the context of heterogeneous azeotropic distillation. The extension of the rigorous column

optimization introduced in Section 3.3 to heteroazeotropic distillation is proposed in Section 4.6. Again, the rigorous optimization problems will greatly benefit from a continuous reformulation and an initialization by the shortcut evaluation.

Two case studies will be presented in Sections 4.7.1 and 4.7.2. The first case study demonstrates the application of the novel methods to quaternary heteroazeotropic distillation. The second case study, provided by an industrial partner, covers the optimization-based design of a multi-column heteroazeotropic process.

4.1 Phase stability test

A multiplicity of equilibrium solutions occurs in the miscibility gap of a heterogeneous mixture: Both the physically correct VLLE solution and a physically invalid VLE solution can be calculated. Without a reliable phase stability test, the correct VLLE solution may be omitted in favor of the invalid VLE solution, which then leads to an inaccurate column simulation. Hence, a phase stability test needs to be implemented. This test identifies the number of phases on a candidate tray or at a pinch in order to facilitate an automatic switch from a set of VLE to a set of VLLE equations when the profile or the pinch line crosses the binodale. In case of VLLE, eqs. (3.5), (3.7), (3.15), and (3.17) are replaced by

$$y_{n,i} = K_{n,i}(\mathbf{x}_n^I, T_n, p_n)x_{n,i}^I, \qquad n = 1, ...N,\ i = 1, ..., C, \tag{4.1}$$

$$y_{n,i} = K_{n,i}(\mathbf{x}_n^{II}, T_n, p_n)x_{n,i}^{II}, \qquad n = 1, ...N,\ i = 1, ..., C, \tag{4.2}$$

$$\mathbf{x}_n = \varphi_n \mathbf{x}_n^I + (1 - \varphi_n)\mathbf{x}_n^{II}, \qquad n = 1, ..., N, \tag{4.3}$$

$$h_n^L = h^L(\mathbf{x}_n^I, \mathbf{x}_n^{II}, T_n, p_n), \qquad n = 1, ..., N, \tag{4.4}$$

$$\sum_{i=1}^{C} x_{n,i}^I = 1, \quad \sum_{i=1}^{C} x_{n,i}^{II} = 1, \qquad n = 1, ..., N, \tag{4.5}$$

$$y_{p,i} = K_{p,i}(\mathbf{x}_p^I, T_p, p_p)x_{p,i}^I, \qquad p = 1, ...P,\ i = 1, ..., C, \tag{4.6}$$

$$y_{p,i} = K_{p,i}(\mathbf{x}_p^{II}, T_p, p_p)x_{p,i}^{II}, \qquad p = 1, ...P,\ i = 1, ..., C, \tag{4.7}$$

$$\mathbf{x}_p = \varphi_p \mathbf{x}_p^I + (1 - \varphi_p)\mathbf{x}_p^{II}, \qquad p = 1, ..., P, \tag{4.8}$$

$$h_p^L = h^L(\mathbf{x}_p^I, \mathbf{x}_p^{II}, T_p, p_p), \qquad p = 1, ..., P, \tag{4.9}$$

$$\sum_{i=1}^{C} x_{p,i}^I = 1, \quad \sum_{i=1}^{C} x_{p,i}^{II} = 1, \qquad p = 1, ..., P. \tag{4.10}$$

Rigorous methods for the determination of phase splits based on global optimization (e.g. McDonald and Floudas (1995); Bollas, Barton and Mitsos (2009)) or interval

methods (Hua, Brennecke and Stadtherr, 1998) allow for a guaranteed detection of all liquid phase splits. However, their high computational demand and the requirement for a special model formulation make them less appealing for the application in shortcut methods. Computationally efficient local methods (e.g. Pham and Doherty (1990)), on the other hand, are known to fail when good initial values are not available. An excellent review on different concepts for phase split detection and VLLE calculation procedures is given in the work by Cairns and Furzer (1990a).

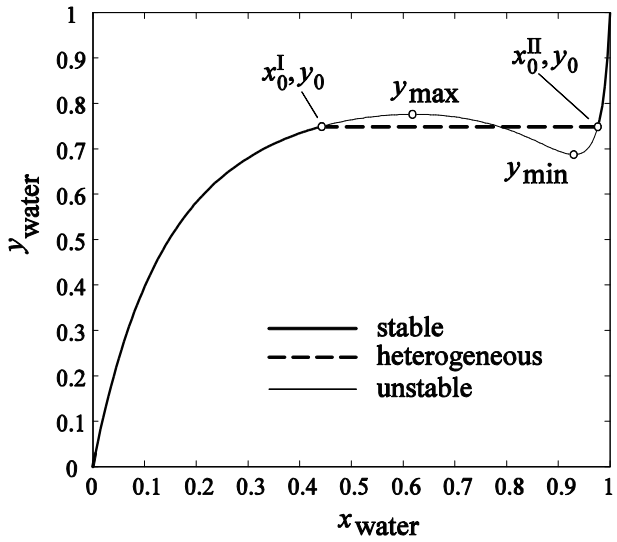

Figure 4.1: Phase stability test: Initialization of the binary miscibility gap for the system water/butanol at p=1.013 bar and boiling temperature (Bausa and Marquardt, 2000a).

In this thesis, an efficient and reliable phase stability test introduced by Bausa and Marquardt (2000a) is applied, a hybrid approach of low computational demand, which is specifically suited for the use in shortcut design procedures. The phase test employs a preprocessing step, where all heterogeneous regions are detected for given pressure and boiling temperature. For this purpose, the VLE of all binary subsystems are searched for local extrema of the vapor phase compositions on the y-x diagram (cf. Fig. 4.1). If no extrema exist, the binary system is homogeneous, since there are no two distinct liquid phases which are in equilibrium with the same vapor phase. For each heterogeneous region a reference state $(\boldsymbol{z}_0, \boldsymbol{x}_0^I, \boldsymbol{x}_0^{II}, \boldsymbol{y}_0, \varphi_0, p_0, T_0)$ is stored. For the very rare cases of heterogeneous regions which do not touch the binary subsystems, Bausa and Marquardt suggest a global search method.

The flash calculations in simulation or optimization runs are then performed by homotopy continuation starting from a stored reference state on a binary edge in a

miscibility gap. The homotopy is given by

$$\mathbf{H}(\mathbf{u}, \lambda) = \lambda \mathbf{F}(\mathbf{u}) + (1 - \lambda)\mathbf{G}(\mathbf{u}), \tag{4.11}$$

where $\mathbf{G}(\mathbf{u})$ is the flash at a reference state and $\mathbf{F}(\mathbf{u})$ is the flash at the composition which is tested for phase stability. In the continuation, λ is gradually increased from 0 to 1. When the binodale is crossed, i.e. when the phase distribution φ leaves the interval $[0, 1]$, VLE behavior is detected. The homotopy continuation guarantees suitable initial values for each calculation step such that the local convergence of the solver is not restrictive. Existing heterogeneous solutions are thus determined reliably, otherwise the homogeneous solution is returned.

4.2 Calculation of tray-to-tray profiles

With the help of the phase test presented in the previous section, tray-to-tray profiles can be calculated also in cases where heterogeneous trays exist inside a column section. The switch from VLE to VLLE calculations, i.e. from eqs. (3.5) and (3.7) to eqs. (4.1)-(4.5), and vice versa can be done automatically.

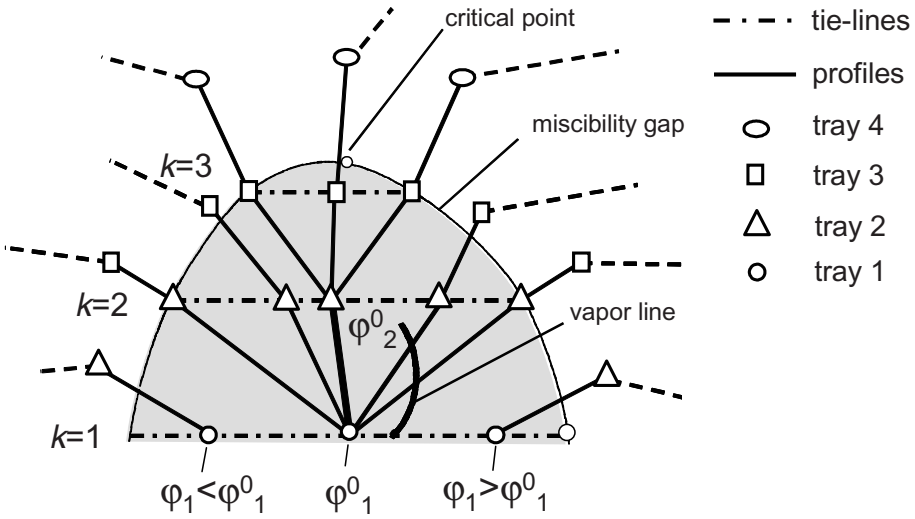

Figure 4.2: Schematic representation of the tree-like structure of the rectifying section profiles within the miscibility gap (Urdaneta et al., 2002). It can be seen that the number of heterogeneous trays k is dependent on the specification of the phase split ratio φ_n.

A specific characteristic of tray-to-tray modeling complicates the downward tray calculation (e.g. for the BVM) when there is heterogeneous behavior in the rectify-

ing section: the course of the rectifying profile within the miscibility gap is not only dependent on the specification of trace components in the distillate, but also on the specification of the liquid phase ratios $\varphi_n = L_n^I/(L_n^I + L_n^{II})$ on the heterogeneous trays. It was shown by Urdaneta et al. (2002) that the liquid phase ratios on the heterogeneous trays are degrees of freedom in the downward tray-to-tray calculation and that only one specific value for the phase ratio on each tray φ_n^0 yields a liquid composition within the heterogeneous region on tray $n+1$. For all other specifications of the liquid phase ratio, the rectifying profile leaves the heterogeneous region. This behavior is illustrated in Fig. 4.2. Instead of specifying the phase splits on all heterogeneous trays, Urdaneta et al. (2002) suggest to specify the number of heterogeneous trays k and the phase ratio on the last heterogeneous tray φ_k to derive suitable values for the other liquid phase ratios $\varphi_{n\neq k}$. Therefore, the downward calculation of trays within the miscibility gap contains the additional degrees of freedom k and φ_k. Note that the upwards calculation of profiles from the reboiler or from any point within the column never requires a specification of k and φ_k, as the liquid phase split on the heterogeneous trays is not a degree of freedom in the upwards calculation (Urdaneta et al., 2002).

The implications of the additional degrees of freedom in the downward profile calculation on the shortcut design methods for heterogeneous distillation will become obvious in Section 4.3.1, where the application of the BVM to heterogeneous distillation is discussed.

4.3 Application of shortcut methods for non-ideal distillation to heteroazeotropic distillation

In this section, the shortcut methods reviewed in Section 3.1 are applied to heteroazeotropic distillation. For this purpose, the methods are supplemented with the phase stability test presented in Section 4.1 to detect liquid-liquid phase split. Furthermore, the assumption of constant molar overflow is dropped, on which most methods reviewed in Section 3.1 rely. Instead, energy balances are added to account for the effects of the strong non-linearity of heteroazeotropic distillation. The strengths and limitations of each method for the heterogeneous case are discussed.

In typical heteroazeotropic designs, a heterogeneous stream is produced at the top of the column and split in a decanter into an entrainer-lean distillate and an entrainer-rich reflux (cf. Fig. 4.3). As an illustrating example we consider a separation of the ternary heterogeneous mixture of isopropanol, water, and cyclohexane defined in Table

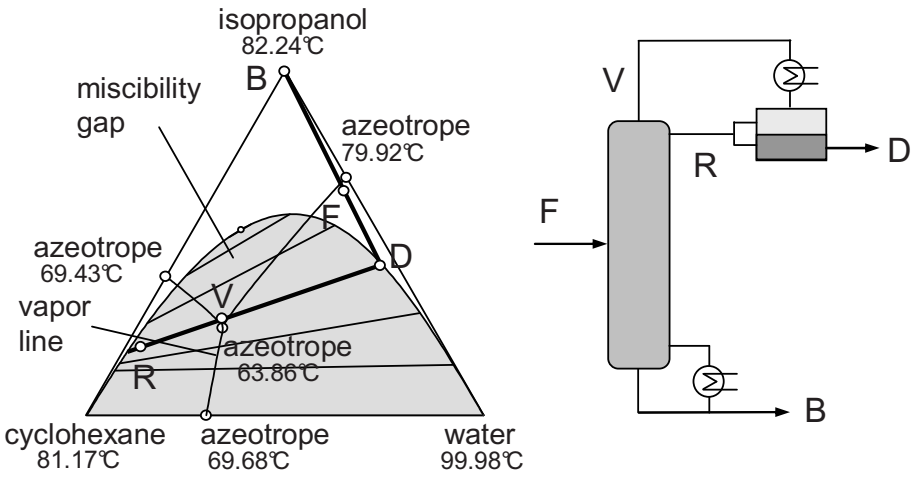

Figure 4.3: Topology of the mixture of isopropanol, water, and cyclohexane at 1.013 bar with column and decanter mass balances for the heteroazeotropic separation in the hybrid process shown on the right.

Table 4.1: Specifications of the heteroazeotropic example separation of a mixture of isopropanol, water, and cyclohexane.

molar composition		
$\mathbf{z}_F$	$\mathbf{x}_D$	$\mathbf{x}_B$
0.665, 0.320, 0.015	0.402, 0.570, 0.028	1, 0, 0
pressure	feed state	g^E-model
1.013 bar	sat. vapor	NRTL

4.1 and Fig. 4.3. The coefficients for the calculation of ideal gas heat capacities and heats of vaporization are given in Tables D.11 and D.20. The parameters for the Antoine vapor pressure equation and the NRTL activity coefficient model were taken from the work by Wang, Wong, Chien, Shih, Liu and Tsai (1998). The mixture exhibits a large miscibility gap between water and cyclohexane as well as three binary azeotropes and one ternary heterogeneous azeotrope, which is the minimum boiler of the system. Pure isopropanol is obtained as the bottoms product and the distillate is drawn off as the water rich phase of the decanter, which is derived from a tie-line close to the minimum-boiling ternary azeotrope. A mixture of both phases (mostly from the organic phase), is recycled back to the column as reflux. Note that the separation mass balance crosses the distillation boundary between the ternary and

the binary azeotrope on the isopropanol-water edge. The vapor profile of the column is however entirely located in the upper distillation region, since the vapor which is drawn off at the top of the column and sent to the decanter has a composition slightly above the ternary azeotrope. The overall mass balance around the distillation column and the decanter is therefore able to cross the distillation boundary in a feasible heteroazeotropic separation.

Table 4.2: MED predicted by various shortcut methods for the heteroazeotropic separation of the ternary mixture specified in Table 4.1.

$Q_{B,\min}/F$ [MJ/kmol]								
rigorous	BVM	RBM	MAC/ZVC	CDRM	Petlyuk	SSLM	FPM	FAM
25.8	31.5	306	27.9	28.9	29.2	25.8	25.8	26.0

4.3.1 Boundary value method

It has been pointed out in Section 4.2 that the downward calculation of tray-to-tray profiles in the heterogeneous region not only depends on the specification of trace components in the products, but also on the number of heterogeneous trays k and the liquid phase ratio φ_k on the last heterogeneous tray. Fig. 4.4 demonstrates that these additional degrees of freedom in heterogeneous distillation complicate the application of the BVM, even for ternary mixtures. Depicted are the rectifying profiles of the sample separation for different isopropanol specifications in the distillate, different number of heterogeneous trays k, and different phase split ratios on the last heterogeneous tray φ_k. Only one of these design parameters is varied in the respective parameter study while all other parameters remain constant. Note that the downward calculation of the rectifying profiles for the BVM for heteroazeotropic distillation is not started at the distillate composition but rather at the reflux composition due to the separation of the two coexisting liquid phases in the decanter. The sensitivity of the rectifying profiles with respect to the design parameters becomes obvious in this study. For the application of the BVM, these design parameters have to be varied in addition to the energy duty in order to determine the particular rectifying profile which intersects with the stripping profile (not shown in Fig. 4.4) at the MED. Hence, this example shows that the evaluation of heteroazeotropic distillation with the BVM is rather cumbersome, even if there are only three components in the mixture and the graphical check for intersection is acceptable. When the effect of liquid phase split

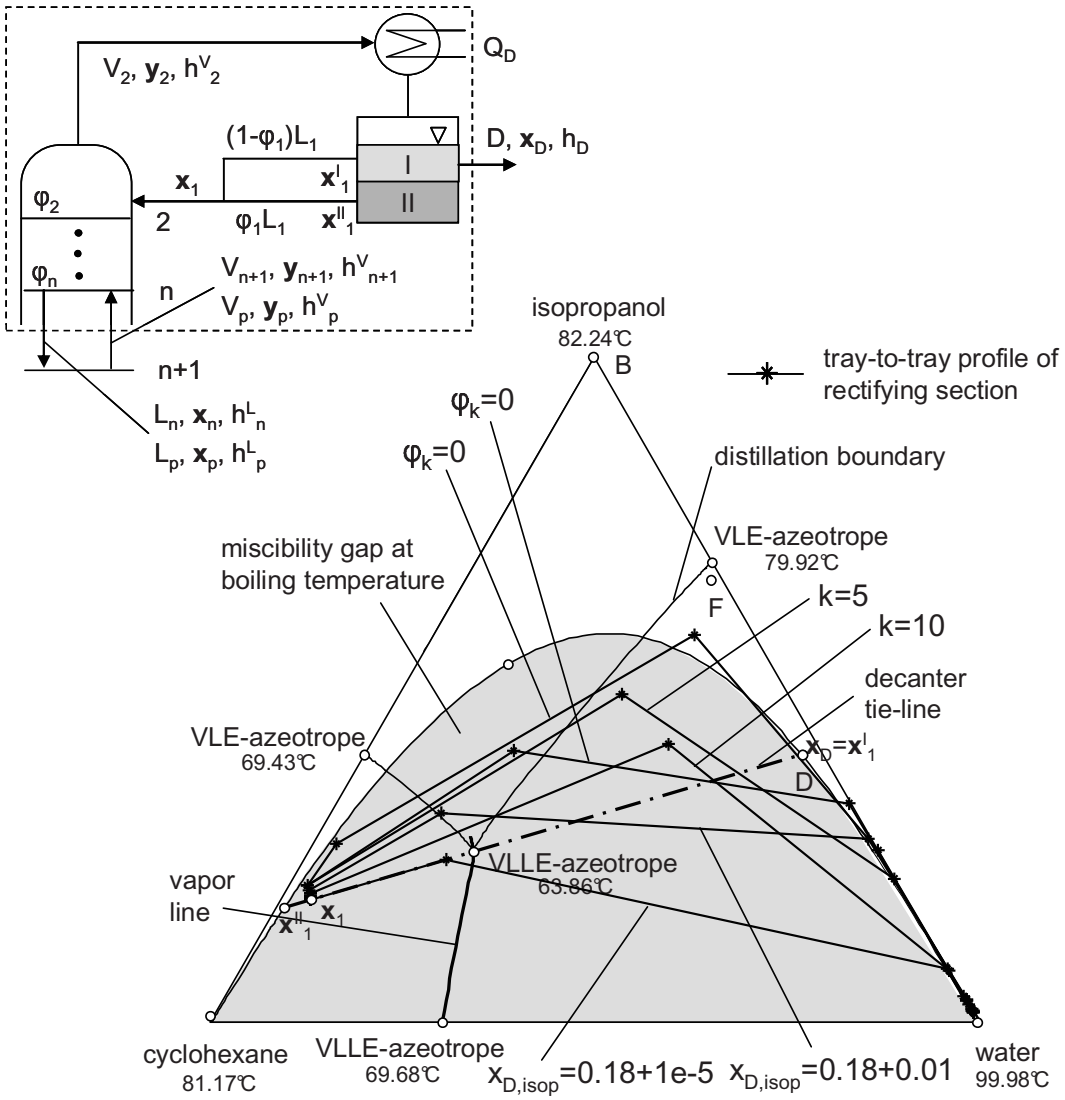

Figure 4.4: Calculation of rectifying section profiles starting from the reflux of the decanter for the BVM. The course of the profiles strongly depends on the specification of product impurities $x_{D,isop}$, the number of heterogeneous trays k and the phase split ratio on the last heterogeneous tray φ_k.

is considered only in the decanter but neglected on the column trays as suggested by Pham et al. (1989), a MED of $Q_{B,min} = 31.5\ MJ/kmol$F is determined, which corresponds to an overestimation by more than 20% (cf. Table 4.2).

4.3.2 Rectification body method

With the help of the phase stability test (cf. Section 4.1), Urdaneta et al. (2002) have extended the procedure for the calculation of the separation pinch points such that all pinch points in the heterogeneous regions are determined reliably. These pinch point solutions allow for an application of the RBM to heterogeneous systems. Bausa (2001) presents a number of examples where the RBM is successfully applied to heteroazeotropic separations. As any pinch-based method, the RBM does not depend on the specification of the number of heterogeneous trays k, the phase split ratio on the last heterogeneous tray φ_k, and the impurities in the products. Since no tray calculations have to be performed, it is a very efficient and user-friendly method.

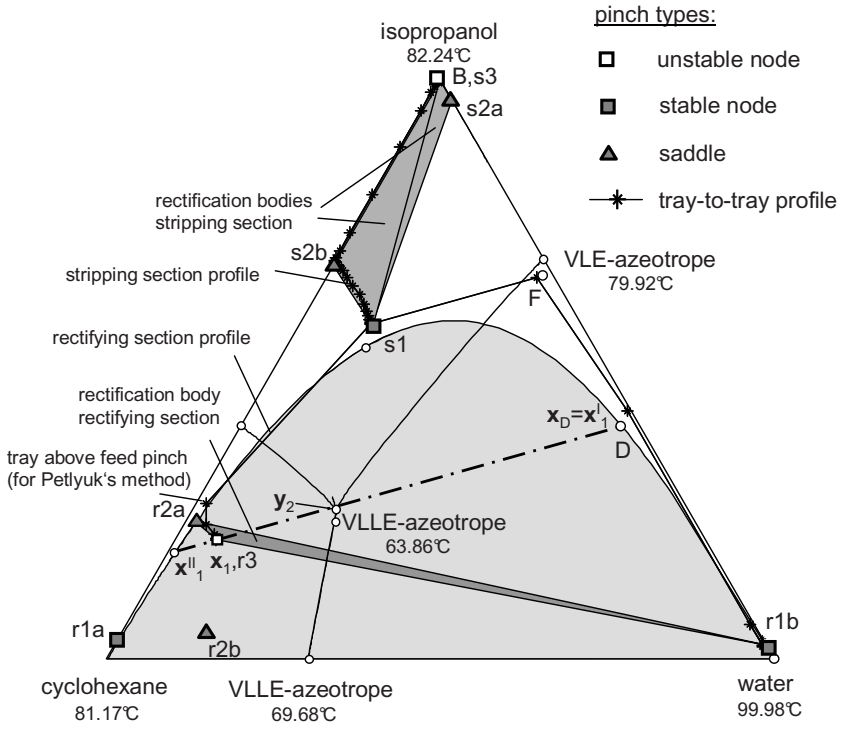

Figure 4.5: Section profiles and relevant rectification bodies for the heteroazeotropic example separation at the rigorously determined MED ($Q_{B,min}/F$ = 25.8 MJ/kmol).

However, the accuracy of the RBM for the MED prediction can be very low for heterogeneous systems, as separations for these systems usually exhibit strongly curved profiles in and close to the region of immiscibility. The rectifying section profile of the example separation is strongly curved towards the isopropanol vertex. While the linear combinations of pinch points at minimum reflux approximate the stripping profiles

very well, they miss the curved profiles of the rectifying section by a large margin as shown in Fig. 4.5. The rectification bodies can be brought to intersection at a significantly higher reflux than the minimum reflux leading to a significant overestimation of the MED (cf. Table 4.2). More examples of inaccurate predictions of the MED for heterogeneous systems by the RBM can be found in Section 4.7. Consequently, the RBM can not be consistently applied to heterogeneous distillation with acceptable approximation error.

4.3.3 Minimum angle and zero-volume criterion

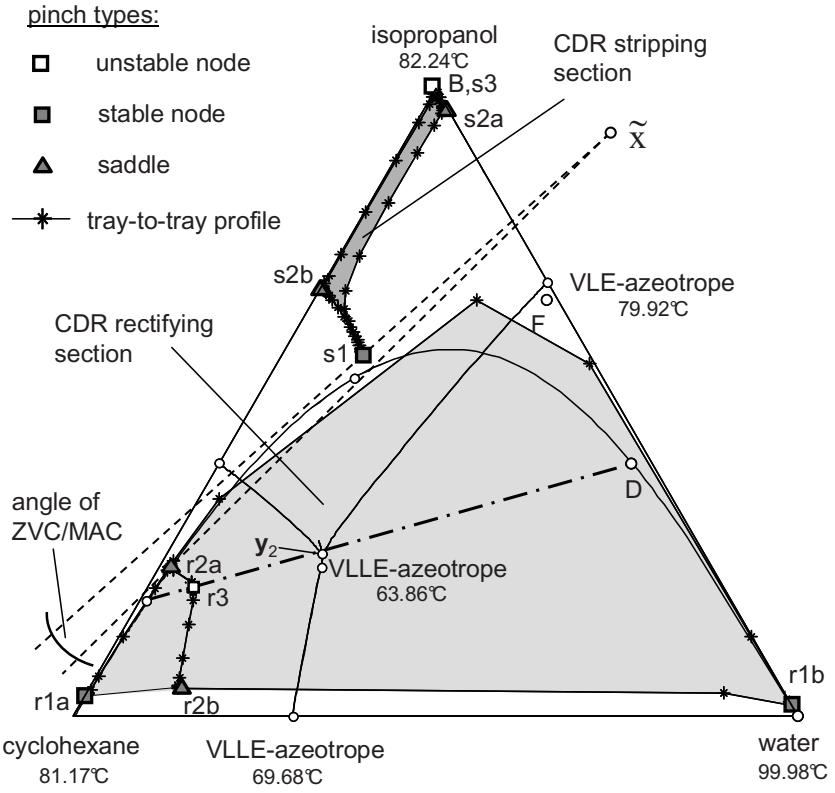

Figure 4.6: Angle of the ZVC/MAC and continuous distillation regions (CDR) for the heteroazeotropic example separation at the rigorously determined MED ($Q_{B,min}/F = 25.8$ MJ/kmol).

The MAC and ZVC can be extended to heterogeneous distillation employing the pinch point analysis for heterogeneous mixtures given by Urdaneta et al. (2002). When the MAC or the ZVC are applied to the example separation, the angle between the line connecting the feed and the stable node pinch of the stripping section *s1* and

the line connecting the feed and the saddle pinch *r2a* of the rectifying section needs to be minimized. As indicated in Fig. 4.6, this angle is quite small at the rigorously determined MED. The angle becomes zero at a slightly higher energy duty. Hence, the MAC or the ZVC overestimates the MED by only 8% in this example (cf. Table 4.2). It should be noted however that the selection of the relevant pinch points, in this case *s1* and *r2a*, is not trivial, especially for mixtures with more than three components.

4.3.4 Continuous distillation region method

As an extension of the eigenvalue criterion, Urdaneta et al. (2002) proposed the continuous distillation region method (CDRM), where curved rectification bodies, so-called continuous distillation regions (CDR), are determined by tray-to-tray calculations starting at an ε-vicinity of the saddle pinch points downwards and upwards in every column section. A single-point intersection of the CDR for the rectifying and stripping section denotes a feasible separation at MED. As a pinch-based method, this procedure has the major advantage over the BVM that the dependency of the profiles - or the CDR - on trace components in the products is eliminated. Since the saddle pinch points describe the extreme locations of the manifold of possible profiles at the specified reflux, the full CDR is identified. For the example mixture, the calculation of the CDR is further simplified by the fact that the heterogeneous region occurs at the top of the column and the relevant saddle pinches are located outside of the heterogeneous region. As a consequence of this property, there is no need to specify k and φ_k as all tray-to-tray calculations within the heterogeneous region are performed upwards. For all other cases, however, k and φ_k still need to be specified properly to determine the full CDR and subsequently the MED. The intersecting CDR of the stripping and rectifying section at the rigorously determined MED are shown in Fig. 4.6 and the MED is given in Table 4.2. The graphical determination of intersection can be accomplished with little effort for this ternary example. Considering the dependence of the profiles on the specification of the ε-distance to the respective saddle pinch point and possibly on the specification of k and φ_k, it is obvious that this manual procedure of trial and error, however, becomes very tedious when processes with several columns connected by a recycle need to be evaluated. Moreover, the construction of multi-dimensional distillation regions out of a few profiles and the check of intersection become impossible for mixtures with more than three components such that the CDRM is effectively limited to ternary systems.

4.3.5 Petlyuk's methodology

Petlyuk (2004) has applied his methodology for the calculation of the MED to ternary heteroazeotropic separations. However, it cannot be deduced from the explanations in this publication whether designs with heterogeneous column trays were considered or if the liquid phase split was only allowed in the decanter.

For the example separation, Petlyuk's shortcut method for a direct split suggests finding the intersection of the line connecting the pinches *r2a* and *r1b* of the rectifying section with the tray above the feed pinch of the stripping section, which is calculated from a simplified mass balance around the feed tray (cf. Fig. 4.5). In order to account for the non-ideality of the example problem, energy balances are added to the original method of Petlyuk, who suggests a constant molar overflow assumption. The corresponding MED is less accurate than the predictions of the MAC and the ZVC (cf. Table 4.2). If the rectification body of the rectifying section is refined by tray-to-tray calculations in a second step as suggested by Petlyuk, the method resembles the CDRM.

4.3.6 Shortest stripping line method

Kraemer, Harwardt, Skiborowski, Mitra and Marquardt (2011) have extended the scope of the SSLM to the separation of heterogeneous mixtures by implementing a phase stability test for the calculation of column profiles which enter the miscibility gap. Furthermore, the constant molar overflow assumption has been dropped and energy balances have been added to the set of tray-to-tray equations. Note that these extensions have not been reported in literature before, though they were indicated already in the original work of Lucia et al. (2008).

The example separation exhibits a feed pinch in the stripping section. The calculation of the stripping section trays is therefore started at the bottoms product. 300 trays are calculated upwards such that the feed pinch point is reached. Here, the switch to the rectifying section is made and 50 trays are calculated upwards from this point. Feasibility of the separation is achieved when the profile reaches the decanter tie-line at the composition of the reflux. When the energy duty is reduced below the MED, the profile does not reach the decanter tie line. In fact, it leaves the composition space as shown in Fig. 4.7. Minimizing the reboiler duty while checking for an intersection of the profile with the decanter tie line yields the MED.

When the feed pinch occurs in the rectifying section, Kraemer, Harwardt, Skiborowski, Mitra and Marquardt (2011) suggest to modify the original SSLM (cf. Sec-

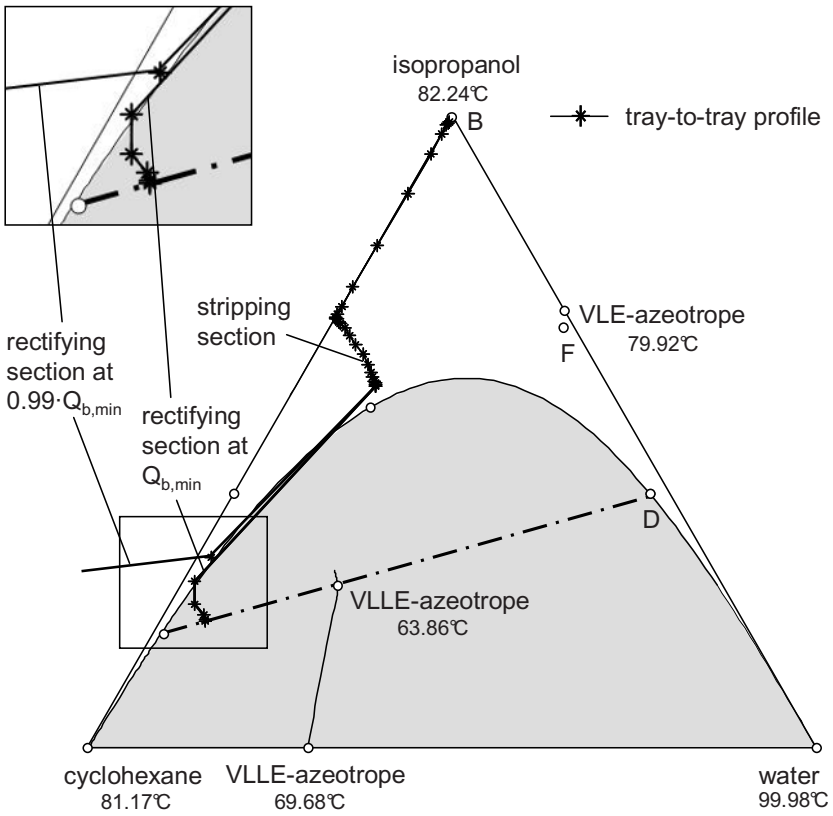

Figure 4.7: Tray-to-tray profile of the SSLM for the heteroazeotropic example separation at the rigorously determined MED ($Q_{B,min}/F = 25.8$ MJ/kmol) and slightly below.

tion 3.1.3) such that the calculation of the profiles is started at the distillate and switched to the stripping section at the feed pinch. Thus, a search for the stripping profile through the feed composition can be avoided.

While the SSLM gives an accurate representation of the MED in the example problem, some drawbacks of the SSLM have been discussed in Section 3.1.3.

4.3.7 Discussion

The application of the existing shortcut methods to heterogeneous distillation has been demonstrated. It has been shown that the disregard of liquid phase split on column trays can lead to a significant miscalculation of the minimum energy demand of heteroazeotropic distillation. The existing methods have therefore been amended with a liquid phase stability test and the equation set for heterogeneous tray and pinch calculations. Furthermore, the constant molar overflow assumption has been dropped by adding energy balances. With these extensions, the methods were applied to heterogeneous distillation with only partial success. Various limitations have been observed, either concerning the accuracy (cf. Table 4.2), the number of components in the mixture, the type of splits, the possible degree of automation, or the computational efficiency. While the MAC/ZVC and the SSLM offer promising performance regarding the accuracy of the MED prediction, they are not universally applicable, at least not in a straight forward manner.

It can be deduced from the analysis of the traditional methods that there is the need for novel shortcut methods for multicomponent heterogeneous distillation. Kraemer, Harwardt, Skiborowski, Mitra and Marquardt (2011) have therefore proposed two novel shortcut methods for heterogeneous distillation by combining elements from the existing methods such that the limitations of these methods can be overcome. These methods are described in the following sections. While the first method (Section 4.4) still shows some limitation, the second method (Section 4.5) is shown to fulfill the following requirements:

- sufficiently accurate,
- applicable to mixtures with any number of components,
- applicable to any kind of sharp split according to the definition in Section 3.1.2,
- fully algorithmic, and
- computationally efficient.

4.4 Feed pinch method

As a first step towards a generally applicable shortcut method for heteroazeotropic distillation, Kraemer, Harwardt and Marquardt (2009b) and Kraemer, Harwardt, Skiborowski, Mitra and Marquardt (2011) have developed the feed pinch method (FPM) for separations characterized by a feed pinch. To this end, a pinch analysis (or the

RBM) is combined with elements from the SSLM. Instead of calculating tray-to-tray profiles from both column ends, the proposed FPM only requires the calculation of one section profile starting from the point that all possible profiles run through, i.e. the feed pinch point. Due to the initialization by a pinch point analysis, the feed pinch of the separation can be determined a priori. Candidate pinches are the stable node pinches of both sections. While the pinch point analysis may yield several possible stable pinch points per column, for sharp splits only one stable pinch point lies on a pinch point curve which runs into the product composition or the decanter tie line of the opposite section. This pinch point approaches the product composition for an infinite amount of trays and an infinite energy supply and can therefore be identified as the feed pinch (cf. Fig. 4.8). For direct or indirect splits, the feed pinch is usually located in the column section where the impure product is drawn off (see also the discussion on splits in Section 3.1.2). The pinch point curves of intermediate or sloppy splits, however, do not run into the product composition of the opposite section. Hence, these splits often exhibit no feed pinch for mixtures with more than three components. The feed pinch method is therefore not generally applicable to intermediate and sloppy splits. Note that one can also perform a RBM to identify the feed pinch. When the rectification bodies intersect at the tip of one body, the intersection marks the feed pinch.

The pinched column section, in our example the stripping section, can then be represented by a rectification body and the respective section profiles do not have to be calculated as the stable pinch can always be reached by the profiles of the respective section. A tangent pinch, as the exception to this rule, can be detected by the pinch reachability check reported by Bausa et al. (1998) (see also Section 3.1.2.3). In this case, the energy is increased until the tangent pinch disappears. The calculation of profiles is only required for the section which does not contain the feed pinch, i.e. when the feed pinch is the stable node pinch of the stripping section, the rectifying section profile is calculated upwards from the feed pinch, which is the case in our example in Fig. 4.8. The tray-to-tray calculation is started at the feed pinch by setting

$$\mathbf{y}_{n_F} = \mathbf{y}_{FP}. \tag{4.12}$$

The rectifying trays located in the homogeneous region are calculated by eqs. (3.1)-(3.7) for $n = 1, ...n_F - 1$. When the phase stability test indicates a phase split, eqs. (3.5) and (3.7) are replaced by eqs. (4.1)-(4.5) for the respective trays. When the feed pinch is the stable node pinch of the rectifying section, the stripping section profile is calculated downwards from the feed pinch.

Feasibility of the separation is detected, when the profile reaches the product composition or the unstable pinch on the decanter tie line, which marks the composition

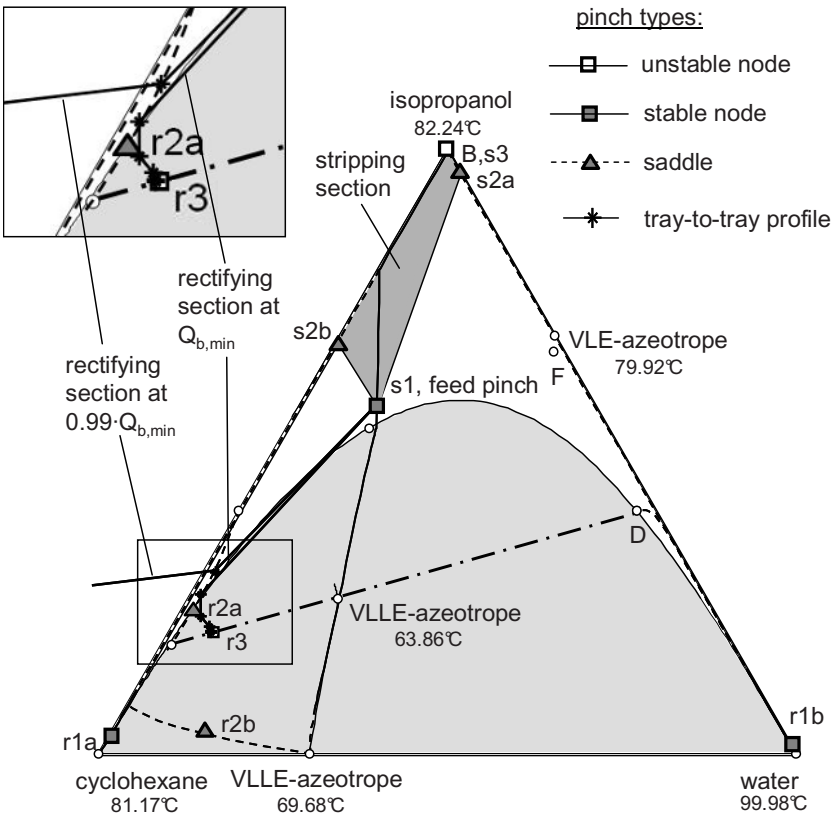

Figure 4.8: Rectification body and tray-to-tray profile of the FPM for the heteroazeotropic example separation at the rigorously determined MED ($Q_{B,min}/F = 25.8$ MJ/kmol) and slightly below.

of the reflux from the decanter. Minimizing the reboiler duty while checking for an intersection of the profile with the product or unstable node yields the MED. If too little reflux is specified, the profile leaves the phase diagram as depicted in Fig. 4.8.

This phenomenon can be further illustrated using McCabe-Thiele diagrams for binary mixtures. At minimum reflux, the operating lines of the rectifying section and the stripping section intersect at the vapor equilibrium line at the feed pinch, resulting in an infinite number of trays for the separation (Fig. 4.9, left). If the energy requirement (or reflux) is reduced below the minimum value, the intersection of the operating lines occurs above the vapor equilibrium line (Fig. 4.9, right). Using the McCabe-Thiele methodology, the profile of the rectifying section, which is constructed between the operating line of the rectifying section and the vapor equilibrium line starting at the feed pinch of the stripping section, does not converge towards the distillate product, but to physically invalid values.

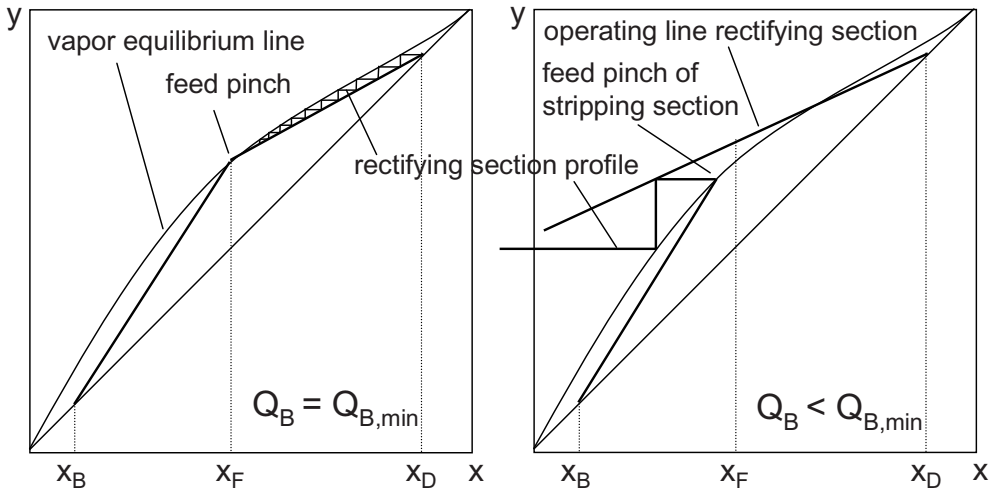

Figure 4.9: Tray-to-tray calculations for the rectifying section of a binary mixture for $Q_B = Q_{B,min}$ (left) and $Q_B < Q_{B,min}$ (right).

The major restriction of the FPM is the requirement of a feed pinch point at the feed tray, where the calculation of the non-pinched column section is started. On the contrary, separations without a pinch at the feed tray cannot be handled as the locus of the feed tray composition cannot be derived from a pinch point analysis.

The check for a feed pinch can be efficiently performed by application of the RBM. When the rectification bodies intersect at the tip of one body, this tip corresponds to the feed pinch (Bausa et al., 1998). On the other hand, an intersection at the edges implies a separation without a pinch at the feed tray. Examples of multicomponent separations without a feed pinch are given by Bausa et al. (1998) and in Appendix B. Note that separations of ternary mixtures usually exhibit a feed pinch, since the rectification bodies typically intersect at the tip of one body. When the initialization by the RBM indicates a feed pinch, the FPM can be applied. For these pinched separations, the FPM offers a number of benefits as pointed out in the following.

For the calculation of profiles, the BVM and the CDRM demand a slight, user-specified perturbation from pure products or saddle pinches, respectively. In contrast, the calculation of the profile for the FPM can be started directly at the feed pinch and, thus, the course of the profile does not depend on the type of perturbation. An additional benefit of the FPM is the independence of the results from the specification of the design variables k and φ_k for heterogeneous distillation. For an explanation of this property, different cases have to be considered:

- When the feed pinch occurs in the stripping section, i.e. when the MED is

determined by the profile of the rectifying section (cf. Fig. 4.8), k and φ_k do not need to be specified, since the tray calculation of the rectifying section is carried out upwards from the feed pinch (Urdaneta et al., 2002).

- When the feed pinch occurs in the rectifying section, i.e. when the MED is determined by the profile of the stripping section calculated downwards form the feed pinch, two scenarios need to be distinguished:
  - The heterogeneous region is located at the top of the column: In this case, the stable node pinches of the rectifying section including the feed pinch are always located outside of the heterogeneous region since one eigenvalue of the pinch equation system is always infinite (Bausa, 2001). Therefore, no heterogeneous trays have to be considered in the stripping section.
  - The heterogeneous region is located at the bottom of the column: In this case, it can be assumed that the stripping profile is located entirely in the heterogeneous region or does not leave the heterogeneous region once it has entered it. With this assumption, there is only one viable specification for the liquid phase ratios on the trays of the stripping section such that the profile does not leave the heterogeneous region but reaches the decanter at the bottom.
- To the best knowledge of the author, there are only very few examples where the heterogeneous region is located in the middle of the column or the column profile repeatedly enters and leaves the miscibility gap. These cases are not yet covered by the FPM.

Due to the independence on specification of k, φ_k, and the trace components, the profile which has to be calculated within the FPM for the determination of feasibility and MED is a function of the energy duty, the pressure, and the feed and the product specifications only.

Like the SSLM, the FPM benefits from a simple feasibility check for direct and indirect splits. Contrary to the BVM and the CDRM, where a multitude of possible profiles have to be checked for intersection in multi-dimensional space, the feasibility check of the FPM for direct or indirect splits offers the following advantages:

- Only one profile needs to be calculated and checked for intersection.
- The intersection occurs at a well-defined location (product composition/unstable node/decanter tie-line).
- Only tray N has to be checked since the profile converges to the unstable node, i.e. the product composition, if enough energy is supplied.

As a consequence, the feasibility check can easily be automated for direct and indirect splits. Like the SSLM, however, the FPM suffers the drawback that an automation of the feasibility check for intermediate or sloppy splits is more challenging. For these splits, the entire section profile needs to be checked for intersection with the end product (see also Section 3.1.3, SSLM).

The application of the FPM to the ternary example is shown in Fig. 4.8. The profile of the rectifying section starts at the feed pinch, i.e. the stable pinch of the stripping section, and reaches the unstable pinch of the rectifying section on the decanter tie line, which marks the composition of the reflux from the decanter. The MED, for which this is possible, is accurately determined to be $Q_{B,min} = 25.8\ MJ/kmol\text{F}$.

4.5 Feed angle method

While the FPM returns an accurate representation of the MED, it can only be applied to separations with a feed pinch, i.e. usually direct or indirect splits for mixtures with more than three components (but usually all types of splits for ternary mixtures, see definition of splits in Section 3.1.2). In addition, the FPM still requires tray-to-tray calculations for one column section such that it is not suited as a shortcut method for process optimization problems in an early design phase. The feed angle method (FAM), which was proposed by Kraemer, Harwardt and Marquardt (2010) and by Kraemer, Harwardt, Skiborowski, Mitra and Marquardt (2011), resolves both of these issues, since it does not rely on numerous tray-to-tray calculations and can be applied to any kind of sharp split. In order to achieve this goal, the FAM revives conceptual elements of the MAC, the ZVC and Petlyuk's methodology and combines these with the FPM such that only one tray per non-pinched section has to be calculated.

Like the FPM, the FAM is initialized by a pinch point analysis (or a RBM), which provides information about the relevant pinch points, identifies possible tangent pinches, and determines an initial value for the MED. For the application of the FAM, it needs to be distinguished between separations with or without a feed pinch (see Section 3.1.2 for comments on splits and pinches).

When a feed pinch is identified in the initialization by the RBM, the pinched section can be approximated by a rectification body as in the FPM since all possible profiles in the pinched section terminate at the feed pinch. The FAM then approximates the MED by the calculation of only one tray above or below the feed tray in the non-pinched column section similar to the shortcut procedure of Petlyuk. In the example considered in Fig. 4.10, the rectifying tray above the pinched feed tray is computed.

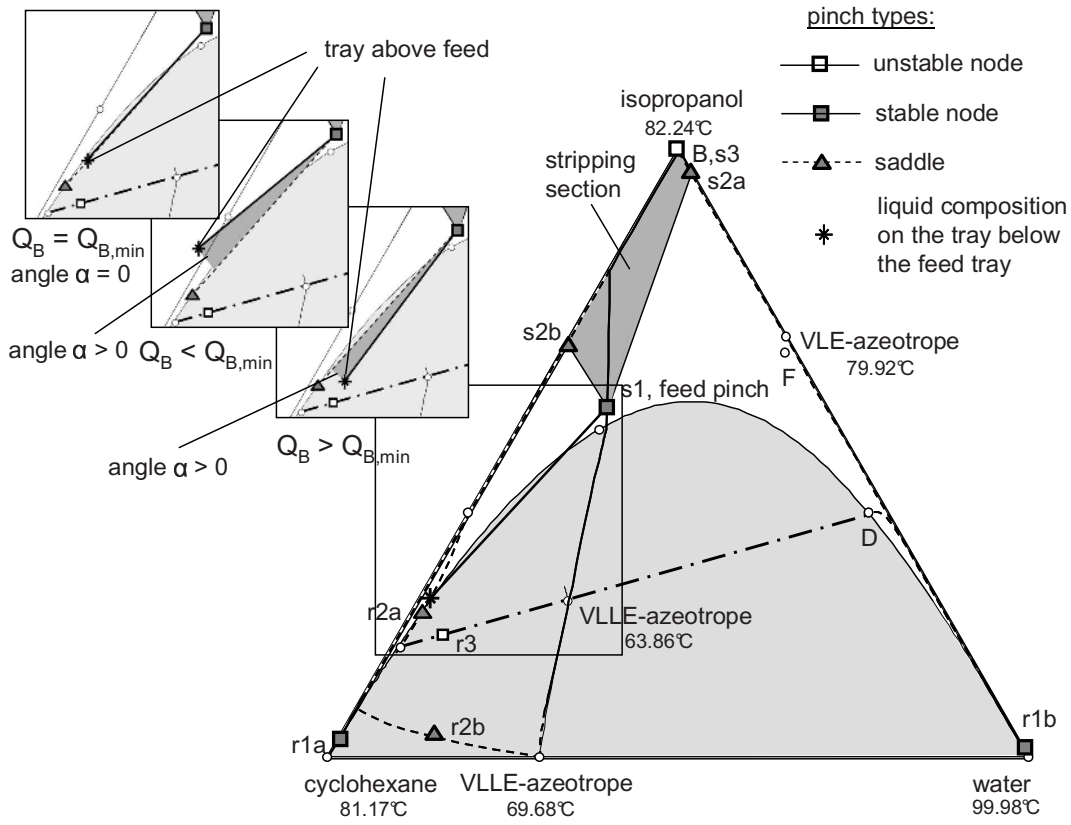

Figure 4.10: Rectification body and tray above the feed pinch in the FAM for the heteroazeotropic example separation at the rigorously determined MED ($Q_{B,min}/F = 25.8$ MJ/kmol) and slightly below and above.

In contrast to Petlyuk's method, however, Kraemer, Harwardt, Skiborowski, Mitra and Marquardt (2011) do not resort to a simplified calculation of this tray under the assumption of constant molar overflow. Note that the line through the feed composition and the feed pinch in the MAC and the ZVC is also defined by a constant molar overflow assumption. While this is a valid approximation in case of a feed pinch and saturated liquid feed due to the close proximity of the vapor compositions on the trays at the feed pinch, the approximation becomes poor if these conditions are not fulfilled (cf. Appendix B). For this reason, the rectifying tray above the pinched feed tray is calculated rigorously by appropriate mass and energy balances and the equilibrium condition, i.e. by eqs. (3.1)-(3.7) in the homogeneous or by eqs. (3.1)-(3.4), (3.6), (4.1)-(4.5) in the heterogeneous case for $n = n_F - 1$.

This tray is then used for the detection of the MED in an algorithmic optimization procedure. Instead of checking the intersection of the tray above the feed tray with

the linearized rectifying section as in Petlyuk's procedure, Kraemer, Harwardt, Skiborowski, Mitra and Marquardt (2011) apply an approach similar to the MAC, where the angle to the relevant saddle pinch point is minimized. For the example separation, the angle between the line connecting the feed pinch *s1* and the tray above the feed pinch and the line connecting the feed pinch *s1* and the relevant saddle pinch *r2a* is minimized. When the line through the tray is located closer to the unstable node on the decanter tie-line than the line through the saddle pinch, the specified energy duty is larger than the required energy duty (cf. Fig. 4.10). Likewise, the energy duty is lower than the MED when the unstable node on the decanter tie-line and the line through the tray are located on opposite sides of the line through the saddle pinch. Mathematically, the FAM for the separation of a ternary mixture and a feed pinch in the stripping section can be formulated as follows:

$$\begin{aligned}
\max \quad & \cos(\alpha), && && (4.13)\\
\text{s.t.} \quad & eqs.\ (3.11)-(3.13), && p \in P_{SP}, && (4.14)\\
& eqs.\ (3.18)-(3.20), && p = p_{FP}, && (4.15)\\
& eqs.\ (3.14)-(3.17), (4.6)-(4.10), && p \in \{P_{SP}, p_{FP}\}, && (4.16)\\
& eqs.\ (3.1)-(3.7), (4.1)-(4.5), && n = n_F - 1, && (4.17)\\
& eqs.\ (4.12), && && (4.18)\\
& \cos(\alpha) = \frac{(\mathbf{x}_{SP} - \mathbf{x}_{FP})^T (\mathbf{x}_{n_F-1} - \mathbf{x}_{FP})}{\|\mathbf{x}_{SP} - \mathbf{x}_{FP}\|_2 \|\mathbf{x}_{n_F-1} - \mathbf{x}_{FP}\|_2}. && && (4.19)
\end{aligned}$$

Note that the maximization of $\cos(\alpha)$ corresponds to a minimization of the angle α, but allows for an easier mathematical formulation. The feed pinch and the relevant saddle pinch points are calculated by eqs. (4.14)-(4.16). The tray above the pinched feed tray is computed by eqs. (4.17) and (4.18). When the feed pinch is located in the rectifying section (e.g. for indirect splits), the tray below the feed pinch and the angle to the relevant saddle pinch in the stripping section are calculated. Feasibility can be assumed when the angle is minimized to zero. The MED determined in this manner is a very good approximation: For the example separation it is only 1% larger than the MED calculated with the more rigorous FPM (cf. Table 4.2). Thus, the FAM gives a better approximation of the MED than the conventional angle methods (ZVC/MAC) reviewed in Section 4.3.3.

4.5.1 Multi-component mixtures

In mixtures with more than three components, more than two pinch solutions are taken into account. Again, the identification of the relevant pinch points for the

FAM can be achieved by means of an initialization by the RBM: The feed pinch and the saddle pinches of the rectification plane which intersects with the feed pinch are selected to construct the angle (cf. Fig. 4.11). Then, a hyperplane defined by the feed pinch and the relevant saddle pinches is constructed by means of the normal vector $\mathbf{n}_{SP,FP}$. Comparable to ternary separations, feasibility and the MED are identified when the tray above or below the feed pinch in the non-pinched section is located in this hyperplane. The angle between the line connecting the feed pinch with the tray above or below the feed pinch and the hyperplane is then given by

$$\cos(\alpha) = \frac{\mathbf{n}_{SP,FP}{}^T(\mathbf{x}_{n_F-1} - \mathbf{x}_{FP})}{\|\mathbf{n}_{SP,FP}\|_2 \|\mathbf{x}_{n_F-1} - \mathbf{x}_{FP}\|_2}, \tag{4.20}$$

which replaces eq. (4.19) in the formulation of the FAM above.

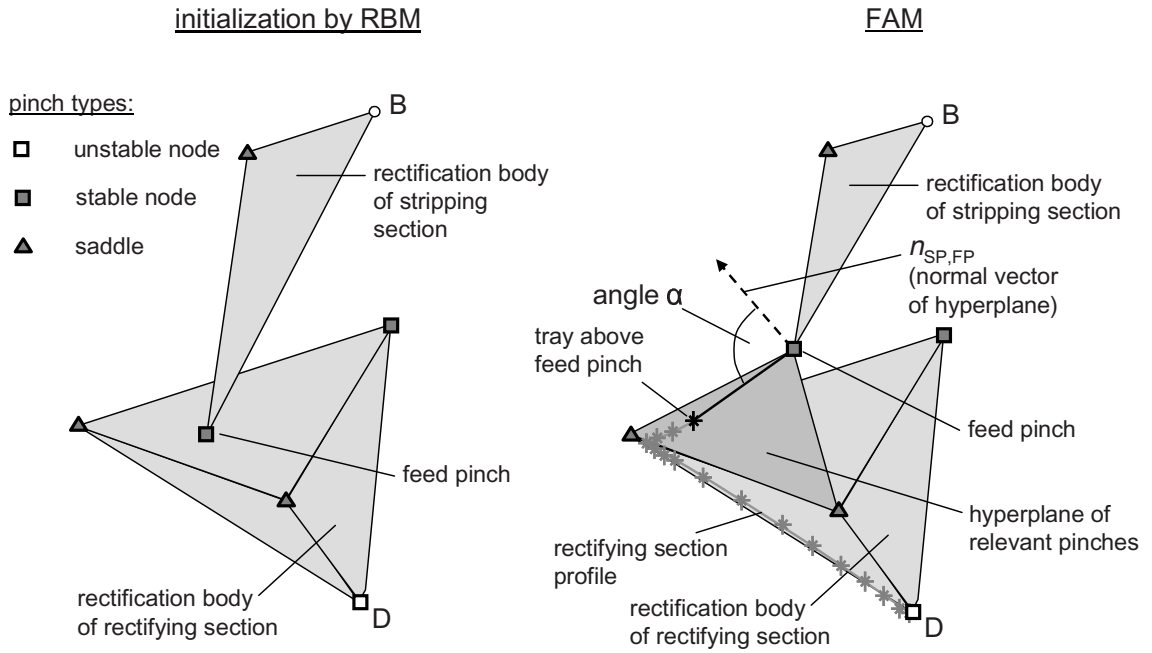

Figure 4.11: FAM for a fictitious separation of a quaternary mixture: Identification of the relevant pinches by an initialization with the RBM (left) and illustration of the construction of the angle between the tray and the hyperplane of the relevant pinches (right).

When the tray is located in the hyperplane, the normal vector is perpendicular to the line connecting the feed pinch and the tray such that $\cos(\alpha)$ becomes zero and eq. (4.13) needs to be replaced by

$$\min \quad (\cos(\alpha))^2. \tag{4.21}$$

Examples of quaternary and quinternary mixtures are given in Sections 4.7.1 and 5.4.3, respectively.

4.5.2 Extension to multi-column processes

Since the FAM is fully algorithmic and computationally efficient, it is perfectly suited for the evaluation of multi-column processes with recycles as shown in the case study in Section 4.7.2. Here, the algorithmic nature of the FAM enables an optimization of the process operating point, i.e. the recycles. For such a process optimization, however, the minimum angle objective (eq. (4.13) or eq. (4.21)) needs to be replaced by a minimum process energy objective:

$$\min \quad \sum_c Q_{B,c}. \tag{4.22}$$

The angles determined by the FAM are then simply set to zero by

$$\cos(\alpha) = 1, \tag{4.23}$$

if the angle is calculated according to eq. (4.19) for a ternary mixture, or by

$$\cos(\alpha) = 0, \tag{4.24}$$

if the angle is calculated according to eq. (4.20) for a multi-component mixture. Alternatively, a positive slack variable ε could be added to the above equations such that eq. (4.22) reads as

$$\min \quad \sum_c Q_{B,c} + M \cdot \varepsilon. \tag{4.25}$$

Here, M is a sufficiently large constant. Eq. (4.23) is then substituted by

$$-\varepsilon \leq \cos(\alpha) - 1 \leq \varepsilon, \tag{4.26}$$

or eq. (4.24) is substituted by

$$-\varepsilon \leq \cos(\alpha) \leq \varepsilon. \tag{4.27}$$

The FAM gives a strong indication for separation feasibility if the angle can be minimized to zero. Still, it needs to be noted that feasibility cannot be guaranteed by the FAM as proposed above. When the compositions of the recycles and intermediate flowsheet streams are released to optimize the process operating point, the implementation of formulations to enforce distillation boundaries may be necessary.

Rigorous representations of the boundaries (e.g. via pinch distillation boundaries, see Brüggemann and Marquardt (2011a)) proved to be computationally expensive and restrict their applicability in shortcut evaluations as discussed in Section 3.4.1. Linear approximations between singular points, on the other hand, can easily be added. However, these approximations are rather inaccurate when the boundaries are curved.

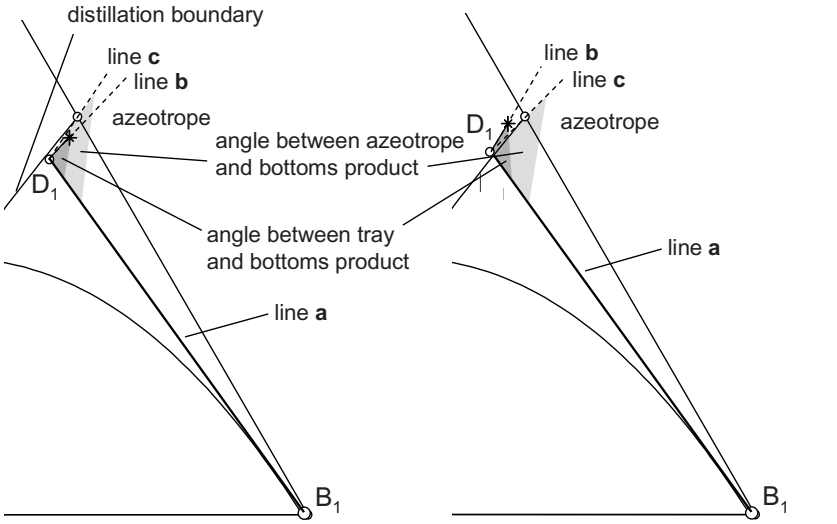

Figure 4.12: Enforcement of distillation boundaries by the FAM for column 1 of the case study in Section 4.7.2: Angle criterion is fulfilled for a feasible separation (left) and violated for an infeasible separation (right).

Kraemer, Harwardt, Skiborowski, Mitra and Marquardt (2011) propose a more accurate approximation for the enforcement of distillation boundaries in the optimization of multi-column processes by an extension of the FAM. This approach again relies on the calculation of angles. The formulation is illustrated by Fig. 4.12, which shows the separation in column 1 of the case study in Section 4.7.2. The location of the distillate composition of this separation is restricted by a distillation boundary (see also Fig. 4.18). Kraemer, Harwardt, Skiborowski, Mitra and Marquardt (2011) suggest to calculate the composition of the liquid on the topmost tray, which is in equilibrium with the vapor stream to the condenser. For the feasibility check, lines are drawn from the distillate to the topmost tray, to the bottoms product, and to the binary azeotrope at the end of the distillation boundary, respectively. For an indication of feasibility, the angle between the lines to the tray and the bottoms product (line b and line a in Fig. 4.12) needs to be smaller than the angle between the lines to the azeotrope and the bottoms product (line c and line a). The left part of Fig. 4.12 illustrates this condition. For an infeasible separation on the other hand,

i.e. when the distillate is located across the distillation boundary, the angle between the tray and the bottoms product (between line b and line a) becomes larger than the angle between the azeotrope and the bottoms product between line c and line a). This condition is shown in the right part of Fig. 4.12. By means of this criterion, the limitation by distillation boundaries could be effectively enforced within process optimization problems as long as the boundaries are not strongly curved. However, a proof of general applicability has not been attempted.

4.5.3 Separations with a tangent pinch

The absence of a tangent pinch is a necessary requirement for the feasibility of distillation. In the RBM, the energy duty is therefore increased until the tangent pinch disappears. This condition is indicated by overlapping rectification bodies at the MED (cf. column 1 in Fig. 4.20 in Section 4.7.2). When the initialization with the RBM reveals that a separation is controlled by a tangent pinch, the FAM proposed above cannot be applied, since it cannot determine the appearance of tangent pinches. This is especially true when the FAM is applied in a gradient-based minimization of the energy demand of a column sequence as in the example in Section 4.7.2, since constraints enforcing the absence of tangent pinches are very difficult to formulate in a mathematical programming problem. Kraemer, Harwardt, Skiborowski, Mitra and Marquardt (2011) therefore propose a different approach for the extension of the FAM to separations with tangent pinches in the following.

Instead of minimizing the angle or the energy duty under the condition that the tangent pinch just vanishes, one can also determine the MED by maximizing the energy duty under the condition that a tangent pinch just appears. The appearance of a tangent pinch can easily be enforced by adding yet another pinch equation system (eqs. (3.11)-(3.17)) to the formulation of the FAM. A maximization of the energy duty such that the tangent pinch equation system is solved then yields the MED. In addition, eqs. (4.23) or (4.24) setting the angle of the FAM to zero need to be dropped, since the rectification bodies overlap at MED (cf. Fig. 4.20). Instead, a constraint is added, which forces the stable node pinch *r1* of the section controlled by a tangent pinch to be located in the adjacent rectification body. The formulation of this condition is given here exemplarily for the separation in column 1 of the example in Section 4.7.2 (cf. Fig. 4.20). The angle between the tray below the stable node pinch *r1* and the bottoms product needs to be smaller then the angle between the

saddle pinch *s2* and the bottoms product, in particular,

$$\frac{(\mathbf{x}_{n_F+1} - \mathbf{x}_{n_F})^T(\mathbf{x}_B - \mathbf{x}_{n_F})}{\|\mathbf{x}_{n_F+1} - \mathbf{x}_{n_F}\|_2 \|\mathbf{x}_B - \mathbf{x}_{n_F}\|_2} \geq \frac{(\mathbf{x}_{p_{SP}} - \mathbf{x}_{n_F})^T(\mathbf{x}_B - \mathbf{x}_{n_F})}{\|\mathbf{x}_{p_{SP}} - \mathbf{x}_{n_F}\|_2 \|\mathbf{x}_B - \mathbf{x}_{n_F}\|_2}. \tag{4.28}$$

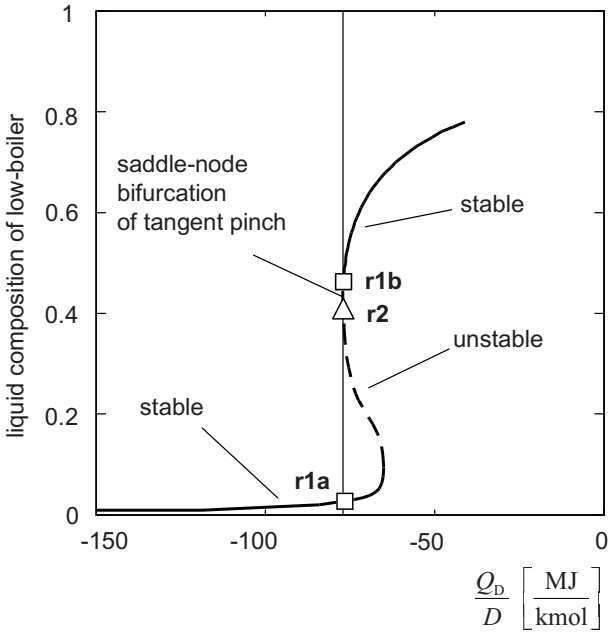

Figure 4.13: Pinch points of the rectifying section of a fictitious separation for an energy duty just below tangent pinch condition (Bausa, 2001).

For the optimization of multi-column processes, however, the maximization of the energy duty for columns controlled by a tangent pinch conflicts with the overall objective of minimizing the process energy duty. The maximization of the energy duty can be dropped when the condition illustrated in Fig. 4.13 is formulated for the column controlled by a tangent pinch (Bausa, 2001): In case of tangent pinch control, a pair of pinches, i.e. a saddle pinch (*r1b*) and a stable node pinch (*r2*, the tangent pinch), appear in the pinched section. At the maximum energy duty for which the tangent pinch still occurs, the pair of pinches merges to a single pinch point. Mathematically, this condition can be formulated by calculating these two pinch points, which are forced to be located in an ε-distance from each other:

$$\|\mathbf{x}_{p_{r1b}} - \mathbf{x}_{p_{r2}}\|_2 = \varepsilon. \tag{4.29}$$

When eq. (4.29) is added to the problem, the MED of columns controlled by a tangent pinch can be calculated reliably, even within the optimization-based evaluation of multi-column processes.

4.5.4 Discussion

To summarize, the FAM can be interpreted as a refinement of the RBM to assess the MED for separations of highly non-ideal mixtures. In the initialization step, the RBM determines whether a feed pinch is present, identifies possible tangent pinches and the relevant saddle pinches, and gives a rough estimation of the MED. In the second step, the FAM adds an additional vertex in form of the tray above or below the feed tray to the non-pinched rectification body in order to account for the curvature of the profiles. While the adjusted rectification bodies of the FAM are still linearized and therefore approximated, the refinement of the linearization results in very good estimations for the MED for many separations as evidenced by the case studies in Section 4.7.

Furthermore, the FAM determines the MED with a very efficient use of computational resources, since the search for relevant pinch points and the analysis of their stability are accomplished in the initialization with the RBM. The FAM then uses only the relevant pinch points and can therefore be integrated effectively into gradient-based process optimization problems. It needs to be mentioned that the selection of relevant pinches can vary within a process optimization, e.g. when the operating point shifts dramatically such that a direct split becomes an indirect split. In this case, the application of the FAM will lead to a miscalculation of the MED. In the experience of the author, however, this limitation is rarely observed, provided that the operating point within the initialization by the RBM is chosen wisely (e.g. minimal recycle streams).

The formulations by eqs. (4.23) and (4.24) imply that the angles can always be minimized to zero when a feasible separation is specified. This was indeed the case for all feasible separations which have been evaluated with the FAM for this thesis. However, a physical explanation for this assumption cannot be provided at this point. It is certainly of interest to further analyze this condition in order to provide a theoretical foundation.

The feasibility check proposed in Section 4.5.2 prevents the crossing of distillation boundaries within the optimization of the operating point of a multi-column process with recycles. As noted in Section 4.5.2, however, this feasibility check is based on an approximation. While this approach proved to be very accurate for distillation boundaries which are not strongly curved, the accuracy can be lower for strongly curved boundaries. Future work will therefore focus on a more rigorous feasibility check based on a-priori calculation and polynomial interpolation of pinch-distillation boundaries (see also Section 8.1.2).

4.6 Rigorous optimization

Besides optimal tray numbers, feed tray locations and optimal operating and capital costs, the rigorous optimization of heteroazeotropic distillation can also provide information about the occurrence of liquid-liquid phase split on column trays. To the author's knowledge, however, there are no examples of rigorous optimization of heteroazeotropic distillation columns in literature. The increased complexity and lack of a robust and efficient phase stability test have so far prohibited the solution of these optimization problems.

In this thesis, the rigorous optimization could be performed for the first time thanks to the addition of the phase stability test of Section 4.1 and the continuous reformulation of the MINLP problem. The necessary extensions to the column model are given in the following.

4.6.1 Rigorous column model

The rigorous optimization model for heteroazeotropic distillation is based on the model for homogeneous distillation given in Section 3.3.1. The optimization superstructure for a heteroazeotropic column with a decanter at the top and variable feed, reflux, and reboil tray locations is shown in Fig. 4.14.

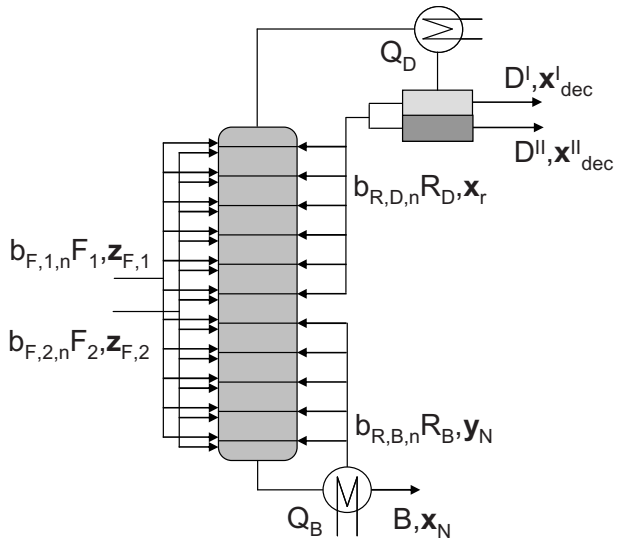

Figure 4.14: Optimization superstructure of a heteroazeotropic column with a decanter at the top and variable feed, reflux, and reboil tray locations.

In the rigorous model for homogeneous distillation (eqs. (3.21)-(3.40)), the equations for the condenser (eqs. (3.24) and (3.25)) are replaced by

$$0 = V_{n+1} - L_{dec} \qquad n = 1, \tag{4.30}$$

$$0 = y_{n+1,i} - x_{dec,i}, \qquad n = 1,\ i = 1, ..., C, \tag{4.31}$$

$$0 = V_{n+1} h^V_{n+1} - L_{dec} h^L_{dec} + Q_D, \qquad n = 1. \tag{4.32}$$

Mass and energy balances for a decanter at the top of the column are added by

$$0 = L_{dec} x_{dec,i} - R_D x_{r,i} - D^I x^I_{dec,i} - D^{II} x^{II}_{dec,i}, \qquad i = 1, ..., C, \tag{4.33}$$

$$0 = L_{dec} h^L_{dec} - R_D h^L_r - D^I h^{L,I}_{dec} - D^{II} h^{L,II}_{dec}, \tag{4.34}$$

$$1 = \sum_i x_{dec,i},\ 1 = \sum_i x^I_{dec,i},\ 1 = \sum_i x^{II}_{dec,i},\ 1 = \sum_i y_{dec,i},\ 1 = \sum_i x_{r,i}. \tag{4.35}$$

Here, $x_{r,i}$ and h^L_r denote the composition and enthalpy of the reflux from the decanter. A decanter at the bottom of the column or connected to the column by side streams can also be implemented with little changes in the model equations. The VLLE equations for the decanter are given by

$$y_{dec,i} = K_{n,i}(\mathbf{x}^I_{dec}, T_{dec}, p_{dec}) x^I_{dec,i}, \qquad i = 1, ..., C, \tag{4.36}$$

$$y_{dec,i} = K_{n,i}(\mathbf{x}^{II}_{dec}, T_{dec}, p_{dec}) x^{II}_{dec,i}, \qquad i = 1, ..., C, \tag{4.37}$$

$$\mathbf{x}_{dec} = \varphi_{dec} \mathbf{x}^I_{dec} + (1 - \varphi_{dec}) \mathbf{x}^{II}_{dec}, \tag{4.38}$$

$$h^{L,I}_{dec} = h^L(\mathbf{x}^I_{dec}, T_{dec}, p_{dec}), \tag{4.39}$$

$$h^{L,II}_{dec} = h^L(\mathbf{x}^{II}_{dec}, T_{dec}, p_{dec}), \tag{4.40}$$

$$h^L_{dec} = \varphi_{dec} h^{L,I}_{dec} + (1 - \varphi_{dec}) h^{L,II}_{dec}. \tag{4.41}$$

In order to allow liquid-liquid phase split on all column trays, VLE and VLLE equations were considered for each tray. The correct identification of phase split was accomplished by the efficient phase stability test described in Section 4.1. When this test detects phase split on a column tray, the VLE set of equations (eqs. (3.31), (3.33)) is automatically replaced by the VLLE set of equations (eqs. (4.1)-(4.5)).

It needs to be noted that the phase stability test and the VLE or VLLE equations for the column trays and the decanter are encapsulated and solved within an external function, which is called by the NLP solver in GAMS. This approach facilitates a robust and efficient execution of the phase stability test. For the column trays, the total liquid and vapor phase compositions $\mathbf{x}_n$, $\mathbf{y}_n$ and enthalpies h^L_n and h^V_n are exchanged between the external function and GAMS in case of either VLE or VLLE, such that no changes to the mass and energy balances of the homogeneous column model have to be made.

The MINLP optimization model for heteroazeotropic columns is reformulated as a continuous problem in the same way as proposed for the homogeneous column model in Section 3.3.2.1, i.e. by replacing the binary variables b_n with continuous variables c_n and adding Fischer-Burmeister constraints (eq. (3.43)). The discrete-continuous optimization problem can thus be solved as a nonlinear programming problem (NLP) with common NLP solvers like in the homogeneous case (cf. Section 3.3.4).

The initialization procedure is adapted from homogeneous distillation as well (cf. Section 3.3.3). Initial temperature and composition profiles are derived from the linear piece-wise combination of the pinch points from the shortcut evaluation with the FAM.

4.6.2 Example

We model the rigorous optimization of the heteroazeotropic distillation example (mixture of isopropanol, water, and cyclohexane, cf. Table 4.1) by the formulation given in Section 4.6.1. A feed flow rate of 5.23 mol/s and a maximum number of 50 trays is specified. A hot utility of 3 bar steam at a price of 12 €/t is used and the depreciation period is assumed to be 5 years. The model is reformulated as a continuous problem by the introduction of Fischer-Burmeister constraints (eq. 3.43) for the continuous decision variables and initialized by the results of the shortcut evaluation as proposed in Sections 3.3.3 and 4.6.1. The continuous problem is solved by reducing the relaxation parameter μ from 0.5 to 0.2 and 0. Table 4.3 lists the total annualized costs and the optimal column configuration. Phase split occurs on eight trays at the top of the column in the optimal solution. Note that the energy duty of the rigorously modeled column is only slightly larger than the minimum energy duty determined in the shortcut evaluation.

The solution time for this complex problem was 141 seconds including the time for the initialization phase. Note that the MINLP solution of this problem did not converge to an integer solution. When the effect of liquid phase split is considered only in the decanter but neglected on the column trays, the separation can be accomplished by only 15 trays and a lower cost of 68.5 k€/a is determined. Obviously, it is necessary to consider phase split on the column trays if an accurate modeling of the separation is desired.

Table 4.3: Results of the rigorous optimization.

TAC [k€/a]	75.1
capital cost [k€/a]	49.1
operating cost [k€/a]	26.0
Q_D/F [MJ/kmol]	67.13
Q_B/F [MJ/kmol]	26.06
number of trays	27
heterogeneous trays	1-8
feed tray	9
diameter [cm]	51.4

4.7 Case studies

This section illustrates the conceptual, optimization-based design of heteroazeotropic distillation by two case studies. The first case study demonstrates the ability of the FPM, the FAM, and the rigorous optimization to deal with multi-component systems efficiently. The conceptual design based on the process synthesis framework introduced in Chapter 2.6 is highlighted with the final case study, which was provided by an industrial partner. Here, heteroazeotropic flowsheet variants are generated for the separation of multiple feed streams in pure components. The process operating points of the flowsheet variants are numerically optimized by means of the FAM in order to determine the most energy-efficient flowsheet, which is then rigorously optimized. The treatment of tangent pinches by the FAM is also demonstrated in this case study.

The application of the proposed shortcut and rigorous methods to the separation of a quinternary heterogeneous system is shown in Chapter 5 in Section 5.4. Furthermore, Appendix B gives an example for the extension of the FAM to intermediate splits without a feed pinch, which cannot be evaluated correctly by any other method reviewed in Section 4.3.

In all case studies, the phase equilibria and the enthalpies are determined by rigorous thermodynamics, i.e. by activity coefficients calculated with common g^E-models. While the tray-to-tray calculations for the FPM are performed in MATLAB, the evaluation with the FAM and the rigorous optimization are performed by means of the

optimization platform GAMS on a 3 GHz standard PC. The sequential quadratic programming solver SNOPT is used for the solution of the NLP problems.

4.7.1 Separation of a quaternary mixture

The first case study considers a direct split of the quaternary heterogeneous mixture water, n-butyl acetate, n-butanol, and acetic acid. The coefficients for the calculation of vapor pressures, ideal gas heat capacities, and heats of vaporization are given in Tables D.2, D.10, and D.22. The liquid activity coefficients are determined by the UNIQUAC model with parameters given in Tables D.38 and D.39. At ambient pressure and boiling temperature, the system exhibits immiscibilities between water and n-butyl acetate and between water and n-butanol. As illustrated in Fig. 4.15, these binary immiscibilities form a coherent miscibility gap. The system has four homogeneous and three heterogeneous azeotropes, most notably a ternary azeotrope within the miscibility gap, which is the minimum boiler of the system.

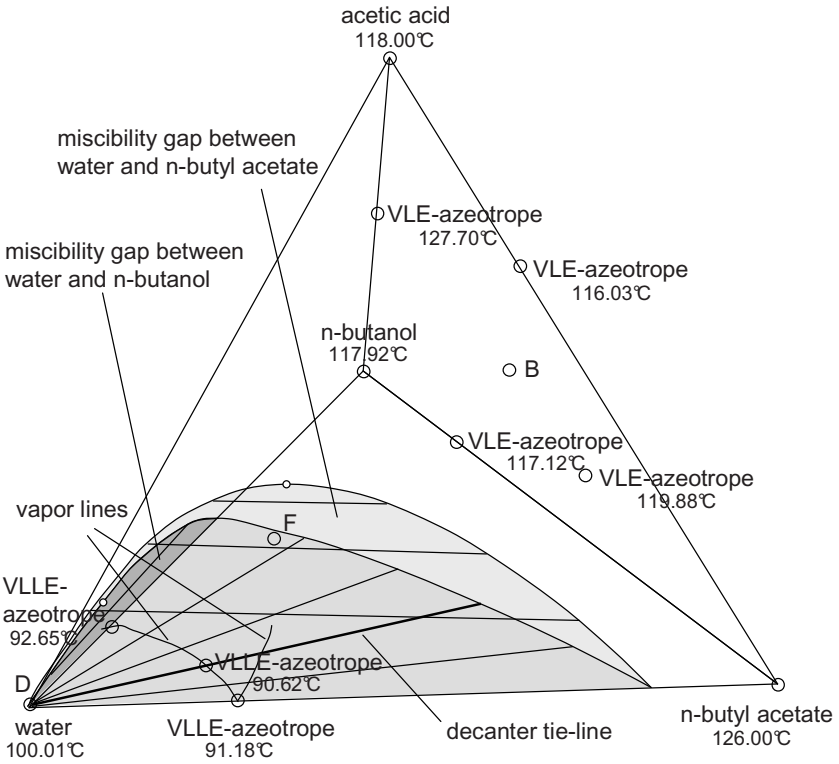

Figure 4.15: Quaternary heterogeneous mixture of water, n-butyl acetate, n-butanol, and acetic acid.

The specified separation given in Table 4.4 is accomplished by a heteroazeotropic

column setup with a decanter at the top of the column, where the water-rich fraction, in this case almost pure water, is drawn off. A ternary mixture of n-butyl acetate, n-butanol, and acetic acid is produced at the bottom. Note that the decanter tie-line runs through the minimum boiling ternary azeotrope such that the separation corresponds to a direct split.

Table 4.4: Specifications and MED of the heteroazeotropic separation of a mixture of water, n-butyl acetate, n-butanol, and acetic acid.

molar composition			
$\mathbf{z}_F$	$\mathbf{x}_D$	$\mathbf{x}_B$	
0.49, 0.17, 0.17, 0.17	0.99, 2e-3, 8e-3, 0	0, 0.33, 0.34, 0.33	
pressure	feed state	g^E-model	
1.013 bar	sat. liquid	UNIQUAC	
$Q_{B,\min}/F$ [MJ/kmol]			
rigorous	RBM	FPM	FAM
35.1	44.5	35.1	35.8

4.7.1.1 Shortcut evaluation

Bausa (2001) inspected this separation with the RBM and determined two relevant rectification bodies, a triangular shaped rectification body for the stripping section and a tetrahedron for the rectifying section as indicated in Fig. 4.16. The intersection occurs at the stable node of the stripping section which marks the feed pinch. The MED determined by the RBM then amounts to $Q_{B,min} = 44.5\ MJ/kmol$F (cf. Table 4.4). It was already noted by Bausa (2001) that the RBM with its linearized rectification bodies might significantly overestimate the MED for this highly non-ideal system. Indeed, the profiles of the rectification section display a distinct curvature, which is illustrated in Fig. 4.16 by two profiles in the vicinity of the saddle pinches *r2* and *r3*. Note that these profiles pass by the sides of the stripping section rectification body with a considerable distance to the edges of the rectification body. It is therefore a very tedious, if not impossible task to determine the CDR for the rectifying section according to the CDRM (Section 4.3.4) and identify an intersection at minimum reflux.

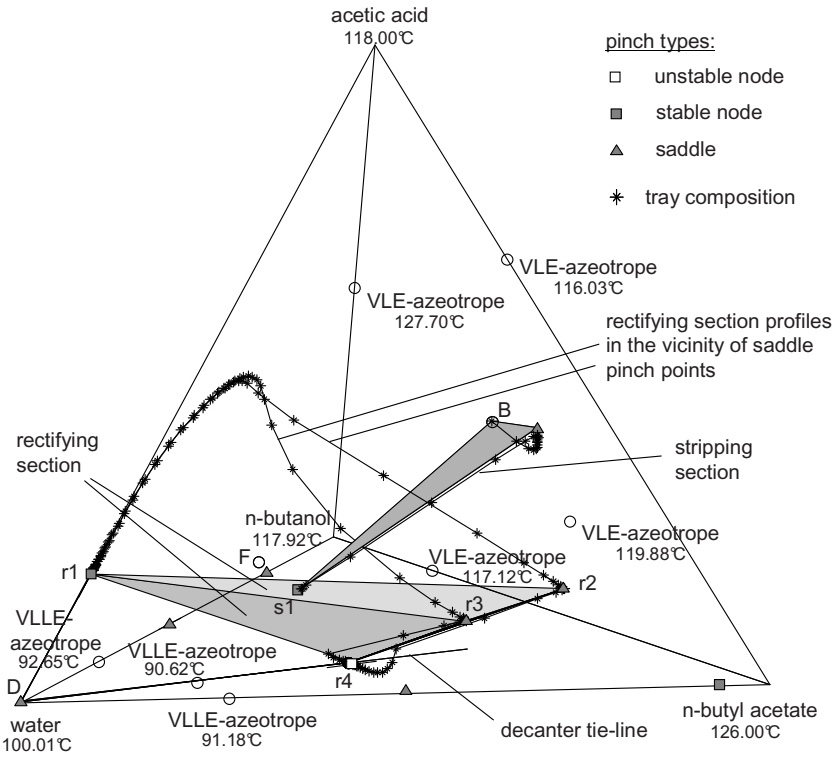

Figure 4.16: Rectification bodies and profiles for the quaternary heteroazeotropic example at the energy duty determined by the RBM ($Q_{B,min}/F$ = 44.5 MJ/kmol).

Despite the significant overestimation of the MED, the RBM helps us to identify the relevant pinch points and an initial value for the MED such that the FPM or the FAM can be applied. The FPM is illustrated in the cutout in Fig. 4.17 for the quaternary example. The upward calculation of 50 trays for the rectifying section profile is started at the feed pinch *s1*. The profile, which is a function of the reboiler duty only, converges to the unstable node *r4* on the decanter tie-line when a sufficient reboiler duty is supplied. The minimum reboiler duty, for which the profile still reaches the unstable node, is determined to be $Q_{B,min} = 35.1\ MJ/kmol$F, about 26% lower than the result of the RBM. The profile leaves the composition space for a reboiler duty lower than the minimum, i.e. $0.99 \cdot Q_{B,min}$, as shown in Fig. 4.17.

The phase diagram in Fig. 4.17 illustrates the application of the FAM. The relevant saddle pinches *r2* and *r3* for the FAM are identified by the RBM. They form the tetrahedron-shaped rectification body of the rectifying section together with the unstable and stable nodes (cf. Fig. 4.16). Since the feed pinch is located in the stripping section, the tray above the feed pinch is calculated. The objective is to minimize the

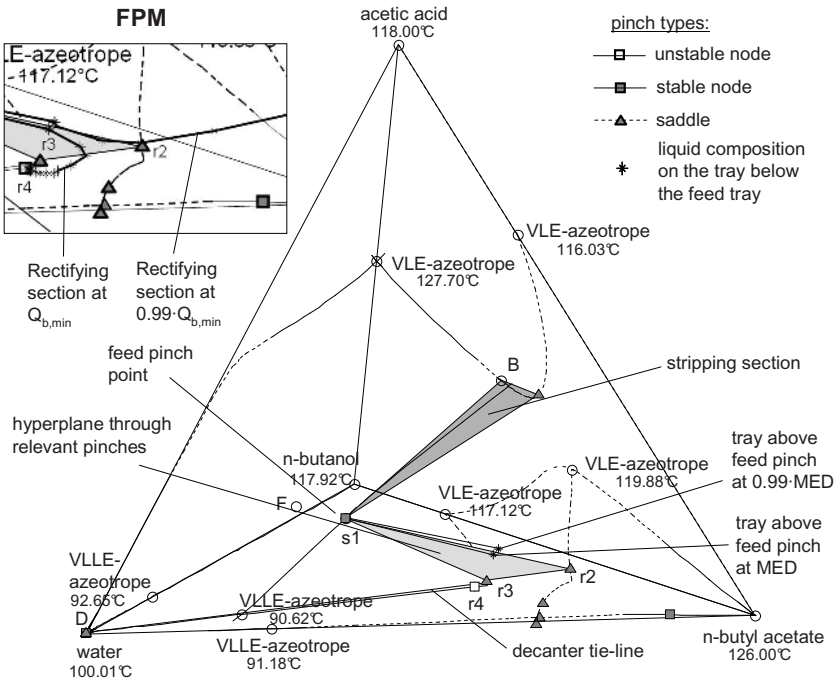

Figure 4.17: Application of the FAM and FPM (cutout) to the quaternary heteroazeotropic example ($Q_{B,min}/F = 35.2$ MJ/kmol). The relevant saddle pinches r2 and r3 were determined from the intersecting rectification plane in Fig. 4.16.

angle between the line connecting the feed pinch *s1* with the tray and the plane defined by the saddle pinches *r2* and *r3* and the feed pinch *s1*. When the angle becomes zero, i.e. when the tray is located in the plane, we determine a slightly higher MED of $Q_{B,min} = 35.8\ MJ/kmol$F when compared to the more rigorous FPM (cf. Table 4.4). The CPU time for the combination of the RBM and the FAM is about two seconds on a standard PC.

4.7.1.2 Rigorous optimization

Table 4.5 lists the results for the rigorous optimization of the quaternary separation example. Phase split occurs only on the feed tray and the tray below the feed in the optimal solution. Again, the energy duty of the rigorously modeled column is only slightly larger than the minimum energy duty determined in the shortcut evaluation.

The solution time for the continuous reformulation of this complex problem was 146 seconds including the time for the initialization phase. The MINLP solution of this problem converged in 3549 seconds to a worse solution of 116.9 k€/a.

Table 4.5: Results of the rigorous optimization for the quaternary heteroazeotropic example.

TAC [k€/a]	112.9
capital cost [k€/a]	30.5
operating cost [k€/a]	82.4
Q_D/F [MJ/kmol]	33.2
Q_B/F [MJ/kmol]	35.1
number of trays	14
feed tray	7
diameter [cm]	43.5

4.7.2 Complex industrial case study

This section illustrates the optimization-based design of a heteroazeotropic distillation process by means of the process synthesis framework presented in Section 2.6. The case study, which is provided by an industrial partner, considers the separation of four streams containing different fractions of propargyl alcohol, monochlorobenzene, and water into pure components. The vapor pressures, ideal gas heat capacities, and heats of vaporization are calculated by coefficients given in Tables D.3, D.12, and D.24 in Appendix D. The NRTL model is used for the calculation of the liquid activity coefficients (cf. Tables D.40 and D.41). The topology of this heterogeneous azeotropic mixture (cf. Fig. 4.18) resembles the one of the example in Section 4.3. The flow rates and the compositions of the different feed streams are given in Table 4.6 and shown in Fig. 4.18. The column pressures are set to 0.23 bar, since the maximum allowed operating temperature in the distillation system is 85°C to prevent decomposition of propargyl alcohol.

Table 4.6: Feed streams for the separation of a mixture of propargyl alcohol, monochlorobenzene, and water.

feed	F_1	F_2	F_3	F_4
flow rate [mol/s]	0.333	0.17	0.18	0.11
molar composition	[0.26,0.74,0]	[0.45,0.1,0.45]	[0.1,0.86,0.04]	[0.03,0.93,0.04]

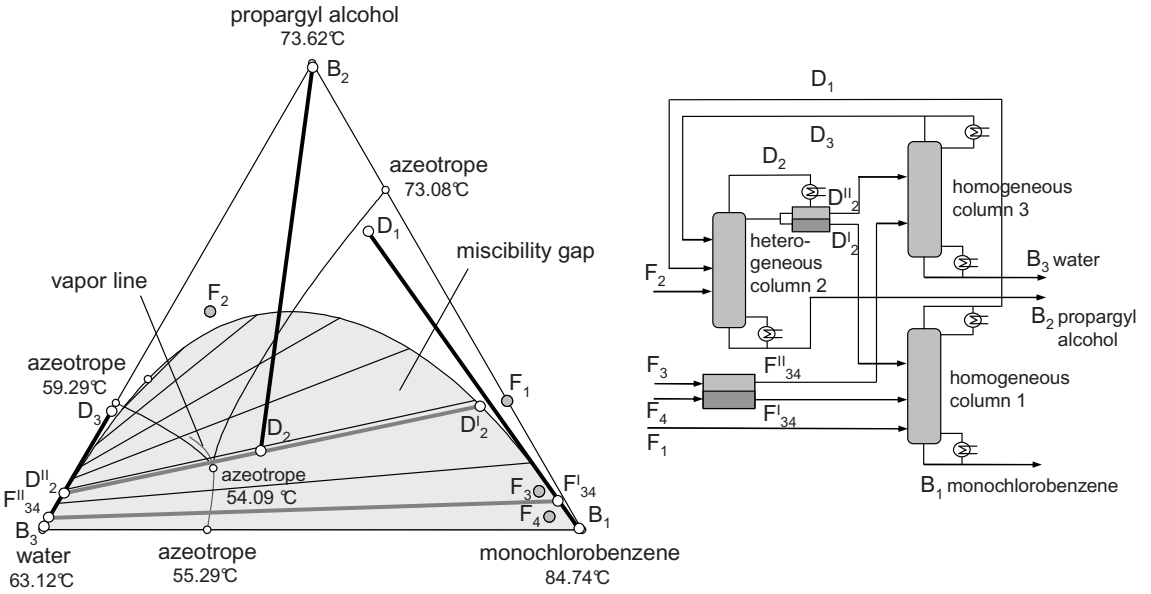

Figure 4.18: Topology of the propargyl alcohol, monochlorobenzene, water system with mass balances of heteroazeotropic flowsheet variant F1 on the right.

Alternative heteroazeotropic distillation flowsheets for this separation task are generated manually; the four most energy-efficient ones are shown in Fig. 4.19 as F1 to F4. F1 and F2 differ from F3 and F4 in the column sequence. Compared to F2, F1 has an additional decanter where the organic and water phases of two feed streams are distributed to the homogeneous columns. F4 has an additional recycle compared to F3. As a measure of heat-integration, the distillates of columns 1 and 3 of all variants are drawn off as a saturated vapor and fed to column 2 in this state. It will be shown by the rigorous optimization in Section 4.7.2.2 that the capital costs are considerably larger than the energy costs in this case study. Hence, additional heat integration between the process condensers and reboilers by variation of column pressures was not considered.

4.7.2.1 Shortcut evaluation

Due to the abundance of distillation boundaries and recycles, feasible process operating points for the flowsheet variants are determined in a first step. This is done by a minimization of the recycle flow rates, where the columns are represented by linear mass balances and the distillation boundaries are approximated by straight lines connecting the singular points. Then each column is evaluated with the RBM at these operating points in order to identify the relevant saddle and feed pinches. This

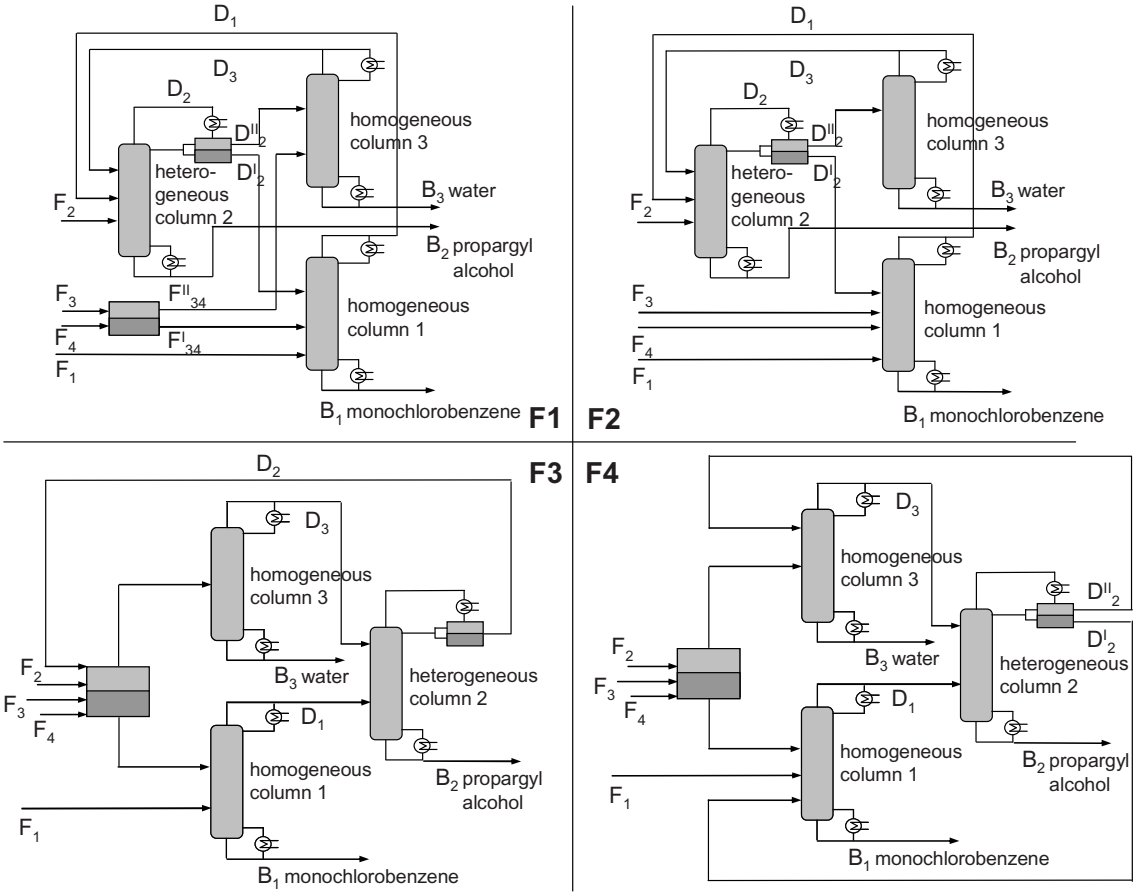

Figure 4.19: The four most energy-efficient flowsheet variants for the separation of pure components.

analysis shows that a tangent pinch controls the separations in column 1 in all of the considered flowsheets (cf. Fig. 4.20).

Table 4.7: Process energy duties for minimized recycle flow rates and linearly approximated distillation boundaries between azeotropes.

flowsheet variant	$Q_{B,\min}$ [kW]
F1	55.9
F2	55.3
F3	73.3
F4	77.3

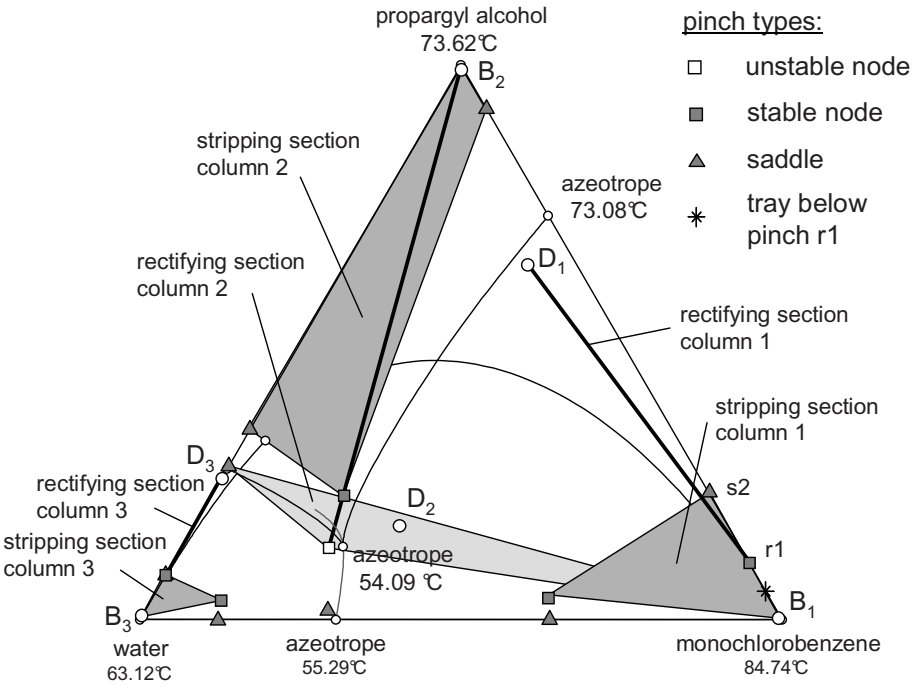

Figure 4.20: Rectification bodies for flowsheet variant F1 determined in the initialization by the RBM.

The four different flowsheets are then evaluated with the FPM for MED at the minimum recycle flow rates with widely different results shown in Table 4.7. Yet a meaningful comparison of the different process variants can only be accomplished at the respective optimal process operating points. The fully algorithmic FAM offers the computational efficiency and robustness required for the optimization of operating points of large-scale processes. Hence, a numerical minimization of the process energy duties of the four best flowsheets is performed in the following.

This optimization-based design step is illustrated by flowsheet variant F1, for which the column mass balances are shown in Fig. 4.18. For initialization, the three distillation columns are evaluated separately by the FAM. Here, column 1 is evaluated by the FAM for separations controlled by a tangent pinch as proposed in Section 4.5.3, while columns 2 and 3 are evaluated by the regular FAM as in eqs. (4.13)-(4.19). Finally, the columns are connected by the flowsheet streams and the previously fixed operating point is released. Since the sum of the reboiler duties is minimized in the resulting NLP problem, the FAM objective of minimum angles eq. (4.13) needs to be dropped. Instead, the angles are simply set to zero by eq. (4.23) as proposed in Section 4.5.2.

Now that the process operating point is released, feasibility of the separation needs

to be ensured by enforcing the distillation boundaries. The feasibility of column 2 can easily be enforced by setting a bound on the vapor composition at the top of the column since the extreme locus of this composition is known: The vapor may not move below the ternary azeotrope on the vapor line in the miscibility gap. The mass balances of columns 1 and 3 do not extend towards singular points but towards distillation boundaries between singular points. Here, the formulations to enforce the boundaries proposed in Section 4.5.2 are introduced (cf. Fig. 4.12). When these formulations are added to the optimization problem in this case study, it can be guaranteed that distillation boundaries are not crossed within a single column. It needs to be noted that the boundary constraints are not active in the example problem, since the column end products move away from the boundaries in the optimization.

Table 4.8: Process energy duties determined by means of the FAM and an optimization of the process operating points.

flowsheet variant	$Q_{B,\min}$ [kW]
F1	41.9
F2	43.1
F3	55.1
F4	55.6

The results, i.e. the optimized MED for the alternative flowsheet variants, are given in Table 4.8. Thanks to the optimization of the operating points, the energy demands of the flowsheets have not only been reduced considerably, but the rank order has also been revised. Due to the computational efficiency of the FAM, the CPU time required for the optimization of the different flowsheet variants amounts to only 10 seconds per variant on a 3 GHz standard PC, including the initialization of the single columns. Thus, the evaluation can be nicely integrated in the engineering workflow.

In Fig. 4.21, the process reboiler duty is plotted over the sum of the recycle flow rates for flowsheet variant F1. It can clearly be seen, that there is an optimal recycle flow rate, for which the process reboiler duty is minimal. Yet, at the minimum sum of the recycle flow rates, the distillates of columns 1 and 2 approach the respective distillation boundaries leading to a considerably higher MED when compared to the MED at the optimal recycle flow rate. Hence, this example impressively demonstrates that it is often not advisable to optimize process operating points for minimum recycle flow rates and compare alternative flowsheet variants based on these operating points.

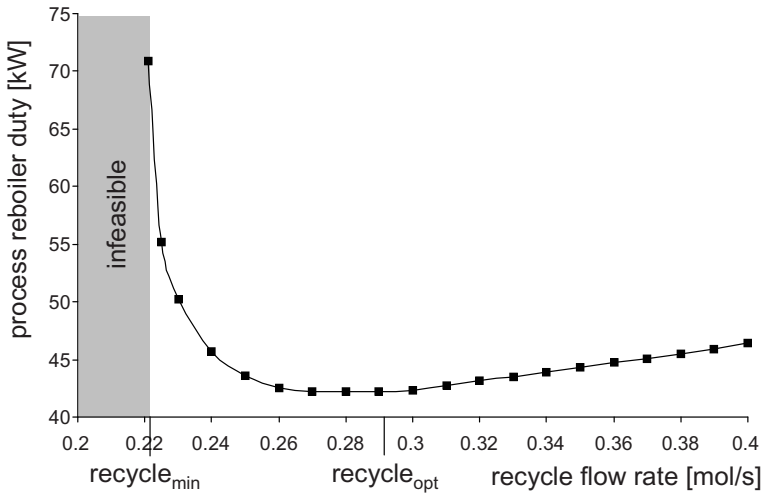

Figure 4.21: Process reboiler duty over the sum of the recycle flow rates for flowsheet variant F1. Indicated are the optimal and the minimal recycle flow rate, beyond which the process becomes infeasible.

An optimization of the recycle flow rates for minimum process energy demands allows a much more meaningful comparison of flowsheet variants.

For a similar heteroazeotropic distillation process, Ryan and Doherty (1989) formulate the heuristic that the distillate composition from the entrainer recovery column should be set close to the distillation boundary. The authors suggest that this degree of freedom can therefore be removed from the list of optimization variables. Yet, it is shown above that the heuristic of Ryan and Doherty (1989) is not valid for the example in this section. The distillate composition of the entrainer recovery column (column 1) moves away from the respective distillation boundary in the optimization, thereby significantly reducing the energy demand of the process. Hence, it is very useful to declare the impure products of the process as optimization variables. Due to the algorithmic optimization procedures proposed in this thesis, there is no need to specify some of these variables by means of heuristics.

4.7.2.2 Rigorous optimization

Flowsheet variant F1 was determined to be the most energy-efficient flowsheet in the shortcut evaluation and was therefore chosen for rigorous optimization. This design step is highly demanding not only due to the non-ideal thermodynamics and the liquid phase split but also due to the manifold of feeds, columns, and recycles.

The rigorous optimization is initialized by the operating point and linearly approx-

imated profiles from the shortcut evaluation step as proposed in Sections 3.3 and 4.6.1. The maximum tray numbers are set to 50, 40 and 20 trays for columns 1, 2 and 3, respectively, yielding a problem of about 2400 variables, including 460 decision variables. The problem is reformulated as a continuous problem as proposed in Section 3.3.2.1 and solved by the solution procedure presented in Section 3.3.4. The optimization results for the costs, number of column trays, feed tray locations, and recycles are displayed in Table 4.9. In the optimal solution, phase split occurs on the six topmost trays of the heteroazeotropic column 2.

Table 4.9: Costs, column configurations and recycles (molar fractions of propargyl alcohol, monochlorobenzene, and water) for all columns of flowsheet F1.

TAC [k€/a]	36.2		
	Col 1	Col 2	Col 3
TAC [k€/a]	15.3	18.5	2.4
capital cost [k€/a]	11.1	14.7	1.9
operating cost [k€/a]	4.2	3.8	0.5
condenser duty [kW]	10.4	35.9	0.4
reboiler duty [kW]	25.7	19.6	3.1
number of trays	13	24	10
feed trays	6/7/10	6/8/13	2/7
diameter [cm]	22.8	20.1	4.7
recycle D_1	0.315 mol/s, [0.51,0.44,0.05]		
recycle D_3	0.061 mol/s, [0.19,4e-3,0.81]		

Due to the favorable initialization and the reformulation as a continuous problem, the resulting NLP problem could be solved in only 305 seconds including the initialization. In contrast, the MINLP solution did not converge for this large-scale example.

The benefit of the rigorous optimization is highlighted by a comparison of the operating points of the shortcut and rigorous evaluations. In the rigorous optimization, the cumulated recycle flow rate was raised from 0.29 mol/s (Fig. 4.21) to 0.42 mol/s (Table 4.9). The higher recycle flow rate comes with lower recycle purities such that less column trays are required. Apparently, the savings in capital costs through the lower tray numbers offset the increased energy costs.

4.8 Summary

Hybrid processes of distillation assisted with decantation, also termed heteroazeotropic distillation processes, occur frequently in industry. Yet, the optimal design of these processes still remains challenging. In literature, very few publications can be found on the systematic design of heteroazeotropic distillation, particularly concerning algorithmic methods. In this chapter, the extension of the process synthesis framework to the optimization-based design of heteroazeotropic distillation processes was presented. For this purpose, both shortcut and rigorous methods were developed, which are able to handle heterogeneous mixtures.

First, various shortcut methods for homogeneous non-ideal distillation based on tray-to-tray calculations, pinch point analysis, or a combination thereof were supplemented with a powerful phase stability test and studied for the application to heteroazeotropic distillation. As shown by a thorough analysis, these methods are either restricted by inaccuracies due to high non-idealities, limited to ternary mixtures, or limited to certain kinds of splits.

Yet, by combining elements from the existing shortcut methods two novel methods have been proposed, which overcome the limitations of the existing methods. The feed pinch method (FPM) combines the RBM for the identification of the feed pinch with a tray-to-tray calculation of the non-pinched section starting from this feed pinch. Compared to methods which require the calculation of full column profiles, significantly less trays have to be calculated. In addition, the FPM offers a simple check for feasibility, especially for direct and indirect splits: When the profile of the non-pinched column section reaches the product composition, feasibility is guaranteed. Unfortunately, the FPM can only be applied to separations with a feed pinch, i.e. direct or indirect splits in case of mixtures with more than three components. Furthermore, the FPM is not suited for application in process optimization due to the requirement of tray-to-tray calculations.

To further improve, the feed angle method (FAM) has been proposed, which resolves the limitations of the FPM. The FAM approximates the MED by the minimization of the angle between one tray above or below the feed pinch and the relevant saddle pinches in the non-pinched column section. The relevant pinches can be identified by an initialization with the RBM. Thus, the FAM can be interpreted as a sequential refinement of the RBM for highly non-ideal mixtures, where an additional vertex is added to the linearized rectification bodies in order to account for the curvature of the profiles. An extension of the FAM to mixtures with any number of components, to tangential pinches, and to intermediate splits (cf. Appendix B) was shown to be

straightforward. Due to its computational efficiency and algorithmic nature, the FAM is perfectly suited for application in process optimization.

Concerning the rigorous optimization, the necessary extensions for the application to heteroazeotropic distillation were introduced in Section 4.6. Due to the robust and efficient implementation of the phase stability test presented in Section 4.1, a rigorous optimization of heteroazeotropic columns could be successfully performed for the first time. Moreover, a sound initialization and continuous reformulation facilitated excellent solution properties for the complex optimization problems in the case studies. Although initialized by the same routine, the respective MINLP solutions of the optimization problems did not converge or required a significantly longer time to converge to a solution of lower quality.

When the effect of liquid phase split was considered only in the decanter but neglected on the column trays, incorrect energies or costs where identified in both the shortcut and rigorous evaluation steps. To conclude, the novel methods seem to fully overcome the restrictions in conceptual design of heteroazeotropic distillation processes. Thereby, the application of the novel methods within the process synthesis framework facilitated the optimization-based design of a complex heteroazeotropic distillation process consisting of three columns, two decanters and two recycles with unprecedented reliability and efficiency.

Chapter 5

Extraction coupled with distillation

Liquid-liquid extraction facilitates an energy-efficient recovery of products from aqueous or organic mixtures, for instance from liquid phase reactions or fermentation. Extraction may be an appropriate separation alternative when distillation is impractical due to azeotropic mixture behavior, high boiling temperatures, low relative volatilities, low product concentrations, or heat-sensitive components. In these cases, a suitable solvent may allow the extraction of certain components from the medium by the difference in solubility. Application examples include the removal of aromatics from reformate streams, the purification of waste streams, pharmaceutical processes like the production of vitamins and antibiotics, and the refining of fats and oils in food processing.

In order to recycle the solvent and obtain pure products, extraction must be combined with additional unit operations in a hybrid separation process. Distillation is well suited for combination with extraction, as long as the solvent does not form azeotropes with the products and the boiling points are sufficiently far apart. Thanks to the low energy consumption of extraction, such hybrid separation processes offer a significant energy savings potential compared to pure distillation processes.

Besides the selection of a suitable solvent, the conceptual design of extraction units involves the specification of the extraction temperature, the solvent flow rate, the number of extraction stages, and the dimensions of the apparatus. An accurate modeling of extraction often requires the consideration of mass transport limitations (Mohanty, 2000). Furthermore, various authors have studied the design of extraction columns by means of drop-population balances. Here, model parameters are regressed from the study of individual drops and drop swarms in lab-scale experiments (Valentas, Bilous and Amundson, 1966; Goodson and Kraft, 2004; Adinata, Ayesterán, Buch-

bender, Kalem, Kopriwa and Pfennig, 2011). However, extraction columns have also been modeled by equilibrium-based tray-to-tray models (Beviá, Rico and Gomis, 1984; Sattler, 1988; Marcilla, Gomez, Reyes and Olaya, 1999). Even these simplified equilibrium models can be computationally expensive when a large number of column trays is considered and favorable initial values are not available. Hence, these rigorous models might not be well suited for an evaluation of process alternatives in the early conceptual design phase, where the optimization of process operating points requires particularly robust and efficient methods. In this phase, shortcut methods may perform better.

In Section 5.1, shortcut methods for the evaluation of extraction columns published in literature are reviewed and a novel algorithmic shortcut method as an extension of the feed angle method for distillation is introduced. Subsequently, a discrete-continuous model for the rigorous optimization of extraction columns is proposed in Section 5.2. Based on the novel shortcut and rigorous methods, Section 5.3 presents examples for the evaluation and design of extraction columns. Finally, Section 5.4 illustrates the optimization-based process synthesis according to the framework of Chapter 2.6 by the design of a large-scale hybrid extraction-distillation process for the separation of butanol from fermentation broth. This case study has recently been published by Kraemer, Harwardt, Bronneberg and Marquardt (2011).

5.1 Shortcut methods for extraction columns

Various authors have proposed shortcut methods for extraction systems using equilibrium-based tray-to-tray models and graphical techniques like the Ponchon-Savarit method for distillation (e.g. Hunter and Nash (1934); Treybal (1963); Sattler (1988)). Due to the graphical nature, these methods are limited to the evaluation of ternary mixtures. By application of projection techniques, Beviá et al. (1984) extended the graphical approach to quaternary mixtures. Still, the methods require manual evaluation and are therefore not suited for the application in process optimization problems.

The feasibility of extraction columns and the minimum solvent flow rate as a measure for the economic potential can also be assessed by the evaluation of pinch points. These points, which constitute the fix-points of the tray-to-tray recursion, usually constrain the extraction of multicomponent mixtures in extraction columns. Comparable to distillation, the separation driving force vanishes at these points. The pinch points can be calculated by the pinch equation system, which is formulated for counter-current cascades (Fig. 5.1) by

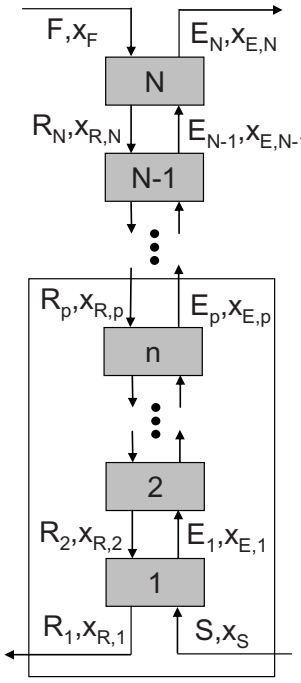

Figure 5.1: Counter-current cascade for liquid-liquid extraction and balance envelope for the calculation of pinch points.

$$0 = S - R_1 + R_p - E_p, \tag{5.1}$$

$$0 = Sx_{S,i} - R_1 x_{R,1,i} + R_p x_{R,p,i} - E_p x_{E,p,i}, \qquad i = 1, ..., C, \tag{5.2}$$

$$0 = \gamma_i(\mathbf{x}_{R,1}, T, p) x_{R,1,i} - \gamma_i(\mathbf{x}_{E,1}, T, p) x_{E,1,i}, \qquad i = 1, ..., C, \tag{5.3}$$

$$0 = \gamma_i(\mathbf{x}_{R,p}, T, p) x_{R,p,i} - \gamma_i(\mathbf{x}_{E,p}, T, p) x_{E,p,i}, \qquad i = 1, ..., C, \tag{5.4}$$

$$1 = \sum_{i=1}^{C} x_{R,p,i}, \; 1 = \sum_{i=1}^{C} x_{E,p,i}, \; 1 = \sum_{i=1}^{C} x_{R,1,i}, \tag{5.5}$$

$$x_{R,1,i} = \text{purity}, \qquad i = \text{solute}. \tag{5.6}$$

Eqs. (5.1) and (5.2) are the total and component material balances for the solvent stream S, the raffinate stream R_1, and the raffinate and extract streams at the pinch points, R_p and E_p. Eqs. (5.3) and (5.4) calculate the liquid-liquid phase equilibrium and eq. (5.6) is the purity constraint for the key solute in the raffinate.

A pinch-based shortcut method for the separation of ternary mixtures in extraction columns has been proposed by Minotti, Doherty and Malone (1996). The method has been extended by Wallert (2008) for the evaluation of quaternary separations, for

which it relies on graphical inspection. These methods are briefly reviewed in the following two subsections. Subsequently, a novel, fully algorithmic shortcut method is introduced, which has been developed for the efficient optimization-based evaluation of extraction columns (Kraemer, Redepenning, Recker, Skiborowski and Marquardt, 2012). This method extends the shortcuts of Minotti et al. and Wallert with concepts of the FAM for distillation (cf. Section 4.5) such that mixtures with any number of components can be handled.

5.1.1 Minotti et al.'s shortcut method for ternary mixtures

According to the geometric criterion for ternary mixtures of Minotti et al. (1996), a specified separation is feasible when no pinch occurs in the extraction column. Two different cases of pinched separations have to be distinguished for the inspection of this criterion: *feed pinch control* and *tangent pinch control*.

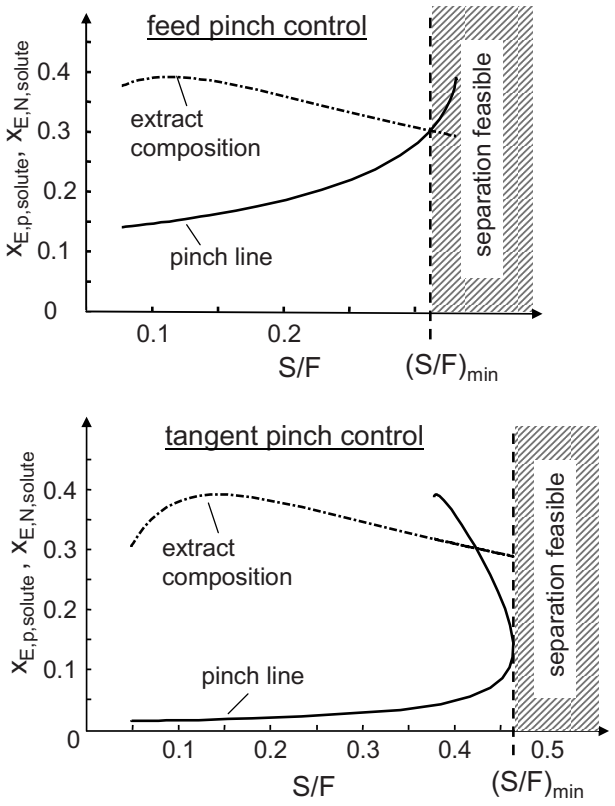

Figure 5.2: Illustration of alternative operating conditions: feed pinch control (top) and tangent pinch control (bottom).

The operating condition *feed pinch control* is illustrated by Fig. 5.2 (top). In this case, the separation is only feasible when the pinch line is located above the extract line, i.e. when $x_{E,p,solute} \geq x_{E,N,solute}$. For $\frac{S}{F} < \left(\frac{S}{F}\right)_{min}$ the profile converges at the feed pinch without reaching the extract composition. In the limiting case of minimum solvent flow rate, the pinch and extract lines cross each other and a pinch occurs at the column end where the feed is introduced. Mathematically, this can be formulated as a NLP problem which maximizes the solvent flow rate such that the solute fraction of the pinch is smaller than the solute fraction of the extract:

$$\max \quad S \tag{5.7}$$

$$\text{s.t.} \quad eq.\ (5.1) - (5.6), \tag{5.8}$$

$$0 = Sx_{S,i} - R_1 x_{R,1,i} + Fx_{F,i} - E_N x_{E,N,i}, \qquad i = 1, ..., C, \tag{5.9}$$

$$0 = \gamma_i(\mathbf{x}_{R,N}, T, p)x_{R,N,i} - \gamma_i(\mathbf{x}_{E,N}, T, p)x_{E,N,i}, \qquad i = 1, ..., C, \tag{5.10}$$

$$1 = \sum_{i=1}^{C} x_{R,N,i},\ 1 = \sum_{i=1}^{C} x_{E,N,i}, \tag{5.11}$$

$$x_{E,p,i} \leq x_{E,N,i}, \qquad i = \text{solute}. \tag{5.12}$$

For ternary mixtures, the location of the pinch point only depends on the solvent flow rate when the temperature, the pressure, the feed, and the purity of the raffinate are specified. Hence, the problem of eqs. (5.7)-(5.12) has one degree of freedom. The degree of freedom reduces to zero when eq. (5.12) is formulated as an equality constraint. However, the problem is given as an optimization problem here, such that the the same set of equations apply to the condition of *tangent pinch control* as described in the following paragraph.

Fig. 5.2 (bottom) illustrates qualitatively the operating condition *tangent pinch control*. In this case, more than one pinch point can appear for a certain range of the solvent flow rate. Comparable to distillation with a tangent pinch, however, the separation is only feasible when the solvent flow rate is large enough such that no stable pinch appears in the extraction column. In the limiting case of minimum solvent flow rate, a single tangent pinch occurs in the middle of the column. This criterion can be checked by solving the same NLP problem (eqs. (5.7)-(5.12)) as in case of *feed pinch control*.

5.1.2 Wallert's shortcut method for quaternary mixtures

When the mixture in the extraction column contains four or more components, the binodale extends to a hyperplane and the ratios of the solutes in the raffinate and the extract constitute additional degrees of freedom. As a consequence, the geometric criterion of Minotti et al. is no longer valid.

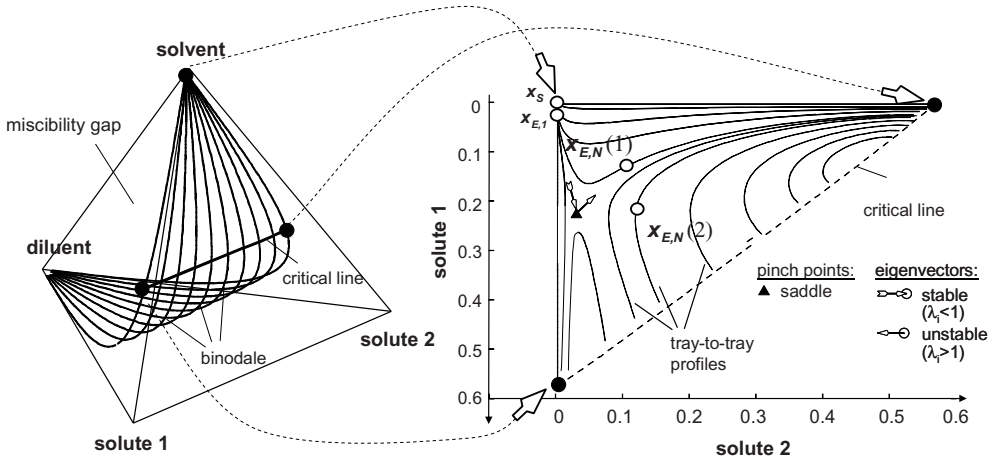

Figure 5.3: Quaternary liquid-liquid phase diagram (left) and projection of extract side of binodale plane in 2-dimensional space (right). Pinch point, tray-to-tray profiles, feasible (1) and infeasible (2) specifications of $\mathbf{x}_{E,N}$ are shown.

Wallert (2008) proposed an extension of Minotti et al.'s method such that the extraction of quaternary mixtures can be evaluated. Wallert's method relies on the visualization and analysis of the separation pinch points by means of a projection of the extract side of the binodale plane in two-dimensional space (cf. Fig. 5.3). The binodale plane is then divided into separation regions based on the occurrence of saddle pinch points. Comparable to distillation, the products need to be located in the same separation region. The identification of the separation regions based on the information of the pinch points solely, however, is a very challenging task. Hence, a number of tray-to-tray profile calculations are necessary to identify the regions reliably. An additional drawback of the method is the dependence on visual inspection of the separation topology to determine feasibility and minimum solvent flow rate. As a consequence, the method cannot be applied to mixtures with more than four components, i.e. more than two solutes. In addition, the shortcut cannot be integrated into algorithmic process simulation or numeric process optimization problems.

5.1.3 Feed angle method for extraction of multi-component mixtures

Many industrial applications involve the extraction of mixtures with more than four components (e.g. the example in Section 5.4). Kraemer et al. (2012) propose a novel shortcut method which can be applied to mixtures with any number of components. Aside from its applicability for multi-component mixtures, the proposed shortcut method is fully algorithmic such that it can be integrated into numeric process optimization problems (cf. Section 5.4).

These properties are achieved by borrowing concepts of the feed angle method for distillation (FAM, Section 4.5) and integrating these elements with the shortcut methods of Wallert and Minotti et al.. In the following, the novel method is therefore termed FAM for extraction.

The FAM for extraction is first introduced for the case of *tangent pinch control*, where the separation pinches occur in the middle of the column, which is usually the case for multi-component separations. For the determination of the feasibility and the minimum solvent flow rate, two criteria have to be met:

- As illustrated by Fig. 5.2 (bottom), the minimum solvent flow rate coincides with the occurrence of a single tangent pinch in the column. Comparable to the criterion by Minotti et al. and the FAM for tangent pinch controlled distillation, a maximization of the solvent flow rate subject to the appearance of a pinch yields the minimum feasible solvent flow rate.
- For multicomponent extraction, the column products need to be located in one separation region. Instead of resorting to a graphical inspection of the separation topology as proposed by Wallert, the procedure to detect this condition is borrowed from the FAM for distillation. For non-ideal distillation, the FAM assesses feasibility and the minimum energy demand using the information of one tray composition vector at the feed, which needs to point towards the saddle pinch. Likewise, the FAM for extraction requires the calculation of the extract composition on tray $N-1$. For feasibility, the solute components of the vector $\overrightarrow{\mathbf{x}_{E,N}\mathbf{x}_{E,N-1}}$ need to point directly towards the tangent saddle pinch (cf. Fig. 5.4). For a solvent flowrate below the minimum, the profile in Fig. 5.4 would not converge to $\mathbf{x}_{E,1}$ but into the separation region below the saddle pinch, i.e. to higher concentrations of solute 2. A solvent flowrate above the minimum would shorten the path of the profile to $\mathbf{x}_{E,1}$ such that the profile would pass by the saddle pinch in a distance.

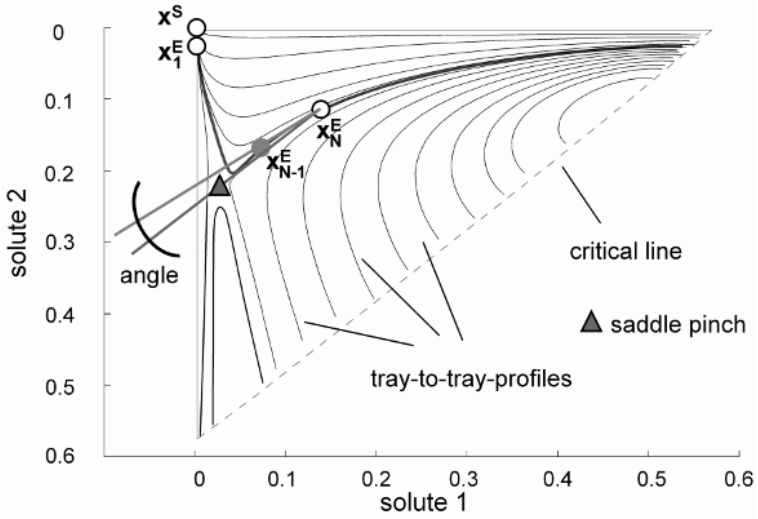

Figure 5.4: Illustration of the FAM for extraction. The vector from $\mathbf{x}_{E,N}$ to $\mathbf{x}_{E,N-1}$ points in the direction of the saddle pinch point at the minimum solvent flow rate.

The FAM for extraction can be formulated as

$$\max \quad S \tag{5.13}$$

$$\text{s.t.} \quad \textit{eq.}\ (5.1)-(5.6), \tag{5.14}$$

$$\textit{eq.}\ (5.9)-(5.12), \tag{5.15}$$

$$0 = Sx_{S,i} - R_1 x_{R,1,i} + R_N x_{R,N,i} - E_{N-1} x_{E,N-1,i}, \qquad i = 1,...,C, \tag{5.16}$$

$$0 = \gamma_i(\mathbf{x}_{R,N-1}, T, p) x_{R,N-1,i} - \gamma_i(\mathbf{x}_{E,N-1}, T, p) x_{E,N-1,i}, \quad i = 1,...,C, \tag{5.17}$$

$$1 = \sum_{i=1}^{C} x_{R,N-1,i},\ 1 = \sum_{i=1}^{C} x_{E,N-1,i}, \tag{5.18}$$

$$x_{E,N-1,i} = x_{E,p,i} + m \cdot (x_{E,N,i} - x_{E,p,i}), \qquad i \in \text{solutes}. \tag{5.19}$$

Here, eqs. (5.16)-(5.18) calculate the extract composition of the tray adjacent to the feed tray $\mathbf{x}_{E,N-1}$. Eq. (5.19) models the collinearity criterion, which guarantees that the solute components of the tray composition vector $\overrightarrow{\mathbf{x}_{E,N}\mathbf{x}_{E,N-1}}$ point towards $\mathbf{x}_{E,p}$ (cf. Fig. 5.4). The only degree of freedom of the optimization problem is the solvent flow rate, when temperature, pressure, feed, and the concentration of one solute in the raffinate are specified.

In case of *feed pinch control*, which rarely occurs in multicomponent examples, Minotti et al.'s procedure is valid for mixtures with any number of components when

eq. (5.12) is formulated for all solutes. Since $\mathbf{x}_{E,N}$, $\mathbf{x}_{E,N-1}$, and $\mathbf{x}_{E,p}$ are identical in case of *feed pinch control*, the collinearity constraint in eq. (5.19) is also fulfilled for these separations. Although not needed, eqs. (5.16)-(5.19) can therefore be solved for the case of *feed pinch control* such that the problem formulation of eqs. (5.13)-(5.19) applies to both *feed pinch* and *tangent pinch control*.

5.1.3.1 Integration of the extraction shortcut in process evaluation problems

Extraction is usually combined with distillation for the recovery of the solvent (cf. Sections 5.3.2 and 5.4). In these hybrid processes, the solvent flow rate and the purity of the extract stream are degrees of freedom, which need to be optimized for an assessment of the economic potential. Such an optimization problem requires the formulation of an objective function, which minimizes the overall energy demand or the overall costs. As a consequence, the maximization of the solvent flow rate as objective of the extraction shortcut needs to be substituted, for example, by

$$\min \quad \sum_{c} Q_{B,c}. \tag{5.20}$$

However, the shortcut then becomes invalid, since the tangent pinch criterion is not fulfilled anymore and the pinch point can move into the region of infeasibility on one of the pinch branches (cf. Fig 5.2). In this case, the tangent pinch condition can be formulated in a similar way as proposed for the FAM for tangent pinch controlled distillation (cf. Section 4.5.3). In particular, a second pinch x_{E,p_2} is calculated, which is forced to be located in an ε-distance from the original pinch $\mathrm{x}_{E,p}$ by

$$0 = Sx_{S,i} - R_1 x_{R,1,i} + R_{p_2} x_{R,p_2,i} - E_p x_{E,p_2,i}, \qquad i = 1, ..., C, \tag{5.21}$$

$$0 = \gamma_i(\mathbf{x}_{R,p_2}, T, p) x_{R,p_2,i} - \gamma_i(\mathbf{x}_{E,p_2}, T, p) x_{E,p_2,i}, \qquad i = 1, ..., C, \tag{5.22}$$

$$1 = \sum_{i=1}^{C} x_{R,p_2,i}, \; 1 = \sum_{i=1}^{C} x_{E,p_2,i}, \tag{5.23}$$

$$\|\mathbf{x}_{E,p} - \mathbf{x}_{E,p_2}\|_2 = \varepsilon. \tag{5.24}$$

It is clear from the inspection of Fig. 5.2 (bottom) that the set of the two pinch equation systems and the ε-distance constraint in eq. (5.24) can only be solved when the pinch points are located in a very close distance to the tangential pinch. A value of $1 \cdot 10^{-5}$ was chosen for ε, which is sufficiently large such that $\mathbf{x}_{E,p}$ and $\mathbf{x}_{E,p_2}$ are identified as two separate pinch points. By adding eqs. (5.21)-(5.24) to the original problem of eqs. (5.14)-(5.19), the minimum feasible solvent flow rate can thus be

determined reliably without a maximization of the solvent flow rate. The shortcut can then be integrated into a process optimization problem with the objective in eq. (5.20).

5.2 Rigorous optimization of extraction columns

As a pinch-based method, the shortcut for multicomponent extraction introduced in Section 5.1.3 relies on the assumption of an infinite number of column trays. While this method provides an accurate assessment of feasibility and minimum solvent flow rate, it cannot give any information on the number of column trays required to reach the specified purity of the raffinate or extract streams. However, this information can be gained by a rigorous extraction model based on tray-to-tray calculations. With the information on tray numbers, the economic trade-off between operating costs (affected by the solvent flow rate) and capital costs (defined by the number and size of the trays) can be determined. The tray number can be lowered by using a larger solvent flow rate than the minimal value. As a consequence, it is recommended to formulate the rigorous model as a discrete-continuous optimization problem to find the tray number, which yields the lowest overall costs.

When the extraction column is integrated in a hybrid process with solvent recovery, the total annualized costs for the whole process, i.e. for extraction and distillation columns, need to be determined. As discussed above, the capital costs of the extraction column can be lowered by choosing a solvent flow rate above the minimum value. Higher solvent flow rates, however, yield higher operating and capital costs for the solvent recovery in the distillation columns. On the other hand, higher solvent flow rates also yield lower concentrations of solutes in the extract, which typically correspond to a reduced selectivity of the extract for the diluent. A significantly reduced selectivity for the diluent, in turn, may correspond to smaller recycles and, thus, lower energy demands for the downstream columns.

Obviously, a multitude of trade-offs need to be optimized in the conceptual design of extraction-distillation hybrid processes. Since the evaluation with shortcut models relies on the condition of minimum solvent flow rate and provides no information on capital costs, a process optimization with rigorous models becomes all the more important.

5.2.1 Rigorous model

The rigorous extraction column model is based on equilibrium trays and tray-to-tray material balances with stagewise countercurrent extract and raffinate flows. For the discrete-continuous optimization, the tray-to-tray model needs to be superimposed by a superstructure which allows a variable number of column trays (cf. Fig. 5.5). For this purpose, Reyes-Labarta and Grossmann (2001) proposed a general disjunctive programming model for countercurrent liquid-liquid extraction columns. In this thesis, a MINLP superstructure with a variable feed (cf. Fig. 5.5) similar to the one proposed by Franke (2006) is used. The MINLP problem for the minimization of the capital costs reads as

$$\min \quad \mathrm{TAC} = f_c \cdot C_{cap}, \tag{5.25}$$

$$\text{s.t.} \quad 0 = F x_{F,i} + S x_{S,i} - R_1 x_{R,1,i} - E_N x_{E,N,i}, \qquad i = 1, ..., C, \tag{5.26}$$

$$0 = b_{F,n} F x_{F,i} + R_{n+1} x_{R,n+1,i} - R_n x_{R,n,i} + E_{n-1} x_{E,n-1,i} - E_n x_{E,n,i}, \qquad n = 1, ..., N,\ i = 1, ..., C, \tag{5.27}$$

$$0 = \gamma_i(\mathbf{x}_{R,n}, T, p) x_{R,n,i} - \gamma_i(\mathbf{x}_{E,n}, T, p) x_{E,n,i}, \qquad n = 1, ..., N,\ i = 1, ..., C, \tag{5.28}$$

$$1 = \sum_{i=1}^{C} x_{R,n,i},\ 1 = \sum_{i=1}^{C} x_{E,n,i}, \qquad n = 1, ..., N, \tag{5.29}$$

$$1 = \sum_{n=1}^{N} b_{F,n}, \tag{5.30}$$

$$x_{R,1,i} = \text{purity}, \qquad i = \text{solute}, \tag{5.31}$$

$$N_{col} = N - \sum_{n=1}^{N} \sum_{n=1}^{n} b_{F,n}, \tag{5.32}$$

$$C_{cap} = f(N_{col}, D_{col}). \tag{5.33}$$

Here, eqs. (5.26) and (5.27) are the overall and tray-to-tray material balances. Eq. (5.28) calculates the liquid-liquid phase split on the trays. Correlations for the column diameter D_{col} and the capital cost C_{cap} are taken from the works by Douglas (1988) and Franke (2006) and are given in Appendix A. For the initialization of the rigorous optimization, an initial column profile is derived by a linear combination of the product and the pinch point compositions from the shortcut evaluation.

It needs to be noted that the superstructure of the MINLP optimization problem

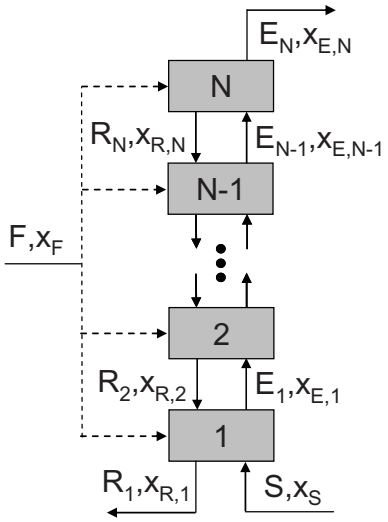

Figure 5.5: MINLP superstructure for the discrete-continuous optimization of countercurrent extraction columns. The variable feed models the number of extraction stages.

in eqs. (5.25)-(5.33) is formulated in a tight way such that the relaxed binary decision variables $b_{F,n}$ take on discrete values at the local minima of the total process cost. This is due to the fact that a distributed feed yields reduced flows at the feed trays in the countercurrent cascade. These reduced flows in turn correspond to reduced separation driving forces which induce a penalty on the costs. Comparable to the rigorous optimization of distillation columns, the binary decision variables $b_{F,n}$ can therefore be replaced by continuous decision variables $c_{F,n}$ to model the discrete decision on the optimal number of column stages. This allows a robust and efficient solution of the column model as a continuous NLP problem instead of a discrete-continuous MINLP problem. Since the local cost minima are found for discrete numbers of trays, special constraints like Fischer-Burmeister functions to force integer decisions (cf. Section 3.3.2) are not required.

5.3 Illustrating examples

The following subsections give examples for the shortcut and rigorous evaluation of extraction columns by the methods introduced in Sections 5.1.3 and 5.2.1. Quaternary mixtures are chosen in these examples for the purpose of graphical representation. The application of the methods to the extraction of a quinternary mixture is demonstrated

subsequently in Section 5.4. The NLP problems were formulated for the optimization platform GAMS 22.7 and solved by the SQP-solver SNOPT on a 3 GHz standard PC.

5.3.1 Acetone, acetic acid, water, and chloroform

The extraction of acetone and acetic acid from water with the solvent chloroform has been studied by Wallert (2008). Table 5.1 gives the specifications for this separation. The coefficients for the calculation of vapor pressures, ideal gas heat capacities, and heats of vaporization are given in Tables D.4, D.13, and D.26. The non-idealities of the liquid-phase are modeled by the UNIQUAC equation with parameters given in Tables D.42 and D.43. The application of the FAM for extraction is illustrated by Fig. 5.6 and the results are given in Table 5.1. Note that the shortcut converges without an initialization step in less than one second. The tray vector at the feed end of the column points directly to the tangential pinch point at the minimum solvent flow rate, which is in good agreement with the value determined by Wallert ($(\mathrm{S/F})_{min} = 0.603$). These values are only slightly smaller than the solvent flow rate determined by a tray-to-tray model with 50 trays (cf. Table 5.1). In contrast to distillation columns with a high tray number, the concentrations are not converging at the ends of the extraction column with 50 trays. It needs to be noted that the extract product compositions $\mathbf{x}_{E,N}$ are also in good agreement.

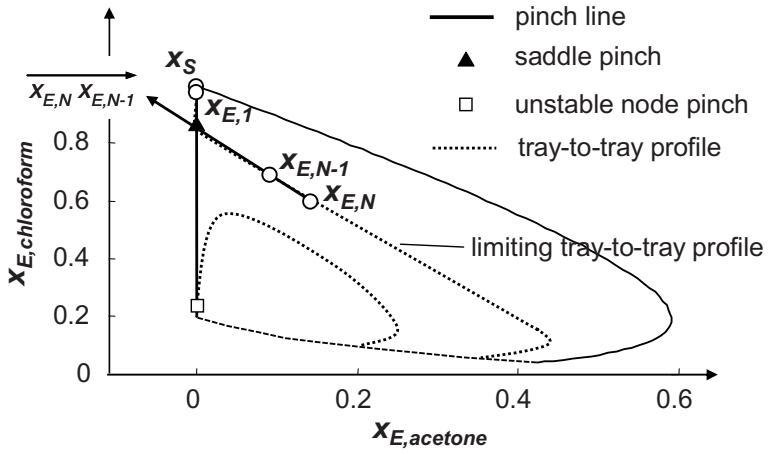

Figure 5.6: FAM for the example of acetone, acetic acid, water, and chloroform. The vector from $\mathbf{x}_{E,N}$ to $\mathbf{x}_{E,N-1}$ points in the direction of the saddle pinch point at the minimum solvent flow rate.

Table 5.1 also shows the results of the rigorous optimization of the extraction col-

Table 5.1: Specifications and results for the extraction of acetone, acetic acid, water, and chloroform at 1.013 bar and 25°C. The tray-to-tray calculations were performed for 50 trays.

	acetone	acetic acid	water	chloroform
$\mathbf{x}_F$	0.15	0.15	0.7	0
$\mathbf{x}_S$	0	0	0	1
$\mathbf{x}_{R,1,acetic\ acid}$	0.01			
$\mathbf{x}_{E,N}$ (FAM)	0.146	0.141	0.108	0.605
$\mathbf{x}_{E,N}$ (tray-to-tray)	0.137	0.132	0.095	0.637
	FAM		tray-to-tray	rigorous optimization
S/F	0.621		0.697	1.127
number of trays			50	6
TAC (F=1kmol/s)				211 k€

umn. Six stages and a solvent flow rate of 1.8 times the minimum are determined to be optimal. The value for the solvent flow rate is relatively large, since the cost for the recovery of the solvent is not considered in this example. It needs to be noted that the calculation time for the rigorous optimization is only slightly larger than the calculation time for the shortcut evaluation of the single column in this example. It will be shown in Section 5.4.3, however, that the evaluation of a hybrid process with several columns benefits greatly from the robustness and efficiency of the shortcut method.

5.3.2 Xylene, toluene, heptane, and propylene carbonate

Fig. 5.7 illustrates the application of the novel shortcut method to the extraction of the aromatics o-xylene and toluene from n-heptane with the solvent propylene carbonate. This example has already been studied by Minotti et al. (1996) and Wallert (2008). The specifications for the separation and the results are given in Table 5.2. The coefficients for the calculation of vapor pressures, ideal gas heat capacities, and heats

of vaporization are given in Tables D.5, D.14, and D.28. The non-idealities of the liquid-phase are modeled by the UNIQUAC equation with parameters from Salem, Hamad and Al-Naafa (1994). The solvent flow rates determined by the different shortcut methods and by the tray-to-tray model are in good agreement. Again, the rigorous optimization cuts the number of stages drastically and raises the solvent flow rate by a large margin, since the cost for the solvent recovery is not considered.

Table 5.2: Specifications and results for extraction of o-xylene, toluene, n-heptane and propylene carbonate at 1.013 bar and 25°C. The tray-to-tray calculations were performed for 50 trays.

	o-xylene	toluene	n-heptane	propylene carbonate
$\mathbf{x}_F$	0.3	0.3	0.4	0
$\mathbf{x}_S$	0	0	0	1
$\mathbf{x}_{R,1,xylene}$	0.01			
$\mathbf{x}_{E,N}$ (FAM)	0.121	0.122	0.032	0.725
$\mathbf{x}_{E,N}$ (tray-to-tray)	0.120	0.121	0.032	0.728
	FAM		tray-to-tray	rigorous optimization
S/F	1.777		1.803	3.709
number of trays			50	5
TAC (F=1kmol/s)				287 k€

5.4 Case study: separation of butanol from fermentation broth

This section presents a case study for the conceptual design of large-scale hybrid extraction-distillation processes by means of the process synthesis framework presented in Chapter 2.6 and the methods introduced in this chapter. This case study, which has been published by Kraemer, Harwardt, Bronneberg and Marquardt (2011), considers the synthesis of a hybrid downstream process for the separation of butanol

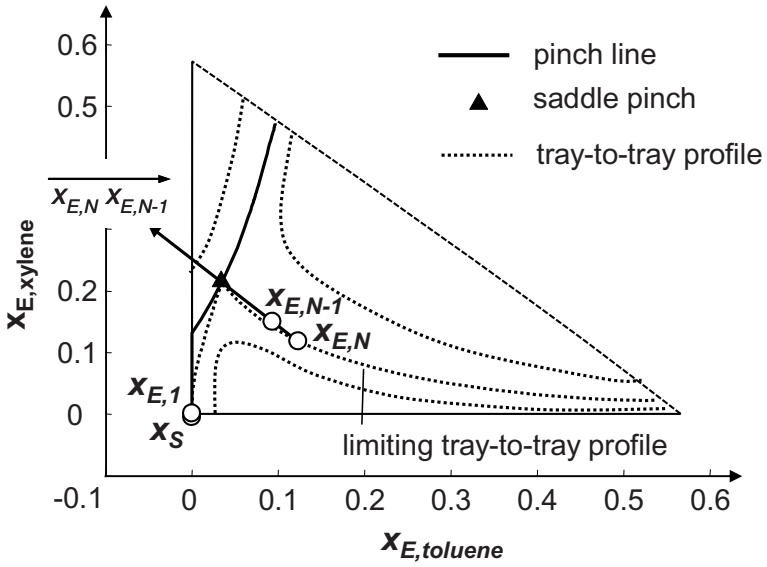

Figure 5.7: FAM for the example of xylene, toluene, heptane, and propylene carbonate. The vector from $\mathbf{x}_{E,N}$ to $\mathbf{x}_{E,N-1}$ points in the direction of the saddle pinch point at the minimum solvent flow rate.

from acetone-butanol-ethanol fermentation. Butanol is a promising candidate for a sustainable biofuel to supplement or replace fossil fuels. Since the depletion of fossil resources as a carbon source will raise the need for novel processes to produce platform chemicals, fuels and products from renewable resources, the example of bio-butanol downstream processing is of great relevance. It also represents a whole class of new bio-based processes.

The identification of the optimal process routes and the design of the optimal flowsheets for these novel processes is a complex process synthesis task. The availability of different feedstocks and the variety of possible bio-based platform chemicals or products makes this synthesis problem particularly challenging. In addition, innovative unit operations, hybrid processes and novel solvents have to be considered during the design phase to tap the full sustainability potential. In the following sections, it will be shown that significant progress in the design of downstream processing can be achieved by the application of systematic and optimization-based process synthesis. A novel hybrid extraction-distillation downstream process will be proposed, which cuts the energy demand of existing downstream processes for bio-butanol production by a large margin.

Section 5.4.1 gives a brief introduction in the fermentative production of butanol and

reviews various options for hybrid downstream processes. We will have a closer look at extraction-distillation downstream processes and study the performance of common solvents for the extraction of butanol from fermentation broth. Section 5.4.2 presents the search for novel solvents with excellent extraction properties via computer-aided molecular design. The systematic optimization-based design of novel energy-efficient hybrid downstream processes by shortcut evaluation and rigorous optimization is then demonstrated in Sections 5.4.3 and 5.4.4.

5.4.1 Fermentative production of butanol from biomass

Butanol can be produced from a wide variety of cellulosic biomass. It has been identified as a superior bio-fuel with excellent fuel properties. Compared to ethanol and other fermentation-derived fuels, butanol offers several advantages as a bio-fuel, such as higher energy content, lower volatility, lower hygroscopy and better miscibility with gasoline (Qureshi and Ezeji, 2008). Apart from its use as a bio-fuel, butanol also makes a suitable platform chemical for further processing to advanced bio-fuels such as butyl-levulinate (Harwardt, Kraemer, Rüngeler and Marquardt, 2011).

Bio-butanol is typically produced via acetone-butanol-ethanol (ABE) fermentation from renewable feedstock using various strains of Clostridium acetobutylicum or Clostridium beijerinckii in anaerobic conditions. Until the 1950s, ABE fermentation has been the industrial standard for butanol production. Bio-butanol production almost ceased in the second part of the 20th century due to the availability and low cost of fossil carbon feedstock. In recent years, ABE fermentation is starting to become appealing to industry again (Hess, 2006). The largest growth is recorded in China, where the annual production of bio-butanol amounted to 210000 tons in 2008 and is expected to reach 1 Mio. tons in the next few years (Ni and Sun, 2009).

The economic competitiveness of bio-butanol production is, however, still hindered by several challenges which need to be addressed in order to make the large-scale production economically viable (Duerre, 2008; Qureshi and Ezeji, 2008). The major challenges are

- expensive feedstock,
- strong product inhibition by butanol and acetone (typically 20 g/l ABE with a mass ratio of 3:6:1 is achievable),
- low productivity (up to 0.6 g/l/h) and ABE yields (0.3) in batch fermentation.

Since the butanol-producing microorganisms are able to catabolize a wide variety of carbohydrates, efforts are being made to use agricultural residues and energy crops

such a switchgrass to reduce the cost of feedstock (i) (Qureshi and Ezeji, 2008). To address product inhibition (ii), hyper-butanol-producing strains are being developed, including C. beijerinckii BA101, which produces ABE up to 33 g/l with a 50% productivity threshold at about 12.5 g/l butanol (Qureshi and Blaschek, 2001). Genetic engineering of butanol producing strains should allow for even lower product inhibition, enhanced productivity and butanol yield (iii) in the future (Woods, 1995). Apart from advanced butanol producing strains, productivity and yield has also been improved by continuous fermentation processes with cell recycle membrane reactors, immobilized cells reactors or packed bed reactors (Groot, der Lans and Luyben, 1992; Qureshi, Schripsema, Lienhardt and Blaschek, 2000; Huang, Ramey and Yang, 2004). Continuous fermentation processes enable the use of concentrated sugar solutions, reduce product inhibition by integrated product removal, and lower the cost of wastewater treatment. ABE productivities of up to 15.8 g/l/h have been achieved in immobilized cell reactors (Qureshi et al., 2000). Various authors also report improved productivities by staged fermentation processes, i.e., reactor cascades where the fermentation conditions are adapted to the respective cell stadium (Afschar, Biebl, Schaller and Schügerl, 1985; Liu et al., 2004).

5.4.1.1 Product removal in downstream processing

Despite the accomplished advances in ABE fermentation, the expensive product removal from the dilute fermentation broth still hinders an industrial production of biobutanol. Pure distillation downstream processes suffer from a high energy demand due to the large content of water in the fermentation broth. These large amounts of water have to be evaporated completely in a distillation column since butanol has a higher boiling point than water. According to Qureshi, Hughes, Maddox and Cotta (2005), the energy required for the separation of butanol in a pure distillation process is therefore often higher than the energy content of butanol itself.

To bring down the cost of separation a variety of authors proposed hybrid downstream processes involving different separation techniques. Examples include distillation columns coupled with liquid-liquid extraction (Ishii, Taya and Kobayashi, 1985), pervaporation (Groot, Schoutens, Van Beelen, Van den Oever and Kossen, 1984), gas stripping (Groot, Van der Lans and Luyben, 1989), perstraction (Groot, Soedjak, Donck, Van der Lans, Luyben and Timmer, 1990), or adsorption (Milestone and Bibby, 1981) units. Groot et al. (1992) and Qureshi et al. (2005) give quantitative comparisons of these hybrid downstream processes. According to Groot et al., hybrid processes with pervaporation or extraction are most attractive for product removal

due to high selectivities and operational advantages. Qureshi et al. suggest that adsorption and extraction combined with distillation are the most energy efficient alternatives. Liu et al. (2004) also prefer extraction in combination with distillation since only conventional unit operations are involved. Although these innovative hybrid processes constitute a leap in energy efficiency from the pure distillation process, the reported specific energy demands are still considerably higher than 10% of the energy content of butanol, which has been stated as the target for energy efficiency (Oudshoorn, Van der Wielen and Straathof, 2009).

It is the scope of this work to systematically explore possibilities to further lower the energy demand of hybrid downstream processing of ABE fermentation broth. Considering the above mentioned promising experiences of other authors and the preference in industry for established unit operations, the energy savings potential of hybrid extraction-distillation processes is studied in the following.

5.4.1.2 In situ extraction of fermentation products

Most publications on ABE removal via extraction study batch fermentation. Here, the fermentation products are removed in situ, i.e. inside the fermenter, into an organic solvent phase. While the inhibitory solutes are directly removed into the solvent phase in this setup, some authors indicate that extractive fermentation with in-situ product removal may not be suitable for large-scale production due to various reasons:

- slow mass transfer into solvent phase (slower than butanol production) (Roffler, Blanch and Wilke, 1987, 1988),
- formation of emulsions through agitation (Roffler et al., 1988; Groot et al., 1990, 1992; Qureshi, Maddox and Friedl, 1992),
- cell inhibition by solvent (interface toxicity) and loss of cells at interface (Qureshi et al., 1992),
- physical shielding by attraction of cells to interface: real distribution coefficients in fermenter lower than in experiments without cells (Davison and Thompson, 1993),
- precipitates carry water into the solvent phase (Groot et al., 1990),
- difficult process control (Oudshoorn et al., 2009).

For these reasons, external product removal in an extraction column with a recycle of product-lean broth seems to be better suited for large-scale production of bio-butanol (Roffler et al., 1987, 1988; Oudshoorn et al., 2009).

5.4.1.3 Extraction of fermentation products in an external column

The continuous extraction of the fermentation products can also be carried out in an external extraction column with a recycle of the product lean fermentation broth back to the fermenter. For this setup, a large extraction column is needed due to the large recycle of the dilute fermentation broth. In addition, the microorganisms need to be retained inside the fermenter by immobilization or ultrafiltration. But more importantly, there are significant advantages of an extraction in an external column:

- use of powerful but toxic solvents, if the solubility in the aqueous recycle to the fermenter is very low (Eckert and Schügerl, 1987),
- high mass transfer rates in the extraction column (Roffler et al., 1987, 1988),
- extraction can be carried out at optimal temperatures, which can differ from the fermentation temperature.

Considering these advantages and also the drawbacks of in-situ extraction raised in the previous section, only external product removal is considered for the design of the downstream process in this work.

5.4.1.4 Screening of solvents for extraction of fermentation products

The performance of the extraction-distillation downstream process greatly depends on the choice of the extracting agent, regardless whether the extraction is carried out inside or outside the fermenter. Various authors have therefore conducted extensive solvent screenings (Ishii et al., 1985; Dupire and Thyrion, 1986; Matsumura and Kataoka, 1987; Roffler et al., 1987; Groot et al., 1990; Oudshoorn et al., 2009), where a wide range of possible solvents were checked manually against the following criteria:

- high capacity, i.e. high distribution coefficient for butanol $D_{butanol}$,
- high selectivity $D_{butanol}/D_{water}$,
- non-toxicity to cells when extraction is carried out inside fermenter,
- low viscosity,
- different density than water,
- commercially available at low cost.

Two main groups of solvents have been identified, namely alcohols and alkanes. While alcohols exhibit high capacities ($D_{butanol} > 5$ g/g), they have relatively low selectivities ($D_{butanol}/D_{water} < 350$) for butanol, i.e. a large fraction of water in the solvent phase (Groot et al., 1990). Alkanes, on the other hand, offer large selectivities

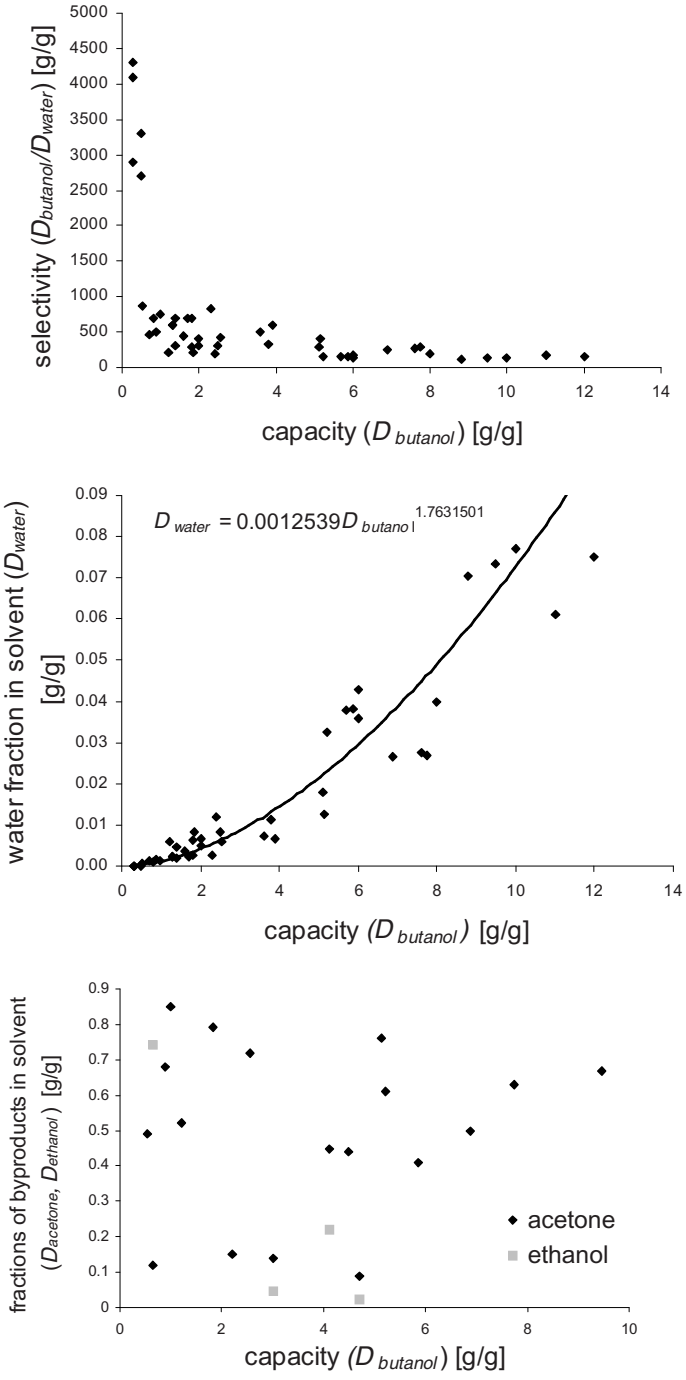

Figure 5.8: Data of 44 solvents for ABE extraction collected from various publications for comparison of their capacity and selectivity (Ishii et al., 1985; Dupire and Thyrion, 1986; Matsumura and Kataoka, 1987; Roffler et al., 1987; Groot et al., 1990; Oudshoorn et al., 2009).

($D_{butanol}/D_{water}$ = 2500-4300) but suffer from low capacities ($D_{butanol} < 0.5$ g/g). The properties of 44 possible solvents have been gathered, which were studied in solvent screenings for ABE extraction by the authors referenced above. The combined data is shown in Fig. 5.8, which plots the selectivity $D_{butanol}/D_{water}$ and the distribution coefficient D_{water}, i.e. the fraction of water in the solvent phase, over the solvent capacity $D_{butanol}$. Based on these data, it can be concluded that the solvent selectivities are typically inversely related to the solvent capacities.

Many authors have chosen oleyl alcohol as extracting agent due to its non-toxicity towards the microorganisms and its relatively high distribution coefficient for butanol ($D_{butanol}$ = 3.8 g/g). Oleyl alcohol has therefore become the solvent of choice for extractive ABE removal and many authors report enhanced cell productivity and butanol yields for extractive fermentations using oleyl alcohol as the solvent (Ishii et al., 1985; Roffler et al., 1987; Qureshi et al., 1992; Davison and Thompson, 1993). However, most studies were carried out as batch fermentations in lab-scale. Under these circumstances, some disadvantages of oleyl alcohol for continuous industrial-scale production have little effect. In particular the low distribution coefficient for acetone ($D_{acetone}$ = 0.34 g/g) requires a large amount of solvent to prevent an accumulation of the inhibitory acetone in the fermentation. The required amount of solvent is therefore determined by the removal rate of the byproducts rather than by butanol itself (Matsumura, Kataoka, Sueki and Araki, 1988). In addition, the high boiling point of oleyl alcohol (330-360°C) makes the separation of the products from oleyl alcohol via distillation in a large-scale process very expensive.

Pitner, Schulte, Gorak, Santangelo and Wentink (2008) propose the use of ionic liquids for the extraction of butanol from fermentation broth. While the authors claim that the considered ionic liquids are biocompatible, they also report moderate selectivities for butanol ($D_{butanol}/D_{water} < 500$).

5.4.1.5 Study of solvent performance in downstream process

In their work on extractive distillation, Kossack et al. (2008) have shown that an entrainer screening based on selectivity or capacity alone is not sufficient and could possibly lead to an unfavorable entrainer choice. Instead, the authors suggest complementing the entrainer screening with an evaluation of the entrainer performance in the flowsheet, i.e. by an evaluation of the separation process performance with shortcut methods. For the complex downstream process, the repeated evaluation of possible flowsheets for many different solvents seems too tedious, even when powerful shortcut methods are available. For ABE extraction, however, the correlation of D_{water},

i.e. the fraction of water in the solvent, and $D_{butanol}$ can be qualitatively approximated by the function given in Fig. 5.8 (center). Assuming that all solvents roughly follow this function, it is possible to identify the region of optimal solvent properties without an individual process evaluation for each solvent. For this purpose, the correlation of D_{water} and $D_{butanol}$ is inserted into a simplified downstream process model (cf. Fig. 5.9), which consists of an extraction column, a solvent recovery column with preheating of the feed, and a purification column. This simplified process model can be used when the solvent is the high boiler of the system (which is the case for all but three of the 44 considered solvents) and when the following two major simplifications are made:

- ideal vapor-liquid equilibrium (VLE), i.e. no distillation boundaries,
- identical relative volatilities, heat capacities, and heat of vaporization for all solvents.

The first simplification is violated at least by a distillation boundary between water and butanol such that the sharp separation of butanol in the second distillation column is not feasible when non-ideal VLE is considered. The relative volatilities, heat capacities, and heat of vaporization of the common solvent oleyl alcohol are used as representatives for the actual values for each individual solvent. While these are significant simplifications, the simplified process model still gives insight into the process behavior and enables a first, quick solvent property evaluation.

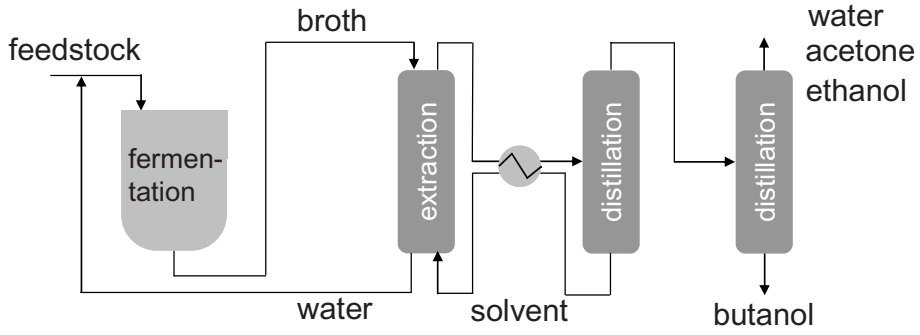

Figure 5.9: Simplified hybrid downstream process for a preliminary study of solvent performance.

The extraction column is modeled by the FAM for extraction (cf. Section 5.1.3). The distribution coefficient for butanol is a degree of freedom in this model. The concentration of water in the organic phase is expressed by the function from Fig. 5.8 (center). It can be seen in Fig. 5.8 (bottom) that the distribution coefficients of acetone and ethanol cannot be correlated to the distribution coefficient of butanol.

Therefore, we assume constant values of $D_{acetone} = 0.34$ g/g and $D_{ethanol} = 0.28$ g/g, which are the values for oleyl alcohol.

In order to keep the distillation models as simple as possible, the distillation columns are modeled by Underwood's method. Note that Underwood's method and the simplifications mentioned above were only used in this section for the purpose of a quick solvent property evaluation. Powerful shortcut methods based on rigorous, non-ideal VLE behavior will be applied in the process evaluation in Section 5.4.3.

The butanol concentration in the broth is set to 8 g/l. This concentration is below the threshold for butanol inhibition and has been reached in continuous fermentations (Roffler et al., 1988; Qureshi et al., 2000). All butanol is removed from the broth in the extraction but fractions of acetone and ethanol are recycled back to the fermenter due to smaller distribution coefficients for these byproducts. A relatively high ethanol concentration in the broth of 5 g/l is therefore assumed. The concentration of acetone in the broth (12 g/l) is determined from a mass balance around the extraction column assuming that the mass ratio of butanol and acetone in the extract stream is 2:1, which is consistent with the ratio produced by the microorganisms in the fermentation (Jones and Woods, 1986). The total concentration of ABE in the broth is allowed to rise up to a concentration of 25 g/l, above which it becomes toxic to the microorganisms (e.g. Qureshi and Ezeji (2008)).

Table 5.3: Results of the solvent performance study for different values of $D_{acetone}$. D_{water} denotes the fraction of water in the solvent.

	$D_{butanol}$ [g/g]	D_{water} [g/g]	$Q_{reboiler,min}$ [MJ/kg butanol produced]
optimum for $D_{acetone} = 0.34$ g/g	1.05	1.37e-3	10.5
oleyl alcohol ($D_{acetone} = 0.34$ g/g), D_{water} from correlation	3.8	1.32e-2	12.9
oleyl alcohol ($D_{acetone} = 0.34$ g/g), real value for D_{water}	3.8	1.14e-2	11.5
optimum for $D_{acetone} = 0.68$ g/g	2.04	4.40e-3	6.0

The approximate downstream process model is formulated as a nonlinear optimization (NLP) problem with $D_{butanol}$ as degree of freedom and the minimization of

the process reboiler duties as objective. The results of this study are shown in Table 5.3. The process reboiler duties are minimized for $D_{butanol} = 1.05$ g/g. For values of $D_{butanol} > 1.05$ g/g, the cost for the separation of water in the columns predominates the savings through lower solvent flow rates. Hence, the energy demand for the common solvent oleyl alcohol is considerably higher than the optimum. Note that the two results for oleyl alcohol in Table 5.3 refer to different assumptions for the fraction of water in oleyl alcohol: (a) D_{water} from the correlation in Fig. 5.8 (center), and (b) real value for D_{water} as given in the work by Matsumura and Kataoka (1987).

Note that higher values of $D_{butanol}$ also result in the condition that the solvent flow rate is controlled by the required removal of acetone rather than butanol. When the distribution coefficient for acetone is doubled from $D_{acetone} = 0.34$ g/g to $D_{acetone} = 0.68$ g/g, a substantially higher optimal value of $D_{butanol}$ and a significantly lower process reboiler duty is obtained (cf. Table 5.3).

The results of this preliminary study apparently support the argument of Matsumura et al. (1988) that the minimum solvent flow rate is often controlled by the removal rate of the byproducts. In addition, an optimal balance between $D_{butanol}$ and D_{water}, is crucial for an energy-efficient downstream process.

5.4.2 A novel solvent for energy-efficient product removal

After the rough estimates in the previous section, a novel solvent is identified next, which fulfills the stated requirements.

5.4.2.1 Solvent screening by computer-aided molecular design

Following the methodology of the process synthesis framework depicted in Fig. 1, the optimal solvent for the extraction of ABE has to be chosen in the first step. Here, progress in solvent screening by computer aided molecular design (CAMD) can be exploited to identify novel solvents. The CAMD solvent selection procedure has been performed with the help of the software package ICAS (Harper and Gani, 2000), which uses a generate-and-test approach to screen molecules. First, thresholds for the desired properties and a selection of functional groups have to be specified by the user. Then, meaningful molecules are generated by CAMD and tested for the desired properties based on thermodynamic group contribution methods, i.e. UNIFAC. These tested molecules can then be ranked and checked against a database to exclude non-existing molecules. Compared to tedious manual solvent screening, the CAMD approach offers a significant speed-up of the solvent screening procedure. In addition, CAMD provides

a larger search space of possible solvents, since the estimation of the relevant properties based on group contribution methods allows the evaluation of molecules for which only limited property data is available.

It will be shown in Section 5.4.2.3 that the predictions of the solvent properties by UNIFAC can be quite inaccurate. Despite the inaccuracies in the absolute values, however, the application of CAMD provides valuable information about suitable solvents and often leads to the selection of superior solvents (see also Peters, Zavrel, Kahlen, Schmidt, Ansorge-Schumacher, Leitner, Buechs, Greiner and Spiess (2008)).

Although ICAS is an easy to use software tool, the application of CAMD for solvent selection requires a careful choice and weighting of selection criteria in order to obtain meaningful solvents. In this work, information on the optimal selection criteria is gained through the preliminary solvent evaluation in Section 5.4.1.5. Based on these results, we particularly emphasize large distribution coefficients for acetone and a favorable balance between the solvent capacity ($D_{butanol}$) and the solubility for water (D_{water}).

When the cells are retained in the fermenter by immobilization or ultrafiltration, powerful but toxic solvents can be used in an external extraction column as long as their solubility in the aqueous recycle to the fermenter is negligible. Hence, we do not exclude toxic solvents but emphasize a very low solubility in water. In addition, we pay attention to operational constraints like viscosity, melting point, and boiling point such that the solvent recovery by distillation is technically feasible and economically viable.

5.4.2.2 Novel solvents

With the help of CAMD and the selection criteria discussed above, novel solvents are identified which exhibit optimal extraction properties for the extraction of ABE from fermentation broth in an external extraction column: these solvents belong to the class of the tri- and tetramethylbenzenes. According to a survey of the literature, these solvents have never been chosen in solvent screenings for ABE removal from fermentation broth before. This is probably due to the expected toxicity to the cells when applied in situ and the relatively low distribution coefficient for butanol at room temperature compared to fatty alcohols. From the tri- and tetramethylbenzenes, 1,3,5-trimethylbenzene (also known as mesitylene) is chosen as the favorite solvent although tetramethylbenzene has a higher selectivity for butanol. Mesitylene, however, is a common solvent in many industrial applications and may therefore also be preferred for the extraction of butanol.

5.4.2.3 Comparison of the novel solvent mesitylene with the common solvent oleyl alcohol

Table 5.4 lists the predicted and measured properties of the new solvent mesitylene and gives a comparison to the measured values for oleyl alcohol, which is the common solvent choice in the literature. The first column contains the properties for the new solvent mesitylene as predicted by UNIFAC at 25°C, which led to the selection in the solvent screening procedure by CAMD. The predicted value for $D_{butanol}$ in mesitylene is considerably lower than $D_{butanol}$ in oleyl alcohol. This is presumably the reason why mesitylene has never been chosen as extracting agent for the ABE removal in an external extraction column before. It is important to note, however, that $D_{butanol}$ in mesitylene is close to the optimal value of $D_{butanol}$ determined in the solvent performance study in Section 5.4.1.5. In addition, the distribution coefficient for acetone in mesitylene is significantly larger than the distribution coefficient for acetone in oleyl alcohol. This is an important advantage of mesitylene since acetone also inhibits cell productivity and needs to be removed from the broth in considerable amounts as well. In fact, it was shown in Section 5.4.1.5 that the minimum flow rate of oleyl alcohol to remove the inhibitory products is determined by the low distribution coefficient for acetone rather than the large distribution coefficient for oleyl alcohol (see also Matsumura et al. (1988)). Note that ethanol is by far the least inhibitory product and, therefore, the relatively low distribution coefficient for ethanol should not be detrimental.

To validate the properties predicted by the UNIFAC group contribution method, the distribution coefficients for acetone, butanol, and ethanol in mixtures of water and mesitylene (cf. Table 5.4) were measured. At 25°C, the measured distribution coefficients are considerably lower than the predicted coefficients, particularly for acetone and ethanol. However, when the temperature was increased to 80°C, well below the boiling point of the broth, significantly higher distribution coefficients were measured such that the conclusions drawn from the predicted values are valid again. It needs to be noted, however, that the measurements of the distribution coefficients given in Table 5.4 point to an inaccuracy of the UNIFAC predictions. Therefore, the measured data of Table 5.4 will be used in the simulations of the extraction column presented in Sections 5.4.3 and 5.4.4.

The solubility of water in mesitylene has also been determined experimentally (cf. Table 5.4). The solubility increases with the temperature but remains remarkably low even at elevated temperatures ($D_{water} = 0.0074$ mol/mol or 0.00113 g/g at 80°C). Note that the solubility of water in mesitylene is well below the curve for common

Table 5.4: Solvent properties of the novel solvent mesitylene compared to the common solvent oleyl alcohol.

	mesitylene			oleyl alcohol
	UNIFAC	measured	measured	(Matsumura, 1987, 1988)
	25°C	25°C	80°C	30°C
$D_{butanol}$ [g/g]	1.3	0.76	2.2	3.8
$D_{acetone}$ [g/g]	1.4	0.43	0.83	0.34
$D_{ethanol}$ [g/g]	0.14	0.03	0.1	0.28
selectivity ($D_{butanol}/D_{water}$)	7879	1650	1970	330
solubility of water in solvent [mol frac]	0.0011	0.0031	0.0074	0.15
solubility of solvent in water [mol frac]	4e-6	7.8e-6 (Zou, 1999)		1.3e-6
viscosity [mPa s]	0.66			26
boiling point [°C]	165			330-360
melting point [°C]	-45			13-19

solvents in Fig. 5.8 (center). Accordingly, mesitylene exhibits a very high selectivity ($D_{butanol}/D_{water} = 1970$ at 80°C), significantly higher than the selectivities of the solvents with a comparable capacity of $D_{butanol} = 2.2$ g/g in Fig. 5.8 (top). Oleyl alcohol on the other hand exhibits a substantially higher solubility for water. This results in significant amounts of water in the organic phase, which raises the cost for the recovery of the oleyl alcohol and the downstream purification of butanol and acetone. Because of the high solubility of water in oleyl alcohol, it was not considered to raise the temperature in the extraction with oleyl alcohol, since this would lead to an even higher water content in the solvent.

The solubility of mesitylene in water at 25°C as given in Table 5.4 was measured by Zou, Yang, Han, Liu and Yan (1999). Since this value is in the ppm-range, toxic effect of mesitylene on the cells in the fermenter is not expected. While the solubility may be higher at 80°C, a decantation of the aqueous recycle at the fermentation temperature of 35°C removes an excess of mesitylene.

In addition to the favorable solvent properties mentioned above, mesitylene offers additional advantages over the common solvent oleyl alcohol. Whereas oleyl alcohol removes the valuable intermediates butyric acid ($D_{butyricacid} = 3.7$ g/g) and acetic acid ($D_{aceticacid} = 0.35$ g/g) from the broth (Matsumura et al., 1988), mesitylene is expected to leave these intermediates ($D_{butyricacid} = 0.6$ g/g, $D_{aceticacid} = 0.04$ g/g, predicted by UNIFAC) in the broth such that they can be catabolized in the fermenter. Groot et al. (1990) and Groot et al. (1992) report fouling inside the extraction column when they use oleyl alcohol as solvent due to its non-toxicity. The anticipated toxicity of mesitylene, however, will presumably reduce fouling. Both solvents have a density that allows for an efficient phase separation (0.85 g/cm3), but the higher viscosity of oleyl alcohol (cf. Table 5.4) results in a diffusion coefficient of only 1.1e-10 m2/s (Groot et al., 1992), which leads to a large height (HETP) of the extraction stages. Significantly smaller HETP values are expected for mesitylene thanks to its low viscosity. The moderate melting and boiling points (cf. Table 5.4) also favor mesitylene. The high boiling point of oleyl alcohol, on the other hand, hinders a separation of the products in a distillation column. The melting point just below room temperature can also complicate large-scale industrial production.

Because of the favorable solvent properties of mesitylene, especially the relatively high distribution coefficient for acetone and the low solubility for water, low flow rates for the removal of the products and little water in the extract phase is expected. This will ultimately lead to an energy-efficient downstream process as will be shown by the process evaluations in Sections 5.4.3 and 5.4.4.

5.4.3 Shortcut evaluation of downstream process variants

As a consequence of the above-mentioned favorable solvent properties of mesitylene, it is expected that the use of mesitylene as the solvent in the hybrid extraction-distillation downstream process can significantly reduce the separation costs. Entire downstream processes for ABE purification are modeled in this section in order to quantify the energy savings in comparison to alternative designs and determine the optimal flowsheet for the novel solvent. Specifically, hybrid extraction-distillation processes using the new solvent mesitylene and the state-of-the-art solvent oleyl alcohol are evaluated. Both hybrid processes are compared to pure distillation processes.

The basic structure of these hybrid extraction-distillation downstream processes is sketched in Fig. 5.10. This flowsheet considers possible heat integration within the recycle loops and between the extraction and the condensers of the purification columns. The heat integration allows the operation of the extraction column at elevated tem-

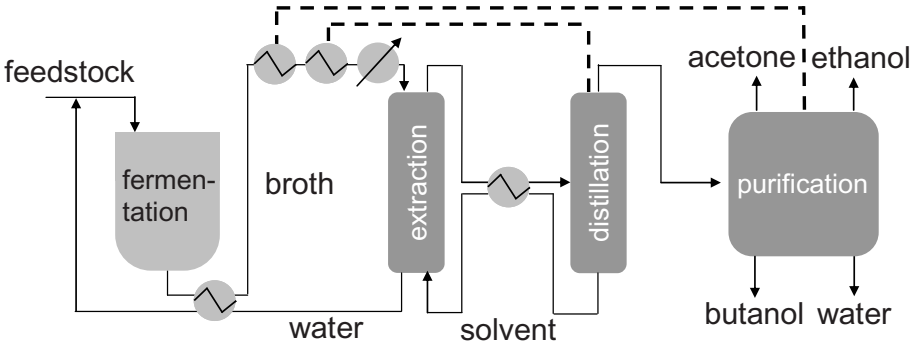

Figure 5.10: Basic structure of hybrid extraction-distillation downstream processes with heat integration. Different sequences of distillation columns are possible within the black box 'purification'.

perature without the drawback of additional energy consumption.

The product purification following the extraction process is performed in the black box "purification" in Fig. 5.10. Many alternative sequences of distillation columns are conceivable for the purification of the strongly non-ideal azeotropic mixture of ABE and water. The occurrence of a liquid-phase split between water and butanol allows the use of decantation for separation. It is important to note that the identification of the feasible and most energy-efficient sequences for the purification process is a non-trivial task and depends on the composition of the distillate stream of the solvent recovery column. Since different solvents in the extraction yield different compositions of this distillate stream, the best sequence for the purification system ultimately depends on the use of the solvent.

The alternative downstream processes offer various operational degrees of freedom with a direct influence on energy demand and investment costs. A major operational degree of freedom of the process with the novel solvent mesitylene is the purity of the aqueous raffinate recycles to the fermenter. Larger fractions of ABE in the raffinate yield a lower solvent flow rate and thus a lower energy duty for the reboiler of the recovery column. In this case, however, the broth flow rate needs to be increased to meet the specified butanol production level, which in turn raises the heat losses induced by the recycling of the product-lean broth at temperatures higher than 35°C. Hence, the optimization of this trade-off can significantly bring down the process energy demand. Another degree of freedom of the process with a large impact on the costs is the temperature difference of the heat exchanger between the broth and raffinate streams. This heat exchanger needs to be very large due to the large flow rates of the very dilute broth. A smaller temperature difference in the heat exchanger

minimizes the heat losses but gives rise to even larger heat exchange areas. Obviously, the determination of an optimal temperature difference minimizes the costs.

The intermediate flows within the sequence of purification columns offer additional degrees of freedom where energy can be saved through optimization. These optimization tasks need to be considered in the shortcut evaluation of the novel downstream process in order to obtain a meaningful assessment of the minimum separation cost. Hence, the suitable shortcut methods for this case study are required to be

- fully algorithmic and computationally efficient,
- applicable to quinternary mixtures,
- sufficiently accurate for the distillation of heterogeneous mixtures.

The FAM for distillation and extraction as introduced in Sections 4.5 and 5.1.3 meets these requirements and is therefore used as shortcut method for the evaluation of the separation. In fact, the downstream processes in this example are perfectly suited to demonstrate the performance of the FAM for highly non-ideal multicomponent separation processes.

5.4.3.1 Shortcut evaluation of novel hybrid downstream process

For an evaluation of alternative hybrid downstream processes with the novel solvent mesitylene a butanol production rate of 40000 t/a is assumed. The butanol concentration in the fermentation broth is set to 8 g/l, which has been reached in continuous fermentations in the literature (Roffler et al., 1988; Qureshi et al., 2000). The concentration of acetone in the broth (10.5 g/l) is determined from a mass balance around the extraction column assuming an acetone:butanol fermentation mass ratio of 1:2 (cf. Section 5.4.1.5). The ethanol concentration is assumed to be 5 g/l.

The liquid-liquid equilibrium is modeled with the measured distribution coefficients for ABE in the water-mesitylene system. As shown in Fig. 5.11, the distribution coefficient for butanol $D_{butanol}$ increases with the overall concentration of butanol. The linear approximation given in Fig. 5.11 has therefore been used for $D_{butanol}$. Constant values can be used for $D_{acetone}$ and $D_{ethanol}$ as shown in Fig. 5.11. The solubility of water in mesitylene is modeled using the measured values at 80°C (cf. Table 5.4). For the solubility of mesitylene in water, values from the literature at 25°C (cf. Table 5.4) are used, since the aqueous recycle is cooled down and passed through a decanter before being recycled to the fermenter. These solubilities are assumed to be constant over the very limited range of concentrations of ABE in the broth and in the solvent ($x_{ABE} < 0.05$). The vapor pressures, ideal gas heat capacities, and heats of

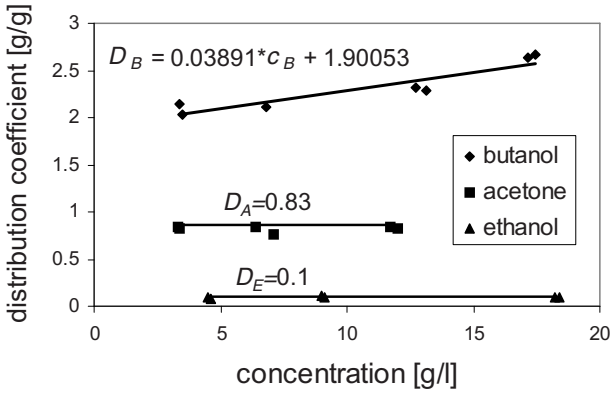

Figure 5.11: Measured distribution coefficients for butanol, acetone and ethanol in water-mesitylene at 80°C and 1.013 bar. Linear regression for butanol.

vaporization are calculated by coefficients given in Tables D.6, D.15, and D.30. The vapor-liquid-equilibrium in the distillation columns is modeled by the NRTL model with missing binary parameters for mesitylene derived from activity coefficient estimation by COSMO-RS (cf. Tables D.44 and D.45).

The flowsheet evaluation has been performed by an optimization of the operating point in a NLP problem. The feasible flowsheet resulting in the lowest energy demand is shown in Fig. 5.12. The main degrees of freedom in the optimization are the purity of the raffinate recycle and the temperature difference of the large heat exchanger Hex 1. Furthermore, the composition of the distillate of column Col 2 has not been fixed but constrained by the distillation boundary between acetone and the ethanol/water/butanol plane. This constraint is checked algorithmically with the help of the FAM as proposed in Section 4.5.2. In order to optimize these degrees of freedom simultaneously, the NLP problem covered the whole downstream process with the exception of the second purification column (Col 3). Since it is not part of a recycle or a heat-integration loop, it can be evaluated separately. The objective function is formulated such that all degrees of freedom can be optimized effectively. Hence, a minimization of the hot utilities of the process is not sufficient. The investment for the large heat exchanger Hex 1, which is also a significant cost factor, has to be minimized as well. The objective function therefore included the costs of the hot utilities for Col 1 and Col 2 and the annualized capital cost of heat exchanger Hex 1. For the shortcut evaluation, this simplified cost function yielded reasonable results while allowing an efficient solution of the optimization problem.

Due to the efficient algorithmic shortcut methods, the optimization problem could be solved in 12 CPU seconds on a 2.66 Ghz PC. At the optimal operating point, the

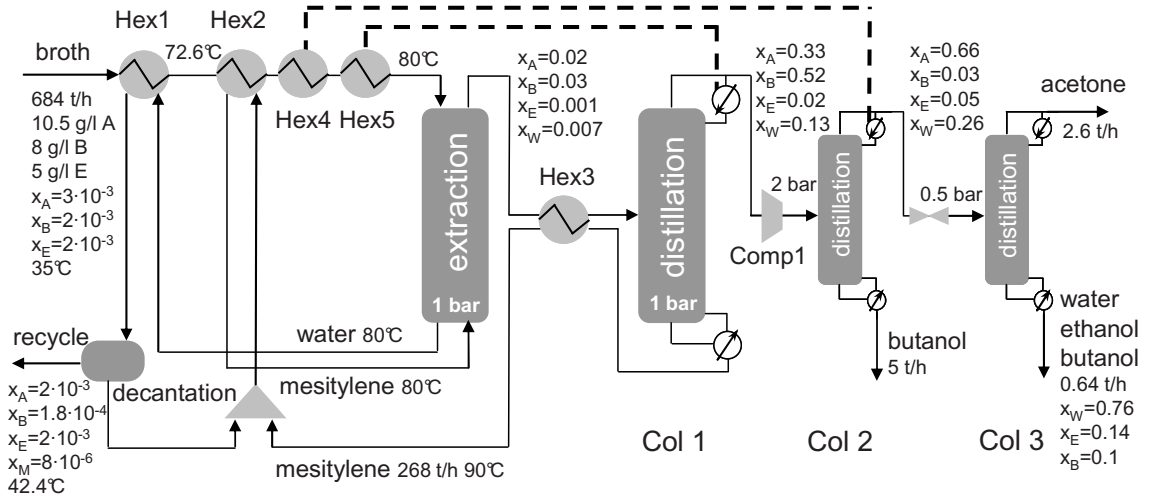

Figure 5.12: Novel extraction-distillation downstream process (solvent mesitylene) with results from the shortcut evaluation for the production of 40000 t/a butanol.

fermentation broth is heated by the raffinate recycles and the condensers of the recovery and the first purification column to 80°C (cf. Fig. 5.12). The cost minimization yielded a logarithmic mean temperature difference of 7.4°C in Hex 1, such that the broth leaves Hex 1 with a temperature of 72.6°C. Thus, an additional heater after the cascade of heat exchangers (cf. Fig. 5.10) becomes redundant. The butanol-lean broth leaves the heat exchanger Hex 1 at 42.4°C and is recycled to the fermentation after being cooled to 35°C in an additional heat exchanger, which is not modeled.

The extraction is carried out at 80°C and 1 bar. A butanol content of $x_{butanol} = 1.8 \cdot 10^{-4}$ in the raffinate recycles is determined to be cost-optimal. The low water content of $x_{water} = 0.13$ in the distillates of the mesitylene recovery column allows an efficient purification of butanol and acetone in a pressure swing column sequence. The pressure of Col 2 is raised to 2 bar in order to shift the distillation boundary between acetone and the water/butanol azeotrope towards the acetone/water edge. This minimizes the amount of butanol which is lost via the distillate of Col 2. Furthermore, the pressure increase raises the temperature in the condenser of Col 2 to 86.4°C such that the heat exchange with the broth stream in Hex 4 is feasible. Due to the pressure-shift to 0.5 bar in Col 3, acetone can be separated efficiently from the remains of water, butanol, and ethanol. The purge stream which is drawn from the bottom of Col 3 still contains some ethanol and butanol. It remains to be studied whether a purification of this purge stream is worthwhile. The distillate streams which are fed into a subsequent column are not condensed but transferred as saturated vapor as a measure of heat

integration. Note that a liquid-phase split does not occur in the distillation columns at the optimal operating point determined in the shortcut evaluation. This is mainly due to the low water content in the extract.

5.4.3.2 Shortcut evaluation of hybrid downstream process with solvent oleyl alcohol

Fig. 5.13 shows the optimal flowsheet determined for the hybrid downstream process using the common solvent oleyl alcohol. Again, the butanol and ethanol concentrations in the broth are assumed to be 8 g/l and 5 g/l, respectively. Due to the low distribution coefficient of oleyl alcohol for acetone, the content of acetone in the broth increases to 12 g/l such that the total ABE content in the broth reaches the maximum non-toxic concentration of 25 g/l. Still, the low distribution coefficient of acetone in oleyl alcohol ($D_{acetone} = 0.34$) results in a significantly higher solvent flow rate than necessary for the sole removal of butanol. The missing binary parameters for the NRTL model were derived from activity coefficient estimation by COSMO-RS (cf. Tables D.44 and D.45).

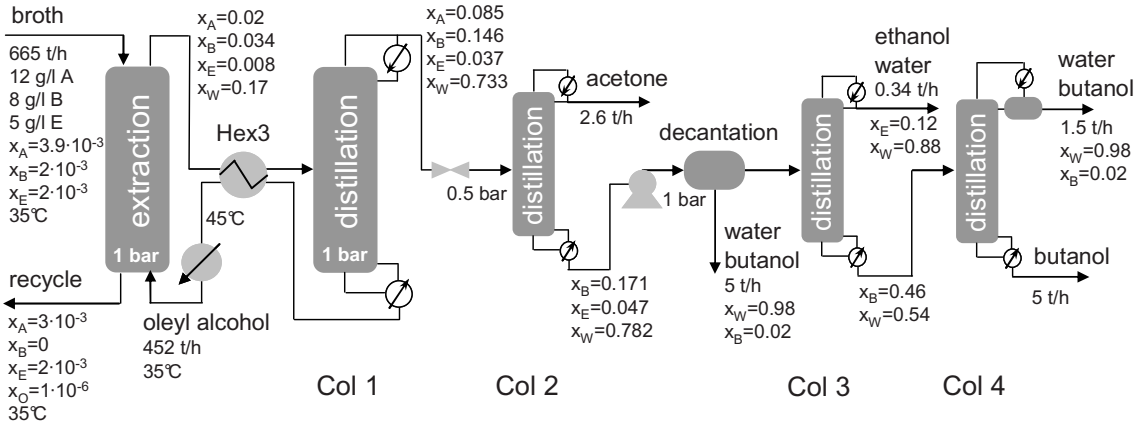

Figure 5.13: Extraction-distillation downstream process (solvent oleyl alcohol) with results from the shortcut evaluation for the production of 40000 t/a butanol.

The extract is preheated by the solvent recycles before it enters the recovery column Col 1. Further preheating of the extract by the condensers of the purification columns is not considered since the pressure of these columns would have to be raised significantly. The considerably higher content of water in the distillates of the recovery column prohibits a simple purification column sequence as in the process for

the solvent mesitylene. Instead, a more complex purification sequence of two simple columns, a decanter and a heteroazeotropic column is determined to be feasible and most energy-efficient. Acetone is separated in the first purification column. The heterogeneous bottoms product of this column is given in a decanter and split in a water-rich and a butanol-rich phase. Note that a considerable amount of about 100 kg/h butanol is purged with the water-rich phase. The butanol-rich phase is fed to the second purification column, where a mixture of water and ethanol is removed at the top. Pure butanol is then separated from the remains of water in a last, heteroazeotropic distillation column. The heteroazeotrope between water and butanol is split with the help of a decanter at the top of this column.

5.4.3.3 Shortcut evaluation of pure distillation downstream process

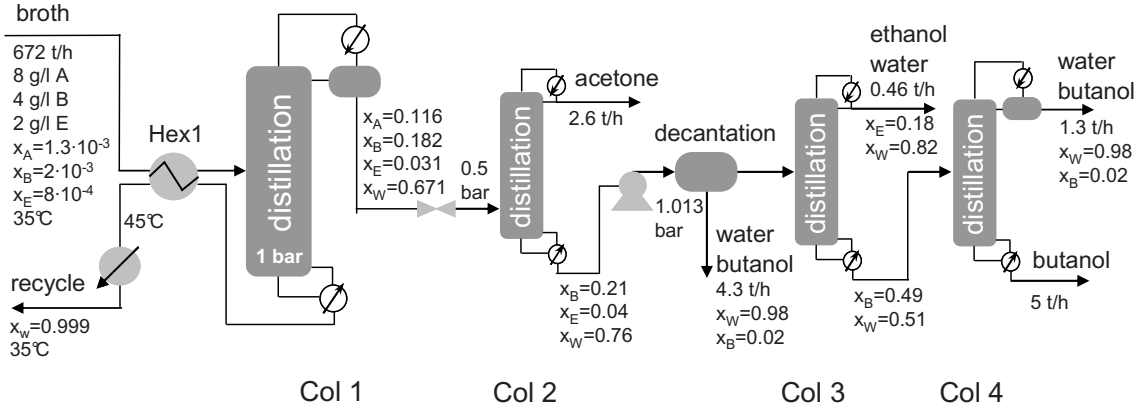

Figure 5.14: Pure distillation downstream process with results from the shortcut evaluation for the production of 40000 t/a butanol.

The optimal flowsheet for the pure distillation downstream process is given in Fig. 5.14. The butanol concentration in the broth of 8 g/l is accompanied by lower concentrations of acetone and ethanol compared to the hybrid processes since all products are separated completely in the first column Col 1. The pure distillation process also benefits from heat integration around Col 1, which reduces the energy demand below the values reported in the literature for pure distillation processes considerably. The distillate from the decanter at the top of Col 1 is located on the butanol rich side of the water/butanol miscibility gap. The large content of water in the distillate of Col 1 leads to a high energy demand of the further purification sequence. Note that the structure of this sequence of distillation columns is identical to the sequence of the hybrid process with the solvent oleyl alcohol. Again, a considerable amount of butanol is purged with the water-rich phase from the decanter.

5.4.3.4 Comparison of minimum energy demands

Table 5.5 compares the minimum energy demands and solvent flow rates of the hybrid distillation-extraction processes and the pure distillation process. Also given are the concentrations of ABE in the broth feed, which are determined as described in Sections 5.4.3.1 - 5.4.3.3. The downstream process with the solvent mesitylene exhibits a specific energy demand of 4.8 MJ/kg butanol produced, which corresponds to 13% of the energy content of butanol. This is a significant reduction compared to the extraction with oleyl alcohol (13.3 MJ/kg butanol), the pure distillation process (18.4 MJ/kg butanol), and the most energy-efficient hybrid downstream process for ABE separation reported in the literature (8.2 MJ/kg butanol via adsorption-distillation (Qureshi et al., 2005; Oudshoorn et al., 2009)). While the latter process is also very energy-efficient, it needs to be noted that adsorption may not be preferred in industrial practice due to the necessity of discontinuous operation and the solids handling.

Table 5.5: Reboiler and compressor energy demands of the hybrid processes with the novel solvent mesitylene and the common solvent oleyl alcohol. Energy demands of the pure distillation process for comparison. Butanol production rate: 40000 t/a. Energy content of butanol: 36 MJ/kg.

	conc. in broth	solvent flow	reboiler/compressor energy demand [MW]						
	[g/l ABE]	[t/h]	Col1	Col2	Col3	Col4	Comp1	total	specific
solvent mesitylene	10.5/8/5	268	5.9	0.35	0.35		0.12	6.7	4.8 MJ/kg butanol
solvent oleyl alcohol	12/8/5	486	14.3	0.5	2.0	1.7		18.5	13.3 MJ/kg butanol
pure distillation	4/8/2		21.2	1.3	1.7	1.4		25.6	18.4 MJ/kg butanol

The main reasons for the relatively large energy demand of the oleyl alcohol process are the high solvent flow rate because of the low distribution coefficient for acetone and the large content of water in the distillate of Col 1 ($x_{water} = 0.70$ for solvent oleyl

alcohol vs. $x_{water} = 0.13$ for solvent mesitylene). Note that the energy demands of the hybrid process with the solvent oleyl alcohol and the pure distillation process can be reduced if further heat integration among the distillation columns is considered by appropriate adjustment of column pressure levels.

5.4.4 Rigorous optimization of the novel downstream process

Following the process synthesis framework, the novel downstream process with the solvent mesitylene as given in Fig. 5.12 is optimized for total annualized cost in the rigorous optimization step. Here, the basic flowsheet structure is fixed at the configuration determined to be optimal in the shortcut evaluation. The column pressure levels from the shortcut evaluation are carried over as well. Considering the large scale and complexity of this downstream process and the nonlinearity of the underlying non-ideal thermodynamics, it is obvious that this optimization problem is particularly hard to solve.

The same butanol production rate and broth concentrations of butanol and ethanol as in the shortcut evaluation (cf. Section 5.4.3.1) is specified. Again, the concentration of acetone in the broth is determined from a mass balance around the extraction assuming a butanol:acetone weight ratio of 2:1 in the fermentation. The maximum number of extraction and distillation stages is set to 100 and 50, respectively. The butanol and acetone product purities are required to be higher than 99.5% and 99%, respectively. Steam at 20 bar and 15 €/t is specified as hot utility for columns Col 1 and Col 2 and steam at 3 bar and 12 €/t as hot utility for Col 3.

Due to the reformulation as a purely continuous problem and the initialization procedure based on the results of the preceding shortcut evaluation, the rigorous optimization can be solved with excellent robustness, efficiency and reliability. The computational time of the rigorous optimization of the entire downstream process apart from Col 3 (250 discrete and about 2000 continuous variables) amounted to only 141 seconds on a 2.66 GHz standard PC, including all the initialization steps. Col 3 is optimized separately since it is not part of a recycle or heat integration loop.

5.4.4.1 Results of rigorous optimization

The optimization results are displayed in Table 5.6 and 5.7. The main cost factors are the solvent recovery column (Col 1) and the heat exchanger in the broth recycle (Hex 1). In Table 5.8, the results of the rigorous optimization are compared to the results of the shortcut evaluation. It can clearly be seen that the approximations of the solvent

flow rate and the energy demands of the distillation columns by the shortcut methods are quite accurate. Compared to the results of the shortcut evaluation the optimal logarithmic mean temperature difference in Hex 1 and the optimal content of butanol in the raffinate recycle is slightly reduced.

Table 5.6: Costs and optimal column configurations for all columns of the novel downstream process with the solvent mesitylene. Butanol production rate: 40000 t/a, depreciation period: 6 years.

	Extraction	Col 1	Col 2	Col 3
TAC [k€/a]	129	1762	126	108
capital cost [k€/a]	129	241	32	52
operating cost [k€/a]		1520	94	56
condenser duty [MW]		3.2	1.1	0.9
reboiler duty [MW]		6.7	0.41	0.17
number of trays	21	41	13	28
feed tray		30	6	26
diameter [m]	4.5	2.7	0.88	1.0

Table 5.7: Costs and specifications for heat exchangers and compressor of the novel downstream process with the solvent mesitylene. Butanol production rate: 40000 t/a, depreciation period: 6 years.

	Hex 1	Hex 2	Hex 3	Hex 4	Hex 5	Comp 1
capital cost [k€/a]	371	43.8	176	32.1	44.2	76.9
operating cost [k€/a]						46.4
$\dot{Q}$ [MW]	30.0	1.7	12.4	1.1	3.2	
area [m^2]	2721	151	1078	110	154	
ΔT [°C]	7.4	11	14.4	10	21	

To assess the prospects of the novel process the energy costs of the alternative processes considered in this work are given in Table 5.9. The hybrid process with

the solvent oleyl alcohol requires a direct fired heater for the reboiler of the recovery column due to the high boiling point of oleyl alcohol (345°C). For a quick estimation of the energy costs, however, steam at 20 bar (212°C) and 15 €/t was used for the recovery column, although the temperature level is not sufficient. For the remaining columns, steam at 3 bar and 12 €/t could be used. The resulting energy costs of 3.9 M€/a are significantly higher than the total costs, i.e. energy plus capital costs, of the novel process (2.9 M€/a). Less expensive steam could be used in the reboiler of the recovery column when the pressure in the column is lowered significantly. As a consequence, however, the temperature drop in the column would then require expensive cooling liquid to be used in the condenser.

Table 5.8: Novel downstream process with the solvent mesitylene: Comparison of results from shortcut evaluation and rigorous optimization. Butanol production rate: 40000 t/a.

	shortcut evaluation	rigorous optimization
solvent flow rate [t/h]	268	288
reboiler energy duty Col 1 [MW]	5.9	6.7
total energy duty of reboilers and compressor [MW]	6.7	7.2
ratio of specific energy demand to energy content of butanol	0.13	0.14
ΔT Hex 1 [°C]	7.365	7.358
butanol content in raffinate [mol frac]	1.85e-4	1.80e-4
mesitylene content in raffinate [mol frac]	7.8e-6	7.8e-6

The pure distillation process requires steam at 3 bar only but the energy costs of this process (4.1 M€/a) are also higher than the total costs of the novel process. A calculation of the capital costs of the pure distillation process and the hybrid processes with the solvent oleyl alcohol is not necessary, since the energy costs of these processes are already higher than the total cost of the novel process.

Table 5.9 also shows the energy costs of an ABE plant in China estimated from the steam requirements given by Ni and Sun (2009). These energy costs are considerably higher than the energy costs of the optimal pure distillation process proposed in this

work. The reasons for this distinct discrepancy might be less heat integration at the plant in China, lower product concentrations in the fermentation broth, steam requirements in other parts of the process, and the fact that the plant in China is a working plant with typical inefficiencies not considered in this design study.

Table 5.9: Comparison of total annualized costs and energy costs for the alternative processes. Butanol production rate: 40000 t/a, depreciation period: 6 years.

	TAC [M€/a]	energy costs [M€/a]	capital costs [M€/a]
hybrid process (solvent mesitylene)	2.8	1.7	1.1
hybrid process (solvent oleyl alcohol)	>3.9	>3.9	>0
pure distillation process	>4.1	4.1	>0
actual plant in China	>9.6	9.6	>0
(Ni and Sun, 2009)		(20 t steam / t butanol)	

5.4.5 Discussion

The total annualized costs of the novel downstream process (2.9 M€/a for a butanol production of 40000 t/a) are considerably lower than the mere operating costs of the hybrid downstream process with the common solvent oleyl alcohol (>3.9 M€/a) or the pure distillation process (4.1 M€/a). It needs to be noted that all considered processes also produce 20000 t/a pure acetone, which is a valuable product as well and can be sold. It can therefore be concluded that the novel downstream process proposed in this work offers an exceptional economic savings potential and constitutes an important step towards an economical production of butanol as bio-fuel. The specific energy demand of the novel downstream process is only slightly higher than 10% of the energy content of butanol, which has been stated as the target for energy efficiency of bio-butanol purification (Oudshoorn et al., 2009).

The interaction of continuous fermentation and downstream processing has not been addressed in this work. For example, the effect of different ABE-concentrations in the

raffinate recycle on yield and productivity of the fermentation has been neglected. Whether this effect can be modeled by simple reaction kinetics remains questionable. In literature, there are very few works on this topic (e.g. Yang and Tsao (1994)), since the investigation of these interactions involves extensive experimental efforts concerning both the fermentation and the downstream processing. Nevertheless, this can be a very interesting topic for further research.

It also needs to be determined by further experiments, whether the nutrients in the broth are extracted into mesitylene in considerable amounts and whether traces of mesitylene in the water recycle have an inhibitory effect on the cells in the fermenter. In addition, the impact of further components in the broth (e.g. fermentation salts) on the downstream process needs to be tested.

In the CAMD procedure, mesitylene was identified as suitable solvent based on the prediction of solvent properties by UNIFAC. These property predictions were determined to be rather inaccurate, since considerably lower distribution coefficients were measured by experiments. In order to regain the distinct advantage of the solvent mesitylene, the temperature in the extraction column had to be raised. While CAMD provided valuable information and led to the selection of the superior solvent mesitylene, a further refinement of property prediction methods will yield more reliable solvent screening results and perhaps even better performing solvents.

5.5 Summary

This chapter covered the optimization-based conceptual design of hybrid processes composed of extraction and distillation by means of the process synthesis framework (cf. Fig. 2.1). The application of the framework required the development of novel shortcut and rigorous methods for multicomponent extraction. A fully algorithmic, pinch-based shortcut method was introduced, which extends the methodology of the FAM for distillation to the extraction of multicomponent mixtures in counter-current columns. Verified by multicomponent examples, this novel method allows an accurate assessment of feasibility and minimum solvent flow rate for mixtures with any number of components. It was shown that the combination of the FAM for distillation and extraction allows a quick evaluation of extraction-distillation processes for the separation of multicomponent mixtures including the numerical optimization of the process operating point.

The robust and efficient rigorous optimization of extraction columns was achieved by a continuous reformulation of the discrete-continuous tray-optimization problem

comparable to the rigorous optimization of distillation columns. Thus, the original MINLP problem could be solved as a NLP problem with common solvers.

The application of the novel shortcut and rigorous methods within the synthesis framework was demonstrated by the optimization-based design of a hybrid extraction-distillation downstream process for the energy-efficient separation of butanol from fermentation broth. It was shown that the application of these recent methodologies to the challenging design problem leads to the identification of novel and sustainable solutions with unmatched economics. In addition, the design effort is significantly reduced by the utilization of the optimization-based design approach instead of simulation studies. It is important to note that the design methodology can easily be applied to further downstream processes. This can be a fruitful topic of research, considering that downstream processes are often the bottleneck in industrial bio-based processes and offer a large potential for energy savings.

Chapter 6

Melt crystallization coupled with distillation

Azeotropic or close-boiling mixtures can be separated efficiently by melt-crystallization, if the melting points are located sufficiently far apart at moderate temperatures. Since enthalpies of fusion are typically lower than enthalpies of vaporization, the substitution of distillation units by melt crystallization units can contribute towards the design of energy-efficient separation processes (Ulrich, Bierwirth and Henning, 1996). When eutectic troughs prohibit a complete separation by crystallization alone, the combination with distillation in a hybrid process may allow the recovery of pure components.

Extensive literature on the design of crystallization-based hybrid processes was published by Ng and his co-workers (Berry and Ng, 1997; Wibowo and Ng, 2000). They propose design procedures based on heuristics and analyses of phase diagrams. Instructions for the economic evaluation of these processes are also given in their later works. A comprehensive review on the design of crystallization-based separation processes was presented by Cisternas, Vásquez and Swaney (2006). The application of shortcut and rigorous evaluation as well as optimization methods for the design of distillation - melt crystallization processes was studied by Franke (2006), Wallert (2008), and Franke et al. (2008).

In this chapter, the process synthesis framework presented in Chapter 2.6 is extended towards the design of hybrid distillation - melt crystallization processes as published by Marquardt, Kraemer and Harwardt (2010). The work builds on the excellent publications by Wallert and Franke et al., but applies recent, powerful shortcut and rigorous models to achieve an optimization-based process synthesis with paramount efficiency, robustness and reliability.

6.1 Shortcut model of melt crystallization

Fig. 6.1 shows the solid-liquid phase diagram of a ternary mixture of isomers. In each crystallization region, one pure isomer crystallizes as product when the temperature is lowered in the crystallizer. The configuration of the crystallizing isomer depends on the crystallization region in which the feed is located. When the temperature is further lowered, the remaining melt reaches a composition on an eutectic trough. The crystallization is stopped then, since a further decrease of the temperature would result in the crystallization of an undesired mix of isomers. The compositions and temperatures along the eutectic troughs e can be calculated by

$$x_{e,i}\gamma_{e,i} = \exp\Big(\frac{\Delta H_{m,i}}{\mathrm{R}}\Big(\frac{1}{T_{m,i}} - \frac{1}{T_e}\Big)\Big), \qquad e \in E, \quad i \in I_e \subset I, \tag{6.1}$$

$$1 = \sum_i x_{e,i}, \qquad e \in E, \tag{6.2}$$

Here, I_e are the sets of the two isomers of the binary eutectic points where the respective eutectic troughs originate. The liquid phase activity coefficients $\gamma_{e,i}$ are determined by a g^E-model with parameters adapted to solid-liquid equilibrium data.

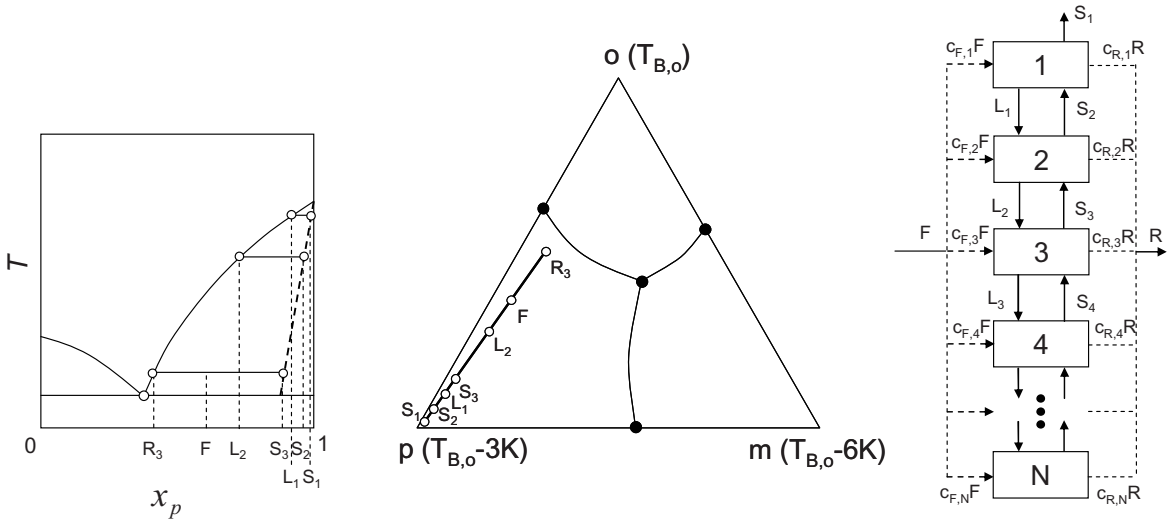

Figure 6.1: Non-ideal melt crystallization of o-\m-\p-isomers: temperature-concentration diagram (left), ternary phase diagram (middle, with boiling temperatures), and crystallization cascade superstructure (right).

Franke (2006) and Franke et al. (2008) assume ideal conditions for their crystallization shortcut model such that the separation of a pure isomer from the remaining melt

at eutectic composition can be accomplished in one crystallization stage. Industrial crystallization processes, however, never operate at ideal conditions due to inclusions of impurities in the solid phase. Thus, melt crystallization processes are carried out as staged processes, where the liquid and solid phases are exchanged between stages in a counter-current pattern (cf. Fig. 6.1 (right)). The energy demand of such a staged process exceeds the energy demand of an ideal, single-staged process by a multitude, e.g. by a factor larger than 5.5 for the crystallization tasks separating the p-isomer in the case study in Section 6.3. In this thesis, the crystallization shortcut is therefore modeled as a non-ideal staged process similar to the shortcut by Wallert (2008).

In contrast to distillation, where the energy demand decreases monotonously with the number of stages, crystallization processes exhibit a clear minimum energy demand at an optimal number of stages and an optimal feed stage location. It is therefore essential to optimize these discrete design variables in the shortcut step in order to facilitate an accurate evaluation of the minimum energy demand. Wallert (2008) formulates this discrete-continuous optimization problem as a general disjunctive programming (GDP) problem, where Boolean operators model the existence of stages and the feed stage location. The GDP problem is then reformulated as a MINLP problem with the help of big-M constraints. Wallert reports that the optimization by a branch & bound solver leads to longer solution times than a simple enumeration of the discrete variables for a maximum number of six stages. Hence, Wallert prefers the solution by enumeration.

While the enumeration of discrete variables may be feasible for a single crystallization unit, it is clear that hybrid processes with several crystallization and distillation units can only be optimized efficiently by powerful optimization algorithms. Yet, the formulation of the crystallization cascade optimization problem with Boolean variables in a GDP yields a very disjunct optimization problem. As a consequence, the reformulation with big-M constraints results in a loose relaxation and long computational times for the solution with MINLP solvers. Marquardt, Kraemer and Harwardt (2010) therefore use a tight MINLP superstructure instead (cf. Fig. 6.1 (right)), which is similar to the superstructure for distillation and extraction column optimization proposed in Sections 3.3.1 and 5.2.1, respectively. More precisely, the number of crystallization stages is modeled by a variable feed and residue melt draw on each stage. Using this tight superstructure, the variable crystallization cascade structure actually takes on a discrete number of stages at the local minima of the energy demand, much like in case of distillation and extraction columns. Obviously, a distributed residue melt draw leads to reduced liquid and solid streams in the counter-current cascade beyond the first partial residue melt draw. This implies a reduced separation driving force and a

penalty on the energy demand for the cascade. Hence, additional measures to force discrete solutions are not necessary.

The crystallization cascade model is given by the following equations:

$$\min \quad Q = Q_C + Q_H, \tag{6.3}$$

$$\text{s.t.} \quad 0 = c_{F,n} F x_{F,i} + S_{n+1} z_{n+1,i} + L_{n-1} x_{n-1,i} - S_n z_{n,i} - L_n x_{n,i} - c_{R,n} R x_{n,i}, \quad n = 1,...,N, \quad i = 1,...,C, \tag{6.4}$$

$$1 = \sum_i z_{n,i}, \quad 1 = \sum_i x_{n,i}, \quad n = 1,...,N, \tag{6.5}$$

$$1 = \sum_n c_{F,n}, \quad 1 = \sum_n c_{R,n}, \tag{6.6}$$

$$0 \le c_{F,n}, c_{R,n} \le 1, \quad n = 1,...,N, \tag{6.7}$$

$$0 = (T_{m,ic} - T_n) - M(1 - z_{n,ic}), \quad n = 1,...,N, \tag{6.8}$$

$$0 = \frac{x_{n,i\neq j,ic}}{x_{F,i\neq j,ic}} - \frac{x_{n,j\neq i,ic}}{x_{F,j\neq i,ic}}, \quad n = 1,...,N, \quad i,j = 1,...,C, \tag{6.9}$$

$$0 = x_{n,ic}\gamma_{n,ic} - \exp\left(\frac{\Delta H_{m,ic}}{\mathrm{R}}\left(\frac{1}{T_{m,ic}} - \frac{1}{T_n}\right)\right), \quad n = 1,...,N, \tag{6.10}$$

$$r_{f,min} \le \frac{S_n}{S_n + L_n} \le r_{f,max}, \quad n = 1,...,N, \tag{6.11}$$

$$0 = \frac{x_{e,i\neq j,ic}}{x_{F,i\neq j,ic}} - \frac{x_{e,j\neq i,ic}}{x_{F,j\neq i,ic}}, \quad e \in E, \quad i,j = 1,...,C, \tag{6.12}$$

$$x_{n,ic} \ge x_{e,ic}, \quad n = 1,...,N, \quad e \in E, \tag{6.13}$$

$$K = \frac{\sum_n S_n}{S_1}, \tag{6.14}$$

$$Q_C = 4 \cdot K \cdot S_1 \cdot \Delta H_{m,ic}, \tag{6.15}$$

$$Q_H = 3 \cdot K \cdot S_1 \cdot \Delta H_{m,ic}. \tag{6.16}$$

The objective function in eq. (6.3) minimizes the energy demand composed of cooling and heating duties. Eq. (6.4) describes the material balances for each stage. The continuous decision variables $c_{F,n}$ and $c_{R,n}$ in the material balance model the location of the feed and the residue melt draw, respectively. Eqs. (6.5) and (6.6) provide closure conditions for concentrations and stream distributions. Based on the results of Matsuoka, Ohishi and Kasama (1986), eq. (6.8) models the non-ideality of the crystallization, i.e. the impurities in the crystal layer, by a linear correlation between temperature in the crystallizer and composition of the crystal layer (cf. Fig. 6.1 (left)). Here, *ic* is the crystallizing component. Together with eq. (6.9), which defines the ratio of the isomers in the melt, we obtain the condition that all liquid and solid compositions are located on a line through the feed composition and the pure isomer

vertex (cf. Fig. 6.1 (middle)). The melt compositions on the stages are related to the crystallization temperatures by eq. (6.10). Again, the liquid activity coefficients are calculated by a g^E-model with binary parameters adapted to solid-liquid equilibrium data. Eq. (6.11) constrains the freezing ratio of a crystallization stage between lower and upper bounds to ensure a feasible operation. Eqs. (6.12) and (6.13) together with eq. (6.1) guarantee that the melt compositions are located in the appropriate crystallization region.

The energy demand of the crystallization cascade is estimated by eqs. (6.14)-(6.16) (Wellinghoff and Wintermantel, 1991). Here, K is the crystallization effort, defined as the ratio of the total amount of crystals produced to the amount of solid product S_1, which accounts for the existence of more than one stage, i.e. the non-ideality of the crystallization. The required energy for cooling the apparatus and pumping the liquor is considered by Wellinghoff and Wintermantel with the factor 4 in eq. (6.15). Note that additional to the cooling duty, the same amount of energy minus the heat induced by the pump is needed for heating the apparatus and melting the crystal layers (eq. (6.16)).

6.2 Rigorous model of melt crystallization

The rigorous crystallization model is based on the shortcut crystallization model. The cascade superstructure of Fig. 6.1 (right) is reused, as are the model equations (eqs. (6.1)-(6.15)). The objective of minimum energy duty (eq. (6.3)) is replaced by the objective of minimum total annualized costs. Correlations for the sizing and costing of the apparatus according to Wallert (2008) and Douglas (1988) are added. These correlations are given in Appendix A. The capital costs are composed of the costs for buffer tanks for each stage and one shell and tube heat exchanger. Comparable to the shortcut evaluation, the variable crystallization cascade structure takes on a discrete number of stages at the local minima of the cost function. A distributed residue melt draw implies a penalty on the energy demand and the cost as explained in Section 6.1 and, thus, binary variables for the existence of stages as in the work by Franke et al. (2008) are not necessary.

6.3 Case study: separation of isomers

The optimization-based design by means of the process synthesis framework is illustrated by an industrial case study, where a ternary mixture of close-boiling ortho-,

meta-, and para-isomers (denoted by o-, m-, and p-isomers) is separated into pure products. Although the separation of the ternary mixture by distillation is not hindered by azeotropic behavior, the close-boiling nature results in a high energy demand for a simple distillation setup. On the other hand, the mixture cannot be separated by crystallization alone because of eutectic troughs, which divide the system in three crystallization regions (cf. Fig. 6.1 (middle)). An efficient separation can be achieved, however, when distillation units are combined with crystallization units in a hybrid separation process.

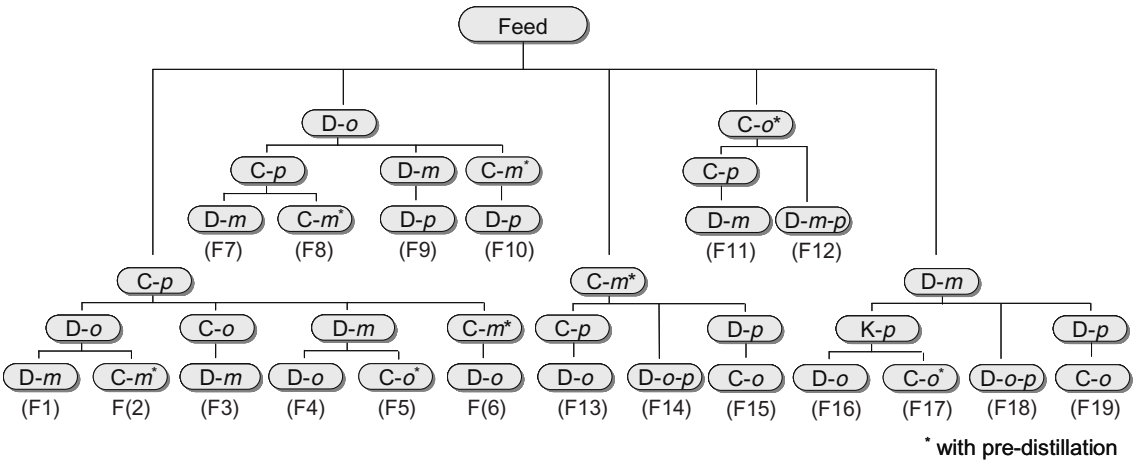

Figure 6.2: Tree of process variants with a maximum of four separation units (from Wallert (2008)).

Certainly, there is a multitude of alternative flowsheet variants, i.e. combinations of crystallization and distillation units, to perform the separation task. By allowing a maximum of four separation units, one can come up with 19 feasible flowsheet variants for a feed of 66% p-, 33% o- and less than 1% m-isomer as given in Fig. 6.2. In the following, it will be shown that the flowsheet variant with the lowest total annualized cost can be identified robustly and efficiently with the help of shortcut and rigorous evaluation steps of the optimization-based synthesis framework described in Chapter 2.6.

Note that this industrial case study of isomer separation has already been studied by Franke (2006), Wallert (2008), and Franke et al. (2008). The work of Wallert, however, is confined to a screening of flowsheet variants with shortcut methods; rigorous discrete-continuous process optimization has not been addressed. In the shortcut evaluation, Wallert resorts to an enumeration of crystallization cascade configurations (number of stages and feed stage location) due to a lack of robust and reliable optimization techniques at the time. Franke et al. presented a comprehensive work on this

case study, considering both shortcut evaluation and rigorous optimization. In the shortcut evaluation step, however, these authors use simplifying methods, which cannot account for non-ideal behavior of the crystallization and distillation tasks. While this approach has computational benefits, the energy demands of the crystallization tasks are underestimated by a large factor. The rigorous optimization problems are then solved by a modified outer approximation algorithm which demands a large number of MILP/NLP iterations to obtain a solution.

In the following two sections, the case study of isomer separation is revisited. It will be shown that further progress beyond the excellent works by Wallert and Franke et al. can be achieved through the application of the powerful shortcut and rigorous optimization models presented in Chapter 3 and Sections 6.1 and 6.2. The optimization problems of the shortcut and rigorous design steps are solved in GAMS 22.7 on a 2.66 GHz standard PC.

6.3.1 Screening of flowsheet variants with shortcut methods

In the shortcut evaluation step, the crystallization tasks are modeled by the shortcut method for melt crystallization cascades proposed in Section 6.1. The distillation tasks are evaluated by the FAM, which was introduced in Section 4.5.

As a first design decision, the operating pressure of the distillation tasks is fixed at a value which allows the use of low pressure steam as hot utility. Impurity bounds are added to the intermediate distillation products in the shortcut evaluation step. These impurity bounds prohibit sharp splits, which would lead to high numbers of trays and expensive capital costs for the distillation tasks in the rigorous optimization step. The impurity bounds are set to 0.2 for the o- and p-isomers. A lower value of 0.1 is chosen for the m-isomer due to the low content in the feed. The intermediate distillate products are not condensed but transferred as saturated vapor as a measure of heat integration. In order to compare the different flowsheet variants at their respective optimal operating point, the degrees of freedom on the flowsheet level, i.e. the flow rates and compositions of the intermediate and recycle streams, are optimized together with the structural decisions for the crystallization cascades.

The initialization applied in this case study is carried out in two steps similar to the initialization of the hybrid processes in Section 4.7.2.1. In the first step, the flowsheet mass balances are initialized at the minimum recycle flow rate. For this purpose, a nonlinear programming (NLP) problem is solved, where the recycle flow rate is minimized such that the flowsheet mass balances, the purity and impurity constraints, and the limitations by eutectic troughs are fulfilled. In the next initialization step,

the flow rates and compositions of the flowsheet streams are fixed at the values of the preceding step and all separation units are evaluated by their respective shortcut method to initialize the shortcut model equations.

In the following shortcut evaluation, the fixed flowsheet variables are released such that the minimum energy demand of the hybrid process can be determined by solving a NLP problem. Here, the objective function is the minimization of a weighted sum of the energy duties of the hybrid process. The weights are introduced, since heating and cooling utilities of different costs are compared. Wallert (2008) and Franke et al. (2008) consider only the cooling duties of the crystallization units besides the heating duties of the distillation units. In this work, the heating duties for the melting of the crystal layers are additionally included as suggested by Wellinghoff and Wintermantel (1991), since the steam required for the heating contributes significantly to the overall energy costs. The objective function is constrained by the product purities, the impurity constraints for the intermediate distillate products, the flowsheet mass balances and the shortcut models of the unit operations. The optimization variables are the independent flowsheet variables and the number of stages and feed stage locations of the crystallization cascades.

Table 6.1: Optimized energy duties for a selection of flowsheet variants.

flowsheet	F1	F16	F13	F6	F9	F18	F7	F3	F11
$Q_{tot}/Q_{tot,min}$	1	1.0007	1.0008	1.045	1.098	1.222	1.239	1.391	1.432

The solution times for the shortcut evaluation of one hybrid process including the initialization takes about 15 seconds. The optimized energy duties for a selection of flowsheet variants are shown in Table 6.1. It can be seen that the pure distillation process (flowsheet F9) requires only 10% more energy than the best hybrid process. Note that the pure distillation processes benefit most from the heat integration by transfer of distillate streams as vapor. Furthermore, it needs to be noted that the constraints for impurities in the intermediate distillate products needed to be dropped for the pure distillation processes. The capital costs for the high numbers of trays for these sharp splits will show in the rigorous optimization in the following section.

The ranking of variants shown in Table 6.1 differs from the ranking given in the work by Franke et al. (2008). This is mainly due to the consideration of non-ideal behavior for the crystallization and distillation units in this work. Since heating duties for the crystallization units are included in this work, the ranking of variants also differs from the results presented in work by Wallert (2008).

6.3.2 Rigorous optimization

A selection of the most promising flowsheet variants is further evaluated in the rigorous optimization step. The rigorous distillation column models are initialized as described in Sections 3.3.3 and 4.6.1 and solved according to the solution procedure proposed in Section 3.3.4. The relaxed decision variables of the crystallization cascades converge to integer values in the local optima even without being constrained to integrality due to the tight crystallization cascade superstructure (cf. Sections 6.1 and 6.2).

The total annualized costs for the three most cost-efficient hybrid processes (F1, F6, F16) and the best pure distillation process (F9) are given in Table 6.2. All three hybrid processes separate the medium boiling p-isomer via crystallization. Flowsheet F6 contains two crystallization units and exhibits the lowest total annual costs despite slightly higher energy demand in the shortcut evaluation compared to processes F1 and F16. The pure distillation process (flowsheet F9) costs almost twice as much as the hybrid processes, mostly due to the large number of trays required for the sharp splits.

Table 6.2: Total annualized costs for the three hybrid processes and one pure distillation process.

flowsheet	F6	F1	F16	F9
$\mathrm{TAC}_{tot}/\mathrm{TAC}_{tot,min}$	1	1.01	1.02	1.95
$\mathrm{TAC}_{D1}/\mathrm{TAC}_{tot,min}$	0.046	0.462	0.065	1.225
$\mathrm{TAC}_{D2}/\mathrm{TAC}_{tot,min}$	0.458	0.063	0.466	0.728
$\mathrm{TAC}_{C1}/\mathrm{TAC}_{tot,min}$	0.485	0.485	0.489	-
$\mathrm{TAC}_{C2}/\mathrm{TAC}_{tot,min}$	0.011	-	-	-

Contrary to the heat integration in the shortcut evaluation, all intermediate distillate products are condensed and transferred as saturated liquid to subsequent distillation columns. Compared to vapor feeds, liquid feeds yield significantly smaller vapor flows in the column. The resulting smaller diameters and lower capital costs for the distillation columns more than compensate for the larger energy duties.

The optimal numbers of stages, locations of feed stages, and flowsheet mass balances of flowsheet F6 are shown in Fig. 6.3. In the optimal solution, all isomers are present in the intermediate products of the distillation units (B1,D2) although the impurity constraints of the shortcut evaluation are dropped in the rigorous optimization.

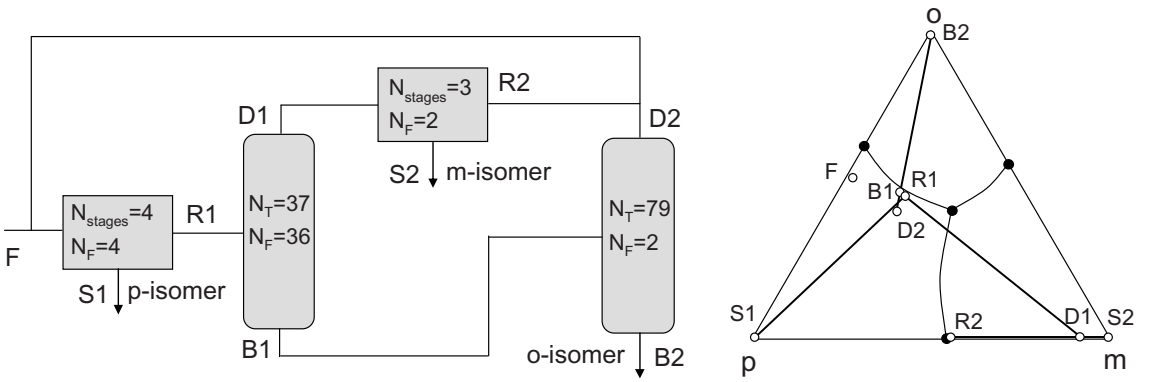

Figure 6.3: Numbers of crystallization stages (N_{stages}) and distillation trays (N_T), feed stage locations (N_F), and flowsheet mass balances of flowsheet F6.

Thanks to the favorable initialization by the shortcut evaluation, the rigorous optimization problems could be solved robustly and good local optima were obtained. Furthermore, the continuous formulation of the crystallization and distillation models provides solutions by solving only very few NLP problems plus the initialization for each hybrid process. Accordingly, the computational time of the rigorous optimization of flowsheet F6 with 320 discrete and about 3000 continuous variables amounted to only 112 seconds, including the initialization phase. Such computational efficiency for large-scale processes cannot be reached by solving a MINLP problem with the common outer-approximation or branch & bounds solvers, which rely on a MILP/NLP iteration or tree search procedure, respectively. Franke (2006) achieved a robust and reliable rigorous MINLP optimization of the hybrid processes for isomer separation with the help of a modified outer approximation solver. Still, he reported 66 NLP and 59 MILP iteration steps for the rigorous optimization of one hybrid process. Note that the costs calculated for the hybrid processes in this work cannot be compared to the costs given in the work by Franke, since different costs functions are used.

6.4 Summary

This chapter demonstrates the optimization-based conceptual design of hybrid processes composed of crystallization and distillation. In particular, a case study for the separation of close-boiling isomers is revisited, which was originally studied by Wallert (2008) and Franke et al. (2008). Progress beyond these excellent works is achieved by the consistent application of powerful optimization techniques developed in this thesis. Thus, a manifold of flowsheet variants could be evaluated by powerful

shortcut methods accounting for the non-idealities of the unit operations. Due to the computational efficiency of these shortcut methods, optimal operating points were determined for the flowsheet variants facilitating an effective comparison of process heating and cooling duties. Initialized by the results of the shortcut evaluation, the subsequent rigorous optimization of a selection of flowsheets could then be performed robustly. The reformulation of these discrete-continuous optimization problems as a purely continuous problems drastically reduced the solution times to about two minutes per process including the initialization phase. Hence, the novel design methods not only assist with identifying optimal solutions but also cut the computational effort for the design of these hybrid processes.

Chapter 7

Reactive distillation

The combination of reaction and separation in one unit is termed reactive separation. The most common example is reactive distillation, but reactive extraction, reactive membrane separation, reactive crystallization, and reactive adsorption processes have been proposed as well (Pai, Doherty and Malone, 2002). When the reaction products are removed from the reaction zone while the reactants accumulate, reactive separation can significantly increase reaction conversion. Yet reactive separation is most effective when it allows to overcome both the reaction equilibrium and the separation boundaries of the mixture. A good example is the synthesis of methyl acetate by the Eastman Chemical Company (Agreda, Partin and Heise, 1990). Here, a single RD column replaced a reactor and about ten separation units.

There are differing views whether reactive separation processes can be classified as hybrid processes. Some authors consider a category of reaction-separation hybrid processes (Kaibel and Schoenmakers, 2002; Qi, Sundmacher, Stein, Kienle and Kolah, 2002), others describe reactive separation as process intensification, since two unit operations are combined in one unit (Franke, 2006). Intensified processes differ from hybrid processes in terms of degrees of freedom. While the design of hybrid processes is characterized by an increase in degrees of freedom, intensified processes are subject to a reduction in degrees of freedom.

Nevertheless, this chapter gives a brief outlook on how the shortcut and rigorous methods developed in the preceding sections can be extended such that the synthesis framework also applies to the design of reactive distillation. In Section 7.2, the extension of the FAM to reactive distillation will be proposed. The rigorous optimization of distillation columns based continuous reformulation as introduced in Section 3.3 has recently been applied to reactive distillation as well. These works will be reviewed

in Section 7.3. It needs to be noted that a large-scale case study on the design of reactive separation processes will not be presented in this chapter. It is the purpose of this chapter, however, to trigger efforts which may lead to a comprehensive design methodology for reactive separation processes.

7.1 Shortcut evaluation of reactive distillation

Barbosa and Doherty (1988) proposed an extension of the boundary value method (BVM, cf. Section 3.1.1) for reactive distillation with equilibrium reactions. Later, the BVM was also applied to kinetically-controlled reactive distillation (e.g. Buzad and Doherty (1994)). Dragomir and Jobson (2005) formulated a similar approach where the so-called stage composition lines form a surface for each column section depending on the specification of reaction holdup. Like the BVM for non-reactive distillation, however, the application of these methods is limited due to the graphical check for intersection. The same limitation holds for the extension of the continuous distillation boundary method proposed by Urdaneta (2005) (see also Section 4.3.4). Lucia et al. (2008) applied the shortest stripping line method (cf. Section 3.1.3) to a reactive distillation column. To reduce the complexity and computational demand of the problem, Lucia et al. assume that equilibrium reactions only take place in one column section. In addition, they use a constant molar overflow assumption and also neglect the heat of reaction.

In order to provide a computationally efficient shortcut method for multicomponent separations, Bausa (2001) has extended the rectification body method (RBM, cf. Section 3.1.2.3) to reactive distillation with equilibrium reactions. In this work, the reactive pinch points are determined from the solution of the reactive pinch equation system. For the rectifying section, the reactive pinch equations are obtained from the pinch equation system for the non-reactive case (eqs. (3.11)-(3.17)) by substituting the mass balances of eqs. (3.11) and (3.12) with

$$0 = V_p - L_p - D + \sum_{j=1}^{N_{reac}} E_j \sum_{i=1}^{C} \nu_{j,i}, \qquad p \in P_D, \tag{7.1}$$

$$0 = V_p y_{p,i} - L_p x_{p,i} - D x_{D,i} + \sum_{j=1}^{N_{reac}} E_j \nu_{j,i}, \qquad p \in P_D,\ i = 1, ..., C, \tag{7.2}$$

and adding the chemical equilibrium by

$$0 = r_j(\mathbf{x}_p, T_p, p_p), \qquad p \in P_D,\ j = 1, ..., N_{reac}. \tag{7.3}$$

Here, E_j is the extent of reaction and ν_j the stoichiometric vector for reaction j. The pinch points of the stripping section can be determined analogously. The degrees of freedom of the system are reduced by one for each reaction.

Like in the non-reactive case, the location of the pinch points is only dependent on the specification of the product compositions $\mathbf{x}_D$ and the energy duty Q_D. From the pinch points, the rectification bodies are constructed as described in Section 3.1.2.3. Note that the reactive pinch points and the rectification bodies of the reactive sections lie on the equilibrium surface. For the minimum energy demand (MED), the rectification bodies of the stripping and rectifying sections must intersect at a singular point. Comparable to non-reactive distillation, the linear approximation of the curved column profiles may lead to a considerable over- or underestimation of the MED in highly non-ideal systems.

Kossack (2010) has shown that the pinch points of reactive distillation with kinetically controlled reactions also lie on the equilibrium surface. Since the equilibrium surface may never be reached in the actual column however, pinch-based methods are not suited for these problems. In the light of these challenges, Kossack (2010) suggests to assume an equilibrium reaction in the shortcut evaluation step. The reaction kinetics can then be considered in the subsequent rigorous optimization to determine the optimal column hold-up based on economic considerations.

7.2 Feed angle method for reactive distillation

The BVM-based shortcut methods referenced above require a graphical inspection of profile intersection. The fully algorithmic RBM, on the other hand, can be quite inaccurate for highly non-ideal reactive distillation (see examples below). In an effort to provide a fully algorithmic, efficient, and accurate shortcut method for reactive distillation under the assumption of reaction equilibrium, the feed angle method (FAM, cf. Section 4.5) is extended to reactive distillation in the work by Avami, Marquardt, Saboohi and Kraemer (2012). The equations for the non-reactive FAM (eqs. (4.13)-(4.19)) are modified as described for the pinch equation system in Section 7.1, i.e. the total and component mass balances are extended by the extent of reaction $\sum_{j=1}^{N_{reac}} E_j \cdot \sum_{i=1}^{C} \nu_{j,i}$ and $\sum_{j=1}^{N_{reac}} E_j \nu_{j,i}$, respectively. Furthermore, the chemical equilibrium (eq. (7.3)) is added.

Table 7.1: Specifications and MED of the reactive distillation of a mixture of di-tert-butylbenzene, m-xylene, tert-butyl-m-xylene, tert-butylbenzene, and benzene. Compositions are given in transformed coordinates.

molar composition in real (top) and transformed coordinates (bottom)		
$\mathbf{z}_F$	$\mathbf{x}_D$	$\mathbf{x}_B$
0.256, 0.453, 0.194, 0, 0.097	0, 1, 0, 0, 0	1, 0, 0, 0, 0
0.647, 0.059, 0.294	1, -1, 1	0, 2, -1
pressure	feed state	g^E-model
1.013 bar	sat. liquid	Wilson
$Q_{B,\min}/F$ [MJ/kmol]		
BVM	RBM	FAM
69	74	69

7.2.1 Illustrative examples

The FAM for reactive distillation is illustrated by a quinternary mixture with two alkylation reactions. In the first reaction, di-tert-butylbenzene ($C_{14}H_{22}$) reacts with m-xylene (C_8H_{10}) to produce tert-butyl-m-xylene ($C_{12}H_{18}$) and tert-butylbenzene ($C_{10}H_{14}$). In the second reaction, tert-butylbenzene and m-xylene form tert-butyl-m-xylene and benzene (C_6H_6):

$$C_{14}H_{22} + C_8H_{10} \rightleftharpoons C_{12}H_{18} + C_{10}H_{14} \tag{7.4}$$

$$C_{10}H_{14} + C_8H_{10} \rightleftharpoons C_{12}H_{18} + C_6H_6 \tag{7.5}$$

The chemical equilibrium constants for these two reactions are $K_{eq,1} = 0.6$ and $K_{eq,2} = 0.16$, respectively (Ung and Doherty, 1995). The coefficients for the calculation of vapor pressures, ideal gas heat capacities, and heats of vaporization are given in Tables D.7, D.16, and D.32. The activity coefficients of the liquid phase are calculated by the Wilson model with parameters given in Tables D.46 and D.47. Table 7.1 specifies a separation to produce pure m-xylene at the top and pure di-tert-butylbenzene at the bottom of a single feed reactive column. Note that the compositions are also given in transformed coordinates as suggested by Ung and Doherty (1995). Fig. 7.1, which is plotted based on these transformed coordinates, illustrates the evaluation of the considered separation by means of the RBM and the FAM. The corresponding tray-to-tray profiles are also shown.

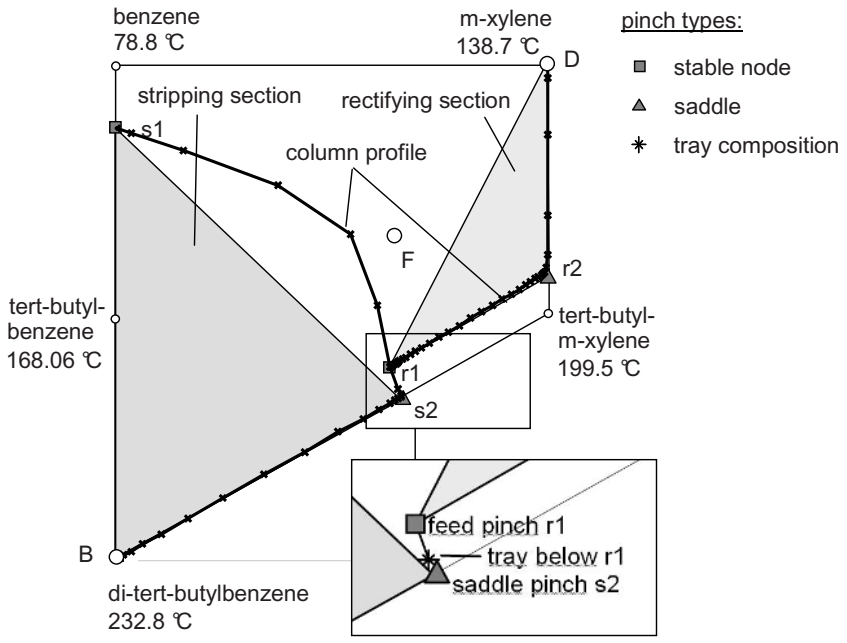

Figure 7.1: Pinches, rectification bodies, and tray-to-tray profiles of the quinternary reactive distillation example at MED. The application of the FAM is illustrated in the cutout.

The minimum energy demands (MED) determined by these methods are given in Table 7.1. Apparently, the RBM overestimates the MED significantly due to the curvature of the stripping profile between pinches *s1* and *s2* (cf. Fig. 7.1). Hence, the rectification bodies for the stripping and rectifying section do not intersect at the correct MED. Yet the FAM determines the correct MED by a minimization of the angle between the feed pinch *r1*, the tray below the feed pinch, and the saddle pinch *s2*, which is illustrated in the cutout in Fig. 7.1.

A second example from the work by Avami et al. (2012) is given in Table 7.2. This example studies the formation and separation of butyl-levulinate ($C_9H_{16}O_3$), which is obtained from levulinic acid ($C_5H_8O_3$) and butanol ($C_4H_{10}O$) by the following esterification:

$$C_5H_8O_3 + C_4H_{10}O \rightleftharpoons C_9H_{16}O_3 + H_2O \tag{7.6}$$

Butyl-levulinate is a promising biofuel candidate with excellent combustion properties. Both levulinic acid and butanol can be obtained from biomass conversion (Harwardt et al., 2011).

Table 7.2: Specifications and MED of the reactive distillation of a mixture of levulinic acid, butanol, butyl-levulinate, and water. Compositions are given in transformed coordinates.

molar composition in real (top) and transformed coordinates (bottom)		
$\mathbf{z}_F$	$\mathbf{x}_D$	$\mathbf{x}_B$
0.5, 0.5, 0, 0	0, 0.02, 0, 0.98	0, 0, 1, 0
0.5, 0.5, 0	0.98, 1, -0.98	0, 0, 1
pressure	feed state	g^E-model
1.013 bar	sat. liquid	NRTL
	$Q_{B,\min}/F$ [MJ/kmol]	
rigorous optimization (Section 7.3)	RBM	FAM
50.6	63	47

The vapor pressures, ideal gas heat capacities, and heats of vaporization are calculated by coefficients given in Tables D.8, D.17, and D.34. The mixture exhibits a miscibility gap between water and butanol. The resulting vapor-liquid-liquid equilibrium is described by the NRTL model with parameters given in Tables D.48 and D.49. The expression for the reaction equilibrium is taken from the work by Harwardt et al.:

$$\ln(K_{eq}) = 2.9275 - \frac{702.97\text{K}}{T}. \tag{7.7}$$

An equimolar mixture of levulinic acid and butanol is fed to the column. Small amounts of sulfuric acid are also added as homogeneous catalyst. Note that these traces of sulfuric acid neglected in the shortcut model for better visualization of the separation in Fig. 7.2. Pure ester is obtained at the bottom of the column and water is drawn off the decanter at the top.

The rectification bodies at the MED are shown in Fig. 7.2. Note that the separation is highly non-ideal due to the combination of reaction and liquid-liquid phase split in one column. Hence, the rectifying section profile exhibits a distinct curvature between the saddle pinch *r2* and the node pinch *r1* such that the rectification bodies do not intersect. An intersection occurs for a reboiler duty of 63 $MJ/kmol$F, which marks a significant overestimation of the MED by the RBM (cf. Table 7.2). The FAM,

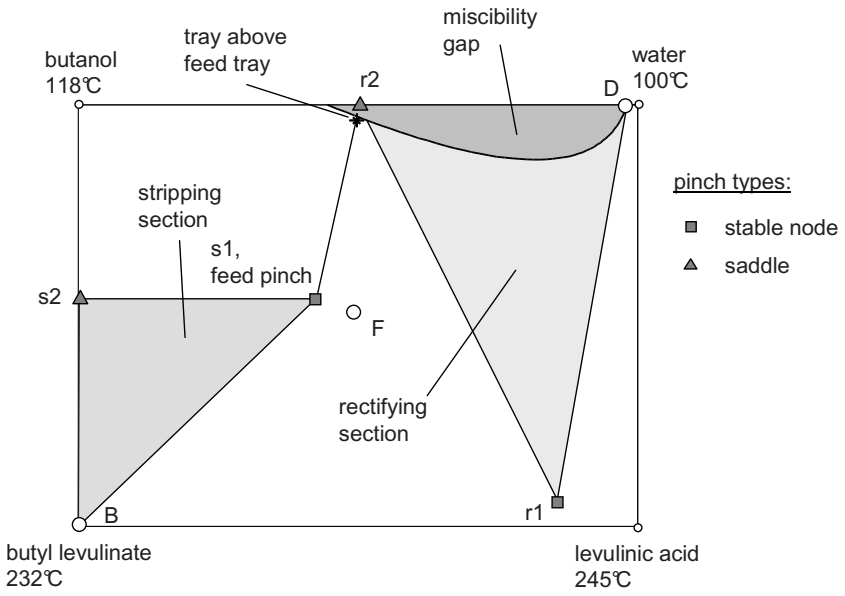

Figure 7.2: Pinches, rectification bodies, and tray above the feed tray for the reactive distillation of butyl-levulinate at the MED.

however, determines the correct MED of 47 $MJ/kmol$F. At this reboiler duty, the tray above the feed pinch points directly towards the saddle pinch of the rectifying section as shown in Fig. 7.2.

7.2.2 Higher-dimensional systems and two-feed columns

For better visualization, reactive distillation examples which can be reduced to two-dimensional systems via transformed coordinates have been chosen above. It needs to be noted that the BVM can be applied to these examples as well, since a graphical check for intersection of profiles can be performed easily. However, Avami et al. (2012) also present an example for a three-dimensional system in their work, which is not suited for an evaluation with the BVM. Specifically, Avami et al. study the esterification of methanol and acetic acid to form methyl acetate and water in the presence of the inert sec-butyl acetate. For this example, the FAM again identifies the correct MED while the RBM overestimates the MED significantly.

Besides single feed reactive distillation, Avami et al. (2012) have also studied the shortcut evaluation of double-feed reactive distillation columns by means of the FAM. Here, pinch points for the rectifying, stripping, and a middle section between the feeds are calculated. Two feed pinches are determined due to the occurrence of two

feeds. The MED is determined by the evaluation of the angle at the feed pinch, which controls the MED. Like in the single-feed case, the identification of the relevant pinches can be accomplished by an initialization with the RBM.

7.3 Rigorous optimization of reactive distillation

Various authors have published works on the rigorous discrete-continuous optimization of reactive distillation. Different optimization techniques have been studied, including MINLP optimization (Ciric and Gu, 1994; Stichlmair and Frey, 2001; Sand, Barkmann, Engell and Schembecker, 2004), simulated annealing (Cardoso, Salcedo, de Azevedo and Barbosa, 2000), or a combination of an evolutionary strategy with a mathematical programming solver (Urselmann and Engell, 2010). Recently, Kossack (2010) and Harwardt et al. (2011) have shown that the methodologies for the optimization of non-reactive distillation proposed in Section 3.3 can be applied to reactive distillation as well, when formulations for equilibrium or non-equilibrium reactions are added.

The work by Kossack focuses on the proper initialization of rigorous column models by the results of a preceding shortcut evaluation with the RBM. In addition, the resulting MINLP problems are reformulated as purely continuous problems for better convergence properties. Examples with both equilibrium and non-equilibrium reactions are presented.

Harwardt et al. propose the production of butyl-levulinate from butanol and levulinic acid in a reactive distillation column (cf. Section 7.2.1). They consider a two-column process, where the second column removes water and recycles the catalyst. This process is rigorously optimized using the methodologies proposed in Section 3.3. While the resulting large-scale rigorous optimization problem can be solved robustly, the solution time is considerably longer compared to the non-reactive examples in this thesis. The optimized reboiler energy duty of 50.6 $MJ/kmol$F corresponds well to the minimum value of 47 $MJ/kmol$F determined by the FAM.

7.4 Summary

In this chapter, the shortcut and rigorous evaluation methods developed in the preceding chapters have been extended to reactive distillation. It is shown that the FAM for distillation can be applied to multicomponent reactive distillation. Examples for

the reactive distillation of quaternary and quinternary mixtures are presented. While the RBM significantly overestimates the MED for these highly non-ideal examples, the FAM provides an accurate estimation. Concerning the rigorous optimization, it is shown that the continuous reformulation allows the economic optimization of reactive distillation processes, even though the computational time increases considerably.

Chapter 8

Conclusions

Hybrid separation processes offer a great potential for energy-efficient, sustainable designs. However, the design of these highly integrated processes is particularly challenging due to the multitude of structural and operative degrees of freedom. A lack of modeling experience and reliable synthesis methods has so far hindered the application of these promising designs in industry.

In industrial practice, conceptual process design is typically conducted by repetitive simulations studies, which require detailed design specifications in an early design phase. Guided by heuristics, these iterative solution procedures result in a high manual effort and, in addition, no guarantee concerning the quality of the solution can be given. Various authors have therefore suggested the use of shortcut design methods, which allow an efficient design of separation processes without the need for detailed specifications (Section 2.3). Others have developed methods for the optimization-based flowsheet generation by means of superstructure optimization (Section 2.4). Marquardt et al. (2008) proposed a framework for the optimization-based process design, which combines shortcut and rigorous evaluation steps (Chapter 2.6). This framework has been successfully deployed to distillation processes (Kossack et al., 2008; Kraemer, Kossack and Marquardt, 2009; Kossack, 2010).

In this thesis, the process synthesis framework of Marquardt et al. is extended towards the optimization-based design of hybrid separation processes. For this purpose, powerful shortcut and rigorous evaluation methods for distillation, heteroazeotropic distillation, extraction, crystallization and reactive distillation are proposed. It is important to emphasize that all of these methods were developed to be fully algorithmic as well as computationally efficient in order to allow an optimization-based design and analysis of large-scale hybrid processes. As a consequence, energy-efficient and

cost-optimal process solutions could be obtained with considerably less effort compared to the use of tedious repetitive simulation studies. It also has to be stressed that the performance of all methods is validated by large-scale industrial case studies. Thus, it has been shown that the process synthesis framework can contribute decisively towards the sustainable solution of today's challenging design problems in chemical engineering.

After the synthesis framework was introduced in Chapter 2.6, the foundation for the subsequent extension of the framework to hybrid processes is laid in Chapter 3. Here, the methodology of the framework is refined for the application to large-scale azeotropic distillation processes, which requires efficient and robust design methods. Progress concerning the rigorous optimization of distillation processes is achieved by measures on two levels. First, the integration in the process synthesis framework allows a reduction of the complexity of the optimization superstructure and provides excellent opportunities for initialization with the results of the preceding shortcut evaluation. Second, the large-scale MINLP problems are reformulated as purely continuous NLP problems by the substitution of binary variables with continuous decision variables. These decision variable are forced to integer values by the introduction of Fischer-Burmeister constraints, which are relaxed at first and gradually tightened in a series of a few easy to solve NLP problems. As a result of these advancements, the optimization-based design of distillation processes for quaternary and quinternary azeotropic mixtures could be accomplished with unprecedented robustness, reliability, and efficiency. The computational times were cut by at least 85% compared to the respective MINLP solutions, which also benefit from the favorable initialization procedure. In addition, the benefit of the efficient rigorous optimization is highlighted by the optimization-based design of complex and heat-integrated column systems.

Chapter 4 then introduces the extension of the process synthesis framework to the optimization-based design of heteroazeotropic distillation processes. First, a multitude of shortcut methods for non-ideal distillation from literature were supplemented with a powerful phase stability test and studied for the application to heteroazeotropic distillation. It is shown by thorough analysis that these methods are either restricted by inaccuracies due to high non-idealities, limited to ternary mixtures, or limited to certain kinds of splits. By combining elements from the existing shortcut methods, two novel methods for multicomponent heteroazeotropic distillation are proposed, which overcome the limitations of the existing methods. The feed pinch method (FPM) offers an accurate calculation of the minimum energy demand but is not suited for application in process optimization due to the requirement of tray-to-tray calculations. This limitation is resolved by the feed angle method (FAM), which is perfectly

suited for application in process optimization due to its purely algorithmic nature and computational efficiency. Both shortcut methods rely on rigorous thermodynamics and incorporate an efficient test for liquid phase stability.

Based on the same efficient phase test, the rigorous optimization of heteroazeotropic columns is achieved for the first time. Comparable to the homogeneous case, these problems are solved with outstanding robustness and computational efficiency due to a sound initialization and the continuous reformulation of the discrete-continuous problem. It is shown by various multicomponent examples that the novel shortcut and rigorous methods overcome the restrictions in conceptual design of heteroazeotropic distillation processes. The consistent application of the synthesis framework is demonstrated by an industrial case study comprising the optimization-based design of a heteroazeotropic distillation process with several columns and recycles.

Chapter 5 extends the scope of the synthesis framework to hybrid extraction-distillation processes. For this purpose, the methodology of the FAM is adapted for the evaluation of counter-current columns in multicomponent extraction. Comparable to distillation columns, the robust and efficient rigorous optimization of extraction columns is achieved by a continuous reformulation of the discrete-continuous tray-optimization problem. The performance of the novel methodologies is demonstrated by the design of a hybrid extraction-distillation downstream process for the energy-efficient separation of butanol from fermentation broth. For this challenging example, the optimization-based design approach reduced the design effort significantly and lead to the identification of sustainable solutions with unmatched economics.

Subsequently, Chapter 6 presents the optimization-based design of hybrid processes composed of crystallization and distillation. It is shown that the consistent application of powerful optimization techniques allows the evaluation and optimization of a multitude of hybrid process variants for the separation of close-boiling isomers with unprecedented efficiency.

Finally, Chapter 7 gives an outlook on the extension of the proposed methods to reactive separation processes. In particular, it is shown that the FAM for distillation can be applied to reactive distillation with good results. Likewise, progress in the rigorous optimization of reactive distillation processes is achieved by the continuous reformulation of the discrete-continuous optimization problem.

8.1 Topics for further research

While this thesis presents a comprehensive methodology for the optimization-based design of hybrid separation processes, it also provides a foundation for further extensions. The most important topics according to the authors' assessment are briefly illustrated in the following subsections.

8.1.1 Further unit operations

Design methods for hybrid processes comprising the unit operations distillation, decantation, extraction, crystallization, and reaction are proposed in this thesis. Hence, the most natural extension is certainly the development of shortcut and rigorous methods for the evaluation of further unit operations to cover the design of additional, promising hybrid processes. While the extension of the methods to absorption is straight forward, the inclusion of adsorption, chromatography, electrodialysis, and solids processing may require more effort.

Hybrid processes combining distillation with pervaporation or permeation membrane separations offer a great potential for the energy-efficient separation of azeotropic mixtures (Lipnizki, Field and Ten, 1999; Sommer and Melin, 2004; Fontalvo, Cuellar, Timmer, Vorstman, Wijers and Keurentjes, 2005). However, the design of these processes is particularly challenging. Different combinations of membrane modules and distillation columns lead to a multitude of process alternatives. The selection of suitable membranes for these process alternatives often requires a high effort, since critical membrane parameters need to be determined by time-consuming experiments. At the Aachener Verfahrenstechnik, a recently started research project in collaboration with the Laboratory of Fluid Separations of the Technical University of Dortmund focuses on the efficient design of hybrid distillation-membrane separation processes. For this purpose, the synthesis framework used in this thesis will be complemented by shortcut and rigorous membrane models to facilitate a reliable design of these highly integrated processes. Particular attention will be given to the optimal experimental design of membrane measurements. The coupling of membrane modeling and experiments is expected to provide an effective parametrization of the membranes while at the same time reducing the number of required measurements significantly.

8.1.2 Approximation of distillation boundaries

Brüggemann (2005) and Brüggemann and Marquardt (2011a) suggested the assessment of distillation feasibility by means of the pinch distillation boundary (PDB), which describes the boundary conditions at minimum reflux (see also Section 3.2). The PDB is calculated by the detection of bifurcation phenomena and homotopy continuation. Supplemented with an algorithmic shortcut method for the calculation of the minimum energy demand and an objective function to minimize the total process energy demand, the PDB can be used for the numerical optimization of process operating points. However, it is shown in Section 3.4.1 that the repeated call of the PDB homotopy continuation in every iteration step of such an optimization procedure can significantly slow down the solution times, even to an extent that the process optimization with shortcut methods requires longer solution times than a rigorous process optimization. Hence, a simplified approach, which requires no calculation of PDBs, was proposed in Section 4.5.2 and used in the shortcut evaluation steps in this thesis. However, this approach relies on an approximate knowledge of distillation boundaries and column splits and may be inaccurate for highly curved boundaries.

A speedup of the PDB-based feasibility check can be achieved by a calculation of the PDB a priori, i.e. before the process optimization. This is possible, since the location of the pinch distillation boundary is only dependent on the column pressure, which is fixed in the process optimization problems in this thesis. The PDB is then approximated by a polynomial interpolation and stored for usage in the process optimization. The polynomial order can be chosen depending on the curvature of the distillation boundary to facilitate a sufficient accuracy and an efficient parametrization for multi-component mixtures. As a consequence, the computational expensive homotopy-continuation for the determination of the interpolation points has to be carried out only once for a fixed column pressure.

8.1.3 Model-based experimental analysis (MEXA) for process design

The MEXA methodology (Marquardt, 2005) aims at an integration of model discrimination and the necessary experiments in order to facilitate an effective identification of model parameters and the optimal experimental setup. As a further step of integration, Kossack (2010) suggested the incorporation of the MEXA methodology within conceptual process design, when missing or uncertain property data requires an extensive use of experiments. Here, approximate process models are used to identify the

concentration, temperature and pressure ranges where accurate data is critical for process evaluation. Optimal experimental design then helps to reduce the experimental effort to obtain required property data, relative volatilities, distribution coefficients, membrane parameters, etc.. With this knowledge, refined process models are derived, which in turn can be used to improve the design of experiments. It is expected that this approach can significantly improve the quality and efficiency of process design in case of missing or uncertain property data.

8.1.4 Software development

The application of the process synthesis framework (or parts thereof) in industrial practice requires the availability of robust software modules, which connect the design methods with a graphical user interface. While the development of design methods for the synthesis framework has been progressed far, the implementation of these methods in user-friendly software is not nearly as advanced. A first step has been made by the development of the process synthesis toolbox Insynto at AIXCAPE e.V. (http://www.aixcape.org/tools/insynto). Insynto integrates shortcut methods for distillation with a graphical user interface. Distillation processes can be evaluated for feasibility with infinity-infinity analysis (Bekiaris and Morari, 1996; Esbjerg, Andersen, Müller, Marquardt and Jørgensen, 1998; Ryll, Blagov and Hasse, 2008) and for the minimum energy demand with the RBM. Property data can be automatically imported from Aspen Plus. Several opportunities for a reasonable extension of Insynto are provided in this thesis. These are listed in the following.

In its current form, the Insynto toolbox does not allow an optimization of process operating points with respect to energy demand. In future work, the introduction of optimization algorithms can provide significant progress in this regard. For azeotropic distillation processes, this extension requires a description of distillation boundaries. Here, an appropriate implementation of the pinch distillation boundary as suggested in Section 8.1.2 may be sufficient. Another promising addition may be the inclusion of rigorous design and optimization methods.

In view of the author, the rigorous optimization methods proposed in this thesis have reached a maturity level which warrants their implementation in the software toolbox. However, these methods require the use of powerful NLP solvers, which are only available in advanced optimization platforms such as GAMS. It may therefore be necessary to develop a parser which generates input files for the optimization platform from the process specifications in Insynto. The optimization results are then returned to Insynto and displayed on the graphical output.

Depending on user requests, shortcut or rigorous design methods for further unit operations can also be integrated. Several of these are proposed in this thesis. Particularly the extension to heteroazeotropic distillation might be fruitful, since these processes occur frequently in industrial practice.

Appendix A

Empirical study on the continuous reformulation of MINLP problems

In Section 3.3.2, the continuous reformulation of MINLP problems as purely continuous NLP problems was presented. It was proposed to replace the discrete decision variables $y \in \{0,1\}$ or $b \in \{0,1\}$ by continuous decision variables $c \in [0,1]$. These continuous variables are forced to integer values by the introduction of NCP-functions in the form of Fischer-Burmeister (FB) functions (eq. (3.42)). In order to improve the solution properties of these highly nonlinear constraints, a relaxation parameter μ was added. The resulting NLP problem is then solved in a series of a few solution steps where μ is reduced to zero.

While the continuous reformulation of mathematical programs with equilibrium constraints (MPEC) has been applied to large MPEC problem libraries with good results (Fletcher and Leyffer, 2004; Baumrucker et al., 2008), continuous reformulation strategies have not been applied to MINLP problem libraries. Hence, Kraemer and Marquardt (2010) studied the performance of continuous reformulation of MINLP problems empirically by means of a large MINLP test problem library.

For this study, the MINLPLib (Bussieck, Drud and Meeraus, 2003) library was chosen. The test problems in MINLPLib are supplied in GAMS (Brooke et al., 2005) syntax by a large number of authors. At the time of the study, MINLPLib contained 271 test problems. Some problems occur in many similar versions which often only differ in a few parameters, variables or equations and have very similar solution properties. Obviously, the problems with many similar versions would have a disproportionate weight in the empirical study. In order to prevent such a distortion, the library was reduced to 98 representative MINLP problems by eliminating similar

versions of a problem a priori, i.e. before the performance was checked.

The 98 MINLP problems of the reduced library were automatically reformulated with the help of FB NCP-functions as in equation (3.42). The FB NCP-functions are relaxed with the relaxation parameter μ and solved in a series of successive NLPs with μ reduced in nine steps from 1 to 0.3, 0.25, 0.2, 0.15, 0.1, 0.05, 0.025 and finally to $\mu = 0$. The solution properties of the reformulated problems, i.e. the value of objective and the solution time, are compared to the solution properties of the MINLP solution with the branch & bound solver SBB (Drud, 2005) and the outer approximation solver DICOPT (Grossman, Viswanathan, Vecchietti, Raman and Kalvelagen, 2008), respectively. All optimization problems were solved in GAMS 22.7 on a PC with a 3 GHz Dual-Core CPU (GAMS runs on one processor only). The NLP problems or subproblems were solved with the SQP-based solver SNOPT (Gill et al., 2008).

The continuous decision variables, which replace the binary variables in the reformulated problems, are initialized with a value of 0.5. In a few instances, the original MINLP program contains initial values for the binary variables. In these cases, the given initial values are carried over to the reformulated problems. It is however important to note that no "good" initial values were assigned to the decision variables other than those given in the original problem. The comparison of the solution quality, i.e. the value of the objective, for the 98 test problems is shown in the upper part of Fig. A.1. More than half of the test problems yielded better solutions when solved with the classical MINLP solvers SBB or DICOPT. The poor performance of the continuous reformulation regarding the solution quality can in part be attributed to the high rate of infeasibility: 61% of the reformulated problems could not be solved to a discrete solution. The percentage of infeasible or non-converging problems is significantly lower for the MINLP solvers SBB (21%) and DICOPT (27%).

The solution times are compared in the lower part of Fig. A.1. Note that here only problems are compared for which both considered solvers yield feasible solutions and at least one solution takes longer than 20 seconds (large-scale problems). The solution procedure for the reformulated problems requires the solution of only 9 NLPs regardless of the complexity of the original MINLP. It is therefore not surprising that most large-scale or complex problems converge faster when reformulated compared to the MINLP solution, where a large number of costly NLP subproblems have to be solved.

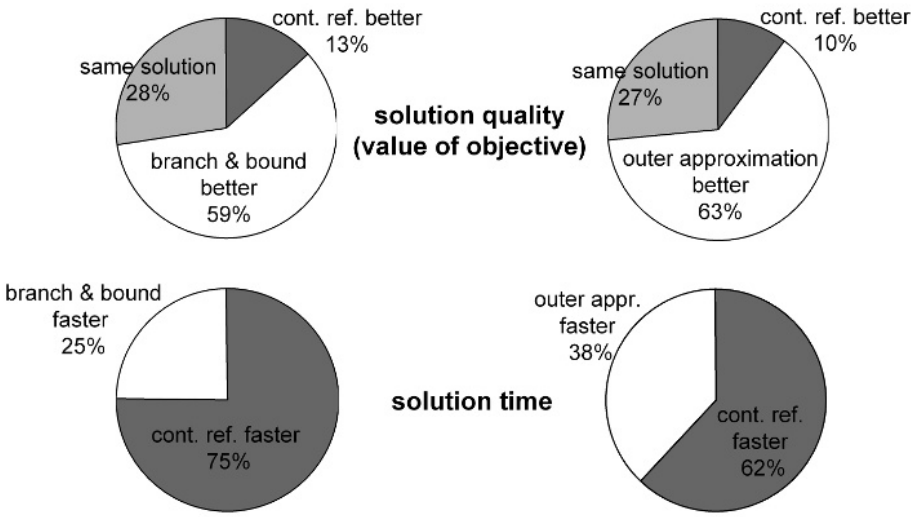

Figure A.1: Performance of continuous reformulation versus branch & bound solver SBB (left) and outer approximation solver DICOPT (right).

A.1 Extension of Continuous Reformulation

Reinitialization Procedure. It was shown that 61% of the reformulated problems turn infeasible when solved as described above. In most cases, the completely relaxed first NLP problem ($\mu = 1$) in the series of successive NLP problems can be solved but the solution becomes infeasible when the relaxation parameter μ is tightened in the subsequent NLPs. An illustration of this property is shown in the upper right of Fig. A.2. Here, the solution procedure for one relaxed binary variable y_i is demonstrated. It is assumed that there is a bound $y_i < 0.8$ on the variable implied by the inequality constraints. ${y_i}^{opt} = 0.68$ is the value of the relaxed decision variable at the solution of the NLP. When the relaxation parameter μ is reduced in the successive solution steps, the feasible region for the relaxed decision variable y_i is split in two disjunct regions. As a consequence, ${y_i}^{opt}$ is pushed to the "right" towards $y_i = 1$ in our example. When the bound imposed by the FB NCP-function and the bound $y_i < 0.8$ overlap for small values of μ, the feasible region on the right side vanishes. Very often, the NLP solver then does not move $y_i = 1$ to the feasible region at the left side but returns an infeasible solution. It is therefore proposed to reinitialize the decision variables, which cause the infeasibility, in the feasible region at the opposite side of their domain. In our example, y_i would be reinitialized with $y_i = 0$.

This reinitialization strategy was implemented in the solution procedure as shown in Fig. A.2. After each NLP, it is automatically checked whether any FB NCP-functions

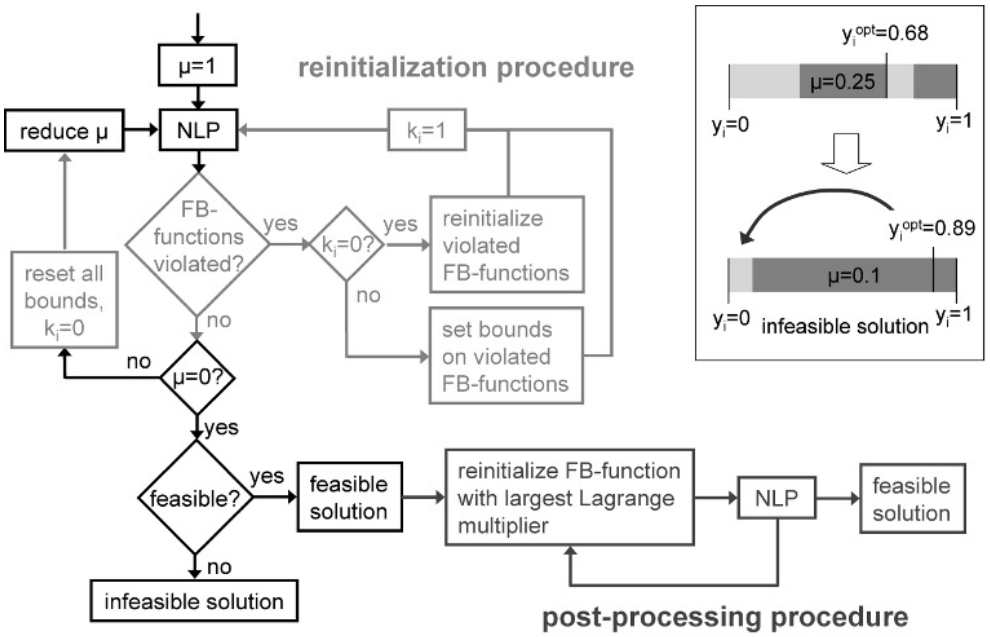

Figure A.2: Solution procedure with reinitialization and post-processing procedures.

are violated. When this is the case, the violated FB NCP-functions are reinitialized by initializing the corresponding relaxed decision variables at the opposite side of their domain (i.e. 0 or 1) as described above. Then the NLP is solved again and when feasible, μ is reduced and the solution procedure is resumed. However, when the same FB NCP-functions are still violated and the reinitialized variables are still at the same side of their domain, these decision variables are forced to the opposite side of their domain by setting bounds on the variables. In our example, y_i would be bounded by $y_i \leq 0$. When the following NLP can be solved, all bounds are released again, μ is reduced, and the solution procedure is resumed. The number of reinitialized problems, which may be solved for each value of the relaxation parameter μ, is limited by an upper bound of m, i.e. the number of binary variables y_i.

Post-Processing Procedure. In order to improve the solution quality (local optima) of the reformulated problems, a post-processing procedure was implemented as shown in Fig. A.2. The post-processing procedure is started when $\mu = 0$ is reached. Then additional NLPs are solved, where single binary variables are fixed at the binary value which is complimentary to the value in the preceding NLP. In other words, the binary variable is fixed at 1 when it was 0 in the optimal solution of the preceding NLP and vice versa. The decision, which binary variable to fix in each post-processing NLP depends on the Lagrange multipliers of the preceding NLP: The binary variable

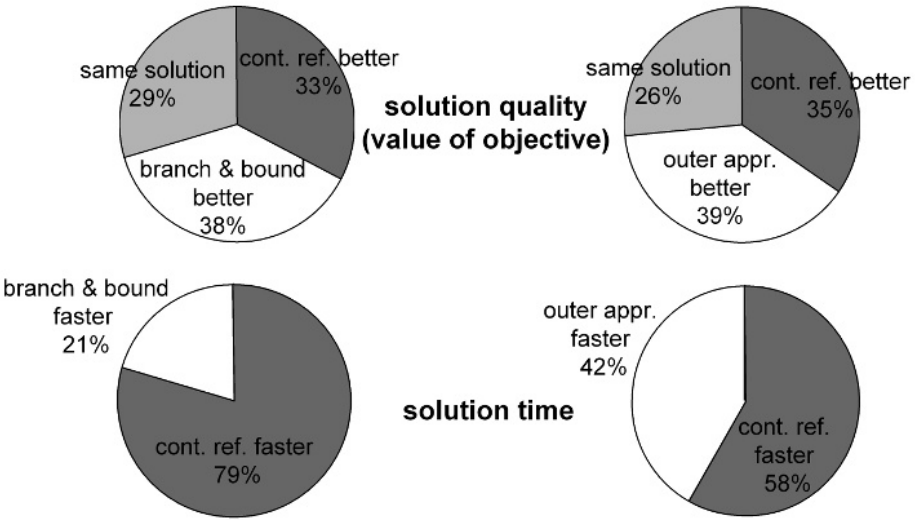

Figure A.3: Performance of extended continuous reformulation versus branch & bound solver SBB (left) and outer approximation solver DICOPT (right).

bounded by the FB NCP-function with the largest associated Lagrange multiplier is chosen. The procedure is stopped when a maximum number of 10 NLPs in the post-processing is reached. Together with the reinitialization procedure for m binary variables and nine decreasing values of the relaxation parameter mu, a maximum number of $9 \cdot m + 10$ NLP subproblems need to be solved. Thus, the maximum number of NLP subproblems is identical to the number of combinations of binary variables for six binary variables and less for more than six binary variables. It is important to note that the maximum number of NLP subproblems was hardly ever reached in the solution of the test problems.

Results. When extended by the reinitialization and post-processing procedures, only 17% of the 98 test problems could not be solved to a discrete solution. This is a significant reduction from the reformulation without the reinitialization and post-processing procedures (61%). In fact, the number is even lower than the number of problems which could not be solved by the MINLP solvers SBB (21%) and DICOPT (27%). The comparison of the solution quality for the 98 test problems is shown in the upper part of Fig. A.3. With the help of the reinitialization and post-processing procedures, the continuous reformulation closed the gap to the classical MINLP solvers: The reformulation yielded better solutions for a comparable number of test problems as the MINLP solvers SBB and DICOPT.

Note that the post-processing procedure improved the solution of 54% of the re-

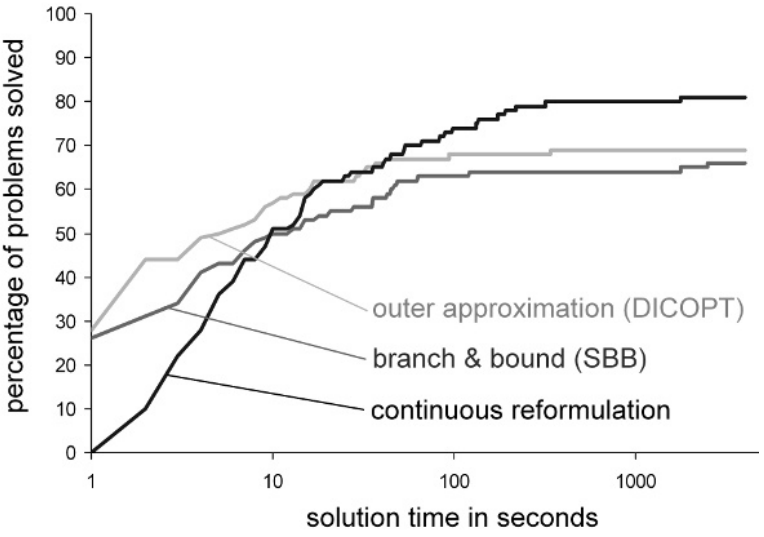

Figure A.4: Comparison of solver performances.

formulated test problems. However, the additional NLPs of the post-processing and reinitialization procedures extended the solution times for the reformulated problems. It becomes apparent in Fig. A.4 that small-scale problems with few binary variables tend to demand longer solution times when they are reformulated. This is because a disproportionally large number of NLPs has to be solved within the reinitialization and post-processing procedures. It needs to be noted, however, that contrary to the subproblems in the fully implemented MINLP solvers, the reformulated problems are solved as consecutive separate NLP problems. As a consequence, GAMS performs a time consuming pre-solve step for each NLP which adds to the solution time especially for the small-scale problems.

Large-scale problems on the other hand, where the classical MINLP solvers need to solve a large number of NLP subproblems, often converge faster when they are reformulated. The solution times of the large-scale problems are compared in the lower part Fig. A.3. Note that only problems are considered for which the solution took longer than 20 seconds with at least one of the compared solvers. In addition, problems are excluded which solutions are infeasible by one or more solvers. Compared to the simple continuous reformulation the solution time advantage over the solver DICOPT has decreased slightly but is still noticeable. Obviously, there is a trade-off between robustness and reliability (quality of the solution) of the reformulation on the one and efficiency on the other hand. The extension with the reinitialization and post-processing procedures has shifted the balance slightly towards robustness and reliability.

It is certainly an important question, for which discrete-continuous optimization problems the continuous reformulation performs better than the existing local MINLP solvers or vice versa. No definite answers can be given to this question as this is still a topic of research. As indicated above, the reformulation offers the prospect of shorter solution times mostly for large-scale problems. Of course, these are in fact the problems were computational efficiency matters most. Regarding the robustness and reliability of the solution, the continuous reformulation tends to perform better for problems with low combinatorial complexity, i.e. problems which are not highly disjunct but where the local optima are located close together in the solution space. For these problems, the tightening of the NCP-functions works more reliably.

A.2 Summary

In Appendix A, 98 representative MINLP test problems of the library MINLPLib were reformulated as continuous problems with the help of FB NCP-functions. When solved in successive NLP steps with a gradually tightened relaxation parameter, the reformulated problems yielded considerably shorter solution times compared to the classical MINLP solvers SBB and DICOPT. As a drawback however, 61% of the reformulated problems could not be solved to a discrete solution. Kraemer and Marquardt (2010) have therefore proposed an extension of the continuous reformulation by a reinitialization and a post-processing procedure. With this extension, the reformulation achieved a comparable performance to the MINLP solvers SBB and DICOPT for the 98 test problems: The reformulation identified better local optima for about the same percentage of problems as the MINLP solvers. Small-scale problems tend to be solved faster by the MINLP solvers whereas large-scale problems are often solved faster by the extended continuous reformulation. Apparently, it is very problem-specific which solver performs best.

In the main part of this thesis, continuous reformulation is applied to column optimization problems, i.e. the discrete-continuous optimization of distillation and extraction columns or crystallization cascades. For these problems of large scale but low combinatorial complexity, the continuous reformulation performs better than the MINLP solvers. Obviously, it would be of great value to be able to predict a priori, whether a discrete-continuous optimization problem qualifies for continuous reformulation. Further research should therefore be directed towards a more detailed characterization of the problems which are suited for reformulation.

Appendix B

FAM for intermediate splits without feed pinch

In Chapter 4, the feed angle method (FAM) has been applied to direct or indirect splits (see Section 3.1.2 for a definition of splits). These splits, which are most common for distillation, exhibit a feed pinch. It is important to emphasize that the FAM, in contrast to the FPM and the ZVC, can also be applied to sharp split separations without a feed pinch, e.g. to intermediate splits. The shortest stripping line method (Lucia et al., 2008) requires the solution of a MINLP problem to find a feasible feed tray composition for these splits.

The application of the FAM to intermediate splits is illustrated by the quaternary azeotropic heterogeneous mixture of acetone, ethanol, water, and butanol. The coefficients for the calculation of vapor pressures, ideal gas heat capacities, and heats of vaporization are given in Tables D.6, D.15, and D.30. The liquid activity coefficients are determined by the NRTL model with parameters given in Tables D.50 and D.45. An intermediate split has been specified as shown in Table B.1. The rectification bodies detected in the initialization by the RBM are shown in Fig. B.1. It can be clearly seen that the rectification bodies intersect at the edges, since the separation does not exhibit a feed pinch. In fact, this separation will never have a feed pinch, no matter how many trays or how much energy are specified. Note that Fig. B.1 shows no intersection for the column section tray-to-tray profiles calculated for MED determined by the RBM. Therefore, one can conclude that the RBM underestimates the MED in this case.

The task of the FAM is to find a feed tray composition $\mathbf{x}_{n_F}$ and the MED such that the tray above and the tray below the feed tray point towards the respective

Table B.1: Specifications and MED for an intermediate heterogeneous split of a heterogeneous mixture of acetone, ethanol, water, and butanol.

molar composition		
$\mathbf{z}_F$	$\mathbf{x}_D$	$\mathbf{x}_B$
0.23, 0.23, 0.35, 0.2	0.45, 0.45, 0.1, 0	0, 0, 0.6, 0.4
pressure	feed state	g^E-model
1.013 bar	sat. liquid	NRTL
$Q_{B,\min}/F$ [MJ/kmol]		
RBM	FAM	MAC
39.6	44.2	40.7

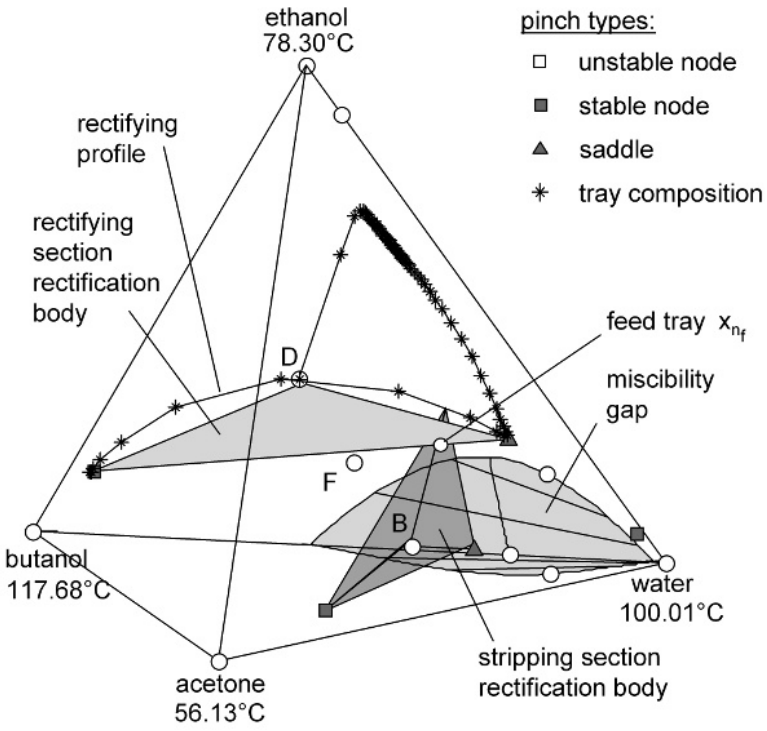

Figure B.1: Rectification bodies and rectifying section profile for the intermediate split at the energy duty determined by the RBM ($Q_{B,min}/F = 39.6$ MJ/kmol).

saddle pinches (cf. Fig. B.2). The point of intersection of the rectification bodies can be used as initial feed tray composition for the FAM. The angles between the lines

connecting the feed to a tray below and above and the lines connecting the feed to the saddle pinches in the rectifying and stripping sections are determined as described above. Note that the example separation exhibits two relevant saddle pinches in the stripping section (cf. Fig. B.2). Consequently, the angle between the line connecting the feed to the tray below and the hyperplane through the saddle pinches and the feed tray is calculated for this section. The angles for the rectifying and stripping sections are then minimized by solving a nonlinear programming problem (NLP) where the feed tray composition and the energy duty are degrees of freedom:

$$\max \quad \cos(\alpha_D) + \cos(\alpha_B), \tag{B.1}$$

$$\text{s.t.} \quad Eqs.\ (3.11) - (3.20), (4.6) - (4.10), \qquad p \in P_{SP}, \tag{B.2}$$

$$Eqs.\ (3.1) - (3.3), \qquad n = n_F - 1, \tag{B.3}$$

$$Eqs.\ (3.8) - (3.10), \qquad n = n_F + 1, \tag{B.4}$$

$$Eqs.\ (3.4) - (3.7), (4.1) - (4.5), \qquad n \in [n_F - 1, n_F + 1] \tag{B.5}$$

$$\cos(\alpha_D) = \frac{(\mathbf{x}_{p_{SP}} - \mathbf{x}_{n_F})^T (\mathbf{x}_{n_F-1} - \mathbf{x}_{n_F})}{\|\mathbf{x}_{p_{SP}} - \mathbf{x}_{n_F}\|_2 \|\mathbf{x}_{n_F-1} - \mathbf{x}_{n_F}\|_2}, \tag{B.6}$$

$$\cos(\alpha_B) = \frac{\mathbf{n}_{SP,\mathbf{x}_{n_F}}^T (\mathbf{x}_{n_F+1} - \mathbf{x}_{n_F})}{\|\mathbf{n}_{SP,\mathbf{x}_{n_F}}\|_2 \|\mathbf{x}_{n_F+1} - \mathbf{x}_{n_F}\|_2}. \tag{B.7}$$

Since the angles between the relevant saddle pinches in the resulting NLP are minimized to zero, feasibility of the separation can be assumed and the MED is determined as given in Table B.1. In order to verify the results, full tray-to-tray profiles for both column sections are calculated at MED determined by the FAM (cf. Fig. B.2). These profiles intersect at the optimized feed tray composition; hence, the results of the FAM are verified. Note that the CPU time required to solve FAM conditions is about two seconds on a standard PC, since only two trays and three pinches have to be calculated.

The MAC can be applied to separations without a feed pinch as well. In this case the angle between the feed composition $\mathbf{x}_F$ and the relevant saddle pinches is minimized. Since the additional information of the tray adjacent to the feed trays is missing the MAC underestimates the MED like the RBM by about 9% (cf. Table B.1). In addition, it is important to note that the angle minimized by the MAC for separations without a feed pinch will always be greater than zero. Hence, no conclusions can be drawn regarding the feasibility of the separation. In contrast, the angle minimized by the FAM contains information about the feasibility of a separation task: If the angle between the relevant saddle pinches can be minimized to zero, feasibility is determined.

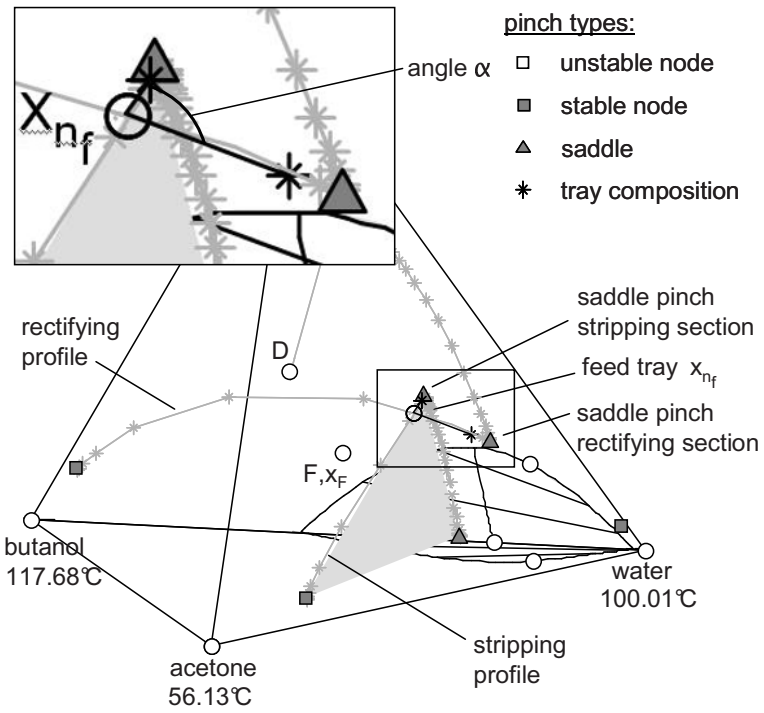

Figure B.2: Tray above and below the optimized feed tray in the FAM for the intermediate split at the MED determined by the FAM ($Q_{B,min}/F$ = 44.2 MJ/kmol). Full profiles are also shown (in grey) for the verification of the MED.

Appendix C

Sizing and costing functions

The rigorous optimization problems in the case studies of this thesis minimize the total annualized costs given by

$$TAC = \dot{C}_{op} \cdot t_a + f_c \cdot C_{cap}. \tag{C.1}$$

The operating cost $\dot{C}_{op}$ is obtained from the utility costs for cooling and heating by

$$\dot{C}_{op} = \sum_k C_{steam,k} \dot{m}_{steam,k} + C_{cw} \dot{m}_{cw} + C_{cool} Q_{cool}, \quad k \in \{3bar, 10bar, 20bar\}, \tag{C.2}$$

and multiplied by the annual operating time t_a =8000 h/a. Here, Q_{cool} is the cumulated duty of chilled water (5°C). Steam costs of $C_{steam,3bar} = 12$ €/t, $C_{steam,10bar} = 13$ €/t, and $C_{steam,20bar} = 15$ €/t are assumed. The costs for cooling water and chilled water are $C_{cw} = 0.05$ €/t and $C_{cool} = 7.77\text{e-}6$ €/kJ, respectively. The mass flows of steam and cooling water are derived by

$$\dot{m}_{steam,k} = \sum_k \frac{Q_{steam,k}}{r_k}, \qquad k \in \{3bar, 10bar, 20bar\}, \tag{C.3}$$

$$\dot{m}_{cw} = -\frac{Q_{cw}}{c_{p_w} \cdot \Delta T_{cw}}, \tag{C.4}$$

where $Q_{steam,k}$ denotes the cumulated heating duties for steam of pressure k and Q_{cw} the cumulated cooling water duties.

The capital costs C_{cap} are multiplied by the capital charge factor f_c, which models the depreciation time including interest. The capital charge factor is typically set to 0.25/a in this thesis such that the investments are depreciated in 5 years. The capital costs are composed of the costs for column shells $C_{s,j}$, column internals $C_{int,j}$, heat

exchangers $C_{hex,j}$, and tanks $C_{t,j}$ for equipment j:

$$C_{cap} = \sum_j (C_{s,j} + C_{int,j} + C_{hex,j} + C_{t,j}), \qquad j \in J. \tag{C.5}$$

The cost functions for the equipment are derived from those of Guthrie (1969) and Biegler, Grossmann and Westerberg (1997) by a currency conversion from \$ to € and an update with the Marshall&Swift index ($M\&S_{2007}$=1.4088, $M\&S_{1968}$=0.28):

$$C_s = 1000\$ \frac{M\&S_{2007}}{M\&S_{1968}} \frac{1}{1.35} \frac{€}{\$} \Big(\frac{D_{col}}{0.914\text{m}}\Big)^{1.05} \Big(\frac{H_{col}}{1.22\text{m}}\Big)^{0.81} (MPF + MF - 1), \tag{C.6}$$

$$C_{int} = 180\$ \frac{M\&S_{2007}}{M\&S_{1968}} \frac{1}{1.35} \frac{€}{\$} \Big(\frac{D_{col}}{0.61\text{m}}\Big)^{1.45} \Big(\frac{H_{col}}{3.05\text{m}}\Big)^{0.97} (MPF + MF - 1), \tag{C.7}$$

$$C_{hex} = 5000\$ \frac{M\&S_{2007}}{M\&S_{1968}} \frac{1}{1.35} \frac{€}{\$} \Big(\frac{A_{hex}}{37.16\text{m}^2}\Big)^{0.65} (MPF + MF - 1), \tag{C.8}$$

$$C_t = 690\$ \frac{M\&S_{2007}}{M\&S_{1968}} \frac{1}{1.35} \frac{€}{\$} \Big(\frac{D_t}{0.914\text{m}}\Big)^{1.05} \Big(\frac{H_t}{1.22\text{m}}\Big)^{0.81} (MPF + MF - 1). \tag{C.9}$$

Here, MPF are material and pressure factors and MF is the module factor given in the work by Guthrie (1969).

For distillation, the column diameter D_{col} is calculated from the gas load at the bottom of the column by

$$D_{col} = \sqrt{\frac{4R_B}{\pi F_G} \sqrt{\frac{\text{R} \cdot T \sum_i y_{n,i} \cdot M_i}{p}}}, \qquad n = N. \tag{C.10}$$

The F-factor F_G is set to $2\text{Pa}^{0.5}$. When a vaporous feed is specified, the gas load in the rectifying section dominates. In this case, the diameter is calculated at the top of the column by substituting R_B with V_2 and setting $n = 1$ in eq. (C.10). The diameter of an extraction column is derived from the volumetric flow rates of the feed and the solvent and the maximum velocity w_{max} by

$$D_{col} = \sqrt{\frac{F \sum_i \frac{x_{F,i} \cdot M_i}{\rho_i} + S \sum_i \frac{x_{S,i} \cdot M_i}{\rho_i}}{w_{max}}}. \tag{C.11}$$

In this expression, w_{max} is set to 50 m/h according to Perry and Green (1997).

The hight of the columns is given by

$$H_{col} = N_{col} \cdot H_{tray} + H_0. \tag{C.12}$$

For distillation, the hight of the trays H_{tray} and the clearance for the liquid distributors H_0 are assumed to be 0.5 m and 4 m, respectively. For extraction columns, these values were set to 0.3 m and 2 m, respectively.

The required areas of the heat exchangers are obtained from

$$A_{hex} = \frac{Q}{\Delta T \cdot k}. \tag{C.13}$$

Here, the logarithmic mean temperature difference is used for the calculation of ΔT for condensers, while the simple temperature difference between evaporating and condensing media suffices for reboilers. When the column products are known, these temperature differences can be fixed during the rigorous optimization of distillation columns. The heat transfer coefficient k is typically set to $800\frac{W}{m^2K}$.

The capital cost of a crystallization unit is dominated by the costs for a shell and tube heat exchanger. The required area of this heat exchanger is calculated from the number of tubes N_T and their diameter D_T and length L_T by

$$A_{hex} = N_T \pi D_T L_T. \tag{C.14}$$

According to Wallert (2008), the maximum number of tubes is given by

$$N_T = \frac{t_{cryst} S_{max} M_s}{\epsilon \pi L_T \rho_s \frac{D_T}{2}^2}. \tag{C.15}$$

Here, ϵ is the load factor, which is assumed to be 0.5. In the rigorous optimization, it is not known a priori on which crystallization stage the maximum rate of solid product S_{max} is obtained. Therefore, eq. (C.15) is substituted by

$$N_T \geq \frac{t_{cryst} S_n M_s}{\epsilon \pi L_T \rho_s \frac{D_T}{2}^2}, \qquad n = 1, ..., N. \tag{C.16}$$

The crystallization time t_{cryst} is obtained from

$$t_{cryst} = \frac{1}{w_{cryst}} \frac{D_T}{2} (1 - \sqrt{1 - \epsilon}), \tag{C.17}$$

where a value of $1 \cdot 10^{-6} \frac{m}{s}$ is specified for the crystallization velocity w_{cryst} (Franke, 2006).

In addition to the heat exchanger, buffer tanks for the storage of residue melt have to be considered for each crystallization stage. The volume of these buffer tanks is given by

$$V_{t,n} = t_{cryst} \frac{(L_{n-1} + c_{F,n} F) M_R}{\rho_l}, \qquad n = 1, ..., N. \tag{C.18}$$

In the rigorous optimization, the residue melt flow rates L_n become zero for non-existing stages such that only buffer tanks for existing stages are considered.

Appendix D

Physical Property Calculation

D.1 Vapor pressure

The extended Antoine equation for the vapor pressure p in Pa at the temperature T in K is given by

$$\ln p_i = C_{1,i} + \frac{C_{2,i}}{T + C_{3,i}} + C_{4,i}T + C_{5,i}lnT + C_{6,i}T^{C_{7,i}},\ i = 1, ..., C. \tag{D.1}$$

Table D.1: Antoine equation parameters for the system of acetone, chloroform, benzene, and toluene (Chapter 3).

	$C_{1,i}$	$C_{2,i}$	$C_{3,i}$	$C_{4,i}$	$C_{5,i}$	$C_{6,i}$	$C_{7,i}$
acetone	73.2391	-5626.84	0	$6.25888 \cdot 10^{-3}$	-8.05705	$1.27440 \cdot 10^{-17}$	6
chloroform	49.4950	-4909.24	0	$6.97118 \cdot 10^{-4}$	-4.04868	$1.02370 \cdot 10^{-17}$	6
benzene	73.8624	-5970.44	0	$5.53760 \cdot 10^{-3}$	-8.07976	$6.61298 \cdot 10^{-18}$	6
toluene	71.2775	-6413.29	0	$4.16630 \cdot 10^{-3}$	-7.50535	$5.41998 \cdot 10^{-18}$	6

Table D.2: Antoine equation parameters for the system of water, n-butyl acetate, n-butanol, and acetic acid (Chapter 4).

	$C_{1,i}$	$C_{2,i}$	$C_{3,i}$	$C_{4,i}$	$C_{5,i}$	$C_{6,i}$	$C_{7,i}$
water	73.649	-7258.2	0	0	-7.3037	$4.1653 \cdot 10^{-6}$	2
n-butyl acetate	71.34	-7285.8	0	0	-6.9459	$9.9895 \cdot 10^{-18}$	6
n-butanol	93.173	-9185.9	0	0	-9.7464	$4.7796 \cdot 10^{-18}$	6
acetic acid	53.27	-6304.5	0	0	-4.2985	$8.8865 \cdot 10^{-18}$	6

Table D.3: Antoine equation parameters for the system of propargyl alcohol, monochlorobenzene, and water (Chapter 4).

	$C_{1,i}$	$C_{2,i}$	$C_{3,i}$	$C_{4,i}$	$C_{5,i}$	$C_{6,i}$	$C_{7,i}$
propargyl alcohol	113.01	-8141.8	0	0	-14.526	$1.5774 \cdot 10^{-2}$	1
monochlorobenzene	54.1440	-6244.4	0	0	-4.5343	$4.703 \cdot 10^{-18}$	6
water	73.6490	-7258.2	0	0	-7.3037	$4.1653 \cdot 10^{-6}$	2

Table D.4: Antoine equation parameters for the system of water, acetone, chloroform, and acetic acid (Chapter 5).

	$C_{1,i}$	$C_{2,i}$	$C_{3,i}$	$C_{4,i}$	$C_{5,i}$	$C_{6,i}$	$C_{7,i}$
water	73.6490	-7258.2	0	0	-7.3037	$4.1653 \cdot 10^{-6}$	2
acetone	69.006	-5599.6	0	0	-7.0985	$6.2237 \cdot 10^{-6}$	2
chloroform	146.43	-7792.3	0	0	-20.614	$2.4578 \cdot 10^{-2}$	1
acetic acid	53.27	-6304.5	0	0	-4.2985	$8.8865 \cdot 10^{-18}$	6

Table D.5: Antoine equation parameters for the system of o-xylene, toluene, n-heptane, and propylene carbonate (Chapter 5).

	$C_{1,i}$	$C_{2,i}$	$C_{3,i}$	$C_{4,i}$	$C_{5,i}$	$C_{6,i}$	$C_{7,i}$
o-xylene	90.356	-7948.7	0	0	-10.081	$5.9756 \cdot 10^{-6}$	2
toluene	80.877	-6902.4	0	0	-8.7761	$5.8034 \cdot 10^{-6}$	2
n-heptane	87.829	-6996.4	0	0	-9.8802	$7.2099 \cdot 10^{-6}$	2
propylene carbonate	83.087	-9788	0	0	-8.5515	$3.1842 \cdot 10^{-6}$	2

Table D.6: Antoine equation parameters for the system of acetone, ethanol, water, n-butanol, mesitylene, and oleyl alcohol (Chapter 5).

	$C_{1,i}$	$C_{2,i}$	$C_{3,i}$	$C_{4,i}$	$C_{5,i}$	$C_{6,i}$	$C_{7,i}$
acetone	69.006	-5599.6	0	0	-7.0985	$6.2237 \cdot 10^{-6}$	2
ethanol	73.304	-7122.3	0	0	-7.1424	$2.8853 \cdot 10^{-6}$	2
water	73.6490	-7258.2	0	0	-7.3037	$4.1653 \cdot 10^{-6}$	2
n-butanol	107.09	-9914.7	0	0	-117.68	$1.0925 \cdot 10^{-17}$	6
mesitylene	88.697	-8317	0	0	-9.733	$5.3187 \cdot 10^{-6}$	2
oleyl alcohol	123.911	-15785.3	0	0	-13.5208	$2.91259 \cdot 10^{-18}$	6

Table D.7: Antoine equation parameters for the system of di-tert-butylbenzene, m-xylene, tert-butyl-m-xylene, tert-butylbenzene, and benzene (Chapter 7).

	$C_{1,i}$	$C_{2,i}$	$C_{3,i}$	$C_{4,i}$	$C_{5,i}$	$C_{6,i}$	$C_{7,i}$
di-tert-butylbenzene	21.0017	-4096.3	-103	0	0	0	0
m-xylene	94.6023	-7884.68	0	$7.245 \cdot 10^{-3}$	-11.12	$4.183 \cdot 10^{-18}$	6
tert-butyl-m-xylene	20.9517	-3850.38	-88.75	0	0	0	0
tert-butylbenzene	136.263	-9750.76	0	0.0144	-17.906	$1.766 \cdot 10^{-17}$	6
benzene	73.8624	-5970.44	0	$5.538 \cdot 10^{-3}$	-8.08	$6.613 \cdot 10^{-18}$	6

Table D.8: Antoine equation parameters for the system of levulinic acid, butanol, butyl levulinate, and water (Chapter 7).

	$C_{1,i}$	$C_{2,i}$	$C_{3,i}$	$C_{4,i}$	$C_{5,i}$	$C_{6,i}$	$C_{7,i}$
levulinic acid	158.19	-15257	0	0	-19.116	$7.233 \cdot 10^{-6}$	2
butanol	107.09	-9914.7	0	0	-11.768	$1.0925 \cdot 10^{-17}$	6
butyl levulinate	22.5302	-4898.5	-65.6	0	0	0	0
water	773.6490	-7258.2	0	0	-7.3037	$4.1653 \cdot 10^{-6}$	2

D.2 Ideal gas heat capacity

The ASPEN polynomial for the ideal gas heat capacity $c_{p,i}^{ig}$ in J·kmol−1K−1 at the temperature T in K is given by

$$c_{p,i}^{ig} = C_{1,i} + C_{2,i}T + C_{3,i}T^2 + C_{4,i}T^3 + C_{5,i}T^4 + C_{6,i}T^5, \text{ for } C_{7,i} \leq T \leq C_{8,i}, \quad \text{(D.2)}$$

$$c_{p,i}^{ig} = C_{9,i} + C_{10,i}T^{C_{11,i}}, \text{ for } T \leq C_{7,i}. \quad \text{(D.3)}$$

The DIPPR equation 107 is defined by

$$c_{p,i}^{ig} = C_{1,i} + C_{2,i}\left(\frac{\frac{C_{3,i}}{T}}{\sinh(\frac{C_{3,i}}{T})}\right)^2 + C_{4,i}\left(\frac{\frac{C_{5,i}}{T}}{\cosh(\frac{C_{5,i}}{T})}\right)^2, \text{ for } C_{6,i} \leq T \leq C_{7,i}. \quad \text{(D.4)}$$

Table D.9: Parameters of the ASPEN ideal gas heat capacity polynomial for the system of acetone, chloroform, benzene, and toluene (Chapter 3).

	$C_{1,i}$	$C_{2,i}$	$C_{3,i}$	$C_{4,i}$	$C_{5,i}$	$C_{6,i}$	$C_{7,i}$	$C_{8,i}$
acetone	6301.13	260.586	-0.125269	$2.03772 \cdot 10^{-5}$	0	0	300	2049.2
chloroform	24002.9	189.327	-0.184094	$6.65701 \cdot 10^{-5}$	0	0	300	921.790
benzene	-33917.3	474.364	-0.301701	$7.13012 \cdot 10^{-5}$	0	0	300	1410.5
toluene	-24354.6	512.464	-0.276538	$4.91112 \cdot 10^{-5}$	0	0	300	1665.4
	$C_{9,i}$	$C_{i,10}$	$C_{i,11}$					
acetone	33256	7.7938	1.5					
chloroform	33256	6.30760	1.5					
benzene	33256	1.10550	1.879					
toluene	33256	13.965	1.5					

Table D.10: Parameters of the ASPEN ideal gas heat capacity polynomial for the system of water, n-butyl acetate, n-butanol, and acetic acid (Chapter 4).

	$C_{1,i}$	$C_{2,i}$	$C_{3,i}$	$C_{4,i}$	$C_{5,i}$	
water	33738.1	-7.01756	0.0272961	$-1.665 \cdot 10^{-5}$	$4.3 \cdot 10^{-9}$	
n-butyl acetate	13619.7	548.889	-0.227846	$-7.913 \cdot 10^{-7}$	0	
n-butanol	3265.7	418.01	-0.224161	$4.68503 \cdot 10^{-5}$	0	
acetic acid	4839.94	254.851	-0.175301	$4.9488 \cdot 10^{-5}$	0	
	$C_{6,i}$	$C_{7,i}$	$C_{8,i}$	$C_{9,i}$	$C_{10,i}$	$C_{11,i}$
water	$-4.17 \cdot 10^{-13}$	200	3000	33256	$1.9 \cdot 10^{-20}$	9.2846
n-butyl acetate	0	300	1197	33256	23.961	1.5
n-butanol	0	300	1594.9	33256	14.723	1.5
acetic acid	0	300	1180.8	33256	6.466	1.5

Table D.11: Parameters of the DIPPR ideal gas heat capacity equation 107 for the system of isopropanol, water, and cyclohexane (Chapter 4).

	C_1	C_2	C_3	C_4	C_5	C_6	C_7
isopropanol	57230	191000	1421	121550	626	150	1500
water	33363	26790	2610.5	8896	1169	100	2273.15
cyclohexane	43200	373500	1192	163500	-530.1	100	1500

Table D.12: Parameters of the DIPPR ideal gas heat capacity equation 107 for the system of propargyl alcohol, monochlorobenzene, and water (Chapter 4).

	C_1	C_2	C_3	C_4	C_5	C_6	C_7
propargyl alcohol	93600	70700	1239	$-3.44 \cdot 10^{7}$	7.58	300	1500
monochlorobenzene	80110	231000	2157	204600	897.6	200	1500
water	33363	26790	2610.5	8896	1169	100	2273.15

Table D.13: Parameters of the DIPPR ideal gas heat capacity equation 107 for the system of water, acetone, chloroform, and acetic acid (Chapter 5).

	C_1	C_2	C_3	C_4	C_5	C_6	C_7
water	33363	26790	2610.5	8896	1169	100	2273.15
acetone	57040	163200	1607	96800	731.5	200	1500
chloroform	39420	65730	928	49300	399.6	100	1500
acetic acid	40200	136750	1262	70030	569.7	50	1500

Table D.14: Parameters of the DIPPR ideal gas heat capacity equation 107 for the system of o-xylene, toluene, n-heptane, and propylene carbonate (Chapter 5).

	C_1	C_2	C_3	C_4	C_5	C_6	C_7
o-xylene	85210	329540	1494.4	211500	-675.8	200	1500
toluene	58140	286300	1440.6	189800	-650.43	200	1500
n-heptane	120150	400100	1676.6	274000	756.4	200	1500
propylene carbonate	80969	210850	1659.8	171900	756.5	200	1500

Table D.15: Parameters of the DIPPR ideal gas heat capacity equation 107 for the system of acetone, ethanol, water, n-butanol, mesitylene, and oleyl alcohol (Chapter 5).

	C_1	C_2	C_3	C_4	C_5	C_6	C_7
acetone	57040	163200	1607	96800	731.5	200	1500
ethanol	49200	145770	1662.8	93900	744.7	200	1500
water	33363	26790	2610.5	8896	1169	100	2273.15
butanol	74540	259070	1607.3	173200	712.4	200	1500
mesitylene	91540	392700	1498	250900	676.9	2.00	1500
oleyl alcohol	358715.76	586642.35	809.84	436882.15	1992.51	200	1500

Table D.16: Parameters of the ASPEN ideal gas heat capacity polynomial for the system of di-tert-butylbenzene, m-xylene, tert-butyl-m-xylene, tert-butylbenzene, and benzene (Chapter 7).

	$C_{1,i}$	$C_{2,i}$	$C_{3,i}$	$C_{4,i}$	$C_{5,i}$	$C_{6,i}$
di-tert-butylbenzene	-60809.1	1411.79	-0.815589	$1.83047 \cdot 10^{-4}$	0	0
m-xylene	-29165.2	629.695	-0.374719	$8.47827 \cdot 10^{-5}$	0	0
tert-butyl-m-xylene	-59264.2	1223.38	-0.708407	$1.59643 \cdot 10^{-5}$	0	0
tert-butylbenzene	-8.6001.1	1101.97	-0.874623	$2.82651 \cdot 10^{-4}$	0	0
benzene	-33917.3	474.364	-0.301701	$7.13012 \cdot 10^{-5}$	0	0
	$C_{7,i}$	$C_{8,i}$	$C_{9,i}$	$C_{i,10}$	$C_{i,11}$	
di-tert-butylbenzene	300	1485.2	33256	50.232	1.5	
m-xylene	300	1473.3	33256	18.292	1.5	
tert-butyl-m-xylene	300	1479.2	33256	41.387	1.879	
tert-butylbenzene	300	1031.5	33256	26.993	1.5	
benzene	300	1410.5	33256	1.1055	1.879	

Table D.17: Parameters of the DIPPR ideal gas heat capacity equation 107 for the system of levulinic acid, butanol, butyl levulinate, and water (Chapter 7).

	C_1	C_2	C_3	C_4	C_5	C_6	C_7
levulinic acid	69480	162350	486.04	158500	1721.2	300	1500
butanol	74540	259070	1607.3	173200	712.4	200	1500
butyl levulinate	182863	306603	756.45	-22.1972	-77.7081	280	530
water	33363	26790	2610.5	8896	1169	100	2273.15

D.3 Heat of vaporization

The Watson equation for the heat of vaporization $\Delta H_{vap,i}(T)$ in J·kmol−1 at the temperature T in K is given by

$$\Delta H_{vap,i}(T) = \Delta H_{vap,i}(T_1) \left(\frac{1 - \frac{T}{T_{c,i}}}{1 - \frac{T_1}{T_{c,i}}} \right)^{C_{1,i}+C_{2,i}(1-\frac{T}{T_{c,i}})}, \text{ for } T > T_{\min}. \tag{D.5}$$

The DIPPR Heat of vaporization equation is defined by

$$\Delta H_{vap,i} = C_{1,i} \left(1 - \frac{T}{T_{c,i}} \right)^{\left(C_{2,i}+C_{3,i}\frac{T}{T_{c,i}}+C_{4,i}\left(\frac{T}{T_{c,i}}\right)^2+C_{5,i}\left(\frac{T}{T_{c,i}}\right)^3\right)}, \text{ for } C_{6,i} \leq T \leq C_{7,i}. \tag{D.6}$$

Table D.18: Parameters of the Watson heat of vaporization equation for the system of acetone, chloroform, benzene, and toluene (Chapter 3).

	$\Delta H_{vap,i}(T_1)$	T_1	C_1	C_2	$T_{\min}$
acetone	$2.91401 \cdot 10^7$	329.4	0.36374	0	178.2
chloroform	$2.97263 \cdot 10^7$	334.3	0.345189	0	209.6
benzene	$3.07814 \cdot 10^7$	353.3	0.349117	0	278.7
toluene	$3.32013 \cdot 10^7$	383.8	0.363993	0	178

Table D.19: Critical temperatures in K for the system of acetone, chloroform, benzene, and toluene (Chapter 3).

	$T_{c,i}$
acetone	508.1
chloroform	536.4
benzene	562.1
toluene	591.7

Table D.20: Parameters of the Watson heat of vaporization equation for the system of isopropanol, water, and cyclohexane (Chapter 4).

	$\Delta H_{vap,i}(T_1)$	T_1	C_1	C_2	T_{min}
isopropanol	$3.98583 \cdot 10^7$	355.4	0.401403	0	184.7
water	$4.06831 \cdot 10^7$	373.2	0.310646	0	273.2
cyclohexane	$2.99775 \cdot 10^7$	353.9	0.357231	0	279.7

Table D.21: Critical temperatures in K for the system of isopropanol, water, and cyclohexane (Chapter 4).

	$T_{c,i}$
isopropanol	508.3
water	647.13
cyclohexane	553.58

Table D.22: Parameters of the Watson heat of vaporization equation for the system of water, n-butyl acetate, n-butanol, and acetic acid (Chapter 4).

	$\Delta H_{vap,i}(T_1)$	T_1	C_1	C_2	T_{min}
water	$4.06831 \cdot 10^7$	373.2	0.310646	0	273.2
n-butyl acetate	$3.60065 \cdot 10^7$	399.2	0.394204	0	199.7
n-butanol	$4.3124 \cdot 10^7$	390.9	0.397885	0	183.9
acetic acid	$2.36973 \cdot 10^7$	391.1	0.370901	0	289.8

Table D.23: Critical temperatures in K for the system of water, n-butyl acetate, n-butanol, and acetic acid (Chapter 4).

	$T_{c,i}$
water	647.13
n-butyl acetate	579.15
n-butanol	563.05
acetic acid	591.95

Table D.24: Parameters of the DIPPR heat of vaporization equation for the system of propargyl alcohol, monochlorobenzene, and water (Chapter 4).

	C_1	C_2	C_3	C_4	C_5	C_6	C_7
propargyl alcohol	$6.652 \cdot 10^7$	0.4113	0	0	0	221.35	580
monochlorobenzene	$5.148 \cdot 10^7$	0.36614	0	0	0	227.95	632.35
water	$5.2053 \cdot 10^7$	0.3199	-0.212	0.25795	0	273.16	647.13

Table D.25: Critical temperatures in K for the system of propargyl alcohol, monochlorobenzene, and water (Chapter 4).

	$T_{c,i}$
propargyl alcohol	580
monochlorobenzene	632.35
water	647.13

Table D.26: Parameters of the DIPPR heat of vaporization equation for the system of water, acetone, chloroform, and acetic acid (Chapter 5).

	C_1	C_2	C_3	C_4	C_5	C_6	C_7
water	$5.2053 \cdot 10^7$	0.3199	-0.212	0.25795	0	273.16	647.1
acetone	$4.215 \cdot 10^7$	0.3397	0	0	0	178.45	508.2
chloroform	$4.186 \cdot 10^7$	0.3584	0	0	0	209.63	536.4
acetic acid	$4.0179 \cdot 10^7$	2.6037	-5.0031	2.7069	0	289.81	591.95

Table D.27: Critical temperatures in K for the system of water, acetone, chloroform, and acetic acid (Chapter 5).

	$T_{c,i}$
water	647.096
acetone	508.2
chloroform	536.4
acetic acid	591.95

Table D.28: Parameters of the DIPPR heat of vaporization equation for the system of o-xylene, toluene, n-heptane, and propylene carbonate (Chapter 5).

	C_1	C_2	C_3	C_4	C_5	C_6	C_7
o-xylene	$5.533 \cdot 10^7$	0.377	0	0	0	247.98	630.33
toluene	$5.0144 \cdot 10^7$	0.3859	0	0	0	178.18	591.8
n-heptane	$5.0014 \cdot 10^7$	0.38795	0	0	0	182.57	540.2
propylene carbonate	$7.1701 \cdot 10^7$	0.32731	0	0	0	223.95	778

Table D.29: Critical temperatures in K for the system of o-xylene, toluene, n-heptane, and propylene carbonate (Chapter 5).

	$T_{c,i}$
o-xylene	630.33
toluene	591.8
n-heptane	540.2
acetic acid	778

Table D.30: Parameters of the DIPPR heat of vaporization equation for the system of acetone, ethanol, water, n-butanol, mesitylene, and oleyl alcohol (Chapter 5).

	C_1	C_2	C_3	C_4	C_5	C_6	C_7
acetone	$4.215 \cdot 10^7$	0.3397	0	0	0	178.45	508.2
ethanol	$5.5789 \cdot 10^7$	0.31245	0	0	0	159.05	514
water	$5.2053 \cdot 10^7$	0.3199	-0.212	0.25795	0	273.16	647.1
n-butanol	$7.7535 \cdot 10^7$	0.49599	0	0	0	184.51	563
mesitylene	$5.9365 \cdot 10^7$	0.35743	0	0	0	228.42	637.3
oleyl alcohol	$9.65 \cdot 10^5$	-11.89	14.069	-2.7275	-0.3885	270	700

Table D.31: Critical temperatures in K for the system of acetone, ethanol, water, n-butanol, mesitylene, and oleyl alcohol (Chapter 5).

	$T_{c,i}$
acetone	508.2
ethanol	514
water	647.096
n-butanol	563
mesitylene	637.3
oleyl alcohol	763

Table D.32: Parameters of the Watson heat of vaporization equation for the system of di-tert-butylbenzene, m-xylene, tert-butyl-m-xylene, tert-butylbenzene, and benzene (Chapter 7).

	$\Delta H_{vap,i}(T_1)$	T_1	C_1	C_2	$T_{\min}$
di-tert-butylbenzene	$4.7269 \cdot 10^7$	535.3	0.41	0	284.2
m-xylene	$3.63833 \cdot 10^7$	412.3	0.378493	0	225.3
tert-butyl-m-xylene	$4.33752 \cdot 10^7$	497.3	0.41	0	271.6
tert-butylbenzene	$3.76393 \cdot 10^7$	442.3	0.379912	0	215.3
benzene	$3.07814 \cdot 10^7$	353.3	0.349117	0	278.7

Table D.33: Critical temperatures in K for the system of di-tert-butylbenzene, m-xylene, tert-butyl-m-xylene, tert-butylbenzene, and benzene (Chapter 7).

	$T_{c,i}$
di-tert-butylbenzene	710.5
m-xylene	617
tert-butyl-m-xylene	679
tert-butylbenzene	660
benzene	562.1

Table D.34: Parameters of the DIPPR heat of vaporization equation for the system of levulinic acid, butanol, butyl levulinate, and water (Chapter 7).

	C_1	C_2	C_3	C_4	C_5	C_6	C_7
levulinic acid	$9.5291 \cdot 10^7$	0.37849	0	0	0	308.15	738
butanol	$7.7535 \cdot 10^7$	0.49599	0	0	0	184.51	563
butyl levulinate	$7.53 \cdot 10^6$	-15.5215	45.7352	-52.9738	22.8607	280	530
water	$5.2053 \cdot 10^7$	0.3199	-0.212	0.25795	0	273.16	647.13

Table D.35: Critical temperatures in K for the system of levulinic acid, butanol, butyl levulinate, and water (Chapter 7).

	$T_{c,i}$
levulinic acid	738
butanol	563
butyl levulinate	688.44
water	647.13

D.4 Liquid activity coefficient models

Table D.36: Binary parameters of the Wilson model based on a gas constant value of 1.98721 for the system of acetone, chloroform, benzene, and toluene (Chapter 3).

	acetone	chloroform	benzene	toluene
acetone	0	28.8819	543.9352	356.0129
chloroform	-484.3856	0	-161.8065	-365.8311
benzene	-182.5230	49.6010	0	377.9760
toluene	13.6840	552.1459	-354.9859	0

Table D.37: Molar volumes of the Wilson model for the system of acetone, chloroform, benzene, and toluene (Chapter 3).

	ν_i
acetone	74.05
chloroform	80.67
benzene	89.41
toluene	106.85

Table D.38: Binary interaction parameter $\tau_{i,j} = \exp(A_{i,j} + \frac{B_{i,j}}{T})$ of the UNIQUAC model for the system of water, n-butyl acetate, n-butanol, and acetic acid (Chapter 4) (temperature T in K).

		water	n-butyl acetate	n-butanol	acetic acid
$A_{i,j}$	water	0	-0.7542	-4.9934	0
	n-butyl acetate	0.9267	0	1.3061	0
	n-butanol	3.7644	-0.7216	0	0
	acetic acid	0	0	0	0
$B_{i,j}$	water	0	48.18740	1569.05	-73.444
	n-butyl acetate	-690.419	0	-566.662	-336.683
	n-butanol	-1446.61	282.768	0	-157.6
	acetic acid	219.66	140.774	277.29	0

Table D.39: UNIQUAC model: values for the surface areas q_i and relative Van der Waals volumes r_i for the system of water, n-butyl acetate, n-butanol, and acetic acid (Chapter 4).

	q_i	r_i
water	1.4	0.92
n-butyl acetate	4.196	4.82729
n-butanol	3.048	3.45419
acetic acid	2.072	2.19512

Table D.40: Binary interaction parameter $\tau_{i,j} = A_{i,j} + \frac{B_{i,j}}{T}$ of the NRTL model for the system of propargyl alcohol, monochlorobenzene, and water (Chapter 4) (temperature T in K).

		propargyl alcohol	monochlorobenzene	water
$A_{i,j}$	propargyl alcohol	0	0	0
	monochlorobenzene	0	0	-8.7003
	water	0	282.768	0.4452
$B_{i,j}$	propargyl alcohol	0	-179.532	-62.3042
	monochlorobenzene	663.814	0	3915.52
	water	701.098	2170.21	0

Table D.41: Non-randomness parameter $\alpha_{i,j}$ of the NRTL model for the system of propargyl alcohol, monochlorobenzene, and water (Chapter 4).

	propargyl alcohol	monochlorobenzene	water
propargyl alcohol	0.3	0.3	0.3
monochlorobenzene	0.3	0.3	0.2
water	0.3	0.2	0.3

Table D.42: Binary interaction parameter $\tau_{i,j} = \exp(A_{i,j} + \frac{B_{i,j}}{T})$ of the UNIQUAC model for the system of water, acetone, chloroform, and acetic acid (Chapter 5) (temperature T in K).

		water	acetone	chloroform	acetic acid
$A_{i,j}$	water	0	-4.8338	0	0
	acetone	-8.6051	0	-1.0178	0
	chloroform	0	1.2757	0	0
	acetic acid	0	0	0	0
$B_{i,j}$	water	0	1612.2	-356.84	-73.444
	acetone	-3122.58	0	535.401	0
	chloroform	-793.15	-555.939	0	151.08
	acetic acid	219.66	0	-166.32	0

Table D.43: UNIQUAC model: values for the surface areas q_i and relative Van der Waals volumes r_i for the system of water, acetone, chloroform, and acetic acid (Chapter 5).

	q_i	r_i
water	1.4	0.92
acetone	2.336	2.5735
chloroform	2.412	2.8675
acetic acid	2.072	2.19512

Table D.44: Binary interaction parameter $\tau_{i,j} = A_{i,j} + \frac{B_{i,j}}{T}$ of the NRTL model for the system of acetone, ethanol, water, n-butanol, mesitylene, and oleyl alcohol (Chapter 5) (temperature T in K).

		acetone	ethanol	water	butanol	mesitylene	oleyl alcohol
$A_{i,j}$	acetone	0	-0.3471	6.3981	-8.8875	3.420361	0.71725097
	ethanol	-1.0787	0	-0.8009	0	-0.0665025	0.37324801
	water	0.0544	3.4578	0	13.1102	10.25	30.02397025
	butanol	10.2979	0	-2.0405	0	1.261211	-0.15907213
	mesitylene	-1.355493	-1.925552	-3.726	-2.488674	0	0
	oleyl alcohol	-0.90311055	-0.97282254	-1.33287836	-0.18357132	0	0
$B_{i,j}$	acetone	0	206.597	-1808.99	3077.281	-977.7501	208.797
	ethanol	479.05	0	246.18	-85.2188	327.881	225.0546
	water	419.9716	-586.0809	0	-3338.954	-230	-5605.73
	butanol	-3326.538	128.5015	763.869	0	-427.9547	47.25265483
	mesitylene	430.1372	1010.222	1970	1321.664	0	0
	oleyl alcohol	124.7683	222.3865	624.8787	57.04243655	0	0

Table D.45: Non-randomness parameter $\alpha_{i,j}$ of the NRTL model for the system of acetone, ethanol, water, n-butanol, mesitylene, and oleyl alcohol (Chapter 5).

	acetone	ethanol	water	butanol	mesitylene	oleyl alcohol
acetone	0	0.3	0.3	0.3	0.61295	0.8
ethanol	0.3	0	0.3	0.3	0.20584	0.8
water	0.3	0.3	0	0.3	0.164	0.16397596
butanol	0.3	0.3	0.3	0	0.17412	0.1
mesitylene	0.61295	0.20584	0.164	0.17412	0	0
oleyl alcohol	0.8	0.8	0.16397596	0.1	0	0

Table D.46: Binary parameters of the Wilson model based on a gas constant value of 1.98721 for the system of di-tert-butylbenzene, m-xylene, tert-butyl-m-xylene, tert-butylbenzene, and benzene (Chapter 7).

	di-tert-butylbenz.	m-xylene	tert-butyl-m-xylene	tert-butylbenz.	benzene
di-tert-butylbenzene	0	-591.5004	-34.4702	80.94379	-91.25845
m-xylene	941.59216	0	484.7771	-23.01521	-544.37571
tert-butyl-m-xylene	-4.06701	-369.52548	0	-508.34779	65.03145
tert-butylbenzene	-95.76331	-47.07077	746.0344	0	408.7681
benzene	10.34257	823.07893	-185.87965	-320.51571	0

Table D.47: Molar volumes of the Wilson model for the system of di-tert-butylbenzene, m-xylene, tert-butyl-m-xylene, tert-butylbenzene, and benzene (Chapter 7).

	ν_i
di-tert-butylbenzene	242.356
m-xylene	122.479
tert-butyl-m-xylene	209.558
tert-butylbenzene	154.455
benzene	88.5091

Table D.48: Binary interaction parameter $\tau_{i,j} = A_{i,j} + \frac{B_{i,j}}{T}$ of the NRTL model for the system of levulinic acid, butanol, butyl levulinate, and water (Chapter 7) (temperature T in K).

		levulinic acid	butanol	butyl levulinate	water
$A_{i,j}$	levulinic acid	0	0	-3.85398	0
	butanol	0	0	-6.40275	-2.0405
	butyl levulinate	9.73414	14.1813	0	-2.41183
	water	0	13.1102	3.61303	0
$B_{i,j}$	levulinic acid	0	0	2398.6	0
	butanol	0	0	2398.59	763.869
	butyl levulinate	-5316.23	-5316.22	0	909.621
	water	0	-3338.95	1.54743	0

Table D.49: Non-randomness parameter $\alpha_{i,j}$ of the NRTL model for the system of levulinic acid, butanol, butyl levulinate, and water (Chapter 7).

	levulinic acid	butanol	butyl levulinate	water
levulinic acid	0.3	0.3	0.3	0.3
butanol	0.3	0.3	0.3	0.3
butyl levulinate	0.3	0.3	0.3	0.3
water	0.3	0.3	0.3	0.3

Table D.50: Binary interaction parameter $\tau_{i,j} = A_{i,j} + \frac{B_{i,j}}{T}$ of the NRTL model for the system of acetone, ethanol, water, and butanol (Chapter B) (temperature T in K).

		acetone	ethanol	water	butanol
$A_{i,j}$	acetone	0	-0.3471	6.3981	-8.8875
	ethanol	-1.0787	0	-0.8009	0
	water	0.0544	3.4578	0	13.1102
	butanol	10.2979	0	-2.0405	0
$B_{i,j}$	acetone	0	206.5973	-1808.991	3077.281
	ethanol	479.05	0	246.18	-85.2188
	water	419.9716	-586.0809	0	-3338.9536
	butanol	-3326.5381	128.5015	763.8692	0

Bibliography

Adinata, D., Ayesterán, J., Buchbender, F., Kalem, M., Kopriwa, N. and Pfennig, A. (2011): Drop-population balances as basis for the design of extraction columns, *Chem. Ing. Tech.* **83**(7), 952–964.

Afschar, A. S., Biebl, H., Schaller, K. and Schügerl, K. (1985): Production of acetone and butanol by clostridium Acetobutylicum in continuous culture with cell recycle, *Appl. Microbiol. Biot.* **22**, 394–398.

Agrawal, R. (2003): Synthesis of multicomponent distillation column configurations, *AIChE J.* **49**(2), 379–401.

Agreda, V. H., Partin, L. R. and Heise, W. H. (1990): High-purity methyl acetate via reactive distillation, *Chem. Eng. Progr.* **86**(2), 40–46.

Amale, A. and Lucia, A. (2008): Non-pinched, minimum energy distillation designs, *Chem. Eng. Res. Des.* **86**(8A), 892–903.

Andrecovich, M. J. and Westerberg, A. W. (1985): An milp formulation for heat-integrated distillation sequence synthesis, *AIChE J.* **31**(9), 1461–1474.

Avami, A., Marquardt, W., Saboohi, Y. and Kraemer, K. (2012): Shortcut design of reactive distillation columns, *Chem. Eng. Sci.* **71**(0), 166 – 177.

Ayotte-Sauve, E., Sorin, M. and Rheault, F. (2010): Energy requirement of a distillation/membrane parallel hybrid: A thermodynamic approach, *Ind. Eng. Chem. Res.* **49**(5), 2295–2305.

Barakat, T. M. and Sørensen, E. (2008): Simultaneous optimal synthesis, design and operation of batch and continuous hybrid separation processes, *Chem. Eng. Res. Des.* **86**(3), 279 – 298.

Barbosa, D. and Doherty, M. F. (1988): Design and minimum-reflux calculations for single-feed multicomponent reactive distillation-columns, *Chem. Eng. Sci.* **43**(7), 1523–1537.

Barkmann, S., Sand, G. and Engell, S. (2008): Modellierungsansätze für die design-optimierung von reaktiven rektifikationskolonnen, *Chem. Ing. Tech.* **80**(1-2), 107–117.

Barnicki, S. D. and Fair, J. R. (1990): Separation system synthesis: A knowledge-based approach. 1. liquid mixture separations, *Ind. Eng. Chem. Res.* **29**(3), 421–432.

Barnicki, S. D. and Fair, J. R. (1992): Separation system synthesis: a knowledge-based approach. 2. gas/vapor mixtures, *Ind. Eng. Chem. Res.* **31**(7), 1679–1694.

Barnicki, S. D. and Siirola, J. J. (2004): Process synthesis prospective, *Comp. Chem. Eng.* **28**(4), 441–446.

Barttfeld, M. and Aguirre, P. A. (2002): Optimal synthesis of multicomponent zeotropic distillation processes. 1. preprocessing phase and rigorous optimization for a single unit, *Ind. Eng. Chem. Res.* **41**(21), 5298–5307.

Barttfeld, M. and Aguirre, P. A. (2003): Optimal synthesis of multicomponent zeotropic distillation processes. 2. preprocessing phase and rigorous optimization of efficient sequences, *Ind. Eng. Chem. Res.* **42**(14), 3441–3457.

Barttfeld, M., Aguirre, P. A. and Grossmann, I. E. (2003): Alternative representations and formulations for the economic optimization of multicomponent distillation columns, *Comp. Chem. Eng.* **27**(3), 363–383.

Bauer, M. H. and Stichlmair, J. (1998): Design and economic optimization of azeotropic distillation processes using mixed-integer nonlinear programming, *Comp. Chem. Eng.* **22**(9), 1271–1286.

Baumrucker, B., Renfro, J. and Biegler, L. (2008): MPEC problem formulations and solution strategies with chemical engineering applications, *Comp. Chem. Eng.* **32**(12), 2903 – 2913.

Bausa, J. (2001): *Näherungsverfahren für den konzeptionellen Entwurf und die thermodynamische Analyse von destillativen Trennprozessen*, Fortschrittberichte VDI, VDI Verlag, Reihe 3, Nr.692, Düsseldorf.

Bausa, J. and Marquardt, W. (2000a): Quick and reliable phase stability test in VLLE flash calculations by homotopy continuation, *Comp. Chem. Eng.* **24**(11), 2447–2456.

Bausa, J. and Marquardt, W. (2000b): Shortcut design methods for hybrid membrane/distillation processes for the separation of nonideal multicomponent mixtures, *Ind. Eng. Chem. Res.* **39**(6), 1658–1672.

Bausa, J., von Watzdorf, R. and Marquardt, W. (1998): Shortcut methods for nonideal multicomponent distillation: 1. simple columns, *AIChE J.* **44**(10), 2181–2198.

Bek-Pedersen, E., Gani, R. and Levaux, O. (2000): Determination of optimal energy efficient separation schemes based on driving forces, *Comp. Chem. Eng.* **24**(2-7), 253–259.

Bekiaris, N. and Morari, M. (1996): Multiple steady states in distillation: ∞/∞ predictions, extensions, and implications for design, synthesis, and simulation, *Ind. Eng. Chem. Res.* **35**(11), 4264–4280.

Berry, D. A. and Ng, K. M. (1997): Synthesis of crystallization-distillation hybrid separation processes, *AIChE J.* **43**(7), 1751–1762.

Beviá, F. R., Rico, D. P. and Gomis, A. F. M. (1984): Liquid-liquid extraction: A graphical method for equilibrium stage calculations for quaternary systems, *Fluid Phase Equil.* **15**(3), 257 – 265.

Biegler, L. T., Grossmann, I. E. and Westerberg, A. W. (1997): *Systematic Methods of Chemical Process Design*, Prentice Hall, New Jersey.

Bollas, G. M., Barton, P. I. and Mitsos, A. (2009): Bilevel optimization formulation for parameter estimation in vapor-liquid(-liquid) phase equilibrium problems, *Chem. Eng. Sci.* **64**(8), 1768–1783.

Bonami, P., Biegler, L. T., Conn, A. R., Cornuéjols, G., Grossmann, I. E., Laird, C. D., Lee, J., Lodi, A., Margot, F., Sawaya, N. and Wächter, A. (2008): An algorithmic framework for convex mixed integer nonlinear programs, *Discrete Optimization* **5**(2), 186–204.

Brooke, A., Kendrick, D., Meeraus, A. and Raman, R. (2005): *GAMS - A Users Guide*, GAMS Development Corporation, Washington.

Brüggemann, S. (2005): *Rapid Screening of Conceptual Design Alternatives for Distillation Processes*, Fortschrittberichte VDI, VDI Verlag, Reihe 3, Nr.841, Düsseldorf.

Brüggemann, S. and Marquardt, W. (2004): Shortcut methods for nonideal multicomponent distillation: 3. extractive distillation columns, *AIChE J.* **50**(6), 1129–1149.

Brüggemann, S. and Marquardt, W. (2011a): Conceptual design of distillation processes for mixtures with distillation boundaries. i. computational assessment of split feasibility, *AIChE J.* **57**(6), 1526–1539.

Brüggemann, S. and Marquardt, W. (2011b): Conceptual design of distillation processes for mixtures with distillation boundaries. ii. optimization of recycle policies, *AIChE J.* **57**(6), 1540–1556.

Buchaly, C., Kreis, P. and Górak, A. (2007): Hybrid separation processes–combination of reactive distillation with membrane separation, *Chem. Eng. Process.* **46**(9), 790 – 799.

Bussieck, M. R., Drud, A. S. and Meeraus, A. (2003): MINLPLib–a collection of test models for mixed-integer nonlinear programming, *INFORMS J. on Computing* **15**, 114–119.

Buzad, G. and Doherty, M. F. (1994): Design of 3-component kinetically controlled reactive distillation-columns using fixed-point methods, *Chem. Eng. Sci.* **49**(12), 1947–1963.

Caballero, J. A. and Grossmann, I. E. (2001): Generalized disjunctive programming model for the optimal synthesis of thermally linked distillation columns, *Ind. Eng. Chem. Res.* **40**(10), 2260–2274.

Caballero, J. A., Grossmann, I. E., Keyvani, M. and Lenz, E. S. (2009): Design of hybrid distillation-vapor membrane separation systems, *Ind. Eng. Chem. Res.* **48**(20), 9151–9162.

Caballero, J. A., Odjo, A. and Grossmann, I. E. (2007): Flowsheet optimization with complex cost and size functions using process simulators, *AIChE J.* **53**(9), 2351–2366.

Cairns, B. P. and Furzer, I. A. (1990a): Multicomponent 3-phase azeotropic distillation. 2. phase-stability and phase-splitting algorithms, *Ind. Eng. Chem. Res.* **29**(7), 1364–1382.

Cairns, B. P. and Furzer, I. A. (1990b): Multicomponent three-phase azeotropic distillation. 3. modern thermodynamic models and multiple solutions, *Ind. Eng. Chem. Res.* **29**(7), 1383–1395.

Cardoso, M. F., Salcedo, R. L., de Azevedo, S. F. and Barbosa, D. (2000): Optimization of reactive distillation processes with simulated annealing, *Chemical Engineering Science* **55**(21), 5059 – 5078.

Ciric, A. R. and Gu, D. (1994): Synthesis of nonequilibrium reactive distillation processes by minlp opttimization, *AIChE J.* **40**(9), 1479–1487.

Cisternas, L. A., Vásquez, C. M. and Swaney, R. E. (2006): On the design of crystallization-based separation processes: Review and extension, *AIChE J.* **52**(5), 1754–1769.

Davison, B. H. and Thompson, J. E. (1993): Continuous direct solvent extraction of butanol in a fermenting fluidized-bed bioreactor with immobilized clostridium Acetobutylicum, *Appl. Biochem. Biotech.* **39-40**, 415–426.

Davydian, A., Malone, M. F. and Doherty, M. F. (1997): Boundary modes in a single feed distillation column for the separation of azeotropic mixtures, *Theor. Found. Chem. Eng.* **31**(4), 327–338.

Diaz, S., Gros, H. and Brignole, E. A. (2000): Thermodynamic modeling, synthesis and optimization of extraction – dehydration processes, *Comp. Chem. Eng.* **24**(9-10), 2069 – 2080.

Diwekar, U. M., Grossmann, I. E. and Rubin, E. S. (1992): An MINLP process synthesizer for a sequential modular simulator, *Ind. Eng. Chem. Res.* **31**(1), 313–322.

Douglas, J. M. (1985): A hierachical decision procedure for process synthesis, *AIChE J.* **31**(3), 353–362.

Douglas, J. M. (1988): *Conceptual Design of Chemical Processes*, McGraw-Hill, New York.

Douglas, J. M. (1995): Synthesis of separation system flowsheets, *AIChE J.* **41**(12), 2522–2536.

Dragomir, R. M. and Jobson, M. (2005): Conceptual design of single-feed kinetically controlled reactive distillation columns, *Chem. Eng. Sci.* **60**(18), 5049–5068.

Drud, A. (2005): Sbb, *GAMS - The Solver Manuals*, GAMS Development Corporation, Washington, p. 377.

Duerre, P. (2008): Fermentative butanol production - bulk chemical and biofuel, *in* J. Wiegel, R. J. Maier and M. W. W. Adams (eds), *Incredible Anaerobes: From Physiology to Genomics to Fuels*, Vol. 1125 of *Ann. N.Y. Acad. Sci*, Blackwell Publishing, pp. 353–362.

Dünnebier, G. and Pantelides, C. C. (1999): Optimal design of thermally coupled distillation columns, *Ind. Eng. Chem. Res.* **38**(1), 162–176.

Dupire, S. and Thyrion, F. C. (1986): Solvent extraction of products from acetone-butanol fermentation, *ISEC'86, Vol. III*, p. 613.

Duran, M. A. and Grossmann, I. E. (1986): A mixed-integer nonlinear-programming algorithm for process systems synthesis, *AIChE J.* **32**(4), 592–606.

Eckert, G. and Schügerl, K. (1987): Continuous acetone-butanol production with direct product removal, *Appl. Microbiol. Biotechnol.* **27**, 221–228.

Eldridge, R. B., Seibert, A., Robinson, S. M. and Rogers, J. (2005): Hybrid separations/distillation technology: Research opportunities for energy and emissions reduction, *Technical report*, U.S. Department of Energy.

Esbjerg, K., Andersen, T. R., Müller, D., Marquardt, W. and Jørgensen, S. B. (1998): Multiple steady states in heterogeneous azeotropic distillation sequences, *Ind. Eng. Chem. Res.* **37**(11), 4434–4452.

Farkas, T., Czuczai, B., Rev, E. and Lelkes, Z. (2008): New minlp model and modified outer approximation algorithm for distillation column synthesis, *Ind. Eng. Chem. Res.* **47**(9), 3088–3103.

Farkas, T., Rev, E. and Lelkes, Z. (2005): Process flowsheet superstructures: Structural multiplicity and redundancy: Part ii: Ideal and binarily minimal MINLP representations, *Comp. Chem. Eng.* **29**(10), 2198 – 2214.

Fletcher, R. and Leyffer, S. (2004): Solving mathematical programs with complementarity constraints as nonlinear programs, *Optimization Methods & Software* **19**(1), 15–40.

Fletcher, R. and Morton, W. (2000): Initialising distillation column models, *Comp. Chem. Eng.* **23**(11-12), 1811–1824.

Fontalvo, J., Cuellar, P., Timmer, J. M. K., Vorstman, M. A. G., Wijers, J. G. and Keurentjes, J. T. F. (2005): Comparing pervaporation and vapor permeation hybrid distillation processes, *Ind. Eng. Chem. Res.* **44**(14), 5259–5266.

Fraga, E. S., Steffens, M. A., Bogle, I. D. L. and Hind, A. K. (2000): An object oriented framework for process synthesis and optimization, *in* M. F. Malone, J. A. Trainham and B. Carnahan (eds), *Foundations of Computer-Aided Process Design, AIChE Symposium Series*, Vol. 323, pp. 446–449.

Franke, M. B. (2006): *Optimierung hybrider Trennverfahren*, Fortschrittberichte VDI, VDI Verlag, Reihe 3, Nr.854, Düsseldorf.

Franke, M. B., Nowotny, N., Ndocko, E. N., Gorak, A. and Strube, J. (2008): Design and optimization of a hybrid distillation/melt crystallization process, *AIChE J.* **54**(11), 2925–2942.

Friedler, F., Tarján, K., Huang, Y. and Fan, L. (1992): Graph-theoretic approach to process synthesis: axioms and theorems, *Chem. Eng. Sci.* **47**(8), 1973–1988.

Gani, R. and Constantinou, L. (1996): Molecular structure based estimation of properties for process design, *Fluid Phase Equil.* **116**(1-2), 75 – 86.

Gill, P., Murray, W., Saunders, M., Drud, A. and Kalvelagen, E. (2008): SNOPT: An SQP algorithm for large-scale constrained optimization, *GAMS - The Solver Manuals*, GAMS Development Corporation, Washington.

Glanz, S. and Stichlmair, J. (1995): Energetic optimization of distillations in hybrid processes, *Comp. Chem. Eng.* **19**, S51–S56.

Goodson, M. and Kraft, M. (2004): Simulation of coalescence and breakage: an assessment of two stochastic methods suitable for simulating liquid-liquid extraction, *Chem. Eng. Sci.* **59**(18), 3865 – 3881.

Groot, W. J., der Lans, R. G. J. M. V. and Luyben, K. C. A. M. (1992): Technologies for butanol recovery integrated with fermentations, *Process Biochem.* **27**(2), 61–75.

Groot, W. J., Schoutens, G. H., Van Beelen, P. N., Van den Oever, C. E. and Kossen, N. W. F. (1984): Increase of substrate conversion by pervaporation in the continuous butanol fermentation, *Biotechnol. Lett.* **6**, 789–792.

Groot, W. J., Soedjak, H. S., Donck, P. B., Van der Lans, R. G. J. M., Luyben, K. C. A. M. and Timmer, J. M. K. (1990): Butanol recovery from fermentations by liquid-liquid extraction and membrane solvent extraction, *Bioprocess. Biosyst. Eng.* **5**, 203–216.

Groot, W. J., Van der Lans, R. G. J. M. and Luyben, K. C. A. M. (1989): Batch and continuous butanol fermentations with free cells: integration with product recovery by gas-stripping, *Appl. Microbiol. Biotechnol.* **32**, 305–308.

Grossman, I. E., Viswanathan, J., Vecchietti, A., Raman, R. and Kalvelagen, E. (2008): Sbb, *GAMS - The Solver Manuals*, GAMS Development Corporation, Washington.

Gupta, O. K. and Ravindran, V. (1985): Branch and bound experiments in convex nonlinear integer programming, *Manage. Sci.* **31**(12), 1533–1546.

Guthrie, K. M. (1969): Capital cost estimating, *Chemical Engineering* (March 24), 114.

Harmsen, G. J. (2004): Industrial best practices of conceptual process design, *Chem. Eng. Process.* **43**(5), 671–675.

Harper, P. M. and Gani, R. (2000): A multi-step and multi-level approach for computer aided molecular design, *Comp. Chem. Eng.* **24**(2-7), 677–683.

Harwardt, A., Kossack, S. and Marquardt, W. (2008): Optimal column sequencing for multicomponent mixtures, *in* B. Braunschweig and X. Joulia (eds), *18th European Symposium on Computer Aided Process Engineering*, Elsevier, pp. 91–96.

Harwardt, A., Kraemer, K. and Marquardt, W. (2009): Optimization based design of heat integrated distillation processes, *In: 8th World Congress of Chemical Engineering, Montreal, Canada*.

Harwardt, A., Kraemer, K. and Marquardt, W. (2010): Identifying optimal mixture properties for HIDiC application, *in* A. B. De Haan, H. Kooijman and A. Gorak (eds), *Distillation & Absorption 2010*, pp. 55–60.

Harwardt, A., Kraemer, K., Rüngeler, B. and Marquardt, W. (2011): Conceptual design of a butyl-levulinate reactive distillation process by incremental refinement, *Chin. J. Chem. Eng.* **19**(3), 371 – 379.

Harwardt, A. and Marquardt, W. (2012): Heat-integrated distillation columns: Vapor recompression or internal heat integration?, *AIChE Journal* pp. n/a–n/a.

Hess, G. (2006): BP and DuPont plan 'biobutanol', *Chem. Eng. News* **84**(26), 9.

Hildebrandt, D., Beneke, D. A., Abbas, R., Holland, S. T., Vrey, M. and Glasser, D. (2010): Column profile maps as a tool for synthesizing complex column configurations, *Comp. Chem. Eng.* **34**(9), 1487–1496.

Hostrup, M., Harper, P. M. and Gani, R. (1999): Design of environmentally benign processes: integration of solvent design and separation process synthesis, *Comp. Chem. Eng.* **23**(10), 1395–1414.

Hua, J. Z., Brennecke, J. F. and Stadtherr, M. A. (1998): Enhanced interval analysis for phase stability: Cubic equation of state models, *Ind. Eng. Chem. Res.* **37**(4), 1519–1527.

Huang, W. C., Ramey, D. E. and Yang, S. T. (2004): Continuous production of butanol by Clostridium Acetobutylicum immobilized in a fibrous bed bioreactor, *Appl. Biochem. Biotech.* **113**, 887–898.

Hunter, T. G. and Nash, A. W. (1934): The application of physico-chemical principles to the design of liquid-liquid contact equipment. ii. Application of phase-rule graphical methods, *J. Soc. Chem. Ind.* **53**, 95–102.

Ishii, S., Taya, M. and Kobayashi, T. (1985): Production of butanol by Clostridium Acetobutylicum in extractive fermentation system, *J. Chem. Eng. Jpn.* **18**(2), 125–130.

Jaksland, C. A., Gani, R. and Lien, K. M. (1995): Separation process design and synthesis based on thermodynamic insights, *Chem. Eng. Sci.* **50**(3), 511–530.

Jiang, H. and Ralph, D. (2000): Smooth SQP methods for mathematical programs with nonlinear complementarity constraints, *SIAM J. Optim.* **10**(3), 779–808.

Jones, D. T. and Woods, D. R. (1986): Acetone-butanol fermentation revisited, *Microbiological Reviews* **50**, 484–524.

Julka, V. and Doherty, M. F. (1990): Geometric behavior and minimum flows for nonideal multicomponent distillation, *Chem. Eng. Sci.* **45**(7), 1801–1822.

Kaibel, G., Miller, C., Stroezl, M., von Watzdorf, R. and Jansen, H. (2004): Industrieller einsatz von trennwandkolonnen und thermisch gekoppelten destillationskolonnen, *Chem. Ing. Tech.* **76**(3), 258–263.

Kaibel, G. and Schoenmakers, H. (2002): Process synthesis and design in industrial practice, *in* J. Grievink and J. van Schijndel (eds), *12th European Symposium on Computer Aided Process Engineering*, Elsevier, pp. 9 – 22.

Karunanithi, A. T., Achenie, L. E. K. and Gani, R. (2005): A new decomposition-based computer-aided molecular/mixture design methodology for the design of optimal solvents and solvent mixtures, *Ind. Eng. Chem. Res.* **44**(13), 4785–4797.

Köhler, J., Aguirre, P. and Blass, E. (1991): Minimum reflux calculations for nonideal mixtures using the reversible distillation model, *Chem. Eng. Sci.* **46**(12), 3007–3021.

Kim, S. B. and Linninger, A. A. (2010): Rigorous separation design. 2. network design solutions for mixtures with various volatility differences and feed compositions, *Ind. Eng. Chem. Res.* **49**(18), 8670–8684.

Kim, S. B., Ruiz, G. J. and Linninger, A. A. (2010): Rigorous separation design. 1. multicomponent mixtures, nonideal mixtures, and prefractionating column networks, *Ind. Eng. Chem. Res.* **49**(14), 6499–6513.

Kocis, G. R. and Grossmann, I. E. (1989): A modelling and decomposition strategy for the minlp optimization of process flowsheets, *Comp. Chem. Eng.* **13**(7), 797 – 819.

Kossack, S. (2010): *A Systematic Synthesis Framework for the Conceptual Design of Distillation Processes*, Fortschrittberichte VDI, VDI Verlag, Reihe 3, Nr.914, Düsseldorf.

Kossack, S., Kraemer, K., Gani, R. and Marquardt, W. (2008): A systematic synthesis framework for extractive distillation processes, *Chem. Eng. Res. Des.* **86**(7A), 781–792.

Kossack, S., Kraemer, K. and Marquardt, W. (2006): Efficient optimization based design of distillation columns for homogenous azeotropic mixtures, *Ind. Eng. Chem. Res.* **45**(25), 8492–8502.

Kossack, S., Refinius, A., Brüggemann, S. and Marquardt, W. (2007): Konzeptioneller Entwurf von Reaktions-Destillations-Prozessen mit Näherungsverfahren, *Chem. Ing. Tech.* **79**(10), 1601–1612.

Kovach, J. W. and Seider, W. D. (1987): Heterogeneous azeotropic distillation: Experimental and simulation results, *AIChE J.* **33**(8), 1300–1314.

Kraemer, K., Harwardt, A., Bronneberg, R. and Marquardt, W. (2011): Separation of butanol from acetone-butanol-ethanol fermentation by a hybrid extraction-distillation process, *Comp. Chem. Eng.* **35**(5), 949 – 963.

Kraemer, K., Harwardt, A. and Marquardt, W. (2009a): Design of heat-integrated distillation processes using shortcut methods and rigorous optimization, *in* R. De Brito Alves, C. Oller do Nascimento and E. Biscaia (eds), *10th International Symposium on Process Systems Engineering*, Elsevier, pp. 993–998.

Kraemer, K., Harwardt, A. and Marquardt, W. (2009b): A novel shortcut method for the design of heteroazeotropic distillation of multicomponent mixtures, *in* M. M.

El-Halwagi and A. A. Linninger (eds), *Design for Energy and the Environment, Proceedings of the Seventh International Conference on the Foundations of Computer-Aided Process Design*, CRC Press, pp. 1035–1052.

Kraemer, K., Harwardt, A. and Marquardt, W. (2010): Shortcut methods for the design of heteroazeotropic distillation of multicomponent mixtures, *in* A. B. De Haan, H. Kooijman and A. Gorak (eds), *Distillation & Absorption 2010*, pp. 515–520.

Kraemer, K., Harwardt, A., Skiborowski, M., Mitra, S. and Marquardt, W. (2011): Shortcut-based design of multicomponent heteroazeotropic distillation, *Chem. Eng. Res. Des.* **89**(8), 1168 – 1189.

Kraemer, K., Kossack, S. and Marquardt, W. (2007): An efficient solution method for the minlp optimization of chemical processes, *in* V. Plesu and P. Agachi (eds), *17th European Symposium On Computer Aided Process Engineering*, Elsevier, pp. 105–110.

Kraemer, K., Kossack, S. and Marquardt, W. (2009): Effficient optimization-based design of distillation processes for homogenous azeotropic mixtures, *Ind. Eng. Chem. Res.* **48**(14), 6749–6764.

Kraemer, K. and Marquardt, W. (2010): Continuous reformulation of MINLP problems, *in* M. Diehl, F. Glineur, E. Jarlebring and W. Michiels (eds), *Recent Advances in Optimization and its Applications in Engineering*, Springer, pp. 83–92.

Kraemer, K., Redepenning, C., Recker, S., Skiborowski, M. and Marquardt, W. (2012): Algorithmic shortcut method for the performance evaluation of multicomponent liquid-liquid extraction, *in preparation* .

Kravanja, Z. and Grossmann, I. E. (1990): Prosyn–an minlp process synthesizer, *Comp. Chem. Eng.* **14**(12), 1363 – 1378.

Kravanja, Z. and Grossmann, I. E. (1993): Prosyn – an automated topology and parameter process synthesizer, *Comp. Chem. Eng.* **17**(Supplement 1), S87 – S94.

Kravanja, Z. and Grossmann, I. E. (1996): A computational approach for the modeling/decomposition strategy in the minlp optimization of process flowsheets with implicit models, *Ind. Eng. Chem. Res.* **35**(6), 2065–2070.

Lang, Y.-D. and Biegler, L. T. (2002): Distributed stream method for tray optimization, *AIChE J.* **48**(3), 582–595.

Lastusilta, T., Bussieck, M. R. and Westerlund, T. (2009): An experimental study of the gams/alphaecp minlp solver, *Ind. Eng. Chem. Res.* **48**(15), 7337–7345.

Levy, S. G., Van Dongen, D. B. and Doherty, M. F. (1985): Design and synthesis of homogeneous azeotropic distillations .2. minimum reflux calculations for nonideal and azeotropic columns, *Ind. Eng. Chem. Fundam.* **24**(4), 463–474.

Li, X. N. and Kraslawski, A. (2004): Conceptual process synthesis: past and current trends, *Chem. Eng. Process.* **43**(5), 583–594.

Lipnizki, F., Field, R. W. and Ten, P. K. (1999): Pervaporation-based hybrid process: A review of process design, applications and economics, *J. Membr. Sci.* **153**(2), 183–210.

Liu, J. H., Fan, L. T., Seib, P., Friedler, F. and Bertok, B. (2004): Downstream process synthesis for biochemical production of butanol, ethanol, and acetone from grains: Generation of optimal and near-optimal flowsheets with conventional operating units, *Biotechnol. Progr.* **20**(5), 1518–1527.

Lucia, A., Amale, A. and Taylor, R. (2006): Energy efficient hybrid separation processes, *Ind. Eng. Chem. Res.* **45**(25), 8319–8328.

Lucia, A., Amale, A. and Taylor, R. (2008): Distillation pinch points and more, *Comp. Chem. Eng.* **32**(6), 1342–1364.

Marcilla, A., Gomez, A., Reyes, J. A. and Olaya, M. M. (1999): New method for quaternary systems liquid-liquid extraction tray to tray design, *Ind. Eng. Chem. Res.* **38**(8), 3083–3095.

Marquardt, W. (2005): Model-based experimental analysis of kinetic phenomena in multi-phase reactive systems, *Chem. Eng. Res. Des.* **83**(A6), 561–573.

Marquardt, W., Harwardt, A., Hechinger, M., Kraemer, K., Viell, J. and Voll, A. (2010): The biorenewables opportunity - toward next generation process and product systems, *AIChE J.* **56**(9), 2228–2235.

Marquardt, W., Kossack, S. and Kraemer, K. (2008): A framework for the systematic design of hybrid separation processes, *Chin. J. Chem. Eng.* **16**(3), 333–342.

Marquardt, W., Kraemer, K. and Harwardt, A. (2010): Systematic optimization-based synthesis of hybrid separation processes, *in* A. B. De Haan, H. Kooijman and A. Gorak (eds), *Distillation & Absorption 2010*, pp. 29–36.

Matsumura, M. and Kataoka, H. (1987): Separation of dilute aqueous butanol and acetone solutions by pervaporation through liquid membranes, *Biotechnol. Bioeng.* **30**, 887–895.

Matsumura, M., Kataoka, H., Sueki, M. and Araki, K. (1988): Energy saving effect of pervaporation using oleyl alcohol liquid membrane in butanol purification, *Bioprocess Eng.* **3**, 93–100.

Matsuoka, M., Ohishi, M. and Kasama, S. (1986): Purification of para-dichlorobenzene and m-chloronitrobenzene crystalline particles by sweating, *J. Chem. Eng. Jpn.* **19**(3), 181–185.

McDonald, C. M. and Floudas, C. A. (1995): Global optimization for the phase-stability problem, *AIChE J.* **41**(7), 1798–1814.

Milestone, N. B. and Bibby, D. M. (1981): Concentration of alcohols by adsorption on silicalite, *J. Chem. Technol. Biotechnol.* **31**, 732–736.

Minotti, M., Doherty, M. F. and Malone, M. F. (1996): A geometric method for the design of liquid extractors, *Ind. Eng. Chem. Res.* **35**(8), 2672–2681.

Moganti, S., Noble, R. D. and Koval, C. A. (1994): Analysis of a membrane distillation column hybrid process, *J. Membr. Sci.* **93**(1), 31–44.

Mohanty, S. (2000): Modeling of liquid-liquid extraction column: A review, *Reviews In Chemical Engineering* **16**(3), 199–248.

Müller, D., Hoppe, J. and Wagner, P. (2010): Steigerung der Energieeffizienz: Verfahrenstechnische Konzepte und Realisierungen, *Chem. Ing. Tech.* **82**(9), 1412–1413.

Neves, F. J. M., Silva, D. C. M. and Oliveira, N. M. C. (2005): A robust strategy for optimizing complex distillation columns, *Comp. Chem. Eng.* **29**(6), 1457–1471.

Ni, Y. and Sun, Z. (2009): Recent progress on industrial fermentative production of acetone-butanol-ethanol by Clostridium Acetobutylicum in China, *Appl. Microbiol. Biotechnol.* **83**(3), 415–423.

Noeres, C., Kenig, E. Y. and Gorak, A. (2003): Modelling of reactive separation processes: reactive absorption and reactive distillation, *Chem. Eng. Process.* **42**(3), 157–178.

Oudshoorn, A., Van der Wielen, L. A. M. and Straathof, A. J. J. (2009): Assessment of options for selective 1-butanol recovery from aqueous solution, *Ind. Eng. Chem. Res.* **48**(15), 7325–7336.

Pai, R. A., Doherty, M. F. and Malone, M. F. (2002): Design of reactive extraction systems for bioproduct recovery, *AIChE J.* **48**(3), 514–526.

Pajula, E., Seuranen, T., Koiranen, T. and Hurme, M. (2001): Synthesis of separation processes by using case-based reasoning, *Comp. Chem. Eng.* **25**(4-6), 775–782.

Perry, H. R. and Green, D. W. (eds) (1997): *Perry's Chemical Engineers' Handbook*, McGraw-Hill.

Peters, M., Zavrel, M., Kahlen, J., Schmidt, T., Ansorge-Schumacher, M., Leitner, W., Buechs, J., Greiner, L. and Spiess, A. C. (2008): Systematic Approach to Solvent Selection for Biphasic Systems with a Combination of COSMO-RS and a Dynamic Modeling Tool, *Eng. Life Sci.* **8**(5), 546–552.

Petlyuk, F. (2004): *Distillation Theory and its Application to Optimal Design of Separation Units*, Cambridge University Press.

Pettersen, T. and Lien, K. M. (1995): Design of hybrid distillation and vapor permeation processes, *J. Membr. Sci.* **102**, 21–30.

Pham, H. and Doherty, M. F. (1990): Design and synthesis of heterogeneous azeotropic distillations iii. column sequences., *Chem. Eng. Sci.* **45**(7), 1845–1854.

Pham, H., Ryan, P. and Doherty, M. F. (1989): Design and minimum reflux for heterogeneous azeotropic distillation columns, *AIChE J.* **35**(10), 1585–1591.

Pitner, W. R., Schulte, M., Gorak, A., Santangelo, F. and Wentink, A. E. (2008): Use of ionic liquids with tetracyanoborate anions as a solvent for extraction of alcohols from aqueous solutions. patent WO 2009152906.

Pöllmann, P., Glanz, S. B. and Blass, E. (1994): Calculating minimum reflux of non-ideal multicomponent distillation using eigenvalue theory, *Comp. Chem. Eng.* **18**(S), S49–S53.

Pressly, T. G. and Ng, K. M. (1998): A break-even analysis of distillation-membrane hybrids, *AIChE J.* **44**(1), 93–105.

Pressly, T. G. and Ng, K. M. (1999): Process boundary approach to separations synthesis, *AIChE J.* **45**(9), 1939–1952.

Qi, Z., Sundmacher, K., Stein, E., Kienle, A. and Kolah, A. (2002): Reactive separation of isobutene from c4 crack fractions by catalytic distillation processes, *Sep. Purif. Technol.* **26**(2-3), 147 – 163.

Qureshi, N. and Blaschek, H. P. (2001): Recent advances in ABE fermentation: hyper-butanol producing Clostridium Beijerinckii BA101, *Ind. Microbiol. Biot.* **27**(5), 287–291.

Qureshi, N. and Ezeji, T. C. (2008): Butanol, 'a superior biofuel' production from agricultural residues (renewable biomass): recent progress in technology, *Biofuels, Bioprod. Biorefin.* **2**(4), 319–330.

Qureshi, N., Hughes, S., Maddox, I. and Cotta, M. A. (2005): Energy-efficient recovery of butanol from model solutions and fermentation broth by adsorption, *Bioproc. Biosyst. Eng.* **27**, 215–222.

Qureshi, N., Maddox, I. S. and Friedl, A. (1992): Application of continuous substrate feeding to the abe fermentation: relief of product inhibition using extraction, perstraction, stripping, and pervaporation, *Biotechnol. Progr.* **8**, 382–390.

Qureshi, N., Schripsema, J., Lienhardt, J. and Blaschek, H. P. (2000): Continuous solvent production by Clostridium Beijerinckii ba101 immobilized by adsorption onto brick, *World. J. Microb. Biot.* **16**, 377–382.

Rajagopal, S., Ng, K. M. and Douglas, J. M. (1992): A hierarchical procedure for the conceptual design of solids processes, *Comp. Chem. Eng.* **16**(7), 675 – 689.

Rathore, R. N. S., Van Wormer, K. A. and Powers, G. J. (1974): Synthesis strategies for multicomponent separation systems with energy integration, *AIChE J.* **20**(3), 491–502.

Reyes-Labarta, J. A. and Grossmann, I. E. (2001): Disjunctive optimization design models for complex liquid-liquid multistage extractors, *AIChE J.* **47**(10), 2243–2252.

Roffler, S. R., Blanch, H. W. and Wilke, C. R. (1987): In-situ recovery of butanol during fermentation, *Bioprocess Eng.* **2**, 1–12.

Roffler, S. R., Blanch, H. W. and Wilke, C. R. (1988): In situ extractive fermentation of acetone and butanol, *Biotechnol. and Bioeng.* **31**, 135–143.

Ruiz, G. J., Kim, S. B., Moes, L. and Linninger, A. A. (2011): Rigorous synthesis and simulation of complex distillation networks, *AIChE J.* **57**(1), 136–148.

Ryan, P. and Doherty, M. F. (1989): Design/optimization of ternary heterogeneous azeotropic distillation sequences, *AIChE J.* **35**(10), 1592–1601.

Ryll, O., Blagov, S. and Hasse, H. (2008): Rechnergestützter konzeptioneller Entwurf von Destillations-/Reaktionsprozessen, *Chem. Ing. Tech.* **80**(1-2), 207–213.

Salem, A. B. S. H., Hamad, E. Z. and Al-Naafa, M. A. (1994): Quaternary liquid-liquid equilibrium of n-heptane-toluene-o-xylene-propylene carbonate, *Ind. Eng. Chem. Res.* **33**(3), 689–692.

Sand, G., Barkmann, S., Engell, S. and Schembecker, G. (2004): Structuring of reactive distillation columns for non-ideal mixtures using minlp-techniques, *in* A. Barbosa-Póvoa and H. Matos (eds), *14th European Symposium on Computer-Aided Process Engineering*, Elsevier, pp. 493 – 498.

Sargent, R. W. H. and Gaminibandara, K. (1976): Optimum design of plate distillation columns, *in* L. C. W. Dixon (ed.), *Optimization in Action*, Academic Press, London, pp. 267–314.

Sattler, K. (1988): *Thermische Trennverfahren: Grundlagen, Auslegung, Apparate*, Wiley-VCH, Weinheim.

Scheel, H. and Scholtes, S. (2000): Mathematical programs with complementarity constraints: Stationarity, optimality, and sensitivity, *Mathematics Of Operations Research* **25**(1), 1–22.

Schembecker, G. and Simmrock, K. H. (1997): Heuristic-numeric design of separation processes for azeotropic mixtures, *Comp. Chem. Eng.* **21**, S231–S236.

Siirola, J. J. (1996): Strategic process synthesis: Advances in the hierarchical approach, *Comp. Chem. Eng.* **20**(Supplement 2), S1637 – S1643.

Skiborowski, M., Mhamdi, A., Kraemer, K. and Marquardt, W. (2012): Model-based structural optimization of seawater desalination plants, *Desalination* **292**(0), 30 – 44.

Sommer, S. and Melin, T. (2004): Design and optimization of hybrid separation processes for the dehydration of 2-propanol and other organics, *Ind. Eng. Chem. Res.* **43**(17), 5248–5259.

Steffens, M. A., Fraga, E. S. and Bogle, I. D. L. (1999): Multicriteria process synthesis for generating sustainable and economic bioprocesses, *Comp. Chem. Eng.* **23**(10), 1455 – 1467.

Stein, O., Oldenburg, J. and Marquardt, W. (2004): Continuous reformulations of discrete-continuous optimization problems, *Comp. Chem. Eng.* **28**(10), 1951–1966.

Stephan, W., Noble, R. D. and Koval, C. A. (1995): Design methodology for a membrane/distillation column hybrid process, *J. Membr. Sci.* **99**(3), 259 – 272.

Stichlmair, J. and Frey, T. (2001): Mixed-integer nonlinear programming optimization of reactive distillation processes, *Ind. Eng. Chem. Res.* **40**(25), 5978–5982.

Stichlmair, J. G. and Herguijuela, J. R. (1992): Separation regions and processes of zeotropic and azeotropic ternary distillation, *AIChE J.* **38**(10), 1523–1535.

Szitkai, Z., Lelkes, Z., Rev, E. and Fonyo, Z. (2002): Optimization of hybrid ethanol dehydration systems, *Chem. Eng. Process.* **41**(7), 631–646.

Tapp, M., Holland, S. T., Hildebrandt, D. and Glasser, D. (2004): Column profile maps. 1. Derivation and interpretation, *Ind. Eng. Chem. Res.* **43**(2), 364–374.

Tawarmalani, M. and Sahinidis, N. V. (2005): A polyhedral branch-and-cut approach to global optimization, *Mathematical Programming* **103**, 225–249.

Thong, D. Y. C. and Jobson, M. (2001): Multicomponent homogeneous azeotropic distillation 3. column sequence synthesis, *Chem. Eng. Sci.* **56**(14), 4417–4432.

Treybal, R. E. (1963): *Liquid Extraction*, McGraw-Hill, New York.

Ulrich, J., Bierwirth, J. and Henning, S. (1996): Solid layer melt crystallization, *Separ. Purif. Method* **25**(1), 1–45.

Underwood, A. (1948): Fractional distillation of multicomponent mixtures, *Chem. Eng. Progr.* **44**(8), 603–614.

Ung, S. and Doherty, M. F. (1995): Vapor-liquid phase-equilibrium in systems with multiple chemical-reactions, *Chem. Eng. Sci.* **50**(1), 23–48.

Urdaneta, R. Y. (2005): *Targeting and Conceptual Design of Heteroazeotropic Distillation Processes*, Fortschrittberichte VDI, VDI Verlag, Reihe 3, Nr.841, Düsseldorf.

Urdaneta, R. Y., Bausa, J., Brüggemann, S. and Marquardt, W. (2002): Analysis and conceptual design of ternary heterogeneous azeotropic distillation processes, *Ind. Eng. Chem. Res.* **41**(16), 3849–3866.

Urselmann, M. and Engell, S. (2010): Optimization-based design of reactive distillation columns using a memetic algorithm, *in* S. Pierucci and G. B. Ferraris (eds), *20th European Symposium on Computer Aided Process Engineering*, Elsevier, pp. 1243 – 1248.

Valentas, K. J., Bilous, O. and Amundson, N. R. (1966): Analysis of breakage in dispersed phase systems, *Ind. Eng. Chem. Fundam.* **5**(2), 271–279.

Viswanathan, J. and Grossmann, I. E. (1990): A combined penalty-function and outer-approximation method for minlp optimization, *Comp. Chem. Eng.* **14**(7), 769–782.

Viswanathan, J. and Grossmann, I. E. (1993): Optimal feed locations and number of trays for distillation-columns with multiple feeds, *Ind. Eng. Chem. Res.* **32**(11), 2942–2949.

Von Watzdorf, R., Bausa, J. and Marquardt, W. (1999): Shortcut methods for nonideal multicomponent distillation: 2. complex columns, *AIChE J.* **45**(8), 1615–1628.

Wahnschafft, O. M., Le Rudulier, J. P. and Westerberg, A. W. (1993): A problem decomposition approach for the synthesis of complex separation processes with recycles, *Ind. Eng. Chem. Res.* **32**(6), 1121–1141.

Wallert, C. (2008): *Konzeptioneller Entwurf und wirtschaftliche Bewertung hybrider Trennprozesse mit Näherungsverfahren*, Fortschrittberichte VDI, VDI Verlag, Reihe 3, Nr.889.

Wang, C. J., Wong, D. S. H., Chien, I.-L., Shih, R. F., Liu, W. T. and Tsai, C. S. (1998): Critical reflux, parametric sensitivity, and hysteresis in azeotropic distillation of isopropyl alcohol + water + cyclohexane, *Ind. Eng. Chem. Res.* **37**(7), 2835–2843.

Wasylkiewicz, S. K. (1999): Design of heterogeneous distillation columns for separation of azeotropic non-reactive and reactive mixtures, *Comp. Chem. Eng.* **23**, S125–S128.

Wasylkiewicz, S. K. (2006): Syntheis of separation systems for azeotropic mixtures: preferred distillation region, *in* W. Marquardt and C. Pantelides (eds), *16th European Symposium on Computer Aided Process Engineering*, Elsevier, pp. 1033–1038.

Wasylkiewicz, S. K., Kobylka, L. C. and Castillo, F. J. L. (2003): Synthesis and design of heterogeneous separation systems with recycle streams, *Chem. Eng. J.* **92**(1-3), 201–208.

Wellinghoff, G. and Wintermantel, K. (1991): Melt trystallization - theoretical presumptions and technical limitations, *Chem. Ing. Tech.* **63**(9), 881–891.

Westerberg, A. W. (2004): A retrospective on design and process synthesis, *Comp. Chem. Eng.* **28**(4), 447–458.

Wibowo, C. and Ng, K. M. (2000): Unified approach for synthesizing crystallization-based separation processes, *AIChE J.* **46**(7), 1400–1421.

Yang, X. and Tsao, G. T. (1994): Mathematical modeling of inhibition kinetics in acetone-butanol fermentation by clostridium Acetobutylicum, *Biotechnol. Progr.* **10**(5), 532–538.

Yeomans, H. and Grossmann, I. E. (2000): Optimal design of complex distillation columns using rigorous tray-by-tray disjunctive programming models, *Ind. Eng. Chem. Res.* **39**(11), 4326–4335.

Zhang, L. B. and Linninger, A. A. (2004): Temperature collocation algorithm for fast and robust distillation design, *Ind. Eng. Chem. Res.* **43**(12), 3163–3182.

Zhang, L. B. and Linninger, A. A. (2006): Towards computer-aided separation synthesis, *AIChE J.* **52**(4), 1392–1409.

Zou, L., Yang, G., Han, B., Liu, R. and Yan, H. (1999): Solubilities of 1,2,3-trimethylbenzene and 1,2,4-trimethylbenzene and 1,3,5-trimethylbenzene in t-butyl alcohol+water mixtures and hydrophobic interaction, *Sci. China, Ser. B Chem.* **42**, 400–410.